UNIVERSITY OF MISKOLC

FACULTY OF MECHANICAL ENGINEERING AND INFORMATICS

Increase the efficiency of the hybrid photovoltaic thermal system

PhD DISSERTATION

Prepared by

Mohammed Alktranee

ISTVÁN SÁLYI DOCTORAL SCHOOL OF MECHANICAL ENGINEERING SCIENCES

MAIN TOPIC GROUP: FUNDAMENTAL SCIENCES IN MECHANICAL ENGINEERING

TOPIC GROUP: TRANSPORT PROCESSES AND MACHINES

Head of Doctoral School
Bognár Vadászné Gabriella
Director of Science, Full Professor

Scientific Supervisor

Bencs Péter
Associate professor

Miskolc
2023

Acknowledgement

Obtaining a PhD degree was a major turning point in my life, as it constituted a bright point in my professional life, which would not have been achieved without the support and assistance of many people.

Firstly, I would like to thank my supervisor, Dr Peter Bencs, for accepting me as a PhD under his supervision, for his great support for the success of scientific research and attendance at various conferences, and for giving me intellectual freedom in my work.

Many thanks to my parents for their moral support and prayers for me. Big thanks to my wife and kids for enduring my absence from them and supporting me in all circumstances.

I would like to thank Mr Peter Bozzay for his help during the experiments, and many thanks to Mohammed Ahmed and Dr Zoltan Nemeth for his help with laboratory work.

Contents

Abstract

In recent years, the energy sector has raised many concerns about the sustainability of energy supplies in future, which constitutes a huge burden on governments worldwide and a great incentive to adopt alternative sources to bridge the shortfall in energy supplies. Renewable energy is considered the most important alternative energy source due to its high potential and reliable performance to compensate for the shortfall in energy supply. Solar energy systems are the most effective and widespread due to their various applications to supply clean electrical and thermal energy without emissions which can cause environmental effects. A hybrid photovoltaic-thermal (PVT) system is an effective solar energy system that simultaneously provides electrical and thermal energy. The mechanism work of the PVT system represents converting solar radiation to electrical energy by Photovoltaic (PV) cells and absorbing the excessive heat of the PV cells to improve their performance and convert it to thermal energy. However, improvements have been made to the PVT system to enhance its performance and maximize its production, but it's still some weaknesses in the methods used to improve performance and system efficiency. Previous studies about improving the efficiency of the PVT system have been reviewed by considering the techniques used. During the depth review of the literature, the gaps found in previous studies have been identified to be addressed during the PhD dissertation by new methods. This PhD dissertation presents a study of using active and passive cooling by new approaches to contribute to improving the PVT system performance. According to thermodynamics laws (the first and second), the energy and exergy of the PVT system have been analyzed to show the quantity and quality of the PVT system's performance.

Passive cooling consists of cotton wicks (CWs) immersed in water as (evaporative cooling). The CW has stacked as one piece attached to the PV module and supplied with water by gravity from top to bottom by the ends of CWs connected in plastic bottles. This cooling approach helped decrease the PV cell's temperature by 22.34%, increase the electrical power by 17.78%, and improve the electrical efficiency to 7.25%. Reducing the PV module temperature contributes to reduced exergy losses and entropy generation by 14% and 14.32%, respectively. The first cooling approach was developed by integrating with aluminium fins to increase the heat dissipation area and enhance the evaporative cooling as a second cooling approach. The new approaches were applied according to hot operation conditions and significantly improved the PV module performance during reduced temperature by 31.20% and increased electrical power by about 23.16 W and electrical efficiency to 8.61%. On another side, the quality of the PV module performance is enhanced by decreasing the exergy losses and entropy generation with achieving appropriate economic feasibility.

The active cooling approaches adopted mono and new hybrid nanofluids as cooling fluids circulated into tubes which a soldered absorber plate attached at the backside of the PV module. Thereby, to prevent the formation of air gaps at the contact region between the backside of the PV module and absorb plate, thermal grease was used; then to reduce the heat convection losses, a new high-performance insulation layer was placed on the tubes. The nanomaterials have been synthesized in different morphologies at the laboratory to avoid the high purchase cost and for more purity of the nanomaterials produced. All manufactured nanomaterials (WO_3, Cuo, TiO_2, Fe_2O_3, TiO_2-CuO and TiO_2-Fe_2O_3) were subjected to different measurements such as crystal structure, morphological and thermophysical properties to investigate their effect on enhancing the thermal performance. The nanofluids have prepared at different volume concentrations

(vol%) and used with the PVT system at different operation conditions, then compared the performance of the PVT system with another previous study to show the effectiveness of the nanofluids used to improve the PVT system performance.

The results indicated that using some mono nanofluids such as Fe_2O_3/ deionized (DI) water has a high performance by reducing the PV cell's temperature by 29.64% and incrementing the electrical power by 76.69%, then incrementing the thermal and electrical efficiency to 12.11%, 43.30% at 0.3 vol% compared with reference PV module. This is attributed to the high thermal properties and surface area of Fe_2O_3 nanorods dispersed in DI water and the configuration of the cooling system. CuO/DI water achieved better performance in the PVT system than in another previous study by reducing the PV cell's temperature by 23.44% and incrementing electrical and thermal energy to 10.31% and 38.9% compared with the reference PV module. The TiO_2 nanofluid was a less performance than the mono nanofluids mentioned above through reduced the PV cells temperature by 14% and incremented the electrical and thermal efficiency to 8.44% and 34.61% compared with the reference PV module, which recorded electrical efficiency that was not excess of 5.3% due to rising their temperature up to 55 ºC.

Improving the nanofluid performance is positively reflected in the PVT system performance; in this dissertation, a new hybrid nanofluid has been applied consisting of TiO_2 nanowires (NWs) loaded on the Fe_2O_3 nanoparticles (NPs) and TiO_2 NWs loaded on CuO NPs which has been dispersed into DI ware at different vol%. Thereby, using a hybrid TiO_2-Fe_2O_3 nanofluid reduced the PV cell's temperature to 37%, then increased the electrical and thermal efficiencies of the PVT system to 12.62% and 48.2% at 0.3 vol%. Then the exergy losses and entropy generation were reduced by 47.3% and 70.47% compared with the reference PV module. In contrast, TiO_2-CuO nanofluid provides a performance no less important than the TiO_2-Fe_2O_3 nanofluid, dispersed 0.3 vol% of TiO_2-CuO nanomaterials help reduce the PV cell temperature by 39.16%, then increment of electrical and thermal efficiency to 12.41% and 45.8%. The exergy losses have been reduced by 37.90% and entropy generation by 69.93%, which is attributed to enhancing the thermophysical properties of hybrid nanofluids reflected by enhancing the PVT system performance. Furthermore, increased volume concentrations of the nanomaterials in DI water directly enhanced the heat transfer coefficient, and the Nusselt number increased with an increased Reynold number.

On another side, increased volume concentrations cause an increase in the density of nanofluids, then a decrease in friction factors and an increased pressure drop. In chapter 7, numerical simulation was conducted on the PVT system to investigate the effect of mono and hybrid nanofluids on the energy and exergy of the PVT system. Experimental results validated the numerical simulation results to confirm the reliability of the simulation results. The simulation results show temperature distribution and heat transfer mechanism between the PVT system components that help to decrease the PV cell temperature. Thereby, improving the thermal parameters of nanofluids has a significant effect by incrementing the energy and exergy efficiencies of the PVT system. The numerical simulation results show logical convergence with experiment results with a deviation not exceeding 4%, confirming the simulation results' reliability. The economic analysis of the passive and active cooling approaches has achieved a good payback period, confirming the feasibility of the cooling approach applied.

Nomenclature

A	Area of the module [m^2]
b	width [m]
Cp	Specific heat [kJ/kg.˚C]
CuO	Copper Oxide
D_{tub}	Tube diameter [m]
D_h	Hydraulic diameter [m]
EVA	Ethylene Vinyl Acetate
f	Friction factor
h	Heat transfer coefficient [$W/m^2 \cdot K$]
g	gravity acceleration [N/kg]
S	Solar radiation [W/m^2]
I_{SC}	Short circuit current
I_{pv}	Current [A]
L	Riser length [m^2]
K	Thermal conductivity [W/m·K]
$\dot{m}$	Mass flow rate [L/min]
n	Number of tubes
Nu	Nusselt number
NWs	Nanowires
PV	Photovoltaic module
P_{pv}	Power [W]
P_{inc}	The percentage improve electrical power [%]
PVF	Polyvinyl fluoride
Q_u	Thermal energy [W]
P_{ref}	Reference power [W]
R	Thermal resistance [°C/W]
R_a	Rayleigh number
Re	Reynold's number
T	Temperature [°C]
U_L	The overall loss coefficient
Voc	Open circuit voltage
V_{pv}	The voltage of the [V]
W	Distance between pipes [m]

Subscript

amb	Ambient
bf	Base fluid
CuO	Copper oxide
DI	Deionized
ele	Etricalecal
FF	Fill factor
Fe_2O_3	Iron oxide nanorods
in	Input
NP	Nanoparticles
nf	Nanofluid
np_s	Nanoparticles
out	Output
PV	Photovoltaic
SEM	Scanning electron microscope
TEM	Transmission Electron Microscopy
TiO_2	Titanium oxide
STC	Stander test condition (25 °C, 1000 W/m^2)
V_{OC}	Open circuit voltage
XRD	X-ray power diffraction
PVT	Photovoltaic-thermal
WO_3	Tungsten trioxide
ZrO_2	Zirconium Oxide
ΔP	Pressure drops [Pa]

Greek symbols

η_{th}	Thermal efficiency [%]
η_{ov}	Overall efficiency [%]
η_{ele}	Electrical efficiency [%]
σ	Boltzmann constant =5.67 × 10^{-8} [W/m^2 K^4]
ε	Emissivity [W/m^2k^4]
η_{el}	Electrical efficiency [%]
ρ	Density [Kg/m^3]
μ	Viscosity [Kg/m·s]
$\dot{E}x$	Exergy [J]
$\eta_{\dot{E}_x}$	Exergy efficiency [%]
$\dot{S}gen$	Entropy generation [W/°C]
φ	Volume concentration [%]
δ	Thickness [mm]

Chapter 1

Introduction

In recent decades, the world has rapidly developed using renewable energy sources, reaching significant usage percentages in several countries, particularly for electricity supply [1]. Energy is the most important requirement of humankind that faces a great challenge in future with the increasing energy demand. Crude oil, natural gas and coal are conventional energy resources representing a significant portion of the energy supply for various industrial, domestic and agricultural sectors [2]. Many factors raise a concern about dependence on conventional sources, such as rapid growth, which increases the requirement exponentially energy demands, and the depletion of conventional energy sources, which may threaten the balance of energy demand in of future. Moreover, the fluctuation of supply costs, the negative influence of political issues between the oil exporting/importing countries and increasing greenhouse gas emissions [3,4]. Modern economies depend on long-term energy availability for future economic growth. The energy sector has manifested significant concerns due to the unavailability of sufficient energy resources and increasing conventional energy demands due to human activities. Although fossil fuels are a significant energy source for power generation, burning fossil fuels increases air pollution and greenhouse gas emissions. Fluctuating fossil fuel prices and significant environmental damages encourage renewable energy sources to be an alternative to conventional energy sources in various applications [5,6]. Sustainable energy source systems are one of the solutions to the mentioned problems that we have faced recently; renewable energy sources are sustainable energy characterized by being reliable, cost-effective, efficient for local usage and environment friendly [7]. Different types of renewable energy systems (i.e., solar energy, wind, biomass, hydroelectric, geothermal energy, ocean) have special advantages for certain applications. Advantages of renewable energy applications include lowering external conventional energy dependence, transformation losses, transmission, reduction of gas emission, etc. [8]. Solar energy is an abundant clean energy source, applicable in various fields and helps reduce environmental impact. The solar energy system converts sunlight into heat or electricity energy, one of the important branches of renewable energy systems and a better alternative to environmental safety; its freely available energy is most sustainable in the future [9].

The solar industry is the best option for future energy due to its availability, accessibility, cost-effectiveness, and efficiency compared to other renewable energies. The solar industry has rapidly developed worldwide due to the increased demand for energy, which became cost-effective because of the aggressive scientific research conducted to develop its performance [10]. Photovoltaic modules (PV) are one of the solar energy systems that convert incident solar radiation into electricity. About 20% of incident solar radiation is converted into electrical energy, and the resting is converted to heat [11]. The PV module consists of semiconductor materials that convert solar radiation (i.e. short-wavelength) to electricity energy [12]. The PV module consists of cells made of silicon; their efficiency depends on the incident solar radiation and the ambient temperature. Increasing the PV cell temperature causes loss of their properties and low conversion efficiency, and then the degradation of the PV module work [13]. The PV module's surface temperature is inversely proportional to the electrical power output of the PV module [14]. The reports indicated that a rise in the PV module temperature by 1 °C decreased the PV module efficiency by 0.45–0.50% [15].

Furthermore, increasing the PV cell temperature leads to drops in the output power, efficiency, durability and lifetime of the PV module affected [16]. Different methods are applied to improve

the efficiency of the PV module by reducing its temperatures. The literature survey in (subsections of chapter 1) covers the main problem and factors that affect the PV module performance and cooling approaches applied to PV modules that help to improve their performance. Thus, highlighting the important designs and cooling methods used to improve the performance of the PV modules to give a future view of the possibilities of cooling methods and identify weaknesses that could be improved to enhance solar systems performance.

1.1 Factors causing failure or damage of the photovoltaic modules

Failure or degradation of PV modules is one of the key factors that should be addressed to reduce this phenomenon, thus increasing its performance and operational lifetime. The PV modules are working outdoors which exposed to different environmental stresses such as sunlight, temperature, moisture, cold, and mechanical loads, which cause degradation or decrease in their performance [17]. Solar radiation is a main environmental factor affecting the PV module's operation. The intensity of solar radiation, incidence angle, and spectral distribution depends on the season, latitude, azimuth angle, time of the day, tilt angle, surface reflection, air pollution and cloud cover [18]. The PV module productivity is proportional to incident solar radiation on the PV module surface; a specific part of incident solar radiation is converted to electrical power and a large part to heat which causes serious problems for PV modules [19]. The PV cells convert solar radiation into electricity. This process causes the heating up of the PV cells and then faster degradation of conversion efficiency [20]. The high solar radiance leads to overheating of the PV cells, thus reducing the conversion efficiency of PV cells and may cause the thermal stress of solar modules [21]. The intensity of solar radiation affects the PV module's short circuit current by the number of photons absorbed by the semiconductor material PV cells are made from [22]. A marginal change by open-circuit voltage with an increase in the intensity of solar radiation, while conversion efficiency is somewhat constant and is reduced with the rising of PV cells [23]. An increase in solar radiation with ambient temperature to a high-level cause reducing the output power of PV modules and a decline in their lifetime [24]. An increase in the ambient temperature causes an increase of PV cells, which leads to a significant decrease in open-circuit voltage when the PV module temperature is above 25 °C with a slight drop by short circuits current, then a reduction in power output. Rising temperature above 45 °C causes degradation of the PV module performance and causes local hotspots when the temperature reaches the extreme range. Therefore, the high irradiance and temperature lead to overheating of the PV module, which may cause a decrease in its performance due to degradation of cell work, a drop in conversion efficiency and then reduce the lifetime of the PV cell [25]. In this subsection, we have focused on the most effective factors on PV module performance, such as the intensity of solar radiation and rising ambient temperature and their effect on the performance of PV modules. The next subsections discuss the methods used to solve the problems of rising PV cells temperature, the type of cooling used and the improvements in applied cooling systems design.

1.2 Hybrid photovoltaic thermal system

Solar energy is abundant energy on earth that is directly used to generate electricity by employing PV modules, including PV cells, made of semiconductor materials (silicon) which convert solar radiation directly into electrical energy in silent operation without emissions [26]. The band gap of thin film silicon allows typical crystalline silicon of PV cells can absorb sunlight in the range of 300–1100 nm [27]. PV cells work on absorbing photons from the sunlight, which are captured by the electron and produced in high electric potential resulting in electric current. Nevertheless, not all photons generate electric current; the photons with high frequencies above threshold frequency produce heat, causing increased PV cell temperature. The rising of the PV cell's temperature above 25-27 °C causes a drop of electrical energy by 0.4-0.65% with a rise of one-degree celsius [28]. An experimental study of the effect of high temperature and solar radiation intensity on the germanium-based PV cells. The results indicated

that the PV cell's conversion efficiency was inversely proportional to the temperature and solar radiation, but the surface of PV cells is recombination with the increase in radiation intensity [29]. A new design of PV cells is germanium-based as the absorber layer to increase the absorption efficiency by using the cross-cone nanostructures to increase microstructure reflection inside the absorber layer. The results show PV cells have high light absorption with a high electrical conversion efficiency of 10.31% [30]. Rising PV cell temperature is an intrinsic problem that leads to a drop in the open-circuit voltage, damaging the PV panel or reducing its productivity [31]. Keeping PV cells close to optimum values of operating conditions is important to avoid hot spots, which significantly drop their efficiency.

Furthermore, increasing the PV cell temperature leads to drops in the output power, efficiency, durability and lifetime of the PV module affected [32]. Different methods are applied to improve the efficiency of the PV module by reducing its temperatures. The hybrid PVT system is one of the most effective solutions to reduce the excess heat of the PV module and use it to produce thermal energy. The PVT system is categorized into two types according to the cooling media used air-based PVT and fluid-based PVT systems. Several experiments and studies have been conducted in developing PVT systems based on air or fluids. In this dissertation, we will examine the PVT system using water and nanofluid-based for cooling the PVT system as active cooling and apply passive cooling to improve the PV module performance. The PVT system consists of a PV module and a heat exchanger attached at the backside of the PV module; air or fluids are used as coolant media. Attaching heat exchanger, which consists of pipes with absorb plate at the backside of the PV module, contributes to reducing the temperature of the PV cells by heat transfer from the backside of the PV module to the absorbing plat then to fluid circulated into pipes by conduction and convection. Figure 1.1 is a cross-section of the PVT system showing the components of the system and the heat transfer mechanism.

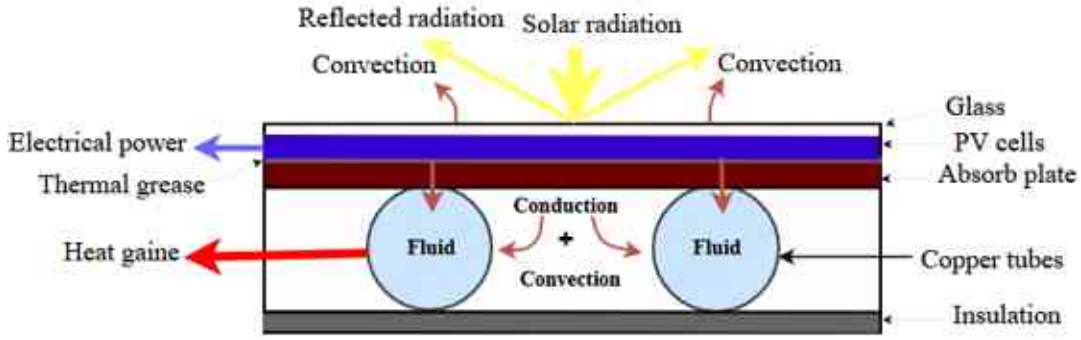

Figure 1.1: A schematic diagram of heat transfer mechanisms between PVT system components

The essential function of the absorbing plate is absorbing the heat of the PV cells from the back of the PV panel and then transferring the heat to copper pipes and the circulating working fluids. The absorber plate is usually made of copper and aluminium. Both materials have high thermal conductivity, are noncorrosive and stable at high temperatures. Different designs have used piping systems to achieve a high level of heat transfer. Aluminium sheets and copper pipes have been arranged as serpentine coils placed at the backside of the PV module. The serpentine coil helps to absorb as much heat as possible from the PV module due to an increase in the time of fluid residence in pipes [33]. Aluminium spiral pipes are a new design for cooling the PV module, which has been used to enhance the PV performance by water as a working fluid [34]. An experimental investigation was conducted using metal-oxide nanofluids to improve the PVT system; the PV module has equipped heat exchanger consisting of a thin copper sheet soldered on serpentine copper tubing [35]. Heat exchanger attached at backside of PV module, which consists of parallel tubes combined with a single pass air heater. The purpose of the cooling system designed is to force the fluid to circulate in the copper tubes and the air in the duct independently to increase the heat dissipation area simultaneously[36]. Figure 1.2 below shows the different heat exchanger designs applied with the PVT system.

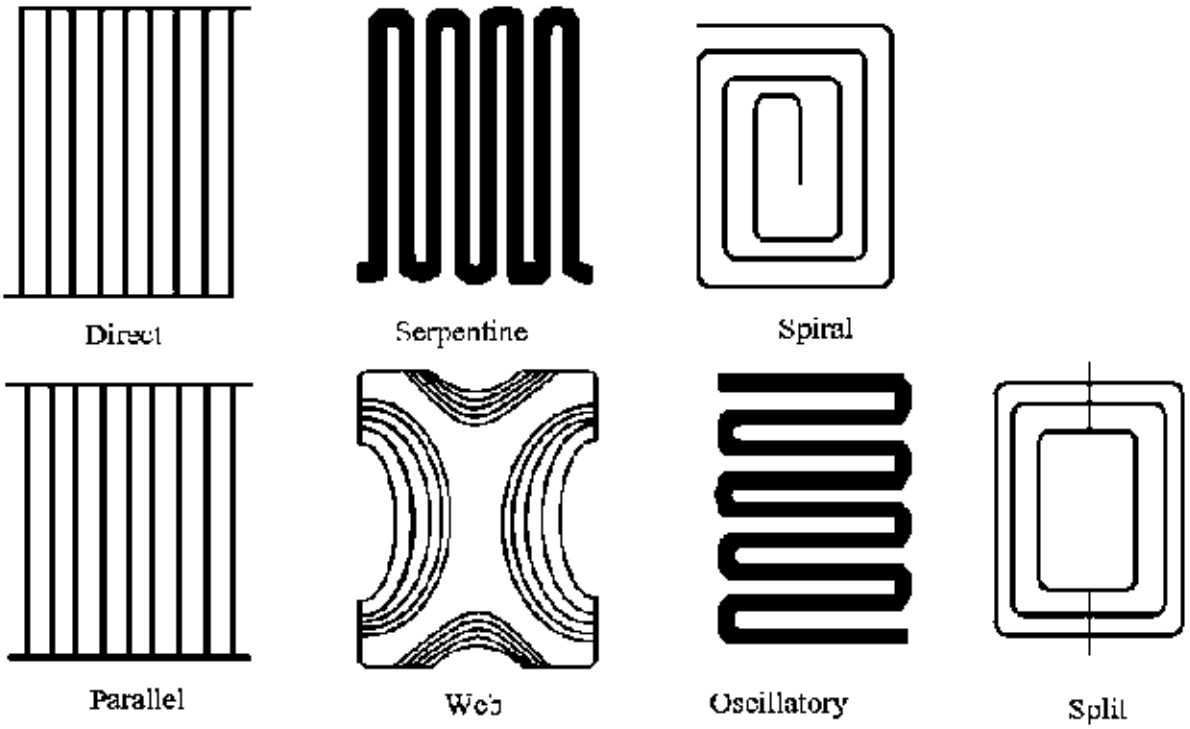

Figure 1.2: Types of heat exchangers used with PVT system

1.3 Cooling systems applied with the photovoltaic thermal system

1.3.1 Passive cooling system

Different cooling techniques help reduce productivity loss and enhance PV module efficiency at high temperatures. Passive cooling techniques are commonly used to maintain PV module performance at high operating temperatures. Passive cooling does not necessarily require external power such pump or fan for cooling the PV module, the opposite of active cooling [10]. In this regard, different passive cooling methods were applied to decrease temperature and enhance the PV module performance. Figure 1.3 shows the progress of PV cooling techniques in the recent decade. A passive cooling technique has been proposed, which consists of Phase Change Material (PCM), including different oils placed in a container designed as a zig-zag geometry to increase the heat transfer surface at the PV module's backside, as shown in Fig. 1.4 Natural water circulating removes heat from the PCM container without any pump system. The technique used enhanced efficiency to 21.19%, 26.88% and 29.24% at solar radiation intensities of 410 W/m^2, 530 W/m^2 and 690 W/m^2, respectively. Mixed PCM with Boehmite nanopowder has better efficiency than the oils used [26]. Another proposed module consisted of cylindrical pin fins with a heat sink; pin fins were arranged uniformly to transmit heat from the PV module to air and enhance the heat exchange with the PV module. A moist wool wood pad was placed at the backside to ensure the touch with the backside surface of the heat sink, and water naturally dropped was used to provide a moist condition for the pad.

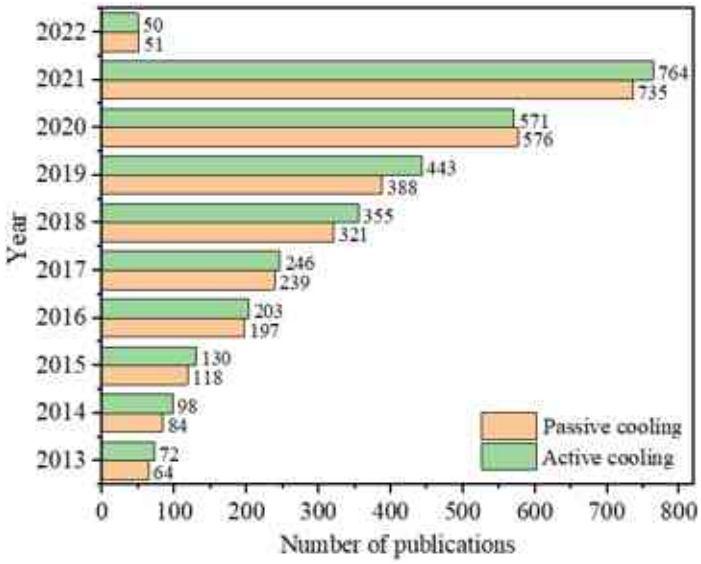

Figure 1.3: Statistics of publications used active and passive cooling of PV modules

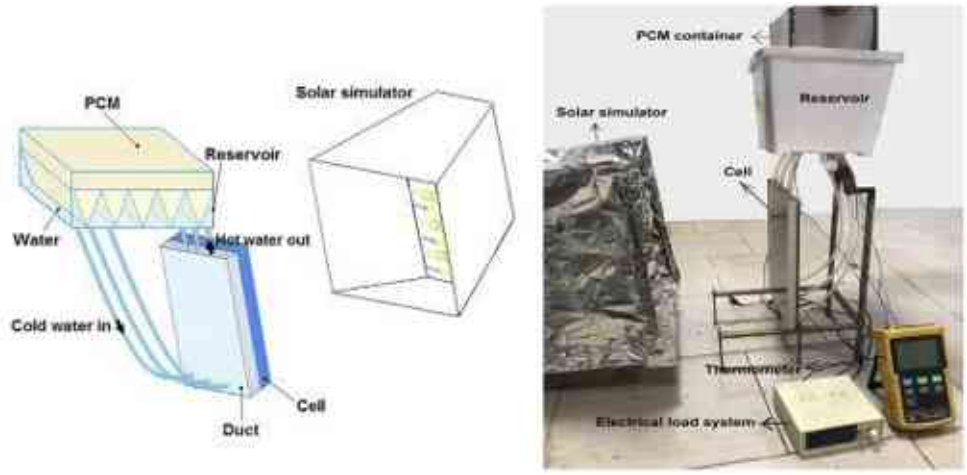

Figure 1.4: The cooling approach applied

The average temperature of the PV module decreased from 61 °C to 45 °C due to the prevailing moist condition at the backside of the PV module, then improving output power by 32.70% and PV efficiency by 31.71%. This cooling technique is characterized by easy maintenance and cost to reduce the PV module degradation [28]. Another method used thin rectangular fins placed longitudinally and integrated on the thin flat metallic sheet attached to the backside of the PV module. Fins helped release heat from the backside of the PV module to air effectively. Thus, the electrical and thermal efficiencies increased by 56.19% and 13.75%, respectively, using four fins under 700 W/m^2 of solar radiation [31]. The Evaporative cooling technique involves a synthetic clay layer covering a perforated copper sheet with a vaporizer and a measuring beaker filled with water used to spray the water on the clay attached at the backside of the PV module, as shown in Fig. 1.5. The evaporating cooling allows the PV module to work at a suitable temperature due to evaporative cooling. The results indicate that this technique improved the performance of the PV module by increasing the voltage by 19.4% and electrical power to 19.10% [37].

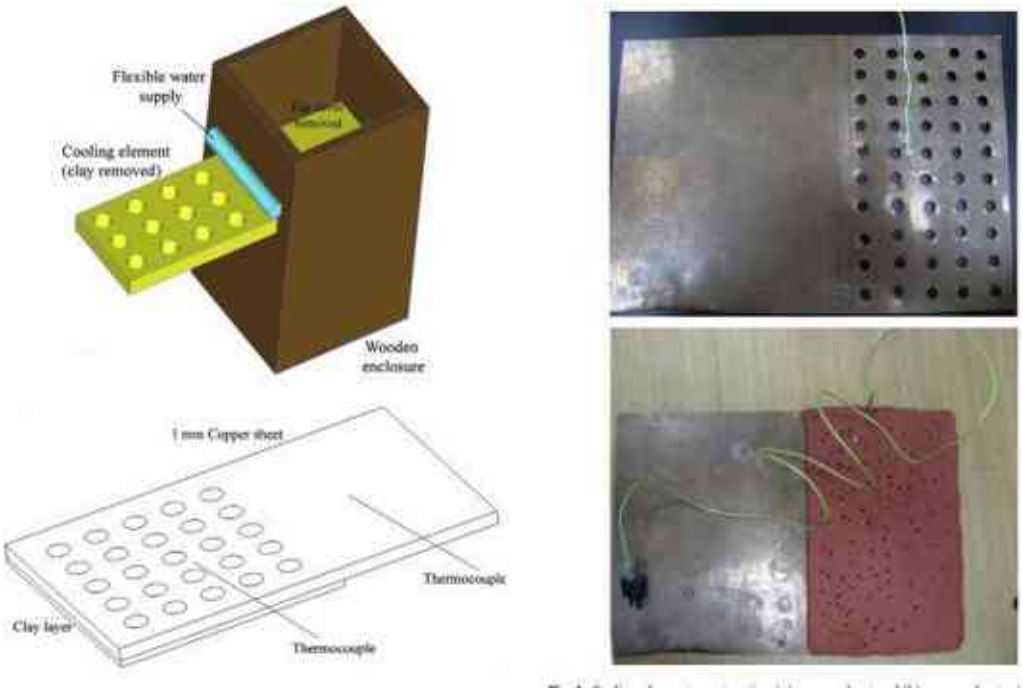

Figure 1.5: Evaporative cooling by synthetic clay layer covering a perforated copper sheet

Chandrasekar et al [38]. Propose fins in conjunction with cotton wicks attached at the backside of PV to control its temperature during operation. The cotton wick was provided with fluid from the bottom to the top of the PV module. The study shows that using fins integrated with cotton wicks increased the electrical yield of PV modules to 14% because of a 12% decrease in the PV module temperature. The use of clay was markedly effective, affordable, and environmentally friendly. Another technique is represented by integrating the desiccant material on the backside of the PV module; at night, when the temperature decreases, desiccants work to adsorb water from the air when the relative humidity is high. During the day, when the temperature increases, water evaporates and takes excess heat from the PV module. The results referred to dropping the PV module's temperature lower than ambient air temperatures that may reduce to 30 °C with evaporative cooling. The yield of PV modules increases by over 10% in sunny conditions [39]. Another configuration representing a stainless-steel tube designed as a serpentine exchanger bonded on a stainless-steel sheet has been placed at the PV module's backside. A two-phase flow of CO_2 passes inside the exchanger by a heat pump system. Decreased solar absorber plate temperature led to an increase in the PV module's electrical power yield. The proposed design helped increase the electrical efficiency from 14.13% to 16% with 1.028 kW of thermal energy, and overall efficiency reached 72.32% [40]. A new trend to restore waste recycling materials in solar systems, aluminium beverage cans filled with paraffin wax have been used to improve the efficiency of PV modules and compare their performance with conventional PV modules simultaneously. Experimental results showed an increment in electrical efficiency from 10.69% to 12.60%, while output power efficiency was from 61.72% and 71.56%, respectively, for PV modules integrated with aluminium beverage cans filled with paraffin wax and conventional [41]. Another passive cooling approach consists of different aluminium and copper fins 5, 10, and 15 attached to the backside of the PV module; Fig. 1.6 shows the fin configuration. Temperature distribution and wind speed vectors were simulating investigated. Passive cooling provided a potential cooling to enhance the performance and decrease the temperature of the PV module. The number of copper fins increased to 15, with a drop in the PV module by 10.2 °C and electrical efficiency by 2.74% [42].

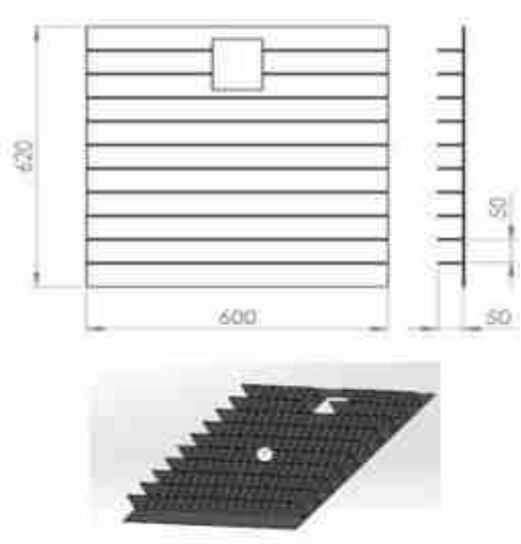

Figure 1.6: Fins configuration attached at the backside of the PV module

The passive cooling approaches applied in the studies above show interesting outcomes and achieve remarkable performance enhancement in the PVT system. However, some important research gaps are still not verified in this domain, such as adopting an evaporative cooling approach more efficiently or hybrid passive cooling. Besides, few studies have investigated the thermodynamic performance of passive cooling, leaving an incomplete thermal view. In his PhD dissertation, two passive cooling approaches are applied, cotton wicks immersed in water and rectangular aluminium fins and cotton wicks combined by fins as a hybrid approach to study their effect on the PV module performance.

1.3.2 Active cooling system

1.3.2.1 Cooling by conventional fluids

Several configurations and cooling fluids have been applied to improve the PV module performance under different conditions. Adopting forced cooling techniques such as circulating fluid into a heat exchanger consisting of tubes and absorb plate attached to the backside of the PV module [43]. The latter method is called a photovoltaic-thermal (PVT) system, which helps to reduce temperature, improve the electrical efficiency of the PV module, and then produce thermal and electrical energy simultaneously [44]. Circulating air or fluids into pipes helps absorb the excessive heat of the backside of the PV module through forced convection due to rising temperature, which improves the electrical efficiency of the PVT system [45]. The dynamic performance of a PVT system has been investigated with direct contact between a simple water box and a mono-crystal PV module. Water was adopted as a coolant to lower the PV module temperature, and it was observed an increment of the maximum thermal energy by 58% with a decrease in the PV module temperature due to heat loss. The electrical efficiency is dropped at noon due to rising solar radiation to the maximum value.
However, the cooling technique has increased the electrical efficiency from 15 to 21.5% compared to the conventional PV module [46]. Water circulation in a dual copper pipeline has been designed for a cooling PVT system tested under solar radiation from (600-1000) W/m^2, the mass flow rate from 2 to 5 L/min, and 26 °C inlet water temperature. The results indicated that the thermal efficiency was enhanced by 59.6% with the increased solar radiation and mass flow rate. Besides, the decreased PV cell temperature has improved the output power and the electrical efficiency by 11.71% compared with the reference module [47]. Another study adopted a water-to-air heat exchanger coupled with a PVT air collector; the heat exchanger consists of pipes with fins linked by the well that contains water at a constant temperature at 5 m depth and works as a geothermal energy source. Thus, the heat exchanger helps transfer energy from and to

the water. The proposed system achieved the required heating and cooling and improved the PV module efficiency to 2% in the winter and 5.1% in the summer. The saved electrical and thermal energies for cooling were 3.14 kWh/day and 24.79 kWh/day [48]. The spiral flow absorber consisting of rectangular hollow tubes made of stainless steel has been proposed as a heat exchanger. The tubes were connected by welding and attached to the backside of the PV module. The performances of PVT were tested under different solar radiation levels and mass flow rates. The results indicated that spiral flow absorbers provide superior performance at solar radiation of 800 W/m^2 and a mass flow rate of 0.041 kg/s. Electrical efficiency was 13.86%, thermal efficiency reached 54.62%, and the overall efficiency of PVT was 68.40% [49].
An investigation used feed water of reverse osmosis for cooling the backside of a PV module, and its effect on the output power and efficiency was studied. The output power generation and the electrical efficiency were improved by 14.17% and 19.80%, respectively, compared to a module without cooling [50]. A numerical study has investigated the impact of cooling system design on the electrical and thermal efficiency of the PVT system by using different tube diameters and lengths, as shown in Fig. 1.7.

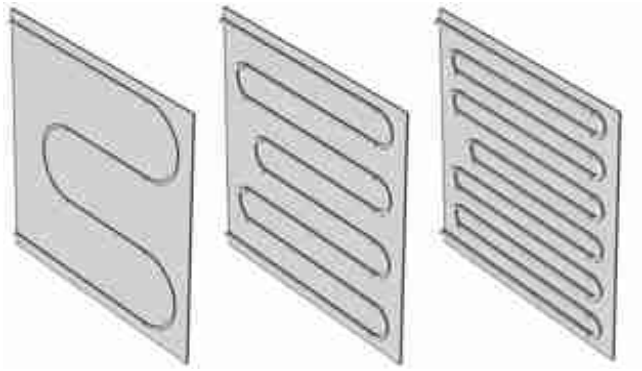

Figure 1.7: Different modes of tube design

The tube's diameters tested were 9.53, 12.70 and 15.88 mm under the flow rate range of 0.5 and 2.5 L/min. The results indicated that the highest electrical efficiency was 14.81% at a tube diameter of 9.53 mm and a flow rate of 2.5 L/min, while the highest thermal efficiency was 79.13%, and overall efficiency was 92% at a used tube diameter of 15.88 mm and 1.5 L/min flow rate. Furthermore, using a 15.88 mm tube diameter and flow rate of 0.68 L/min leads to a lower temperature of the PV module and the increased outlet temperature of the PVT system [51]. Although using water or equivalent base fluids can enhance the performance of the PVT system, this enhancement is still meagre because of the poor thermal conductivity of the conventional fluid (water). The thermophysical properties of the conventional fluid can be enhanced by adding nanoparticles to the fluid, which produces nanofluids with high thermal characteristics.

1.3.2.2 Cooling by nanofluids

In recent years, the use of nanofluids attracted attention because this fluid gives better heat transfer capacity due to its high thermal properties compared to conventional fluids [52]. The literature adopted various nanoparticles at specific volume concentrations, which enhanced the PVT system performance. For instance, an experimental study of the PVT system used a nanofluid of carbon black nanoparticles mixed with water at different concentration ratios from 0-0.4 wt% to control rising PV cell temperature. The results indicated that a 0.21 wt% concentration ratio of nanoparticles in water lowered the surface temperature and increased the output power by 7% compared with pure water [53]. An investigation was conducted on the effect of used Ag/water nanofluid on the energy and exergy efficiencies of the PVT system under different flow regimes and nanoparticle concentrations. The results showed a significant enhancement of energy and exergy efficiencies of the PVT system, which was attributed to

increased nanofluid concentration and flow rate close to turbulent flow. Thus, using 4 wt% nanofluids increased output power by 35% and 10%, and the exergy efficiency increased by 50% and 30% compared with water cooling and without cooling [54]. The performance of the unglazed PVT system was evaluated using water and CuO nanofluid circulated by the cooling system consisting of sheets and tubes placed at the backside of the PV module. The temperature of the PVT system dropped to 15 °C and 23.7 °C with the used water and nanofluid compared with the PV module without cooling, which reached 68.4 °C. The PV cell temperature reduction increases the average electrical efficiency to 35.67% with nanofluid and 12.98% with water, while without cooling is 12.32%. The overall efficiency of the PVT system with nanofluid was higher by 21% than the water-cooled due to the high heat absorption by CuO nanoparticles [55]. A new geometry of the PVT system has been studied with Al_2O_3/H_2O nanofluid applied with a concentration of (0.05–0.5 wt.%) as a coolant working fluid to evaluate their effect on the performance of the PVT system. The cooling system attached at the backside of the PV module consists of the serpentine half-pipe; the PV cells are assembled on an aluminium plate of a 3 mm thickness, with removes the Tedlar to increase the heat transfer in the cooling section, as shown in Fig. 1.8. The results show a remarkable increment of the PVT efficiency, especially at cooling by nanofluid with a concentration of 0.5 wt.% of nanoparticles into pure water. The thermal and electrical efficiency was enhanced by 126.71%, 7.38% compared with pure water, and the overall efficiency of the PVT system is 93.73%, which confirms the feasibility of nanofluids as a better coolant than water [25]. Experimental investigations were conducted on the performance of the PVT system using two types of nanofluids, Cu/water and TiO_2/ water, at the variation of mass flow rate.

The experimental outcomes show enhancing of the PVT electrical efficiency to 5.98% at a 1% volume concentration of Cu/water nanofluid, and at a higher mass flow rate, the temperature of the PV module is reduced to 17.18 °C. Thereby enhancing the electric and thermal efficiency of the PVT system by 2.58% and 5.43%, respectively [56]. Energy and exergy evaluation of the PVT system was conducted using ZnO, TiO_2 and Al_2O_3 nanoparticles dispersed in DI water as coolant fluids at a mass flow rate of 30 kg/h. Based on the data measured, the TiO_2 and ZnO nanofluids gave better energy and exergy efficiencies than Al_2O_3 nanofluids. The overall exergy efficiencies of the PVT were enhanced by 15.45% ZnO/water, 15.93% TiO_2/water, and 18.27% Al_2O_3/water compared with water cooling, which recorded 12.34%. Al_2O_3/water has a better enhancement of entropy generation [35]. A numerical analysis of the PVT system using MgO/water nanofluid that circulated into copper tubes attached at the backside of the PV module, the volume concentration of nanoparticles was 0 and 1% in the base fluid and the volume flow rate from 0.5-4 L/min. The results indicated that it enhances the exergy output by lowering nanofluid flow rates while increasing the flow rate above 0.5 L/min causes reduces the efficiency.

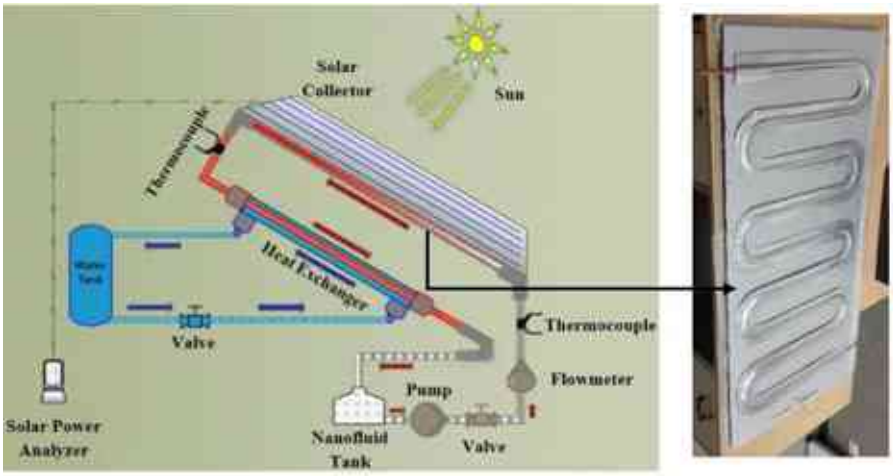

Fig 1.8: The schematic diagram of the experimental with serpentine half-pipe

The exergy efficiency increased by 0.45% by adding 1% volume concentration nanoparticles and 0.5 L/min volume flow rate [57]. A study has proposed using Al_2O_3/water and Cu/water nanofluids as a coolant and the effect of the diameter and number of pipes used on the performance of the PVT system. The results show that using Cu/water nanofluids gives better performance to the PVT system than using Al_2O_3/water nanofluids. The electrical and thermal efficiencies had improved by 4.98% and 5.23%, respectively, by Cu/water nanofluid. The performance of the PVT system was significantly enhanced by increasing the number of tubes with no substantial effect on the diameter of the pipes [58]. Multi-Wall Carbon Nanotubes (MWCNT)/water nanofluid has been used as a coolant to evaluate the PVT system performance at different volume concentrations (0-0.3%) and a constant mass flow rate of 1.2 L/min. Adding MWCNT nanoparticles to water enhanced the thermal properties, which are positively reflected by the electrical and thermal efficiency generated by the system. The temperature of the PV module was reduced by 12 ºC at maximum incident radiation and achieved a maximum overall efficiency of 83.26% [59]. Graphene nanofluid has been proposed as a coolant media to enhance the efficiency of a PVT system at different volume concentrations along with a surfactant (sodium deoxycholate). The results indicated a reduction in the PV module temperature by 20 ºC with an increase in the volume concentration to 0.3 vol% at a mass flow rate of 0.085 kg/s. Then the energy efficiency of the PVT system and PV module was improved by 13% and 23%, respectively [60].

1.4 Objectives of the dissertation

In the literature, it can observe that all the methods and techniques used to improve the performance of the PVT systems are similar. It lacks a comprehensive analysis of quantitative and qualitative performance because it relies on quantitative analysis based on the first law of thermodynamics. In addition to qualitative analysis, it lacks comprehensive analysis, such as exergy losses and entropy generation. Regarding passive cooling in most techniques, I found that some technologies have achieved good results, but without mentioning their reliability in different operating conditions, economic feasibility, and scope of application.

On the other hand, we found that active cooling techniques have occupied a wide range of applications due to their interesting outcomes and durability in simultaneously improving electrical and thermal performance. Nevertheless, limited improvements were made to improve its performance, such as the design of the heat exchanger attached to the back side of the solar panel, the type of coolant used, or the use of integrated cooling methods.

This PhD dissertation addresses the uncompleted gaps in the literature that contributes to improving the general performance of the PVT system by adopting reliable technologies that contribute to improving PVT system performance, such as:

- Comprehensive thermal analysis of the system included energy and exergy analysis, thermal parameters such as Reynolds number, Nusselt Number, fraction factor, pressure drop and heat transfer mechanism with identifying the cooling fluids (Chapter 2).
- Predictive study of the thermal and electrical behaviour of the PV module under different operating conditions and the factors affecting their output, which in turn determine the effective ways to improve performance (Chapter 3).
- Investigation of the effect of thermal parameters of using nanofluids as a cooling fluid at various flow rates and temperatures by using the boiler system to ensure effective of nanofluids under different conditions (Chapter 4).
- Regarding passive cooling, in this PhD dissertation, cotton wicks immersed in water which arranged and stacked as one layer, then attached to the backside of the PV module as a first phase. The rectangular aluminium fins integrated with cotton wicks are used as a second phase to enhance evaporative cooling. These cooling techniques help increase the

evaporating cooling that positively reflects on the PV module performance, and these techniques have been applied according to Iraq conditions (Chapter 5).

- Active cooling is a common cooling technique in most PVT system applications which adopt fluids as a cooling technique. Nowadays, nanofluid is one of the effective cooling fluids used in the PVT system; in this dissertation, new nanofluids have been used (mono and hybrid) nanofluids at different volume concentrations and according to Hungary and Iraq conditions (Chapter 6).
- Numerical investigation of the PVT system's energy and exergy and validation is an important issue that most considers demonstrating the reliability and feasibility of the system and the accuracy of the results by comparing them with the practical results. In this case, numerical simulation was conducted for the PVT system using nanofluid according to Iraq and Hungary conditions and then compared the numerical results by experimental results to determine the deviation of the simulation results (Chapter 7).
- Chapter 8 reviews the important new scientific results of this dissertation.

Chapter 2

Methodology

2.1 Thermal analysis of heat transfer between the photovoltaic thermal system components

The efficiency of the PVT collector requires several factors that must be considered to achieve outstanding performance and stability of the PVT collector, such as solar radiation, ambient temperature, and wind speed. All the factors that have been mentioned affect the PVT collector performance. On the other hand, designed PVT collectors play an intrinsic role in their efficiency, such as absorber area, reduced heat loss, and collector tilt angle. The function of the heat exchanger, which represents the second part of the PVT collector fixed at the backside integrated with the PV, is to transform solar radiation by an absorber (copper plate) to thermal energy as a hot fluid and that depends on the input and output parameters that effect on the efficiency of the PVT collector. The input parameters include the form of design of the PVT collector (collector size, incidence angle, collector tilt angle, etc.), climatic conditions (ambient temperature, solar radiation, wind speed), and operation (nanofluid inlet temperature and the mass flow rate through the collector). While overall efficiency, nanofluid outlet temperature, power production, and quantity of useful heat gain are the output parameters. The mathematical model describes the temperature that transfers across the different components of the PVT system. Therefore, it derived the heat balance transfer across different system components, arranging all the tubes in a parallel fashion, and the space between them is fixed. It is considering that fluid flow rate and temperature are the same in all tubes. Assumptions that all the components' material properties are constant, the edge losses are neglected, calculation of all the heat transfer coefficients in real-time and the fluid flow rate in all tubes are the same. To mathematical modelling of the PVT collector, it writes the energy equation for all the different components of the system with the assumption that in one-dimensional energy balance analysis, the heat transfer is one-dimensional and steady.

In a steady state, the useful output energy of a collector of the area is the absorbed solar energy subtracted from the thermal loss. The absorbed solar radiation per unit area of the collector equals the variation amount between the solar radiation and the optical losses. The concept of an overall loss coefficient is important for the calculation, where the absorbed energy (solar radiation) is distributed to thermal losses through the top and bottom and to useful energy gain; Fig 2.1 shows the heat transfer coefficient mechanism between the PVT system layers. The solar radiation incident on the PV cells with heating the PV cell. The absorber plate that attaches to the PV panel's backside will absorb the heat by conduction and transfer it to the pipes' region [61]. The temperature midway between the pipes will be higher than in the vicinity of the pipe. Because of the pipes' presence and weld metal, the temperature above the pipes will be nearly uniform. The heat energy is transferred to the fluid to heat the fluid, which causes a temperature gradient to exist in the flow direction. Thus, at any region of the PVT collector, the general temperature level is governed by the fluid's local temperature Eq. (2.1) [62] represents the convection heat transfer coefficient between solar radiation and the glass cover of the PV collector.

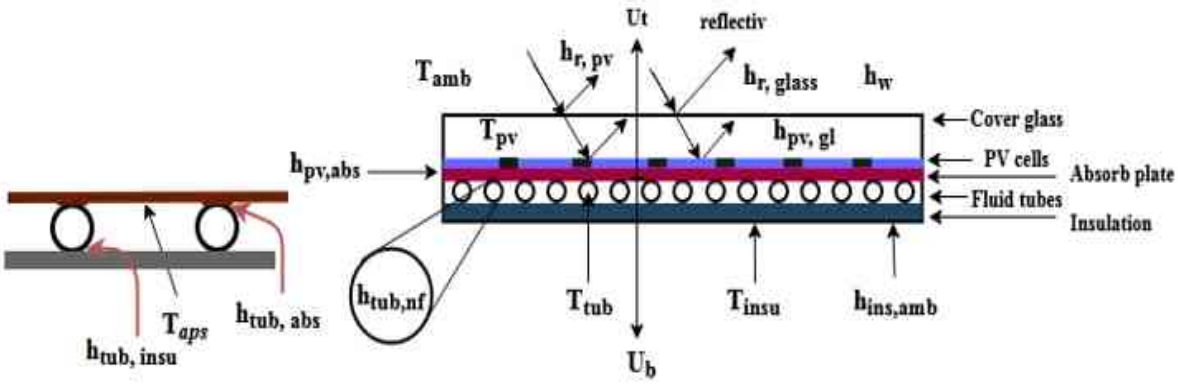

Figure 2.1: Heat transfer coefficient between PVT collector layers

$$h_{r,gl} = \sigma\varepsilon\left(T_s + T_{gl}\right)\left(T_s^2 + T_{gl}^2\right)\left(T_{gl} - T_s\right) \tag{2.1}$$

The sky temperature T_S, is calculated by the equation below, T_{gl} is the glass cover temperature.

$$T_s = 0.0522 * T_{amb}^{1.5} \tag{2.2}$$

The convection heat transfer coefficient between the glass cover and PV cells represents in Eq (2.3) [61].

$$h_{gl,pv} = \frac{k}{L_{gl}} \cdot \left(1 + 1.44\left[1 - \frac{1708(sin\,(1.8\beta))^{1.6}}{R_a\,cos\,(\beta)}\right]\left[1 - \frac{1708}{R_a\,cos\,(\beta)}\right] + \left[\left(\frac{Racos.\,\beta}{5830}\right)^{\frac{1}{3}} - 1\right]\right) \tag{2.3}$$

$$R_a = \frac{g(T_{pv} - T_{gl})L^3}{T_m \nu\alpha} \tag{2.4}$$

$$T_m = \frac{T_{pV} + T_{gl}}{2} \tag{2.5}$$

$T_{amb}$is the ambient temperature, K is the thermal conductivity of the glass, L_{gl} is the distance between the PV cells and cover glass, β is the collector title angle and R_a is Rayleigh number which calculates from Eq (2.4). Thermal diffusivity (α), kinematic viscosity(ν), g is the gravitational constant and T_{PV} The temperature of PV cells. The convection heat transfer coefficient between solar radiation PV cells is given in Eq (2.6) [62].

$$h_{r,pv} = \frac{\sigma\left(T_{pv}^4 - T_{gl}^4\right)}{\frac{1}{\varepsilon_{pv}} + \frac{1}{\varepsilon_{gl}} - 1} \tag{2.6}$$

Where σ is the Stefan-Boltzmann constant = 5.67 × 10^{-8} W/m^2 K^4, ε_{pv}, ε_{gl} are the PV and glass emissivity. The collector overall loss coefficient U_L is the sum of the top, bottom, and edge loss coefficients; Fig. 2.2 shows the thermal resistance to heat flow, and Table 2.1 shows the formulas used to calculate the thermal resistances $R_3 = \frac{k_{abs}}{L_{abs}}$

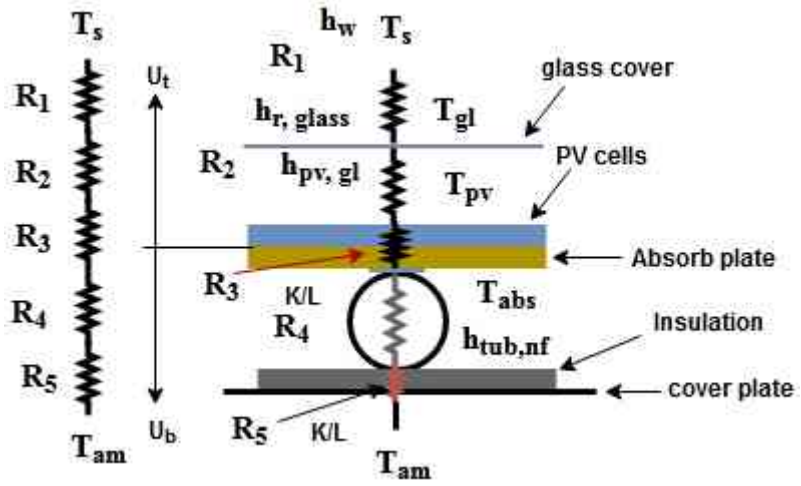

Figure 2.2: Thermal resistance between PVT collector layers

Table 2.1: Thermal resistance formulas [61]

Formula	Thermal resistance
$R_1 = \frac{1}{h_w + h_{r,gl}}$	The thermal resistance between the surroundings and the glass cover
$R_2 = \frac{1}{h_{gl,pv} + h_{r,gl}}$	The thermal resistance between the glass cover and PV cells
$U_t = \frac{1}{R_1 + R_2}$	The total heat transfer coefficient top loss from the PVT system to the ambient
$R_3 = \frac{k_{abs}}{L_{abs}}$	The thermal resistance to heat flow through the absorbing plate
$R_4 = h_{\text{tub, nf}}$	The resistance of the convection heat transfer coefficient between the tube and nanofluid
$R_5 = \frac{k_{insu}}{L_{insu}}$	The resistance to heat flow through the insulation
$U_b = \frac{1}{R_3 + R_4 + R_5}$	The heat loss through the bottom of the PVT system
$U_L = U_t + U_b$	The overall loss coefficient

The heat loss from cover glass exposed to outside winds is important in calculating and by the used formula (2.7)[61].

$$q_{loss,top} = h_{gl,pv} + h_{r,pv}\left(T_{pv} - T_{gl}\right) \tag{2.7}$$

In a steady state, the useful output energy of the PVT collector is given by the equation below.

$$Q_u = A_c\left[S - U_L\left(T_{pv} - T_{amb}\right)\right] \tag{2.8}$$

where S is solar radiation W/m^2, and A_c is collector area.

$$h_{wind} = 3u_a + 2.8 \tag{2.9}$$

where h_{wind} is the convection heat transfer coefficient (W/m^2 K) between PV laminate and ambient air, u_a is the wind velocity [59]. The conduction heat transfer coefficient between the PV cells and the absorber plate $h_{pv,abs}$ that can calculate using the following Eq. (2.10)

$$h_{pv,abs} = \frac{k_{ad}}{\delta_{ad}} \tag{2.10}$$

where δ_{ad} and k_{ad} are thickness and the thermal conductivity of the adhesive. The conductive heat transfer coefficient between the absorber plate and the tube $h_{abs,tub}$, h_{abs} that expressed by Eq. (2.11) [63],

$$h_{abs,\ tub} = \frac{2k_{abs}}{\frac{(W-D_o)}{4}} \tag{2.11}$$

where k_{abs} is the thermal conductivity of the absorber copper plate= 398 W/m·k, W is the tube spacing = 5 cm, D_o is the outer diameter of the pipe = 0.095 cm. The convection heat transfer coefficient between the tube and nanofluid $h_{tub,nf}$ that estimated by using the following correlation (2.12) [62].

$$h_{tub,\ nf} = \frac{Nu_{nf}k_{nf}}{D_{tub}} \tag{2.12}$$

where Nu_{nf} is Nusselt number of nanofluid, k_{nf} is the thermal conductivity of the nanofluid, D_{tub} is the tube diameter. To calculate the conductive heat transfer coefficient between two layers neighboring the tube and the insulation, it uses the correlation (2.13) [64].

$$h_{\text{tub},insu} = \frac{1}{\frac{\delta_{tub}}{k_{tub}}+\frac{\delta_{insu}}{k_{insu}}} \tag{2.13}$$

where δ_{tub} is the thickness of the tube, k_{tub} is the thermal conductivity of the tube. δ_{ins} is the thickness of the insulation, $k_{ins}$is the thermal conductivity of the insulation. To calculate the conductive heat transfer coefficient between the insulation back cover, it uses the correlation (2.14) [64].

$$h_{insu,bcov} = \frac{1}{\frac{\delta_{insu}}{k_{insu}}+\frac{\delta_{b,cov}}{k_{b,cov}}} \tag{2.14}$$

where $\delta_{b,cov}$ is the thickness of the back cover, k_{cov} is the thermal conductivity of the back cover. The amount of heat transferred to the nanofluid can determine by Eq. (2.15) [65].

$$q'_u = WF'\left[S - U_L\left(T_{nf} - T_a\right)\right] \tag{2.15}$$

where T_{nf}, F' is the collector efficiency factor, which calculates from Eq. (2.16) [65], and W is the distance between center pipes, as shown in Fig. 2.3.

$$F' = \frac{1/U_L}{W\left[\frac{1}{U_L[D+(W-D)F]}+\frac{1}{C_b}+\frac{1}{\pi D_i h_{tub,nf}}\right]} \tag{2.16}$$

Adhesive k_b, the average adhesive thickness γ, and the adhesive width b, D is the tube diameter and D_i is the inside diameter of the tube and $h_{tube,nf}$ is the convection heat transfer coefficient between the tube and nanofluid.

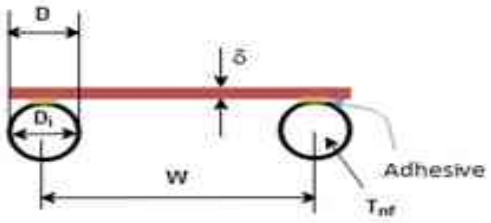

Figure 2.3: Contacting between absorbing plate and pipes

$$C_b = \frac{k_b b}{\gamma} \tag{2.17}$$

The fin efficiency factor F [61].

$$F = \frac{tanh\,[m(W-D)/2]}{m(W-D)/2} \tag{2.18}$$

$$m = \sqrt{\frac{U_L}{k\delta}} \tag{2.19}$$

2.2 Energy balance equations for the photovoltaic thermal system

The mathematical model of the hybrid PVT system involves two parts; the first part is related to calculating the overall efficiency of the PVT system (thermal and electrical efficiency of the PVT system). The second part is related to the properties of nanofluids and the governing equations for the thermo-physical properties of nanofluids. Evaluating the performance of the PV/T system is important to recognize the behaviour components of the system, considering the equations that are governed by the behaviour of the PV/T system. The PVT panel consists of five parts, as shown in Fig. 2.4, cover glass, PV cells, absorb plate, copper pipes, insulation, and the outer cover. A mathematical equation governs each part. Different types of working fluid are used with PVT systems considering thermo-physical proprieties that enhance the system's efficiency. Several assumptions are adapted to writing the heat balance mathematical equation of the PVT panel. We have adopted the heat balance mathematical equation similar to that used [66], as shown below. Solar radiation is the uniform distribution on the photovoltaic panel surface with constant thermal conductivity, particularly for solid materials.

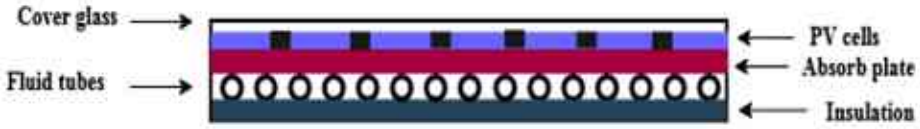

Figure 2.4: Component of PVT collector

The temperature distribution is uniform for each solid material in the PVT system thermodynamic equilibrium with steady-state conditions and the computational domain element. The nanofluid inlet temperature differs from the outlet temperature as a linear variation, with negligible kinetic and gravitational energy balances.

$$\rho_g \delta_{gl} C_{p,gl} \frac{dT_{gl}}{dt} = \alpha_{gl} S + h_{r,gl}\left(T_{sky} - T_{gl}\right) + h_w\left(T_{amb} - T_{gl}\right) + h_{pv,gl}\left(T_{pv} - T_{gl}\right) \tag{2.20}$$

The left side of the equation represents the temporal energy changes in the glass covers. The first item on the right-hand side is the received irradiation by the glass cover; the second item is the irradiative heat transfer between the glass cover and the surroundings. The third item is the convective heat transfer between the glass cover and the outside environment, and the fourth item is the conductive heat transfer from the photovoltaic cells to the glass cover. The rate of absorbed solar radiation by photovoltaic minus the entire heat transfer from the photovoltaic to absorb plate represents the PV module thermal balance [67]. Considering both convection and radiation heat exchange in the environment, as shown in Eqs. (2.21, 2.22).

$$\rho_{pv} \delta_{pv} C_{p.pv} \frac{dT_{pv}}{dt} = \alpha_{pv} \tau_g S - E_{\text{elec}} + h_{pv,gl}\left(T_{gl} - T_{pv}\right) + h_{\,pv,abs}\left(T_{abs} - T_{pv}\right) \tag{2.21}$$

$$E = SP\eta_{el} \tag{2.22}$$

where *S* is the solar radiation, α_{pv} is absorptivity of the PV cells and ρ_{pv} represent the density of the PV cells. while $C_{p,pv}$ is the specific heat of the PV cells. *E, P* and η_{el} are the power of the PV module, the packing factor, and the electrical efficiency. $h_{pv,abs}$ is The conduction heat transfer coefficient between the PV laminate and the absorber plate and T_{abs} is absorber plate temperature. By the internal energy change of the plate, we can calculate the thermal balance of the absorber plate, where the heat transfer from the photovoltaic to the absorber plate minus the

entire heat transfer from the plate absorber to the tube with considering the heat transfer from the absorber plate to the insulation, which is evaluated by the Eq. (2.23) [67].

$$\rho_{abs}\,\delta_{abs}C_{p,abs}\frac{dT_{abs}}{dt} = h_{pv,abs}A_{pv,abs}\left(T_{pv}-T_{abs}\right) - h_{abs,tub}A_{abs,tub}(T_{abs}-T_{tub}) - h_{abs,insu}A_{abs,insu}\left(T_{pv}-T_{insu}\right) \quad (2.23)$$

where T_{ins} is the insulation temperature**,** ρ_{abs} is the density of the absorber plate**,** δ_{abs} is the thickness of the absorbing plate and $C_{p,abs}$ is the specific heat of the absorber plate. The conductive heat transfer coefficients between the absorber and the insulation. The sum of the conduction heat transfer from the tube to the insulation and the convection heat transfer from the tube to the nanofluid minus heat transfer from the absorber plate to the tube represents the thermal balance of the tube is evaluated by Eq. (2.24) [67].

$$\rho_{tub}\,\delta_{tub}C_{p,tub}\frac{dT_{tub}}{dt} = h_{abs,tub}A_{bt}(T_{abs}-T_{tub}) - A_{tub,f}h_{tub,nf}\left(T_{tub}-T_{f}\right) - A_{tub,insu}h_{tub,insu}(T_{tub}-T_{isu}) \quad (2.24)$$

where T_f, ρ_{tub} are the circulating working fluid temperature, the density of the tube, δ_{tub} tube thickness and $C_{p,tub}$ is the specific heat of the tube. The energy balance equation of working fluid is evaluated by Eq. (2.25) below.

$$m_{nf}C_{P,nf}\frac{dT_{nf}}{dt} = \dot{m}_{nf}C_{nf}(T_{out}-T_{in}) + A_{tub,nf}h_{tub,nf}\left(T_{tub}-T_{nf}\right) \quad (2.25)$$

where $\dot{m}_{nf}$ is the fluid mass flow rate, T_{in} is the inlet temperatures and T_{out} is the outlet temperature of the fluid [68]. The energy balance for insulation is the sum of the conduction heat transfer from the tube to the insulation added to the heat transfer from the plate absorber to the insulation, which is evaluated by Eq. (2.26) [67].

$$\rho_{insu}\,\delta_{insu}C_{p,insu}\frac{dT_{i}}{dt} = h_{abs,insu}A_{abs,insu}(T_{abs}-T_{insu}) + A_{tub,insu}h_{tub,insu}(T_{tub}-T_{insu}) + h_{insu,a}\,A_{insua}(T_{insu}-T_{amb}) \quad (2.26)$$

where ρ_{ins} is the density of the insulation material δ_{insu} insulation thickness and $C_{p,ins}$ is the specific heat of the insulation material. $h_{ins,amb}$ represents the convective heat transfer coefficient between the insulation and the ambient air. The convection heat transfer coefficient between the outer aluminium cover plate of the collector and the ambient, $h_{cov,amb}$ can calculate with the Mc-Adams equation below and depending on the wind velocity [69].

2.3 Energy and exergy assessment of photovoltaic thermal system

In this section, the energy and exergy analysis depend on the first and second laws of thermodynamics. The first law asses the energy quantity, while the second law asses the exergy quality of the system [53]. The PVT system produces electricity and thermal energy simultaneously; thereby, the energy analysis of the PVT system is divided into two parts: electrical and thermal performance. The electrical efficiency (η_{ele}) is a measure of the electrical energy performance of the PVT system, which can be calculated from the Eq. (2.27) [70].

$$\eta_{ele} = \frac{P_{pv}\times FF}{S\times A} \quad (2.27)$$

$P_{pv}$is the power of the PV module, which is calculated by Eq. (2.28) [71], $V_{pv}$is the voltage, I_{pv} is the current, and (A) PVT module area. The fill factor (FF) represents the maximum power conversion efficiency of the PV module, which can be calculated from the Eq. (2.29) [38].

$$P_{pv} = V_{pv} \times I_{pv} \tag{2.28}$$

$$\text{FF} = \frac{V_{pv} \times I_{pv}}{V_{oc} \times I_{sc}} \tag{2.29}$$

The effect of using nanofluid as a cooling fluid on the electrical power of the PV module can be noticed by the percentage increment (P_{inc}) of the electrical power Eq. (2.30) [59]:

$$\%P_{inc} = \frac{P_{cooled} - P_{fef}}{P_{ref}} \times 100 \tag{2.30}$$

Thermocouples are placed on the PV module, PVT system surfaces and backsides for measuring the temperature; thus, Eq. (2.31) is used to measure the average temperature of the PV module and PVT system.

$$T_{avg} = \frac{\text{T}_{surface} + \text{T}_{back}}{2} \tag{2.31}$$

The thermal efficiency (η_{th}) indicates the thermal performance of the PVT system. The thermal efficiency calculation of the PVT collector depends on the rate of useful thermal energy Q_u [72], which is calculated using Eq. (2.32) below.

$$Q_u = \dot{m} C_p \times (T_{out} - T_{in}) \tag{2.32}$$

$$\eta_{th} = \frac{Q_u}{S \times A} \tag{2.33}$$

where T_{out} , T_{in} are the input and output fluids (˚C), $\dot{m}$ is the mass flow rate kg/s, and C_p is the specific heat of the fluid (kJ/kg.˚C). The overall efficiency of the PVT system is the collection of the electrical and thermal efficiencies, as presented in Eq. (2.34) [73]:

$$\eta_{ov} = \eta_{ele} + \eta_{th} \tag{2.34}$$

In this dissertation, the nanofluids and DI water are circulated in the serpentine tubes placed at the backside of the PVT system. Thermophysical characteristics of the fluid affect the heat transfer properties and fluid flow velocity. Reynolds number is a parameter for predicting the fluid flow patterns, whether laminar or turbulent flow, which can be calculated from Eq. (2.35) below [74].

$$Re_{nf} = \frac{4\dot{m}}{\pi \mu_f D_{tub}} \tag{2.35}$$

where D_{tub} and μ_f are the tube diameter and the viscosity of the fluid, respectively. Nusselt number represents the ratio of heat transfer by convection to the conductive heat transfer, which can be determined by Eq (2.36) [75, 71].

$$Nu_f = \left(\frac{h\, D_h}{K_{nf}}\right) = \frac{\dot{m}\, C_p (T_{h,i} - T_{h,o})}{A\,(T - T_w)} \times \frac{D_h}{K_f} \tag{2.36}$$

where h, D_h, T *and* T_w *are* the heat transfer coefficient, the hydraulic diameter, the average inlet and outlet temperature and the average wall tube temperature, respectively. In addition, the friction factor is introduced as one of the causes of the pressure drop at the change of Reynold's number, which was calculated by Eq. (2.37) [77], while the pressure drop in the piping system is calculated by Eq. (2.38) [78].

$$f = [1.58 \ln\, Re - 3.82]^{-2} \tag{2.37}$$

$$\Delta P = \frac{f \rho_f L}{2 D_{\text{tubes}}} \left(\frac{4 \frac{\dot{m}_{nf}}{n}}{\rho_f \pi D^2} \right)^2 \tag{2.38}$$

Where n and L are the number of tubes and the riser length of tubes.

The second law of thermodynamics is used for exergy analysis to determine the realistic performance of the PVT systems and evaluate the quality of their electrical and thermal exergy. The change in temperature level destroys the exergy due to increasing the system's entropy compared to the surroundings [79]. Figure 2.5 shows the energy flow of the PVT system considering the PV module unit and the cooling system (absorbing plate and serpentine tube) as a united control volume assuming a steady state condition. The exergy balance equations for the PVT system are written as indicated in Eq. (2.39) [35]:

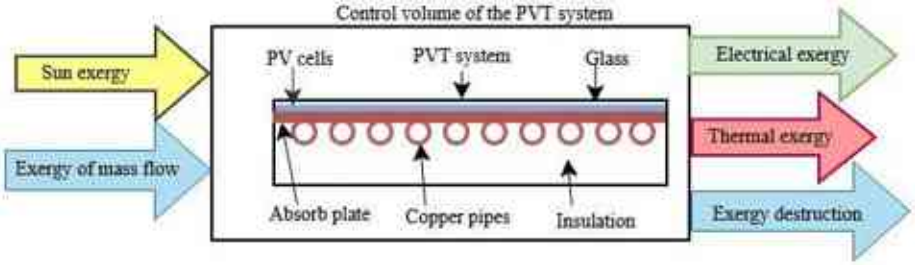

Figure 2.5: Schematic diagram of the Energy flow of a PVT system

$$\sum \dot{E}x_{\text{in}} = \sum \dot{E}x_{\text{out}} + \sum \dot{E}x_{\text{loss}} \Rightarrow \dot{E}x_{\text{solar}} + \dot{E}x_{\text{fluid, in}} = \dot{E}x_{\text{electrical}} + \dot{E}x_{\text{fluid, out}} + \dot{E}x_{\text{losses}} \quad (2.39)$$

$\dot{E}x_{\text{solar}}$, is the input exergy of the solar radiation to the PVT system, which can calculate by Eq. (2.40), [80]. T_{amb} is ambient temperature and T_{sun} sun temperature which considered as (5800 K) [81]. $\dot{E}x_{\text{electrical}}$ is the electrical exergy equivalent to the electrical energy, which can be determined by Eq. (2.41) [80]. $\dot{E}x_{\text{fluid, in}}$, and $\dot{E}x_{\text{fluid, out}}$ are the fluid exergy inlet and outlet, $\dot{E}x_{\text{loss}}$ are the electrical exergy and exergy loss.

$$\dot{E}x_{\text{solar}} = S\left(1 - \frac{T_{amb}}{T_{\text{sun}}}\right) \quad (2.40)$$

$$\dot{E}x_{\text{ele}} = V_{\text{oc}}.I_{\text{sc}} \cdot \text{FF} \quad (2.41)$$

$\dot{\text{E}}\text{x}_{\text{th}}$ is thermal exergy, which is calculated by using Eq. (2.42) [80], $\dot{m}_f$ the mass flow rate and $C_{p,f}$ is the specific heat of fluids. T_{out} and T_{in} are the inlet and outlet fluid temperatures. Then, the thermal and electrical exergy efficiencies are calculated from Eqs. (2.43 and 2.44) [82].

$$\dot{E}x_{th} = \dot{m}_f \cdot C_{p,f}\left[(T_{out} - T_{in}) - T_{amb}\, ln\left(\frac{T_{out}}{T_{in}}\right)\right] \quad (2.42)$$

$$\eta_{\dot{E}x_{th}} = \frac{m_{nf} \cdot C_{p,nf}\left[(T_{out} - T_{in}) - T_{amb}\, ln\left(\frac{T_{out}}{T_{in}}\right)\right]}{S\left(1 - \frac{T_{amb}}{T_{sun}}\right)} \times 100 \quad (2.43)$$

$$\eta_{\dot{E}x\ ele} = \frac{V_{oc}.I_{sc} \cdot FF}{S\left(1 - \frac{T_{amb}}{T_{sun}}\right)} \times 100 \quad (2.44)$$

The exergy efficiency of the PVT is the sum of thermal and electrical exergy efficiency. It can be calculated using Eq. (2.45) as follows:

$$\eta_{\dot{E}x} = \frac{\dot{E}x_{th} + \dot{E}x_{el}}{\dot{E}x_{solar}} \times 100 \quad (2.45)$$

The exergy loss (exergy destruction) is the other parameter which produces the frictional loss in the tubes and heat transfer losses, which can be calculated by Eq. (2.46) [83] as follows:

$$\dot{E}x_{\text{loss}} = \dot{E}x_{\text{in}} - \dot{E}x_{\text{ele}} - \dot{E}x_{\text{th}} \quad (2.46)$$

Entropy generation is a thermodynamic parameter that determines the entropy generation rate in the control volume PVT systems and could be calculated from Eq. (2.47) [77] below.

$$\dot{S}_{gen} = \frac{\dot{E}x_{\text{lost}}}{T_{\text{amb}}} \tag{2.47}$$

2.4 Synthesized nanomaterials

2.4.1 Hybrid titanium oxide-iron oxide nanomaterials

TiO_2-Fe_2O_3 nanomaterials has been produced according to our previous work [84]. $FeCl_3 \cdot 6H_2O$ precursor was dissolved in 100 mL of distilled water to create a homogenous solution. Then, 0.5 g of TiO_2 NWs that had already been produced were added to the solution. Drop by drop, NaOH solution was added while stirring, and when the solution had become base, it was poured into the autoclave and heated to 90 °C for 9 h. The product was dried, calcined at 500 °C for 2 h, and then rinsed with DI water to neutralize pH. The final composition of TiO_2NWs- Fe_2O_3 NPs is 50:50 wt%. To identify and describe the crystal structure of nanomaterials material, XRD was performed. The diffraction peaks are located at 11.9°, 24.2°, 29.1°, 43.1° and 60° index to (200), (002), (310), (602) and (610) originating to $K_2Ti_6O_{13}$ (PDF no. 40-0403). The other peaks at °, 39.2°, 48°, 54.2°, 56.5° and 68.8°, corresponding to (220), (200), (105), (213) and (403), relate to the anatase phase of TiO_2 (JCPDS 21-1272). The diffraction peaks located at 27.4°, 36.1° and 41.2° index to (110), (101) and (111) refer to the rutile phase (JCPDS no-21-1276). The peaks relate to Hematite iron oxide (α-Fe_2O_3) (JCPDS 33-0664) located at 62.4°, 64° and 67.1°, as shown in Fig. 2.6 (a). These results are in good agreement with [85]. A transmission electron microscope TEM technique is used to investigations of the surface morphology of hybrid nanomaterials, which shows the superposition of TiO_2 with Fe_2O_3, as shown in Fig. 2.6 (b).

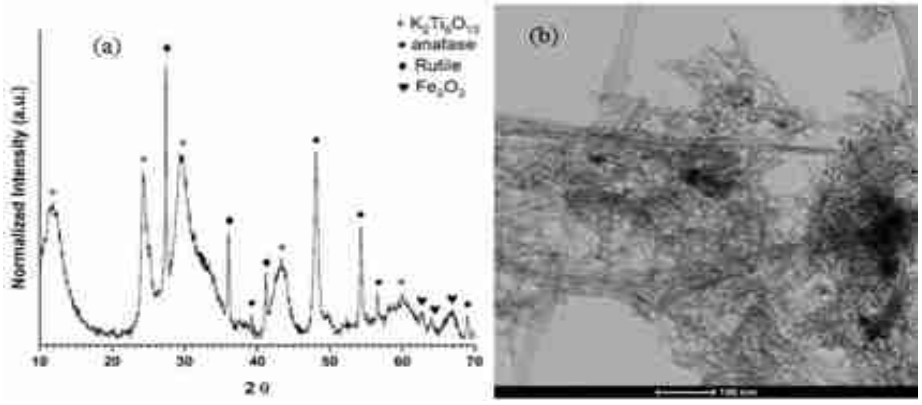

Figure 2.6: The XRD pattern of the synthesized TiO_2-Fe_2O_3 (a) and (b) TEM image of TiO_2- Fe_2O_3 nanomaterials

2.4.2 Hybrid Titanium oxide-copper oxide nanomaterials

TiO_2-CuO nanomaterials was prepared as the following procedure in [84], a calculated amount of (Cu $(CH_3COO)_2$ H_2O) was dissolved in 100 mL of ethanol and stirred vigorously for 30 min. After that, 0.5 g of TiO_2 NW was added to the solution under vigorous stirring for 1 h. The solution was put in an autoclave and heated to 150 °C in a static furnace for 12 h. The product was collected using vacuum filtration, washed, and then calcined at 500 °C for 2 h. The final composition of TiO_2 NWs-CuO NPs is 50:50 wt%. XRD has been performed to describe and identify the crystal structure of nanomaterials material. The diffraction peaks located at 11.9°, 24.2°, 29.1°, 43.1° and 60° corresponding to (200), (002), (310), (602) and (610) refer to K2Ti6O13 (PDF no. 40-0403). The diffraction peaks are located at 25.2°, 48°, 54.2° and 56.6° index to (101), (200), (105) and (213) originating to anatase phase (JCPDS 21-1272). The other peaks located at 27.4°, 36° and 41.2° corresponding to (110), (101) and (111) relate to the rutile phase (JCPDS no-21-1276). Furthermore, the peaks at 38°, 62.7°, 66.2° 68.1° corresponding to (111), (-113), (-311) and (220) refer to copper oxide (JCPDS card number 45-0937), as shown in Fig. 2.7 (a). All these results agree with [84, 79]. A transmission electron microscope TEM

technique is used to investigate the surface morphology of hybrid nanomaterials, which shows the superposition of TiO_2 with CuO, as shown in Fig. 2.7 (b).

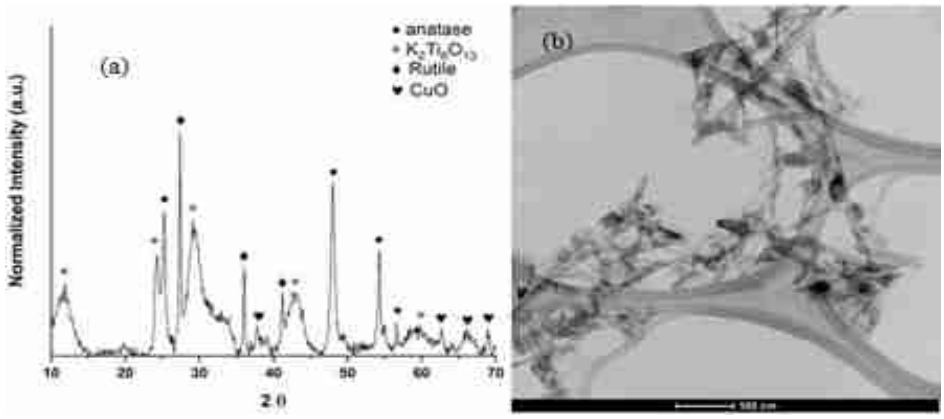

Figure 2.7: The XRD pattern of the synthesized TiO_2-CuO (a) and (b) TEM image of TiO_2-CuO nanomaterials

2.5 Preparation of nanofluids

Stability is an important advantage that nanofluids must have; achieving that is not easy. It undergoes several matters, such as nanoparticle types, purity, size, nanomaterials shapes and base fluid type. The purpose of preparing nanofluids is to improve the thermal properties of the fluids, particularly the thermal conductivity of fluids. Preparing stable nanofluid enhances heat transfer applications depending on the thermophysical characteristics of nanoparticles. The Two-type method is employed to prepare nanofluids, a one-step method consisting of either liquid chemical or physical vapor deposition method to prepare nanofluids. The two-step method is commonly used for dispersing nanomaterials into base liquids [86]. Dispersion of nanoparticles in the base fluid enhances the thermophysical properties of the new working fluid and then improves the heat transfer rate. The good dispersion of nanomaterials into the base fluid at low sedimentation and the high stability of nanofluids depends on the preparation method of nanofluids [87]. In this dissertation, various types of nanofluids have been prepared, such as WO_3/DI water, ZrO_2/DI water, TiO_2/DI water, Fe_2O_3/DI water, CuO/DI water nanofluids, and two types of hybrids nanofluids such as TiO_2-CuO/DI water, TiO_2-Fe_2O_3/DI water. The two-type method is employed to prepare nanofluids at different volume concentrations dispersed in DI water were calculated from Eq. (10). The quantity of nanomaterials was scaled by an electronic scale (type: BOECO BAS of 0.0001g), then dispersed into DI water and mixed with a magnetic stirrer for a different period between 25-30 min. Ultra-sonication probe (Bransonic type 220, Voltage: 240V, Vf: 48kHz) was used from 35-40min depending on the type of nanomaterial employed to avoid the agglomeration of nanoparticles in the nanofluid and to obtain a stable suspension for a long period, as shown in Fig. 2.8. Ultrasonic vibration separates the particles, diverges them from each other, and then spreads them throughout the base fluid. This method delays the agglomeration of nanoparticles and then their deposition for an appropriate period. The time sediment and visualization methods were used to examine the nanofluid's stability for different periods from 3-5 h after sonication and from 2 to 4 days after sonication, as shown in Fig. 2.9 (a-j). The prepared nanofluid showed good stability. Thus, it was prepared in suitable quantities later and directly used in the experiment after the sonication.

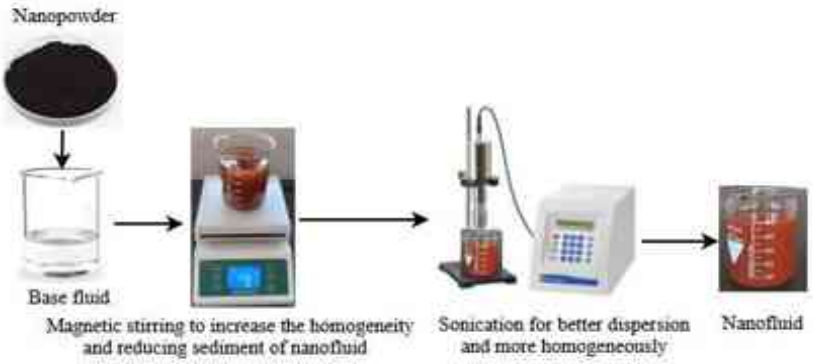

Figure 2.8: Preparation of nanofluid by using two steps method

Figure 2.9: Stability of preparation of nanofluids (a) WO_3/DI water, (b) ZrO_2/DI water, (c) CuO/DI water, (d) Fe_2O_3/DI water, (e) TiO_2/DI water, (f) TiO_2-Fe_2O_3/DI water, (g) TiO_2-CuO/DI water

2.6 Thermophysical properties of nanofluids

2.6.1 Density and viscosity of nanofluid

Density is an essential property of the nanofluid that significantly affects the thermal system's sustainability and achieves a suitable extent of nanofluid stability [88]. Some parameters significantly affect the nanofluid's thermophysical, such as temperature, base fluid, volume fraction, nanoparticle concentration, etc. The density of nanofluid is increased with increased volume concentration and reduced with rising temperature. Thus, an increase in density affects the pumping capacity by increasing power consumption, specifically in thermal applications [89]. On the other hand, increasing the density of nanofluids has a negative impact on the Reynolds number by boosting the friction factor [90]; increased temperatures lead to a low density of nanofluids [91]. The base fluid plays an essential role in nanofluids' density; a limited effect was found for nanoparticles' shape and size on nanofluid density [92]. Equation (2.48) is commonly used to determine nanofluids' density (ρ_{nf}) which depends on the volume concentration (ϕ) of nanoparticles, the base fluid density (ρ_{bf}), and the density of nanoparticles (ρ_{np}) [93].

$$\rho_{nf} = \phi \cdot \rho_{np} + (1 - \phi) \cdot \rho_{bf} \tag{2.48}$$

$$\varphi = \left[\frac{\frac{m_{ap}}{\rho_{np}}}{\frac{m_{np}}{\rho_{np}} + \frac{m_{bf}}{\rho_{bf}}} \right] \times 100 \tag{2.49}$$

were, m_{np} the mass of the nanomaterials m_{bf} the mass of the base fluid.

Viscosity is the essential factor significantly affecting nanofluids' behaviour [94]. Increasing the nanoparticle concentration causes an increase in nanofluids viscosity, which increases pumping power due to pressure drop [95]. The volume concentrations and temperature control the viscosity; the base fluid is the most important factor determining the nanofluid viscosity [96]. Thus, ideal nanofluids must make high thermal conductivity with low viscosity available. In contrast, nanofluid's viscosity is low with increasing temperature [97]. Increasing temperature contributes to increasing thermal conductivity, which leads to lower viscosity and reduces agglomeration of the nanoparticles [73]. Eq. (2.50) is used to determine the nanofluid's viscosity, where μ_{bf} is the viscosity of base fluid.

$$\mu_{nf} = \frac{\mu_{bf}}{(1-\phi)^{2.5}} \tag{2.50}$$

2.6.2 Thermal conductivity and specific heat of nanofluid

Thermal conductivity is one of the most important nanofluid properties in the heat transfer field. Increasing the thermal conductivity of nanofluids is required to enhance the heat transfer of nanofluids. Conventional fluids are poor in heat transfer; the addition of solid nanomaterials materials into the base fluid enhances the high thermal conductivity of nanofluids [98]. On the other hand, increment temperature and concentration of nanoparticles in base fluid cause an increase in the thermal conductivity of nanofluid due to rising kinetic energy that strengthens the collision between particles [99]. Increased thermal conductivity is mainly associated with nanoparticles' type of material by their concentration and size. The shapes of nanoparticles have a role in increasing thermal conductivity [100]. It observes that nanoparticles' instability in base fluid causes agglomerates in the nanofluid, and it's one reason for decreasing thermal conductivity [101]. Eq. (2.51) is used to determine the thermal conductivity of nanofluid, where k_{np}, k_{bf}, k_{nf} are thermal conductivity of nanomaterials, base fluid and nanofluid [102]

$$\frac{k_{nf}}{k_{bf}} = \frac{k_{np}+2k_{bf}+2\emptyset(k_{np}-k_{bf})}{k_{np}+2k_{bf}-\emptyset(k_{np}-k_{bf})} \tag{2.51}$$

The specific heat represents an important property of any thermal fluid; this property plays a vital role in providing the energy that transmits from one body to another [73]. In nanofluids, specific heat is different depending on the nanomaterials used, their concentration in the base fluid, and the type of base fluids [103]. Nanofluids' specific heat increases with increasing temperature while lowering at increased volume concentration [104]. Adding a small volume concentration of nanoparticles in the base fluids enhances the specific heat regardless of the particle shape or type [105]. The nanofluid's specific heat is determined using Eq. (2.52) [93], where $C_{p,nf}$, $C_{p,bf,}$ $C_{p,np}$ are the specific heat of the nanofluid, base fluid and nanomaterials, respectively. Table 2.2 below shows the thermophysical properties of new hybrid nanomaterials used in this dissertation in all experiments.

$$C_{p,nf} = \frac{\phi \cdot (\rho_{np} \cdot C_{p,n}) + (1-\phi) \cdot (\rho_{bf} C_{p,bf})}{\rho_{nf}} \tag{2.52}$$

This chapter presented a deep analysis of the mechanism of heat transfer by conduction, convection, and radiation between the components, considering the energy balance equations for each layer of the PVT system. The inputs and outputs parameters that affect the efficiency of the PV system have been studied and identified weak points that could improve by effectiveness methods by considering the experimental results. The maximum deviation has been noticed at 3.11% by applying the experimental results to the thermal analysis and energy balance equations. According to thermodynamics laws (first and second), energy and exergy analysis has been considered to demonstrate the quantity and quality of the energy produced, adding to identifying the value of exergy destruction. The chapter also presented a synthesis of new hybrid nanomaterials used to prepare new hybrid nanofluids used as cooling fluids of the PVT system and their effect on improving its energy and exergy efficiency. Another mono nanomaterial has also been synthesized by different morphologies (in Appendix A) to use as cooling fluids to compare them with the hybrid nanofluid regarding their effect on the PVT system efficiency.

Table 2.2: Thermophysical properties of the hybrid nanomaterials

Properties	TiO_2-Fe_2O_3	TiO_2-CuO
Density (kg/m^3)	3473	2791
Thermal conductivity (W/m·K)	75.32	79.9
Heat capacity (J/kg·K)	1334	1198

Chapter 3

Factors affecting the photovoltaic module performance

Investigation of the factors that affect the PV module performance is an important issue to avoid any problems facing its work. Climate conditions, such as solar radiation, temperature, wind speed, etc., are the main factors affecting the PV module's performance. Fluctuating incident solar radiation and increased temperature of the PV cells are common problems in most PV module applications. In this chapter, two case studies have been Investigated:
The first case study is a numerical simulation by Ansys software to predict the thermal behaviour of the PV module at different operations conditions in hot and cold weather by adopting different values of solar radiation, temperatures, and wind speed. This case helps predict the PV cells' thermal behaviour at exposure to different solar radiation values and temperatures in different seasons. This case study helps identify the problems PV cells face and then determine the effective technique that improves PV performance.
The second case is an investigation of the electrical behaviour of the PV module depending on the mathematical equations governing PV module performance. The equations have been simulated using the MATLAB-Simulink program as a subsystem and then as one system that undergoes inputs that we can control. The simulation considers variable and constant values of solar radiation and temperature as input to observe output voltage and current and power of the PV module as outputs. This case contributes by giving a general vision of the factors which have the main effect on the PV module performance and helps select the appropriate methods to overcome.

3.1 Simulation study of the photovoltaic module under different operation conditions

This case study studied the effects of temperature distribution on the PV module at various solar radiation values and temperatures under different operation conditions in January and July. A 3D module of the PV panel was simulated with ANSYS software, depending on the various values of temperatures and solar radiation values obtained using mathematic equations. The simulation depended on the layer’s properties of the PV panel, solar radiation values, temperature, and convective heat transfer coefficient of the module to evaluate temperature distribution and identify the appropriate extent of operating conditions of the PV module.

3.1.1 Operation conditions and governing equations

The PV module used type CL-SM50P Polycrystalline, consisting of glass covering, PV cells with two layers of Ethylene Vinyl Acetate (EVA), aluminium frame, and Tedlar (PVF) layer, as shown in Fig. 3.1 below. Table 3.1 below shows the material properties of the PV components inserted in the ANSYS software engineering data. The PV panel datasheet has adopted a reference for comparing the simulation results and the PV panel values under stander test conditions STC (25 °C and 1000W/m^2). According to the manufacturer datasheet, the PV module geometry is built by SolidWorks software with module dimensions. The materials are defined by the Ansys library data of all the PV panel layers. Then the PV module was imported to the Ansys software to analyse the PV module temperature distribution inserted in the software as variable values depending on the different values of beam solar radiation obtained using the mathematical equations below. Thus, according to STC, three solar radiation values have been

used, two of them according to January and July with an estimation of clear-sky radiation and the third solar radiation value under STC.

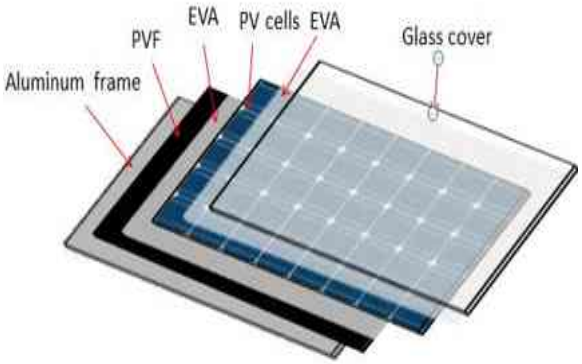

Figure 3.1: The layers of the PV module.

Table 3.1: The layer's properties of the PV panel [106]

Material (Layer)	ρ (kg/m^3)	K (W/m.k)	C_p (J/kg.k)
Glass	3000	1.8	500
EVA	960	0.35	2090
PV	2330	148	677
PVF	1200	0.2	1250
Aluminum Frame	2707	204	996

The heat flux changes with time, which causes a change in the temperature that influences the PV module performance. The temperature was fixed at 4 °C in January, 35 °C in July, and 25 °C in STC. The convective heat transfer coefficient is 14.8 W/m^2. ºC on the panel calculated by using equation (3.1) [107], V_m is the wind speed value that adopted 2.4 m/s according to Miskolc city [108]. The mesh element size of the PV module mesh was 0.002 m, and the number of meshes elements was 278964 with high smoothing; the time simulated was 43.1 min in all initial conditions.

$$h = 5.7 + 3.8V_m \tag{3.1}$$

The mathematical equations were used to predict and estimate direct radiations transmittance (beam radiation) for Miskolc city when a clear atmosphere on 7 January at 11:30 AM and 13 July at 12:30 PM. To achieve that, it needs to find some parameters that help achieve that such angular position of the sun (solar declination (δ)) represents the angle between the line from the sun's centre to the earth's centre equator. The solar declination value is changeable because of the rotating of the earth around the sun and the tilt of the earth on its axis of rotation found by using Cooper's Eq. (3.2) [107], where n is the day of the year of that selected (n = 7 for January and n = 194 for July).

$$\delta = 23.45sin\left(360\frac{284+n}{365}\right) \tag{3.2}$$

The zenith angle is the incidence beam solar radiation angle between the vertical and the line to the sun used with horizontal surfaces and determined by the following Eq. (3.3).

$$cos\ \theta_z = cos\ \phi cos\ \delta cos\ \omega + sin\ \phi sin\ \delta \tag{3.3}$$

Latitude between $-90° \leq \varphi \leq 90°$ for Miskolc, Hungary, is 48.1º, which is an hour angle which is negative in the morning and afternoon positive. Solar time depends on the sun's angular motion in the sky, which may not synchronize with local time [61]. The extraterrestrial radiation

incident is the quantity of solar energy received per unit of time at the mean distance between the sun to the earth. It can be calculated by Eq. (3.4) on the normal plane and is the solar constant.

$$G_o = G_{sc}\left(1 + 0.033\cos\frac{360n}{365}\right) \tag{3.4}$$

Calculating the daily and hourly solar radiation received on a horizontal surface is useful under standard conditions. To calculate the beam radiation transmitted from the sun without scattering by clear atmospheres, consider the zenith angle and altitude of the atmosphere for four climate types from Eq. (3.5) [109].

$$\tau_b = a_0 + a_1 exp\left(\frac{-k}{cos\,\theta_z}\right) \tag{3.5}$$

$$a_0^* = 0.4237 - 0.00821(6 - A)^2 \tag{3.6}$$

$$a_1^* = 0.5055 + 0.00595(6.5 - A)^2 \tag{3.7}$$

$$k^* = 0.2711 + 0.01858(2.5 - A)^2 \tag{3.8}$$

a_0, a_1 are constant, and k represents the standard atmosphere at 23 Km visibility that can be found using the Eqs. (3.6), (3.7), (3.8), and A represent the altitude of the observer in kilometres. Hence, multiply the constant values by correction factors in Table 3.2, $a_0^* \times r_o$, $a_1 \times a_1^*$ and $k \times r_k$ could calculate the beam radiation transmitted. Thus, it can determine the beam radiation for any zenith angle or altitude, even 2.5 km. The normal beam radiation in a clear sky can be found by multiplying the value of the beam radiation transmitted during clear atmospheres τ_b by the value of extraterrestrial radiation incident G_{on}. The value results multiply by the zenith angle to obtain solar radiation's value on the horizontal of the panel G_{cb} [110].

Table 3.2: Correction factors for climate types [107].

Climate Type	r_o	r_1	r_k
Tropical	0.95	0.85	1.02
Mid-latitude winter	1.03	1.01	1
Subarctic summer	0.99	0.99	1.01
Mid-latitude summer	0.97	0.99	1.02

3.1.2. Results and discussion

The PV panel has been simulated under different solar radiation values estimated by mathematical equations and various temperatures. For January, solar radiation values were 176 W/m^2; for July, 735 W/m^2 and under STC was 1000 W/m^2. January's temperature was 4 °C, July's highest temperature was 35 °C, and the PV panel temperature was under STC at 25 °C. The results indicate that the PV module surface temperature distribution was high at the top of the PV panel while the aluminium frame's temperature was lower. The dark blue color refers to the minimum temperature on the panel, the bright red color refers to the maximum temperature on the panel, and other colors represent temperature variations. In January, when the temperature is low, the beam solar radiation is 176 W/m^2. The temperature distribution on the PV module is between a maximum of 15.4 ºC and a minimum of 11.9 ºC, as shown in Fig. 3.2. Thus, this solar radiation range influences PV panel performance represented by power output without leaving any damage or overheating because of the lower PV module temperature.

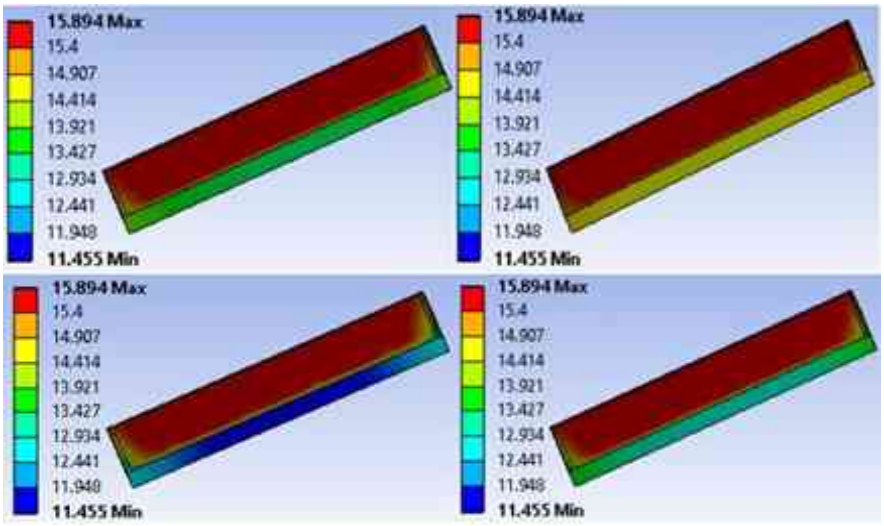

Figure 3.2: At solar radiation 176 W/m^2 and temperature 4 °C

Applied the July solar radiation 735 W/m^2 when the temperature reaches 35 °C, the simulation shows that the PV module is exposed to a maximum temperature of 84.6 °C, while the minimum temperature was 68.4 °C, as shown in Fig. 3.3 below. Increasing the PV panel temperature by 10 ºC above the STC value causes a decrease in its efficiency. This extent of temperature causes other problems for the PV panel, such as overheating, which leads to the burning of some cells or reduced voltage, power, and the PV module output current; thus, the PV module becomes inoperative [111].

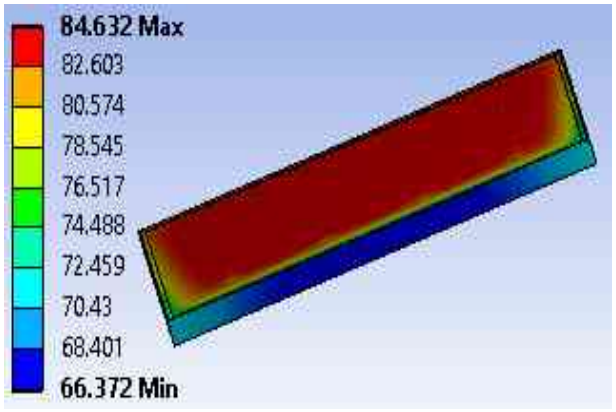

Figure 3.3: At solar radiation 734 W/m^2 and temperature 35 °C

Under STC conditions of the PV module 1000W/m^2 and 25 °C, the PV module temperature was observed until 92.5 °C, while the lowest temperature was 67.7 °C, as shown in Fig. 3.4 below. Therefore, this temperature range is unsuitable for PV module operation due to the rising of the PV cell's temperature and causes the same problems of July values as overheating PV cells or reduced conversion efficiency and production of the PV module. The temperature increase of the PV module is directly proportional to increasing solar radiation. Due to the PV layer's different properties, these layers' temperature is different, as shown in the Figures above; the PV module temperatures surface differs from the aluminium frame. The maximum and average temperatures on the PV panel converged somewhat at increasing the solar radiation, as shown in Table 3.3, for July and STC values. Cooling the PV module to remove the excessive heat is important to continue its work under high temperatures, even with STC values.

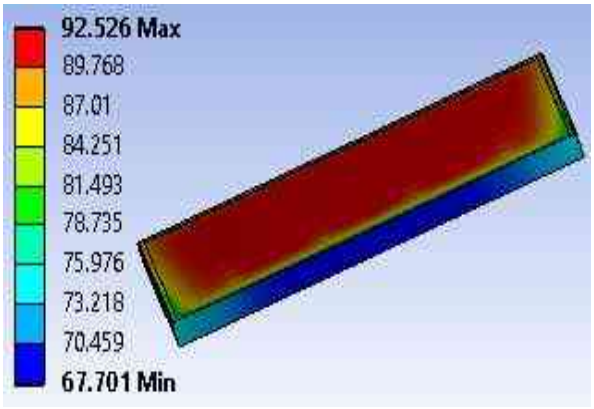

Figure 3.4: At solar radiation 1000 W/m^2 and temperature 25 °C

Table 3.3: Temperatures on the PV panel at different solar radiation.

Solar radiation W/m^2	Max temperature °C	Min temperature °C	Average temperature °C
176	15.8	11.4	15.2
735	84.6	66.3	82.1
1000	92.5	67.7	89.1

3.2. Test the mathematical of the photovoltaic module under different conditions by using MATLAB-Simulink

In this case study, we discuss temperature and solar radiation's effects on the voltage and current of the PV module. MATLAB-Simulink has been used to model the mathematical equations of the PV module to predict the behaviour of the output current and voltage of the PV module. Simulation depends on the constant temperature of the PV module with different solar radiation values and vice versa. Thus, the simulation results are compared with the PV module datasheet under standard test condition STC. The proposed module-derived is a single of the V-I characteristics that will extend for all the string/array of the PV cell depending on the five parameters module and based on the manufacturer datasheet.

3.2.1. Mathematical modelling of photovoltaic module

A specified number of solar cells connected in series and parallel represent the unit build of the solar PV module. The study used MATLAB-Simulink to mathematical module equations of the PV module depending on the variable values of temperatures and solar radiation. The datasheet of the PV module is a reference for comparison with the simulation values with accurate parameters widely used for the analytical characterization of the PV module. The equivalent electric circuit of the PV module consists of a shunt resistor parallel R_{sh} with a higher value than a series resistor R_s with a single diode. The electrical characteristics of the PV module and climatic conditions determined the power output of the PV module. MATLAB-Simulink will module the mathematical equation as subsystems for each equation of the PV module, as shown in Figs. 3.5 and 3.6 (a) and (b), depending on the parameters of the equations.

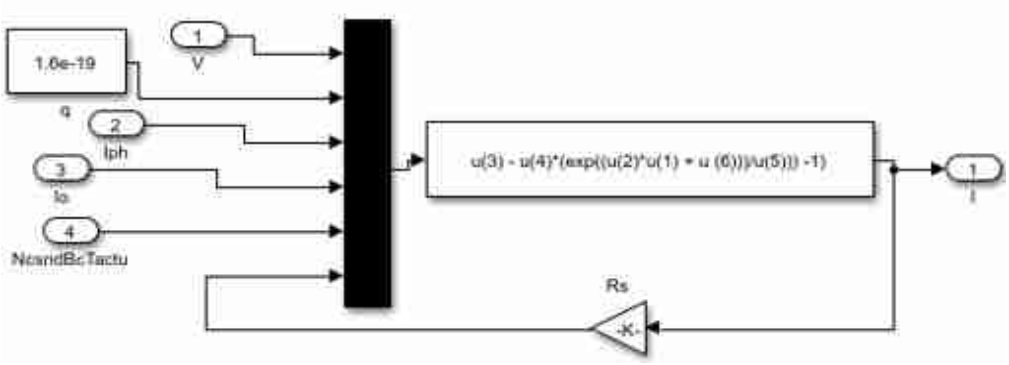

Figure 3.5: Modelling the output current of the PV module

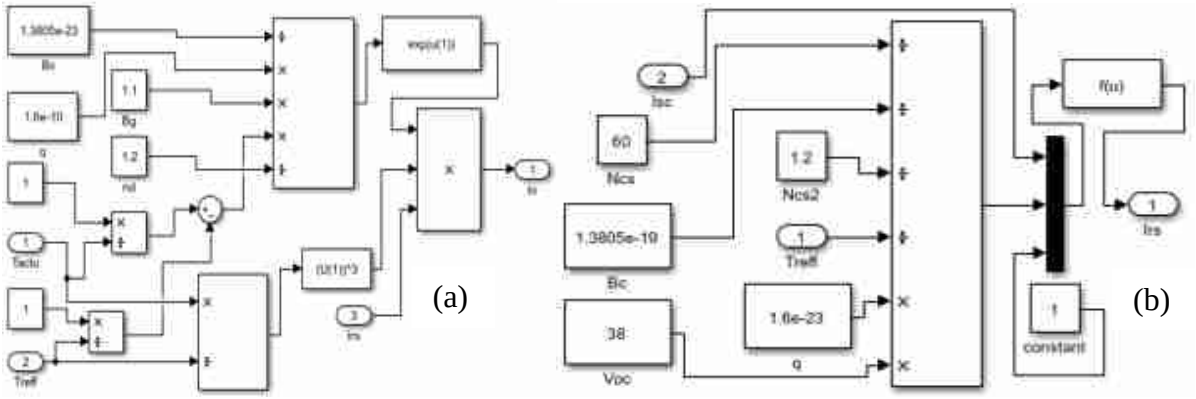

Figure 3.6: Modelling PV equations (a) Saturation current and (b) reverse saturation current

Thus, all the PV module mathematical equations will simulate a PV module to study the PV module's behaviour of I-V and P-V, where Eq. (3.9) [112] represents the I-V characteristic of the PV module.

$$I = I_{ph} - I_O \left[exp^{\left(\frac{q \cdot (V + I \cdot R_S)}{nd \cdot N_{cs} \cdot B_c \cdot T_O}\right)} - 1 \right] - I_{sh} \tag{3.9}$$

where I_{ph} is the PV current, which depends on the irradiation level, I_o is the saturation current obtained from Eq. (3.10). q represents the electron charge (1.60217646 × 10-19 ºC), *I, V,* representing both the output current and the PV module voltage. I_s is a series resistance (0.02 Ω) of the equivalent electric circuit. While *nd* is (1.2) representing the diode's ideality factor (a number between 1 and 2 that typically increases as the current decreases), N_{sc} is the number of PV cells connected in parallel. B_c is Boltzmann's constant (1.3806503 ×10-23 J/K). Thus, both T_o and I_{sh} represents an operating temperature of 24 K and the current resistor through the shunt.

$$I_{sh} = \frac{V + I \,.R_S}{R_{sh}} \tag{3.10}$$

Solar radiation and temperatures are the main parameters that define the value of the PV module current. R_{sh} is shunt resistance (485.5 Ω). I_{ph} could determine by Eq. (3.11) [113] below, and *V* represents the voltage across the diode.

$$I_{ph} = [I_{sc} + I_s(T_o - T_s)] \frac{S}{1000} \tag{3.11}$$

Where I_s represents the short-circuit current of the cell at STC, I_{sh} is the short circuit current (A). T_s represents a solar cell's absolute reference temperature at STC. *S* is solar irradiation. The difference between the cell saturation current I_0 and cell temperature described in Eq. (3.12) [113].

$$I_0 = I_{RS} \cdot \left(\frac{T_o}{T_N}\right)^3 \cdot \exp\left[\frac{qB_g}{nd \cdot B_g}\left(\frac{1}{T_N} - \frac{1}{T_o}\right)\right] \tag{3.12}$$

The reverse saturation current, as seen in Eq. (3.13) [113], and B_g is the band-gap energy of the semiconductor with a value of (1.1 eV). T_N is the average temperature of 25 °C, and V_{oc} is open-circuit voltage (V).

$$I_{RS} = \frac{I_{sc}}{exp^{\left(\frac{q \cdot V_{oc}}{nd \cdot B_c \cdot N_{cs} \cdot T_o}\right)} - 1} \tag{3.13}$$

3.2.2 Simulation of the mathematic module

The simulation has been conducted using MATLAB-Simulink for mathematic equations of the PV module with electrical characteristics that simulated as a subsystem, as shown in Fig. 3.7, using variable and constant parameters. The MATLAB-Simulink illustrates the PV module building by investigating the *V-I* and *P-V* output characteristics. In general, the experiment was conducted under STC, as the first step after that used various solar irradiation and temperature values.

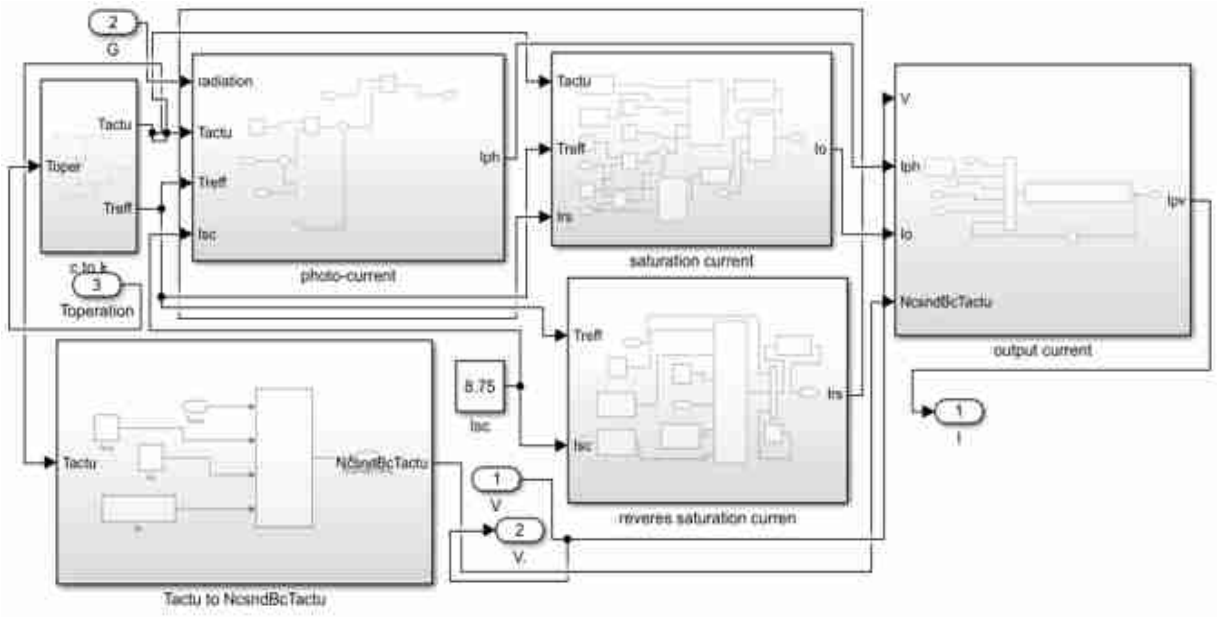

Figure 3.7: A subsystem of the PV module

Different values could change several times in the PV module as input variable parameters, as shown in Fig. 3.8. Therefore, depending on the PV module equations, many subsystems have been created by using MATLAB-Simulink for each equation of the PV module (Saturation current, Reveres saturation current, Shunt current, Photo-current, and PV current) represented as a subsystem of the PV module. Thus, all the subsystems are simulated together after the PV module is linked.

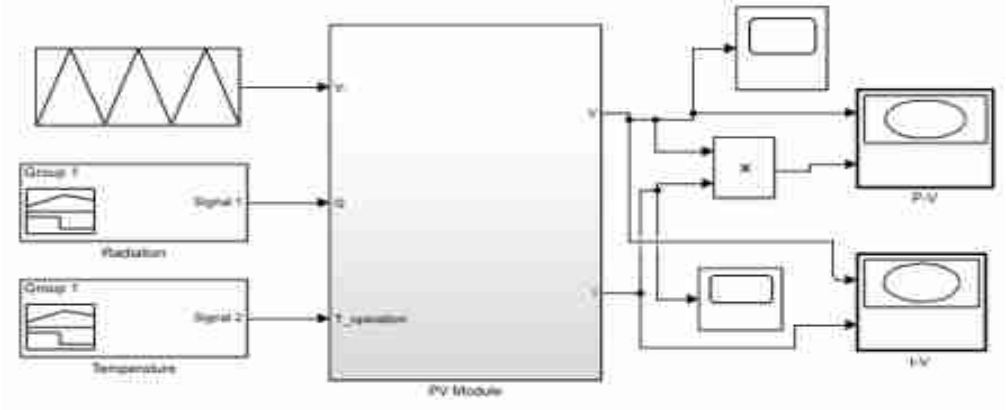

Figure 3.8: Simulink model of the PV module

3.2.3 Results and discussions

The simulations results of the PV module depended on the variable values of solar radiation and temperatures in Miskolc climate conditions. The datasheet of the PV module under (STC) to recognize the behaviour of the PV module of the *I-V* and *P-V* values. The PV module current has been slightly affected by power output due to rising temperatures, even with the drop in solar radiation, as shown in Fig. 3.9. This study considers two cases when solar irradiation values are constant with various temperatures and vice versa. The first case is when solar radiation values are lower than 1000 W/m^2, and the temperature is constant at 25 °C.

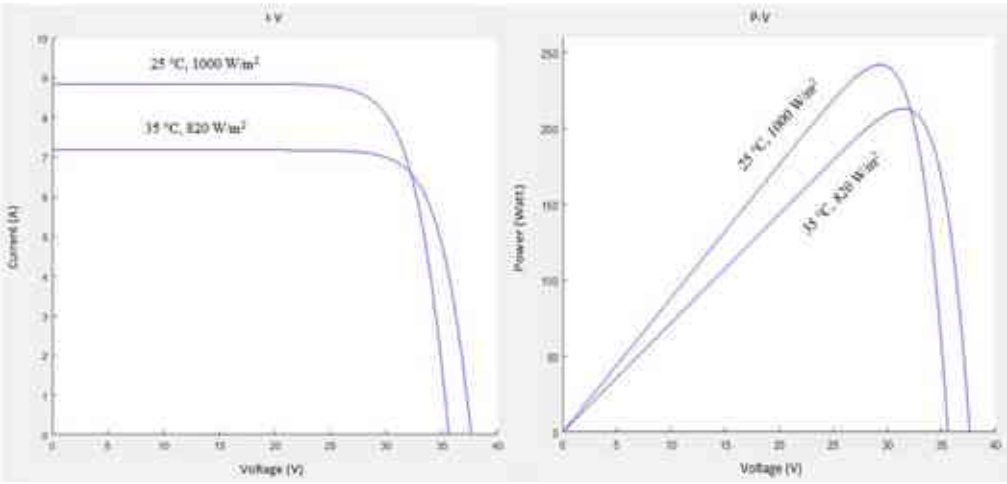

Figure 3.9: Characteristics of PV module under STC and 35 ºC, 820W/m^2

The output current of the PV module dropped from 8.75 to ~7.2 A, with little change with the PV module's output power of 250 W to ~220 W compared with stander case STC at 25 °C, 820 W/m^2. It noticed the reduction in output current and power of the PV module from 8.75A to ~ 4.8 A, and the output power value decreased from 250W to ~140W when the temperature and solar radiation were 25 °C, 535 W/m^2. The continuous reduction in the solar irradiation value at 25 ºC, 185 W/m^2, causes a significant drop in the output current of the PV panel from 8.75A to ~1.7A. In contrast, the output voltage of the PV module dropped from 250 W to ~ 45 W compared with the datasheet of the PV module under STC, as shown in Fig. 3.10.

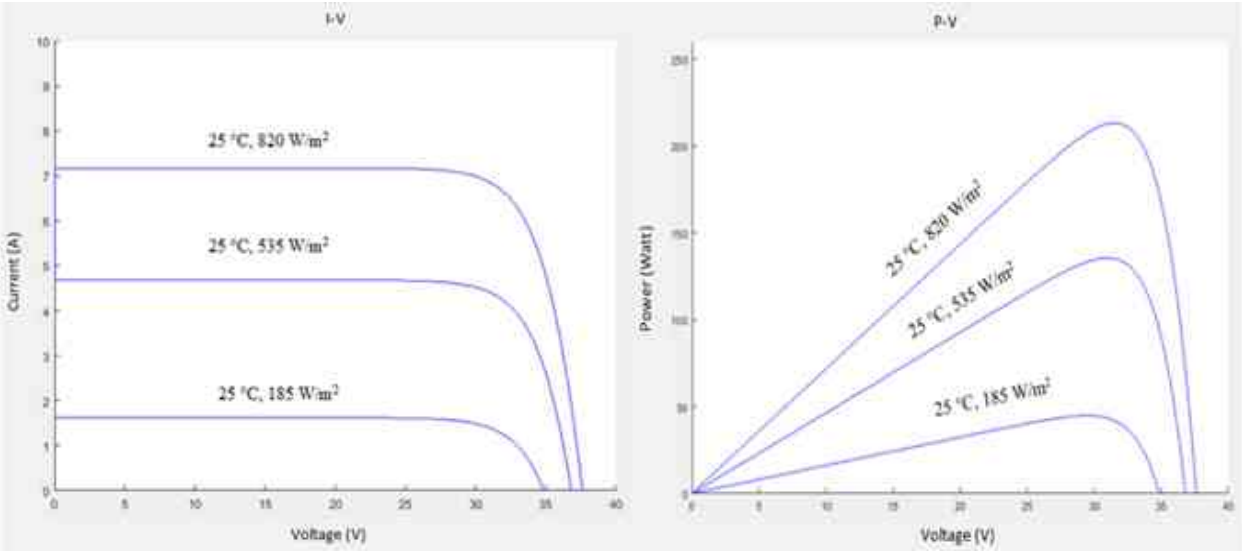

Figure 3.10: Characteristics of the PV module at 25 °C with various radiations

The second case is when solar irradiation is constant at 1000W/m^2 with various temperature values at 35 ºC, 24 °C, and 18 °C. The high temperatures cause PV cells to rise, thus affecting the performance of the module. It's noticed at 35 ºC, 1000W/m^2, a slight drop by the PV module's output current (8.75 - 7.75) A, and the output power also decreased up to ~ 210 W compared with the datasheet of the PV module under STC. Increasing the output current and power of the PV module at 24 ºC, 1000 W/m^2, as shown in Fig. 3.11.

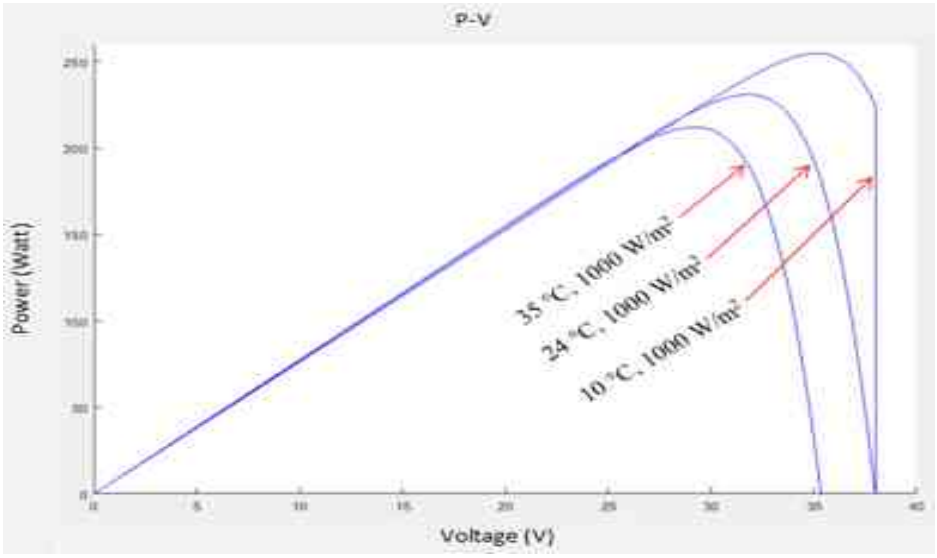

Fig. 3.11: *P-V* characteristics of PV module at various temperatures and constant radiation

Due to the closer temperature and radiation values of the stander datasheet of operation PV module parameters. The output current and power of the PV module continuously increase with a temperature reduction at 10 °C even with 1000W/m^2 of solar radiation, compared with the values when the temperature was high, as shown in Figure 28 above.

3.3 New contributions results

Contribution 1

- The first case study is characterized by using predicted equations that can be adopted to test the PV module's thermal behaviour under different conditions and give a general impression of temperature distribution on the PV module. I found that the thermal behaviour of the PV

module is a variable with solar radiation change during the day, which was clear by temperature distribution on the PV module surface. The lower the solar radiation value and temperature (176 W/m^2, 4 °C), the lower the intensity of solar radiation affects the PV module's short circuit current by the number of photons absorbed by the semiconductor material that PV cells are made from. The average temperature at the solar radiation mentioned above was 15.2 °C; this temperature level is not causing damage to the PV module but reduces its electrical power and efficiency. Increasing solar radiation and temperature to (734 W/m^2, 35 °C) causes an increase in the PV module temperature that causes reduction in power output with damage to PV cells at continuously increased temperatures. An increase in the ambient temperature causes an increase of PV cells, which leads to a significant decrease in open-circuit voltage when the PV module temperature is above 25 °C with a slight drop by short circuits current, then a reduction in power output. Rising temperature to 82 °C causes degradation of the PV module performance and causes the appearance of local hotspots when the temperature reaches the extreme range.

- In the second case, we have modelled the PV module through equations that can control as one system undergoes controllable inputs and outputs that depend on the parameters we are setting, thus helping predict the PV module's electrical behaviour and then identifying the appropriate parameters to achieve better electrical performance. It found that reducing the solar radiation to less than STC, even with 35 °C, reduces the PV module voltage and current to 21.52% and 13.63%, respectively. Constant temperature with a gradual lowering of solar radiation is a significant effect by reducing the current and voltage of the PV module, which confirms the importance of the intensity of solar radiation on power produced. Constant solar radiation values and gradually lowering temperature has a slight effect on the current of the PV module and a higher effect by reducing the voltage compared with constant temperature and variable solar radiation. It was found that decreased temperature of the PV cells with constant solar radiation slightly affects the PV module performance. The second case has confirmed the effect of the intensity of solar radiation and temperature on the open-circuit voltage and short-circuit current that affects the PV module performance.

Chapter 4

Investigation of the effect of using nanofluids on the boiler system behaviour

The current case study contributes to increasing knowledge of the thermal behaviour of nanofluids proposed as a new cooling media and their influence on greater thermal system efficiency. Iron oxide (Fe_2O_3) nanoparticles and tungsten trioxide (WO_3) nanoflakes suspension at a specific volume concentration in DI water were proposed. Thus, investigate their effect on the heat transfer rate, Nusselt number and heat transfer coefficient, drop in the friction coefficient, friction factor and Reynolds number. MATLAB/Simulink has been used to validate the experimental and simulation to confirm the accuracy of the results and compare the results with other studies.

4.1. Data reduction

The nanofluids of Iron oxide Fe_2O_3 and Tungsten trioxide WO_3 nanoparticles were prepared using two-step methods. More information about synthesizing the Fe_2O_3 and WO_3 nanoparticles is available in Appendix A. The volume concentration of Fe_2O_3 was 0.015 vol%, and WO_3 was 0.01 vol%, which is calculated according to equation (49). The parameters of heat transfer rate, Reynolds number, Nusselt number, friction factor, and pressure drop were calculated from Eqs. (2.32, 2.35, 2.36, 2.37, and 2.38), as mentioned in subchapter 2.3, and the heat transfer coefficient was calculated by Eq. (4.1) [114] as follows:

$$h = \frac{\dot{m}C_p \times (T_{out} - T_{in})}{A(T - T_w)} \tag{4.1}$$

Here, *A* is a pipe's peripheral area, which is calculated in Eq (4.2), while *T* represents the average inlet and outlet temperature.

$$A = 2 \times (W_t + H)l \tag{4.2}$$

W_t, *H*, and l are the tube's width, height, and length.

4.2 System description

The system consists of an electric water heater with 81 litres (Model: GCVS 804420 B11 TSR) and a heat exchanger with a surface area of 0.21 m^2 inside the electric water heater. The heat exchanger of the electric heater is connected to a water tank (90 litres) which involves a second heat exchanger inside it with a 15 mm diameter connected with an electric water heater by an inlet pipe. The second tank contains a nanofluid with a pump and mass flow rate sensor (Model: YF-S201) connected to an inlet pipe, a nanofluid tank, and an electric water heater. Eight thermocouples (T-type of 0.2 mm ± 1 °C accuracy and ± 0.5 °C limits of error) were used to measure the temperature of each part of the system, as shown in Fig. B1.1. Thermocouples were distributed of the inlet, outlet, water tank, nanofluid tank, electric heater wall, water inside of the electric heater, ambient temperature, and temperature between the water tank and nanofluid tank. The measured temperature is recorded by the National instrument model NI 9213 and read by IN Signal Express 2015 software. The National Instruments Compact DAQ (NIC) system contacts the thermocouples read and recorded by driver software installed by the laptop.

4.3 Validation of experimental

The system has been modelled with MATLAB/Simulink; this model represents a small water electric heater set to work between the temperature of 60-63 °C and a pressure of 0.6 MPa. Four ports were connected to a heat exchanger; the first port represents the (cold inlet fluid) connected by a reservoir involving cold water at a specific temperature with a pump and mass flow rate sensor, as shown in Fig. B1.2. The second port is (the hot outlet fluid) connected by a temperature sensor to measure the temperature variation between the inlet and outlet. The other ports are connected to an electric water heater to circulate the hot water and make it homogeneous. The heat exchanger models the heating of fluids through conduction heat from hot water on the outer wall to water circulating inside heat exchanger pipes with a temperature less. The thermophysical properties of the liquid are defined and set on the thermal liquid tab.

4.4 Results and discussion

4.4.1. Effect of volume concentration on friction factor and Reynolds number

Adopted Fe_2O_3/DI water and WO_3/DI water as nanofluids, which achieved interesting changes in the heat transfer, thus affecting other parameters by improving the thermal characteristics. Heat transfer of the Fe_2O_3 nanofluid used achieved better performance than WO_3 nanofluids, reflecting enhanced working fluid characteristics due to increased thermal conductivity and decreased viscosity at the outlet. Figure B1.3 (a) shows the variation of inlet and outlet temperature of the DI water and nanofluids on the thermal performance of the working fluid. An increase in inlet hot fluids temperature causes decreased friction factor and a slight decrease in the viscosity of fluids. In contrast, increasing Reynolds number leads to a decreased friction factor. The friction factor is affected by the volume concentration of nanoparticles; at 0.015% and 0.01% nanoparticles volume concentration in the base fluid, the viscosity of nanofluids increases compared to DI water, and the friction factor increases. Figure B1.3 (b) shows the decreased friction factor with an increase of the average Reynolds number due to the volume concentration and viscosity of Fe_2O_3 nanofluid being the highest compared with WO_3 nanofluid and DI water. Figure 4.1 shows the effect of mass flow rate on increasing Reynolds number at different volume concentrations of nanofluids. Fe_2O_3 nanofluid achieved increment by Reynolds number of about 2.51% and 3.80% compared with WO_3 nanofluid and DI water. Thus, increasing the Reynolds and Nusselt numbers increases the heat transfer rate to a more significant extent.

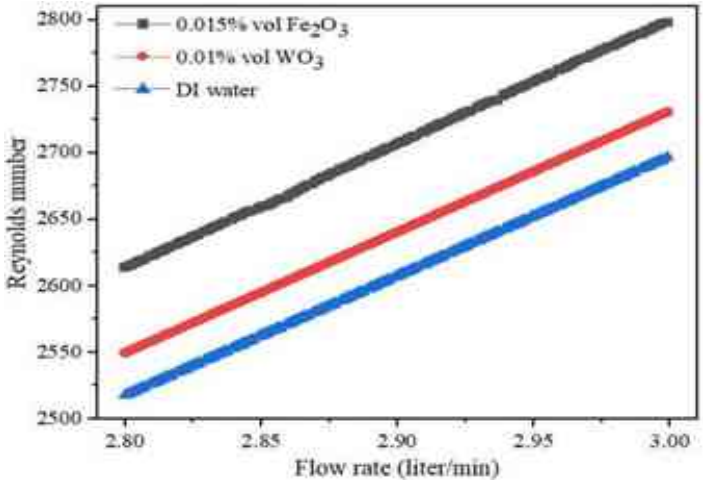

Figure 4.1: Effect of flow rate and volume concentration on Reynolds number

4.4.2. Heat transfer coefficient and heat transfer rate

An increment in the thermal conductivity of the fluid has a positive effect on the convective heat transfer coefficient, thus enhancing the Nusselt number. Increasing the mass flow rate of the nanofluids increased the heat transfer coefficient; thereby, the volume concentration of nanoparticles, inlet temperature, and flow rate contributed by an increment of the heat transfer coefficient of the working fluid. Figure 4.2 shows the heat transfer coefficient enhancement with Fe_2O_3 nanofluid at about 9.61%, higher than other studies [115] that used Fe_2O_3 and CuO/water at 0.15%, 0.4%, 0.65 vol%, and temperatures from 50 to 80 °C.

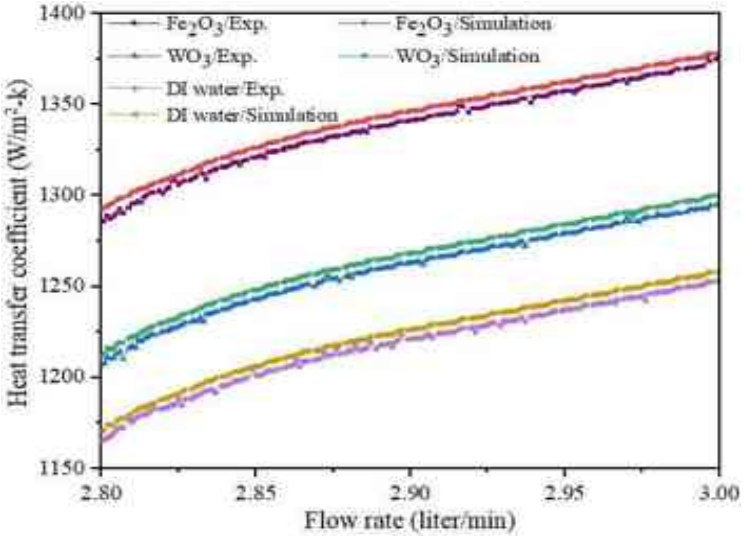

Figure 4.2: Influence of flow rate and inlet temperatures on heat transfer coefficient

Using WO_3 nanofluid at 0.01 vol% achieved an increment of heat transfer coefficient higher than DI water and less than Fe_2O_3 nanofluid by 6%. A slight variation was observed by the experimental and simulation results regarding the heat transfer coefficient of about 2% for the fluids used. Adopting a low concentration of nanoparticles into base fluid achieved better heat transfer characteristics and avoided agglomeration of nanoparticles into pipes. Depending on the thermophysical properties of nanofluids and DI water to determine the heat transfer rate for both fluids, it considered the volume concentration of nanoparticles suspended by water and its effect on the thermal behaviour of the liquid. The experiment was conducted under a temperature range between 61-63 °C with a fluctuation flow rate between 2.8-3 L/min. Fe_2O_3 nanofluid recorded increment by the heat transfer rate higher than WO_3 nanofluids and DI water by about 4.11% and 5.80%, respectively, due to the high potential of their thermal properties that positively reflected on the heat transfer performance from the boiler to the storage tank. Figure 4.3 indicates the difference in heat transfer rate between used nanofluids and DI water; the increment of heat transfer rate was uniform under the operating temperature range and flow rate at three hours, confirming the stability of the nanofluid used during the operation. Compared to another study by [116] that used silver nanoparticles mixed with water with 0.05 vol% as a nanofluid, it achieved an increment of the heat transfer rate of about 4.40%. In the present study, 0.015 vol% of Fe_2O_3 gives an increment of about 5.81% heat transfer rate, which indicates that Fe_2O_3 nanofluid can be a cooling fluid more efficient than WO_3 nanofluid that shows enhancement better than conventional cooling fluid. A slight variation in the heat transfer rate accentual during simulation compared with experimental results validate the measurement of experimental results.

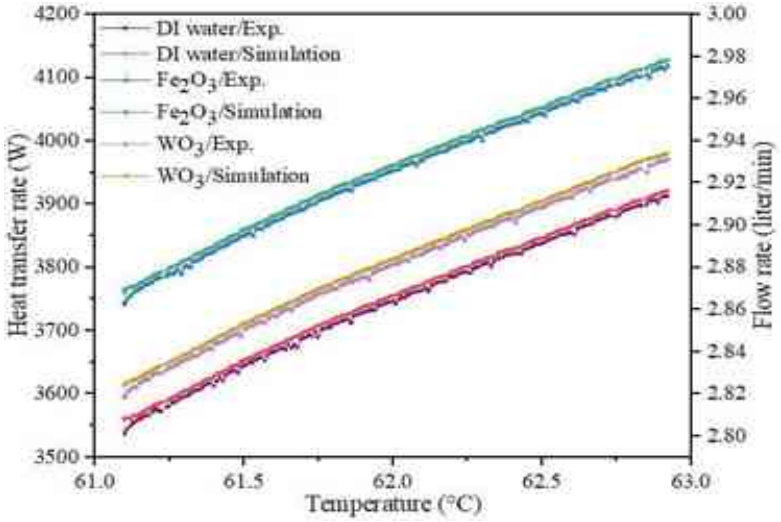

Figure 4.3: Heat transfer rate of working fluids at variation temperatures and flow rate

4.4.3 Nusselt number

Nusselt number is influenced by the volume concentration of nanoparticles and fluids temperature, as shown in Figs. B1.4 (a). The Nusselt number significantly increases with an increase in the temperature of the working fluids; it can be seen in the difference in the Nusselt number used Fe_2O_3 nanofluid compared to WO_3 nanofluid and DI water. Using Fe_2O_3 nanofluid led to an increment of Nusselt number about 6.21%, 8.51% higher than WO_3 nanofluids and DI water at a maximum temperature of 63 °C. It is evident in this study that three parameters significantly affect the Nusselt number: thermal conductivity of the working fluid, Hydraulic diameter, and heat transfer coefficient of the working fluid. Figure B1.4 (b). show the increase in the Nusselt number with an increase in mass flow rate; the range of flow rate help suspend nanoparticles in the base fluid, thereby more nanofluid stability. Compared with this study, an experiment conducted by [114] used aluminium nanoparticles mixed with water at 0.2 vol% and 0.3 vol % enhanced the Nusselt number by 3.37% and 5.08%. The present experiment used Fe_2O_3/DI water at 0.015 vol%, enhancing Nusselt number by 8.51%. A lower volume concentration of Fe_2O_3/DI water gave a high Nusselt number of Al/waters.

4.4.5 Conclusions

The volume concentration of nanoparticles, flow rate, and inlet hot fluid temperature influence an increase in Reynolds number. Increasing of volume concentration of nanoparticles cause an increased friction factor, while the increase of Reynolds number leads to a decrease in friction factor. Fe_2O_3 nanofluid achieved increment by Reynolds number of about 2.50% and 3.81% compared with WO_3 nanofluid and DI water. Furthermore, volume concentration, inlet temperature, and flow rate increase nanofluids' heat transfer coefficient by 9.60% and 6%, respectively, compared with DI water. Suspending 0.015 %vol of Fe_2O_3 nanoparticles into DI water led to an increment of Nusselt number by 6.2%, 8.5% higher than WO_3 nanofluids and DI water at a maximum temperature of 63 °C. A slight variation observed by the experimental and simulation results of about 2% confirms the accuracy of the results. Thus, lower volume concentrations have been adopted in this study to avoid the agglomeration of nanoparticles into pipes and avoiding increasing the viscosity of nanofluids viscosity causing more power consumption of the pump.

Chapter 5

Effect of passive and active cooling on the efficiency of the photovoltaic and photovoltaic thermal system

This chapter consists of four experimental case studies which applied new cooling techniques under hot conditions.
The first study investigates using evaporative cooling as a passive cooling technique to absorb the generated heat from the PV module and lower its temperature by using cotton wicks immersed in the water (CWIWs) attached to the backside PV module. CWIWs help decrease air dry temperature and increase humidity, then produce cool air that helps cool PV modules.
The second study investigates the effect of cotton wicks integrated with rectangular aluminium fins (CWIRAFs). Integrated aluminium fins with cotton wicks immersed in water from the top to the bottom help to increase the heat transfer area and the effective evaporative cooling at the back surface of the PV module. Under the same experimental condition, the passive cooling technique was compared with the active cooling of the PVT system, which used water as a cooling fluid. The cooling techniques' results are compared with other studies according to thermal behaviour, efficiency, and power yield to identify the appropriate cooling technique and calculate the payback period.
The third case is an investigation of using a new nanofluid zirconium oxide (ZrO_2) as a coolant at different volume concentrations dispersed in DI water to reduce the temperature of the PV cells. The nanofluid is circulated in the tubes of the heat exchanger attached to the backside of the PV module to absorb excess heat and then enhance the performance of the PV module. Thus, energy and exergy efficiencies of the PVT system have be analyzed from thermodynamic viewpoints to investigate the effect of the use of nanofluid on the PVT system entropy generation and exergy losses. Adding to the effect of dispersion of nanoparticles on heat transfer coefficient, Reynolds number, Nusselt number, fraction factor and pressure drop.
The fourth case is a proposed heat exchanger consisting of fluid circulating in a serpentine tube and a thermal absorber plate attached at the backside of the PV module to reduce the PV cell's temperature and enhance its efficiency. This case experimentally investigates the effect of employing a new nanofluid tungsten trioxide (WO_3) on a PVT system's energy and exergy efficiency at different volume concentrations 0. 5 vol%, 0.75 vol%, and 1 vol%. Then, the effects of increased volume concentration of nanoparticles on the heat transfer coefficient, Nusselt number and Reynolds number, and pressure drop.

5.1 Effect of evaporative cooling (cotton wicks immersed in the water) on photovoltaic module performance

The present work investigates using the evaporating cooling technique to absorb the heat generated at the backside of the PV by cotton wicks immersed in the water (CWIWs). The CWIWs help decrease air dry temperature and increase humidity, producing cool air and contributing to cool PV modules.

5.1.1 Cooling technique and instruments used

Two polycrystalline 50 W PV modules were used with dimensions of 0.65 m × 0.55 m. The first PV modules were equipped with CWIWs, while the second was used as a reference without

cooling to compare them during operation. The height of PV modules from the ground and the tilt angle (29°) allows great air to flow on the backside of PV modules. The current technique contributes to generating the evaporating cooling by exposure of the wetted cotton wicks to the surrounding air, which decreases dry air temperature and increases humidity, producing evaporating cooling that can exploit it to absorb the rising heat from the backside of the PV module. The experiment used cotton wicks (CWs), commonly used for lanterns or locally available lamps. The CWs have a high absorbent ability, which helps in the transmission and distribution of water to all CWs arranged at the backside of the PV module and is characterized by a suitable heat transfer coefficient and lower thermal conductivity, as shown in Table B2.1 The appropriate cost and ease of use made its application feasible compared to other techniques. \ The CWs were arranged as serpentine forms and attached to the backside of the PV module. The arrangements of cotton wicks avoided any space between them and were fixed by thermal silicon, as shown in Fig. 5.1. At the top edge of the PV module are eight ends of CWs immersed in the bottom of two plastic bottles full of water; this immersion method allows absorbing and transfer of the water from the top to the bottom of the PV module. The gravity-free flow of water helps transmit the water to the CWs without extra power.

Figure 5.1: A sight of the experimental setup, (1-4) thermocouples distribution on the surface of the PV module, (5-8) on the backside, (9) solar power meter, (10) ends of CWs supplier for water, (11) data logger, (12) electric supply, (13), plastic bottles

The temperature was measured through thermocouples installed at different PV module surfaces and backsides. Temperature, voltage and current were measured using a data logger multi-channel Arduino programmed to record the data. The data logger consisted of 17 thermocouples for measuring temperature, two sensors to measure the voltage and two current sensors. Table B2.2 shows the specifications of devices used for the measure used in all experiments conducted in Iraq. The data logger recorded the measured data with 10 min time step throughout the experiment days and saved the data in portable storage memory of 8 GB. Two 18-V lamps completed the electrical circuit between the PV module voltage and current sensors.

5.1.2 Results and discussion

The experiments were conducted according in August 2021. The solar radiation values were obtained throughout the experiment days; Fig. B2.1 shows the average solar radiation recorded at the beginning of the early morning; the solar radiation values increase until a higher value between 12:10 to 13 PM; after that, it decreases. Figure 37 also shows the average ambient temperature recorded during the experiment period, 43.8 °C, and according to (Iraqi Agricultural Meteorological Centre 2021), the average wind speed was between 2.84 - 6.64 m/s.

5.1.2.1 Energy analysis of the photovoltaic modules with and without cotton wicks immerse in water

The PV modules were equipped with thermocouples to investigate the thermal behaviour of the PV modules is an important issue conducted by fixed four (T_1, T_2, T_3, and T_4) thermocouples distributed in different places on the surface and other four (T_5, T_6, T_7, and T_8) thermocouples on the backside of the PV modules. Depending on the average temperature recorded for each 10 min for the PV modules and throughout the experiment periods, it could notice that the variation in the temperature on the surface and backside of the PV module recorded by thermocouples was very slight, as shown in Figs. 5.2 (a). The temperature of the PV module surface was higher than the backside due to being directly exposed to intense solar radiation. The PV module with CWIWs cooling showed thermal behaviour closer to the ambient temperature throughout the experiment due to evaporating cooling of CWs. The airflow on the wet surface of the cotton wicks has a major role in enhancing the evaporation process due to a convection mass transfer and decreasing the PV module temperature, enhancing the evaporation cooling rate. The highest temperature recorded of the PV module with the CWIWs was 46.1 °C at 12:20 PM, while the ambient temperature was 43.8 °C.

In contrast, it simultaneously increased the average PV module temperature without cooling to 56.4 °C during the experiment, as shown in Fig. 5.2 (b). Rising the temperature at this level causes the PV cell's performance degradation and drops the energy yield discussed in the next section. The wet CWIWs exposed to wind have provided adequate cooling that effectively reduces the PV module temperature to 10.3 °C, positively reflecting the PV module performance. The flowing of the air over the wetted surface of the cotton wicks causes water evaporates and cools the air that absorbs the heat from the PV module by forced convection and transfers it to air, which the productivity of the PV module enhances. The maximum output voltage and current obtained from the PV module without cooling were 8.9 V and 1.6 A, respectively, at 12:20 PM.

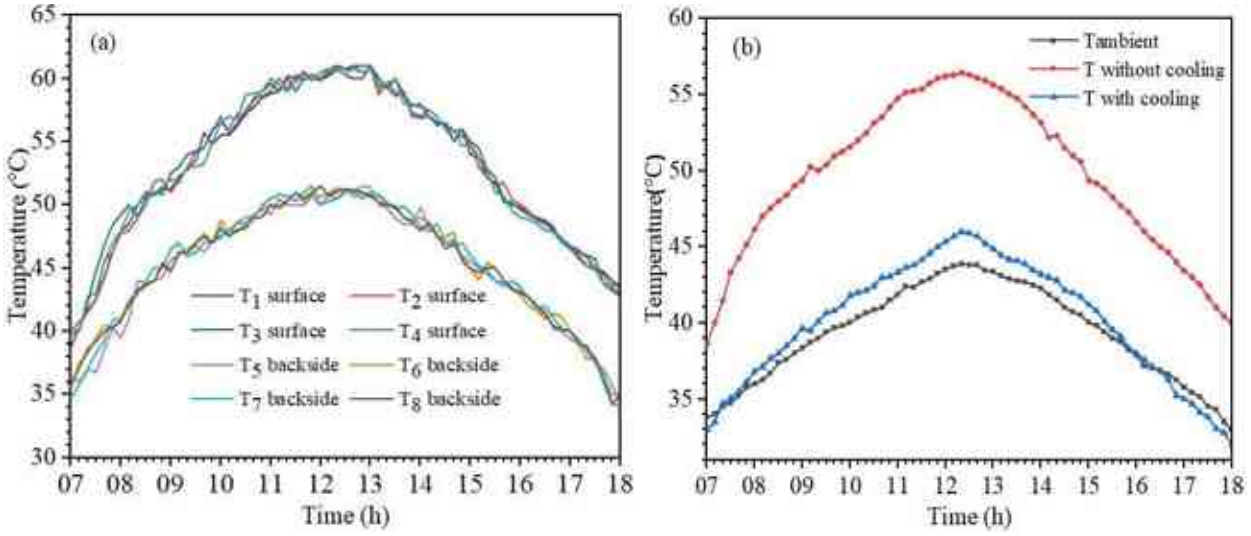

Figure 5.2: Temperature distribution on (a) PV module and (b) average temperature of the PV modules with and without CWIWs

Figure 5.3 (a) shows the maximum output power of the PV module without cooling was 14.2 W, which refers to the influence of an increase in the temperature on the PV module performance, and that was clear by dropping the efficiency to 3.41%, which confirmed the deterioration performance due to rising temperature. Moreover, the tilt angle of the PV module helps run-off of wind in the backside of the PV modules; the airflow on the wet surface of the cotton wicks has a major role in enhancing the evaporation process due to a convection mass transfer and decreases the PV module temperature. Used CWIWs improved the output power of the PV

module to 30.5 W due to an increase in the output voltage values and current to 16.3 V 1.872 A, respectively. Because the cotton bristles immersed in water and exposed to the wind have provided continuous cooling improved, the power yield with an increment of about 16.3 W compared without cooling. Figure 5.3 (b) shows the variation of the PV module's efficiency of both cooling and without cooling, maximum efficiency of the PV module with CWIWs being 7.25%. The mechanism of evaporative cooling used has enhanced the performance of the PV module better than in other studies conducted by [36,109 and 118] used different evaporation cooling techniques, which makes it more reliable for application. Table B2.3 shows the PV module performance compared with previous studies that used similar cooling methods to improve the PV module performance.

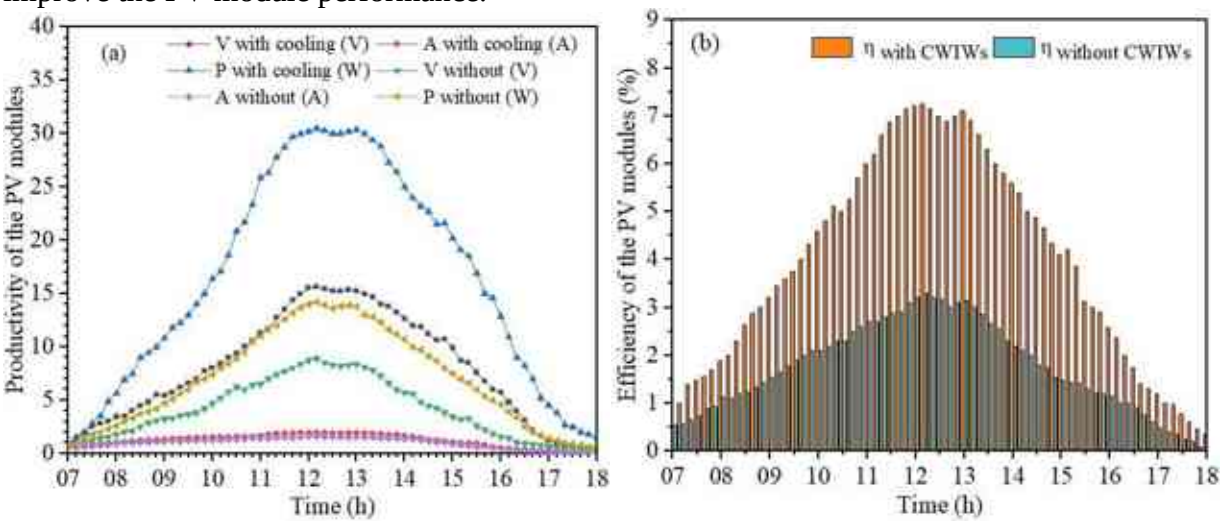

Figure 5.3: The variation value of (a) productivity of PV modules and (b) Efficiencies of the PV modules with and without CWWs

5.1.2.2 Exergy and entropy generation

Exergy analysis is important for estimating the real performance of the PV module. The maximum average PV module temperature without cooling was recorded at 56 °C at 12: 20 PM. The evaporating cooling helped absorb the generated thermal exergy and dissipate it into the surrounding air, reducing the PV module temperature. As mentioned in Eq (55), the output electrical power of the PV module is equal to the exergy electrical. Figure 5.4 (a) shows the relation of electrical exergy with temperature; it can observe the increment gradual of the electrical exergy and exergy efficiency with increased temperature until 56 °C. Maximum electrical exergy and exergy efficiency was 29.8 W, 7.21%; it was a slight variation from electrical energy and efficiency, as shown in Table B2.4, which confirms the effect of evaporative cooling on the performance of the PV module. Using CWIWs with a PV module reduces the exergy losses due to absorbing the heat generated by PV cells by the CWIWs and dissipating it to the surroundings. Based on the second law of thermodynamics, lowering the exergy losses affects the entropy generation in the PV module because of the irreversibilities. Figure 5.4 (b) shows the average entropy generation; using CWIWs leads to a decrease in entropy generation due to reducing the exergy losses exergy by about 14% lower than the PV module without cooling. The lower average entropy generation of the PV module with CWIWs compared to that of the PV module without cooling. Maximum entropy generation with CWIWs 8.45 W/°C and without cooling was 9.66 W/C at 12:20 PM; after that, it dropped with a lowering of the temperature. Comparing performance with and without passive cooling, the PV module that used CWIWs was distinguished with high performance during the experiment by achieving higher power yield and efficiency than the PV module without cooling. Water absorbed by cotton wicks with rising temperature led to created evaporation cooling helps absorb heat from the backside of the PV module. Figure B2.2 compares the PV module performance using

CWIWs and without; the PV module temperatures used CWIWs have a noticeable effect that contributed by decreasing about 22% of the PV temperature compared with the PV module without cooling. Reduction of the temperature effectively contributes to enhanced productivity of the PV module by incrementing the power yield of the PV module to 16.3 W.

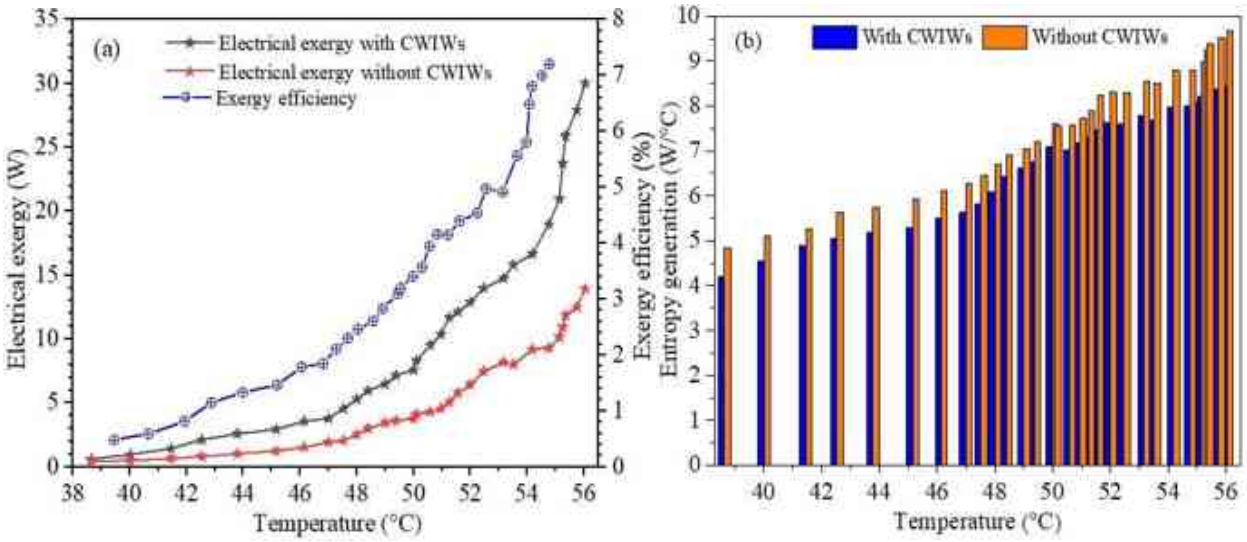

Figure 5.5: The effect of temperature on (a) electric exergy and exergy efficiency and (b) Entropy generation with and without CWIWs

. Due to the increase in output voltage and current of the PV module, the efficiency enhanced to 7.25% compared to cooling, which recorded 3.41% with 14.2 W output power. According to evaporating cooling, the generated heat at the backside of the PV module is absorbed and dissipated into the surrounding air. The electrical energy (output power) under evaporating cooling was the same as the electrical exergy at high temperatures. Enhancing the PV module performance is attributed to using CWIWs to provide the appropriate cooling, decrease the temperature, and increase the electrical exergy and exergy efficiency. It was observed that a significant deterioration in the PV module performance without cooling, thus negatively influence the power yield and efficiency in areas with hot climate conditions.

5.2 Effect of cotton wicks integrated with rectangular aluminium fins cooling on photovoltaic module performance

The present study investigates the effects of passive and active cooling on the PV module performance using different configurations (namely cotton wicks integrated with rectangular aluminium fins (CWIRAFs)) and photovoltaic thermal PVT collectors under hot conditions. Few studies on this method have been conducted with different techniques and operating conditions than the present research. Integrated aluminium fins by cotton wicks immersed in water from the top to the bottom help to increase the heat transfer area and the effective evaporative cooling at the back surface of the PV module, leading to temperature dissipation of the PV module into the surrounding air, then, improve its performance. The experimental results of each cooling technique applied are compared with other studies according to thermal behaviour, efficiency, and power yield to identify the appropriate cooling technique.

5.2.1 Cooling techniques used and experiment procedure

Cotton wicks (CWs) were attached with rectangular aluminium fins (RAFs) by thermal silicon and attached at the rear of the PV module by thermal silicon adhesive. Fins are used as a partial rectangle (i.e., 52 cm long, 3 cm wide, and 1.5 mm thick) and uniform distance between RAFs. CWs were arranged in serpentine on the backside of the PV module, and fins formed contiguously without space between them. Table B2.4 shows the specifications of the CWIRAF

components [119, 120]. The CWs are characterized by a suitable heat transfer coefficient, lower thermal conductivity, and high absorbent capacity, which helps to distribute water to all CWs attached behind the PV module without using extra power. In addition, it's locally available, cost-effective and does not require maintenance. A total of 11 CW ends were submerged at the bottom of three plastic bottles full of water to supply water to CWIRAFs during the experiment, as shown in Fig. B2.3 (a). The CW ends placed in the water tank continuously provide water from the top to the bottom of the PV module. Therefore, four thermocouples were placed on each of the surfaces of the PV modules at different places, three were placed on the backside, and one was used to measure ambient temperature. PVT solar collector consists of a PV module with a 9.5-mm diameter copper pipe arranged in serpentine and attached to an absorbent copper plate with 1.5-mm thickness placed on the rear side of the PV module. Copper pipes are covered by a layer of thermal wool insulation and aluminium cover. PVT collector uses water as a medium that enters and exits from an inlet and outlet of the collector. The outlet water passes via two copper pipes with small holes to re-cool the water before being collected in an insulated storage tank with 0.75 kg of ice added in the storage tank every 30 min. The storage tank cover is partially opened to enable air to circulate. The flow rate was 1.4 L/min, pumped by a tiny pump placed inside the storage tank. After that, two thermocouples were placed at the inlet and outlet of the PVT collector to measure water temperature.
Figure B2.3 (b) shows additional details of the system. The CWIRAF module and PVT collector performance are compared with conventional PV modules without cooling installed individually under the same operating conditions. The experiments were conducted from 25 June to 15 July 2021 in Iraq (latitude: 30.5˚; longitude: 48.14˚). The weather during the experiments was sunny with a clear sky, and there was no substantial variation in temperature during the experiment days. According to the Iraqi Agricultural Meteorological Center, the average wind speed was 1.9–6.6 m/s [121]. Solar radiation values increased gradually from the start of the experiment and decreased in the afternoon. Three 50-W polycrystalline PV modules were used with dimensions of 0.65 m × 0.55 m × 0.03 m. The modules have a tilt angle of 29˚. The distance between PV modules and the ground allows air to pass on the backside of PV modules, which boosts the rate of evaporative cooling because of a convection mass transfer. The output power (Pout) of the PV modules with CWIRAFs and PVTC is calculated by using Eq. (1) [38], depending on the output voltage (V_{out}) and current (C_{out}) of the modules obtained every 10 min.

5.2.2 Results and discussion

PV module with CWIRAFs was supplied with water for two hours to ensure that all CWs were wet before the experiment began. The start of the experiment was simultaneous with the beginning of sunrise when the value of solar radiation is low but increases with an increase in sunlight intensity. Figure B2.4 (a) presents the average solar radiation during the experiment, which gradually increases with operation hours until 12:30 PM. The maximum solar radiation recorded was 1157 W/m^2 but reduced progressively. Increasing the ambient temperature is associated with increased solar radiation intensity, in which the average ambient temperatures are variable along the experiment period. At the beginning of the experiment, the ambient temperature increased gradually, and the maximum ambient temperature reached 48.4 °C at 12:20 PM. After that, it decreased to 40.8 °C when the experiment was over. In July, most days are sunny with rising temperatures and dropping humidity with moderate winds, as shown in Fig. B2.4 (a).

5.2.2.1 Performance of photovoltaic module using cotton wick integrated with rectangular aluminium fins

Figures B2.5 (a and b) show the temperature distribution on the surface and backside of the PV module with used CWIRAFs and without cooling, respectively, throughout the experiment period. Temperature distribution on the sides of the PV module gives significant convergence,

and this reason is logical to depend on the average temperature of the PV module in calculations. The maximum temperature was recorded from 12:00 PM to 12:50 PM before decreasing until the end of the day. Figure B2.5 (c) shows the surface, backside and PV module's average temperature using CWIRAFs. By contrast, the PV module temperature without cooling was recorded at 80.2 °C, 72 °C for both sides and 76.1 °C the average temperature of the PV module. The evaporative cooling and increased heat dissipation area represented by integrating the rectangular aluminium fins with WC wicks have increased the heat transfer area of the PV module's backside and reduced the PV module temperature. Maximum temperatures for both sides of the PV module with CWIRAFs recorded at 12:30 PM were 54.2 °C and 49.8 °C, the maximum ambient temperature was 48.4 °C, and the average temperature of the PV module was 52 °C. The evaporative cooling in CW provides an appropriate cooling environment that lowers approximately 47.97% of the surface PV module temperatures compared with the PV module without cooling. Thus, evaporative cooling in CW has provided an appropriate cooling environment, leading to lowers of approximately 46.34% of the PV module temperatures compared with the PV module without cooling.

Figure B2.5 (d) presents the temperature variation of the PV module without cooling that increases to a critical scale, causing degradation of the PV module. The effectiveness of active cooling causes the backside of the PV module temperature to decrease below the ambient temperature at 2:50 PM, as shown in Fig. B2.5 (c), owing to reduced ambient temperature and increased wind speed. The decrease in the backside temperature was attributed to using CWIRAFs because of the effects of using evaporative cooling. PV module's power and efficiency values vary due to solar radiation and ambient temperature variables, and PV module temperature significantly affects its production, output voltage variation and current PV module. The CWIRAFs have enhanced the PV module's performance by reducing the temperature, which can be noticed in the increased output power shown in Fig. 5.6 (a). Compared with the PV module without cooling, the output voltage and current with CWIRAFs increased by approximately 55.40% and 25%, respectively. Therefore, the used passive cooling represented by CWIRAFs has achieved an impressive performance that increased the PV module's output power. Maximum output power was recorded at 34.75 W at 12:10 PM, an increase of 23.16 W compared with the PV module without cooling, and efficiency up to 8.63%. Figure 5.6 (b) shows the degradation of the PV module without cooling that affects its performance, which is evident by significantly dropping both its voltage and current. Increasing the PV module temperature to 76.11°C without cooling caused a significantly low output power of 11.59 W, representing maximum output power. The maximum efficiency of the PV module without cooling was recorded at 3.12%, attributed to the significant deterioration of the PV module performance. Note the PV module productivity and efficiency fluctuation, decreasing between 12:10 and 1:00 PM. After that, it increased but declined again until the experiment ended due to increasing temperature and direct solar radiation on the PV modules.

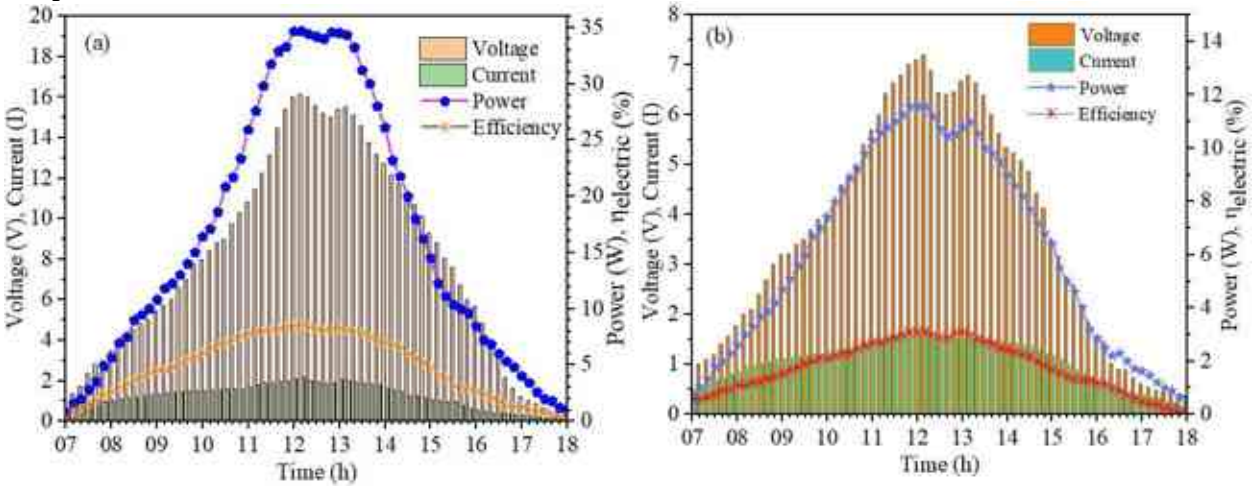

Figure 5.6: Performance of PV module with CWIRAFs (a) and (b) without cooling

5.2.2.2 Performance of the PVT system

Heat flows from the hot surface directly exposed to the intensity of solar radiation to the cold surface resulting in a higher backside temperature of the PV module than the ambient temperature. At the beginning of the experiment, the PVT system surface temperature was 41.4 °C, and the back side (absorb plate) of the PVT collector was 38.2 °C, but it gradually increased. The maximum temperature of the PVT surface was 67.2 °C at 12:20 PM. The backside was 55.4 °C, as shown in Fig. B2.6 (a). The used absorbing plate with water circulates into copper pipes attached to the backside of the PV module as active cooling has reduced the module temperature. Based on the average temperature, the surface and backside temperatures of the PVT collector were lower by approximately 19.30% and 29.70%, respectively, compared with the PV module without cooling. Decreased PV module temperature is attributed to conduction heat transfer from the copper plate directly attached to the backside of the PV module to copper pipes. After that, heat convection is transferred to water circulation into the pipes to reduce the PVT collector temperature. Figure B2.6 (b) shows the water temperature difference between the inlet and outlet water, in which the PVT collector recorded an average temperature reached 60 °C. Inlet water temperature slightly approached ambient temperature until 12:40 PM but decreased afterwards, affecting the thermal energy gained.

It can be noticed in the difference between inlet and outlet water temperatures. Using aluminium fins helps to increase the heat transfer area at the back surface of the PV module; integrating aluminium fins with cotton wicks immersed in water and exposed to the wind provides evaporative cooling that helps to reduce the temperature of the PV module. Thus, absorbing the temperature of the PV module and dissipating it into the surrounding air. Circulating the water into copper pipes attached to the absorbing plate removes the PV modules' excess heat. Thus, the temperature of PV cells was reduced because of increased heat transfer by conduction between the absorbing plate and the PV module backside. The yield energy of the PVT system improved compared with another PV module without cooling owing to the thermal conductivity of water that circulated, thereby facilitating the removal of a portion of excess heat from the PV module's backside. A reduction in the temperature of PV cells achieved increased productivity output voltage, current and power yield of the PVT collector, where the maximum output voltage and current were 14.5 W and 1.85 A, respectively, at 12:20 PM, with an output power of 26.8 W, as shown in Fig. 5.7 (a). However, reducing the PVT collector temperature has increased the electric efficiency by approximately 7.90%. The absorbed plate with pipes and water helps transfer the heat and achieve thermal efficiency, reaching 26.30%, as shown in Fig. 5.7 (b), thereby enhancing the PVT system performance by increasing the overall efficiency to 34.21%.

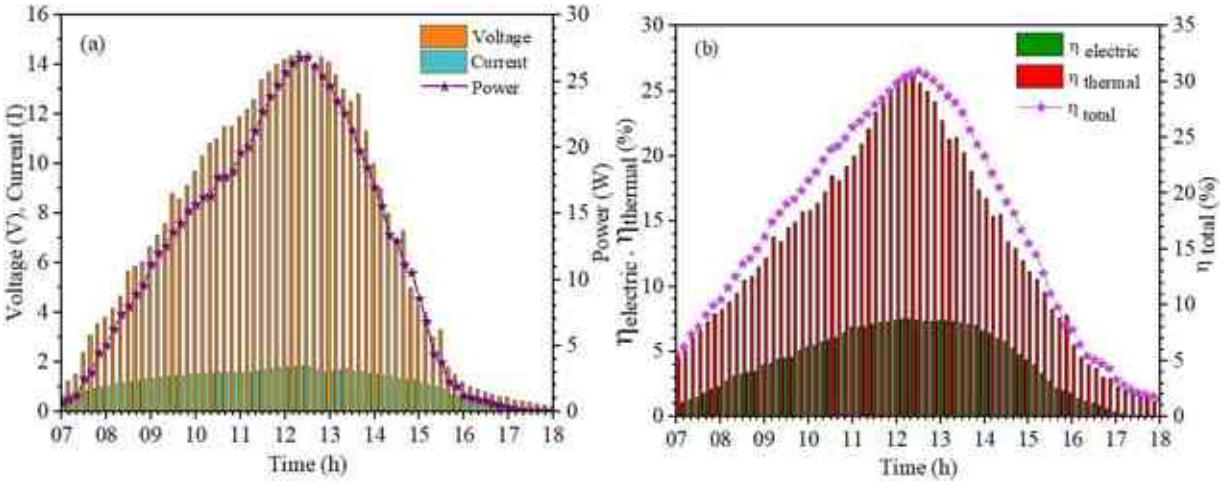

Figure 5.7: Performance of PVT collector (a) energy yield and (b) efficiencies

5.2.2.3 Comparison of performance under different cooling techniques

Increasing the PV cell temperature throughout the experiment affected the performance, particularly without cooling. The PV module output power and efficiency recorded lower values than active and passive cooling. The immersion of CWIRAFs in water with variable wind speed created a cooling environment during the experiment. It contributed to lowering the average temperature of the PV module by 46.34%, while active cooling reduced the PVT system temperature to 19.44% compared PV module without cooling, respectively, at maximum temperature. The CWIRAFs, as passive cooling, achieved better performance than active cooling due to the evaporative cooling with increased heat dissipation area by aluminium fins. Therefore, output power increased by 199.8% and using active cooling increased the output power by 133% compared with PV modules without cooling. The electric efficiency of the passive cooling was enhanced by 175%, compared with active cooling, which recorded an enhancement of 153.21% compared to the PV module without cooling at maximum temperature. Active cooling, represented by water circulation into copper pipes attached to the absorbing plate, facilitates heat removal from the PV module backside and converts to heat energy gained. The maximum thermal energy recorded by the PVT collector was 26.30%, which caused an increase in the overall efficiency of the PVT collector to 34.23%. Figure B2.7 shows the performance of the PV module under different cooling techniques. The PV module without cooling deteriorated performance due to the increasing PV cell temperature. The results obtained in the current study are compared with previous studies, considering factors such as the size of the PV/PVT system, type of cooling media applied, cooling configurations used, and measurement conditions, as shown in Tables B2.6 and B2.7. In the current study, passive cooling by CWIRAF shows better performance than active cooling concerning the reduced PV module temperature and enhanced performance, confirming the effectiveness of passive cooling.

5.2.2.4 Economic analysis of the passive cooling techniques

The purpose of economic analysis and the payback period is to give an effective cost estimation for the cooling techniques proposed [122]. The economic analysis and payback period of the conventional PV module with CWIRAF and conventional PV module have been calculated depending on maintenance, operation, CWIRAFs initial cost, and water supply cost. The net profit is calculated from Eq. (5.1), considering the cost of each element shown in Table 5.1. It can be observed that the payback period of the PV module with CWIRAFs cooling technique was less than the conventional PV module by 77 days. This is a reasonable reason that makes the cooling technique proposed economically effective.

Net profit = Energy produces cost (electric and thermal energy) -Nanofluid cost - Operation cost -Maintenance cost (5.1)

Table 5.1: Economic analysis of PV modules with CWWs and RAFs passive cooling

Element cost	CWWs cost in (IQD)	Conventional PV
Configuration	110000 IQD	90000
Maintenance	250 IQD/ day	115 IQD/day
Water supply	300 IQD /day	--------
Operation	280	0
CWIRAFs	20000 IQD	--------
Energy productivity	1592 IQD/day	522 IQD/day
Net profit	762	407
Payback period	144 days	221 Day

5.3 Effect of zirconium oxide nanofluid on the photovoltaic thermal system behaviour

Experimental investigation of using new zirconium oxide (ZrO_2) nanofluid and serpentine tubes soldered on absorb plate and placed at the backside of the PV modules. Circulating ZrO_2 nanofluid in serpentine tubes helps absorb high heat and enhance the performance of the PV module. Thus, the effect of different volume concentrations (0.015 vol%, 0.025 vol%, 0.0275 vol%) in DI water on energy and exergy efficiencies of the PVT system be analyzed from thermodynamic viewpoints. Then, the effect of dispersion of different volume concentrations of nanoparticles on heat transfer coefficient, Reynolds number, Nusselt number, fraction factor and pressure drop at flow rate 1 L/min.

5.3.1 Experimental setup and work procedure

The experiments were conducted on a typical sunny day from 7:00 am to 5:00 pm, with no significant variation in temperature and solar radiation during the experiment period. Three PV modules of 50 W type polycrystalline were used in this experiment. The first PV module was a reference without cooling, the second PVT module used water as a cooling medium, and a nanofluid cooled the third PVT module. The PVT modules consist of an absorber copper plate integrated at the backside of the PV module with copper pipes arranged in serpentine and fixed on the absorber plate. A thermal wool insulation layer has been placed on the copper pipes and then covered by an aluminium plate. Two copper coils were immersed in a water tank of 35 litres; the first one was connected between the copper coil and the outlet of the nanofluid to reduce the nanofluid temperature. The second was connected between the outlet water and copper coil, then inlet water as a close loop. Thermocouples are placed on the surface and backside of the modules to measure their thermal behaviour of them. A thermocouple was fixed at each inlet and outlet of the PVT modules to measure the variation in fluid temperature. The modules are fixed at a tilt angle of 29° towards the southern. Four thermocouples are distributed on each surface of the PVT modules, and three are on the backside. Thermocouples were placed in the inlet and outlet of the first and second PVT modules to measure the temperature of the cooling medium during the experiment period. Figure 5.8 below shows the experimental setup of the PVT modules.

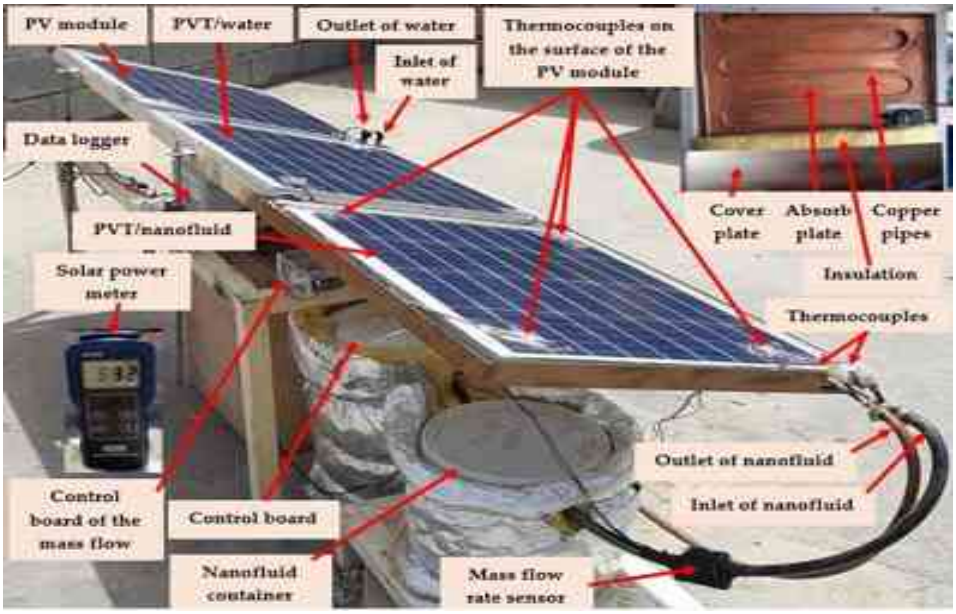

Figure 5.8: A view of the experimental setup

5.3.2 Results and discussion

5.3.2.1 Energy analysis results

Figure B2.8 (a) shows the recorded average ambient temperature and solar radiation values. The maximum ambient temperature was 42.7 °C, while solar radiation was 1004 W/m^2, specifically at 12:20 pm. According to the Iraqi agricultural meteorological centre, the average wind speed was 2.75-2.37 m/s [121] during the experiment days. The thermocouples distributed on the surface and backside for measuring the PV module's temperature show a very slight variation of the measured temperature. It has adopted the average temperature of the temperatures measured for both sides to assess the thermal behaviour of the PVT system considering the ambient temperature. Figure B2.8 (b) shows the variation of the average temperature of the PVT system at different volume concentrations of ZrO_2 fluids, compared with water as coolant and the reference PV module. The average temperature of the reference PV module was recorded at 58.2 °C; circulated DI water in the serpentine pipes attached to the backside of the PV module helped absorb the heat and reduced the PV module temperature by 9.72%. Circulate ZrO_2 nanofluids achieved a remarkable reduction in the PVT system temperature. The gradual increase in the volume concentration of the ZrO_2 nanofluid is accompanied by a noticeable decrease in temperature. At volume concentrations, 0.015 vol%, 0.025 vol%, and 0.0275 vol%, the PVT system temperatures have been reduced to 14%, 18.10% and 21.23%, respectively. Thereby, improving the thermal conductivity of fluids leads to increased heat absorption at the backside of the PV module; using ZrO_2 nanofluid has achieved higher heat absorbed from the PV module than water.

Figure 5.9 (a) confirms the necessity of having a cooling system to enhance the performance of the PV module. It can be observed that the electrical power output of the reference PV module is at a minimum level compared to others that have been coolant. Reduced PV module temperatures effectively contribute to enhancing their performance due to cooling. The increased volume concentration of ZrO_2 nanofluid with a constant mass flow rate of 1 L/min gradually increased the electrical power output. The maximum electrical power of the reference PV module was recorded at 18 W. Using nanofluids at different concentrations of 0.015 vol%, 0.025 vol%, 0.0275 vol% incremented the electrical power output by 11.4 W, 14.7 W and 15.72 W, respectively, compared to DI water that recorded 8.5 W. Figure 5.9 (b) shows the effect of volume concentrations of ZrO_2 nanofluids and water on the enhancing of electrical power, replacing nanofluid with water resulted in a noticeable enhancing due to their thermal properties. The electrical power increment by 15.72 W at 0.0275 vol% compared with DI water. The electrical power output enhancement is positively reflected in the electrical efficiency of the PVT system. Figure 5.9 (c) indicates the growth in the electrical efficiency with increasing volume concentrations of the ZrO_2 nanofluids. At 0.0275 vol%, the electrical efficiency of the PVT system was enhanced by around 54% compared to DI water. Thermal efficiency is an important parameter to evaluate the thermal performance of a PVT system which is affected by the temperature, design of the cooling system applied and type of cooling fluid.

Figure 5.9 (c) show the values of thermal efficiency at different volume concentration; during the experiment's days, the thermal efficiency starts with a low value and then increase to reach a maximum value at noon and then drop until the end of the experiment. Increasing the volume concentration of ZrO_2 nanoparticles in base fluid enhanced the heat removal capacity because of the increased thermal conductivity and convection heat transfer coefficient of the ZrO_2 nanofluid. Thereby the overall efficiency of the PVT system has been boosted by 8.91%, 18.81% and 24.43%, respectively, compared with DI water cooling at 0.0275 vol%. The effect of increasing the volume concentration of ZrO_2 nanoparticles in base fluid and Nusselt number as a function of Reynolds number has been investigated.

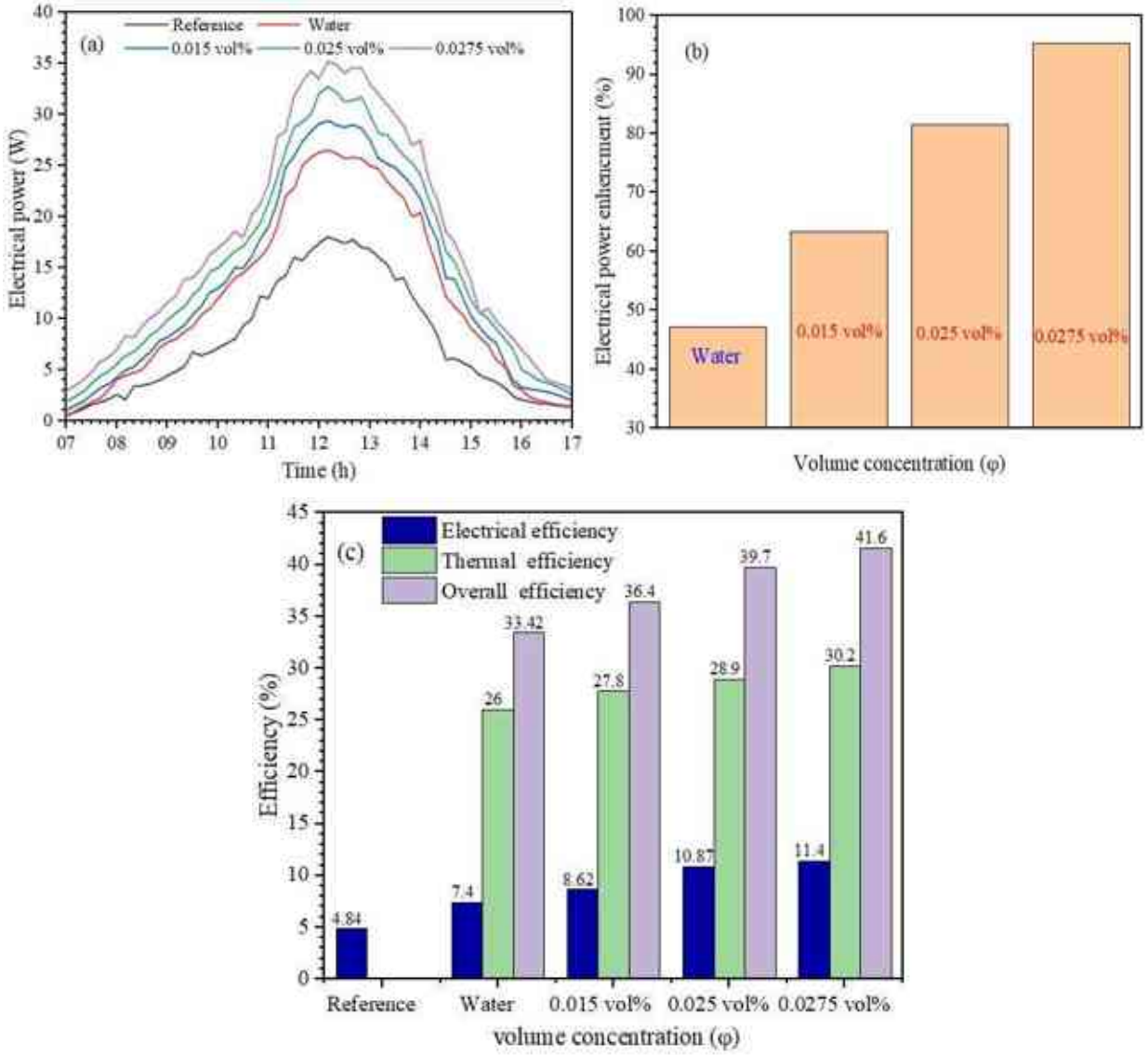

Figure 5.9: The performance of the PVT system Electrical power (a), (b) electrical power-enhancing and (c) overall efficiency as a function of volume concentration

Figure 5.10 (a) shows an increase in the Nusselt number, with Reynold's number increasing due to a gradual increase in the volume concentration of ZrO_2 nanoparticles. Dispersion of ZrO_2 nanoparticles in the base fluid has enhanced the Nusselt number at a maximum value of about 51.71% at 0.0275 vol% compared to the DI water and then enhancement of the thermal properties of the cooling fluid. The increment of Reynolds number leads to an increased heat transfer coefficient of the nanofluid due to enhancing the thermal conductivity of the nanofluid.
Figure 5.10 (b) shows the heat transfer coefficient values with Reynold's number at different volume concentrations. Compared with DI water, the maximum enhanced heat transfer coefficient is 13% at 0.0275 vol%; thus, ZrO_2 nanofluids can increase the heat transfer coefficient, positively reflecting a lower PV temperature than DI water. Increasing the volume concentration enhances the thermal conductivity of nanofluid and increases the density, which affects the pressure drop. Fig. 5.11 (a) shows the effect of increased Reynolds number and volume concentrations in the pressure drop; it can notice increased pressure drop by using ZrO_2 nanofluid to 31.52% compared with DI water which was less due to the low flow resistance of DI water. Figure 5.11 (b) shows the effect of increased volume concentration and Reynolds number on the decrease of friction factor. Compared with DI water, the fraction factor of ZrO_2 nanofluid was high, returning to the increased nanofluid viscosity. At a high Reynolds number

with 0.1% volume concentration, the friction factor was 0.37 higher than DI water, which recorded 0.29 due to lower density.

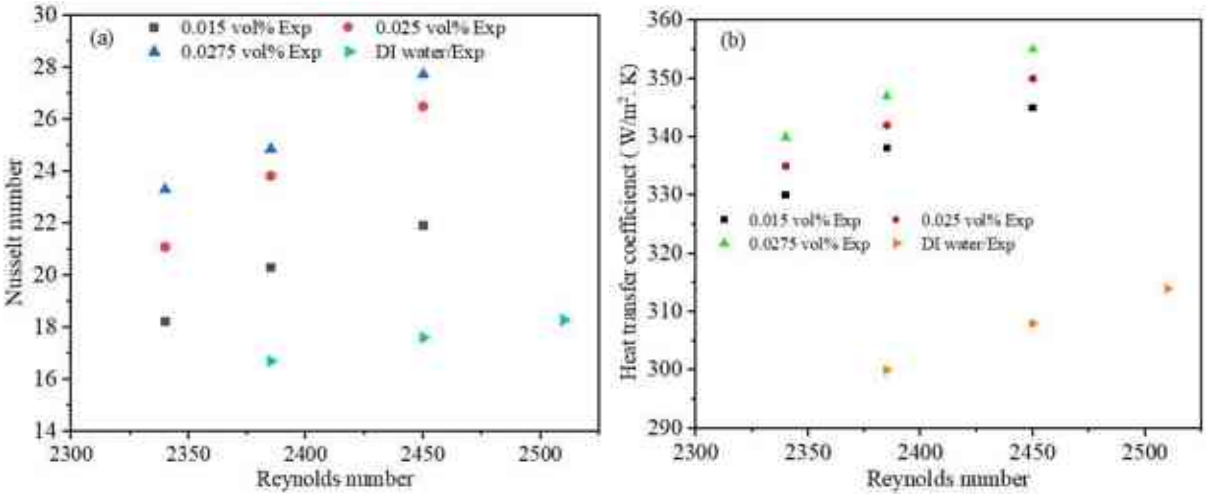

Figure 5.10: Effect of Reynolds number and volume concentration on (a) Nusselt number and (b) heat transfer coefficient

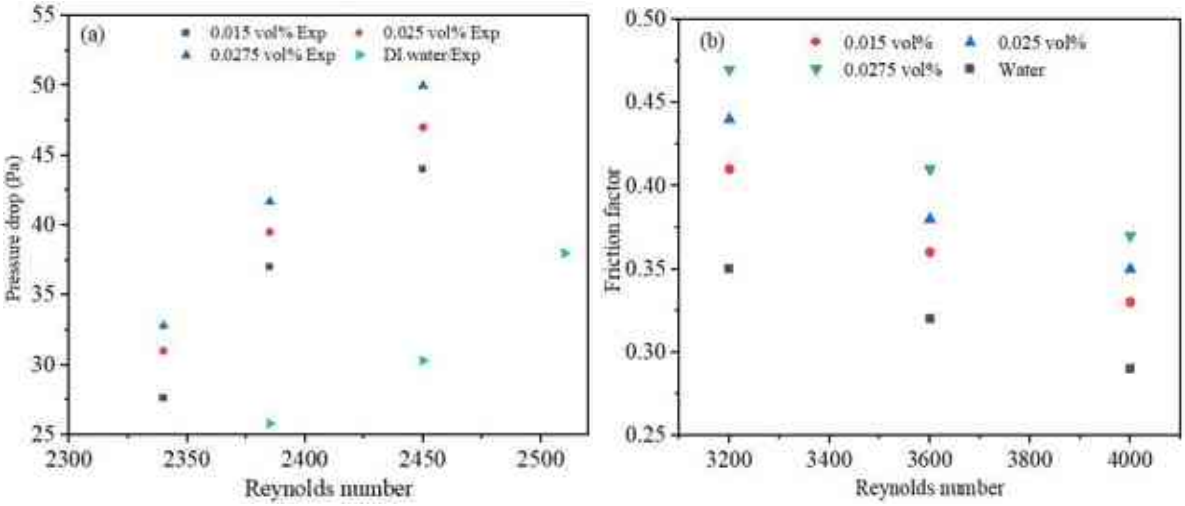

Figure 5.11. Effect of Reynolds number and volume concentration on (a) fraction factor and (b) pressure drop

5.3.2.2 Exergy analysis results

Depending on the second law of thermodynamics, this subsection evaluates the effect of using ZrO_2 nanofluid and water on the thermal exergy and electrical exergy efficiency, entropy generation and exergy losses of the PVT system. Based on Eq. (40), the inlet exergy from solar irradiation has been calculated for the maximum, average and minimum solar exergies during experiments days to be 997 W/m^2, 668.33W/m^2 and 328.58 W/m^2, respectively. Figure 5.12 (a) shows the value of the thermal exergy that was significantly lower than the electrical exergy due to the closer of the fluid outlet temperature of the PVT system to the ambient temperatures. The output thermal exergy is influenced by the specific heat of the working fluid and mass flow rate. Due to the high thermal properties of the nanofluid, it was noticed that the thermal exergy is enhanced more with the ZrO_2 nanofluid than with water. To evaluate the quality of the thermal and electrical efficiencies, Fig. 5.12 (b) shows the effects of ZrO_2 nanofluid on the PVT system's thermal and electrical exergy efficiencies. The low thermal exergy value significantly affects the thermal exergy efficiency; however, a relative increment of the thermal exergy was noticed by increases in the volume concentrations of ZrO_2 nanofluid compared with DI water. The overall

exergy efficiency is impacted by the thermal exergy efficiency, the electrical exergy efficiency, the exergy of solar radiation and ambient temperature. Thereby, the exergy efficiency effectively contributes to the increment of the overall exergy efficiency of the PVT system; the maximum overall exergy efficiency obtained at 0.0275 vol% is 11.86% while cooling by DI water was 7.11%, which confirms the feasibility of ZrO_2 nanofluid as a working fluid. Using nanofluids as a coolant for the PVT system instead of conventional fluids helps enhance the performance of the PVT system due to its high thermal conductivity that increases the convective heat transfer. Evaluation of each thermodynamic system's exergy loss and entropy generation is important for specifying the system losses and irreversibilities. In this case, the exergy loss of the PVT system was calculated using Eq. (40) with ZrO_2 nanofluid and DI water.

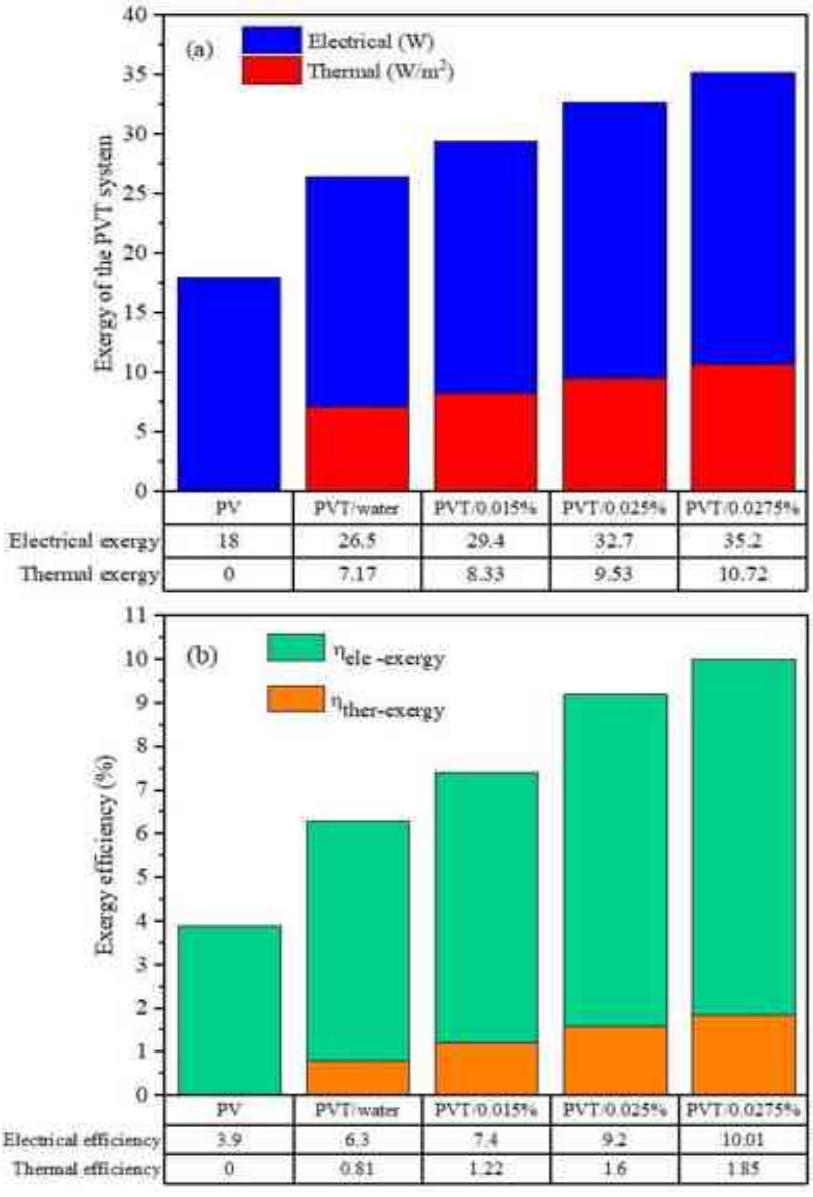

	PV	PVT/water	PVT/0.015%	PVT/0.025%	PVT/0.0275%
Electrical exergy	18	26.5	29.4	32.7	35.2
Thermal exergy	0	7.17	8.33	9.53	10.72

	PV	PVT/water	PVT/0.015%	PVT/0.025%	PVT/0.0275%
Electrical efficiency	3.9	6.3	7.4	9.2	10.01
Thermal efficiency	0	0.81	1.22	1.6	1.85

Figure 5.12: Exergy of the PVT system (a) electrical and thermal exergy (b) electrical and thermal efficiency

Figure 5.13 (a) and (b) show the high exergy losses of the PVT system and PV module without cooling due to a drop in the overall exergy efficiency of the systems lower than the input exergy, specifically thermal exergy efficiency and increased temperature of the PV module surface. Table B2.8 highlights the important results obtained by cooling with ZrO_2 nanofluid.

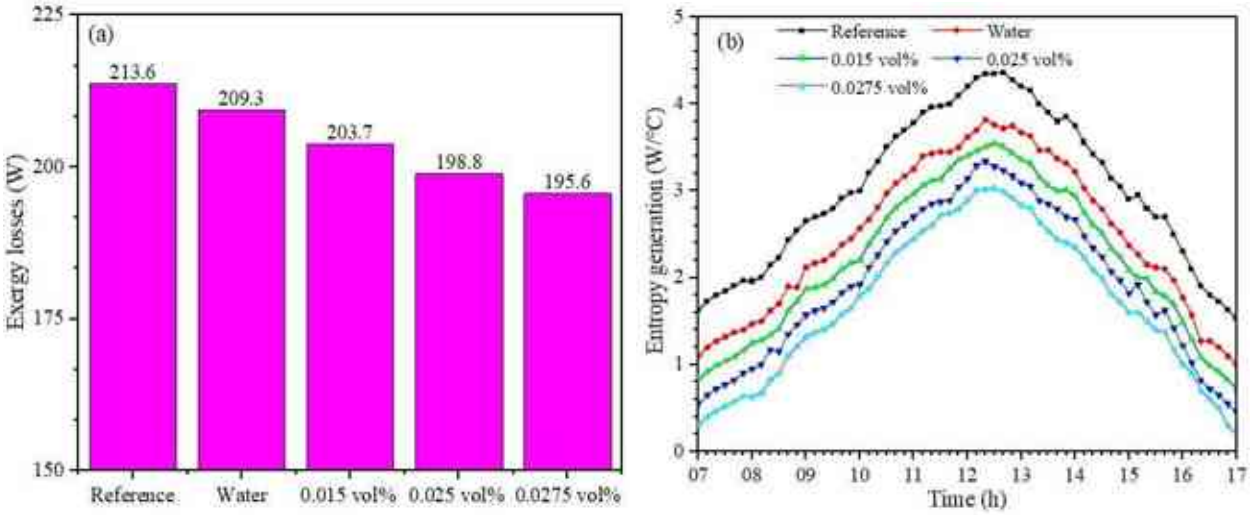

Figure 5.13: Exergy evaluation of the PVT system (a) exergy losses (b) entropy generation

5.4 Energy and exergy assessment of PVT system using tungsten trioxide nanofluid

This work aims to experimentally study the effects of a new metal-oxide WO_3/DI water nanofluid as a cooling fluid for a PVT system on electrical power generation and overall efficiency at different volume concentrations and constant flow rates. Moreover, exergy analysis of the PVT system and the effects of using WO_3/DI water nanofluid on the entropy generation and exergy losses have been evaluated and discussed.. The current work experimentally investigates the effect of using tungsten trioxide (WO_3) nanofluids on a PVT system's energy and exergy efficiency at different volume concentrations 0. 5 vol%, 0. 75 vol%, and 1 vol%.

5.4.1 Results and discussions

Figure B2.9 presents the average daily weather data measured during the experiments for every 10 mins, where the average ambient temperature was 43.3 °C, and the maximum incident solar radiation was 1014 W/m^2. The variation of the ambient temperature and solar radiation can be observed with a maximum ambient temperature and solar radiation recorded at 12:20 PM, which gradually dropped until the end of the experiment.

5.4.1.1 Energy analysis

The surface temperature increment of the reference PV module is noticeable due to direct exposure to solar radiation and the ambient temperature, reaching 58.8 °C. Figure 5.14 (a) shows the thermal behaviour of the PVT system under different volume concentrations of nanoparticles in the base fluid. The difference in the PVT system temperature can be noticed when cooling by DI water and WO_3 nanofluid. The temperature of the PVT system module is high with the base fluid and reduced more with the rising concentration of nanoparticles in the base fluid. Increasing the volume concentrations of nanoparticles in base fluid causes an increase in its thermal conductivity and then increases the nanofluid heat transfer coefficient. Thus, removing more heat from the PVT system through fluid circulation. The PVT system temperature was reduced using the DI water and WO_3 nanofluid at different volume concentrations (0.5 vol%, 0.75 vol%, and 1 vol%) by 9.91%, 13%, 18%, and 21%, respectively. The electrical power output is directly influenced by the operating temperature of the PV cells. Therefore, reducing the PVT system temperature reflects on the electrical power generation. Figure 5.14 (b) shows the effect of cooling by water and nanofluid at a different vol% on the electrical power output of the PVT system with time. The results indicated that using WO_3 nanofluid enhanced electrical power by decreasing the temperature of the PVT system. The maximum electrical power of the reference PV module was recorded at 17.84 W, which shows that the rise in the PV module

temperature has lowered the generated electrical power by the PV module. On the other hand, using WO_3 nanofluid at different concentrations (0.5 vol%, 0.75 vol%, 1 vol%) gradually increased the electrical power by 7.87, 9.95, and 11.15 W, respectively, compared to the reference PV module. The electrical power generation increment of the PVT system was attributed to the increased volume concentration of nanoparticles in the base fluid by 44%, 55.73%, and 62%, respectively, and with DI water by 35.90% compared to the reference PV module. WO_3 nanofluid has enhanced the heat removal capacity due to the increased convection heat transfer coefficient of the WO_3 nanofluid.. Increasing the volume concentration of WO_3 nanoparticles in the base fluid (0.5 vol%, 0.75 vol%, 1 vol%) caused an increment in the electrical efficiency by 31.60%, 48.30% and 52.31%, respectively, compared to DI water cooling.

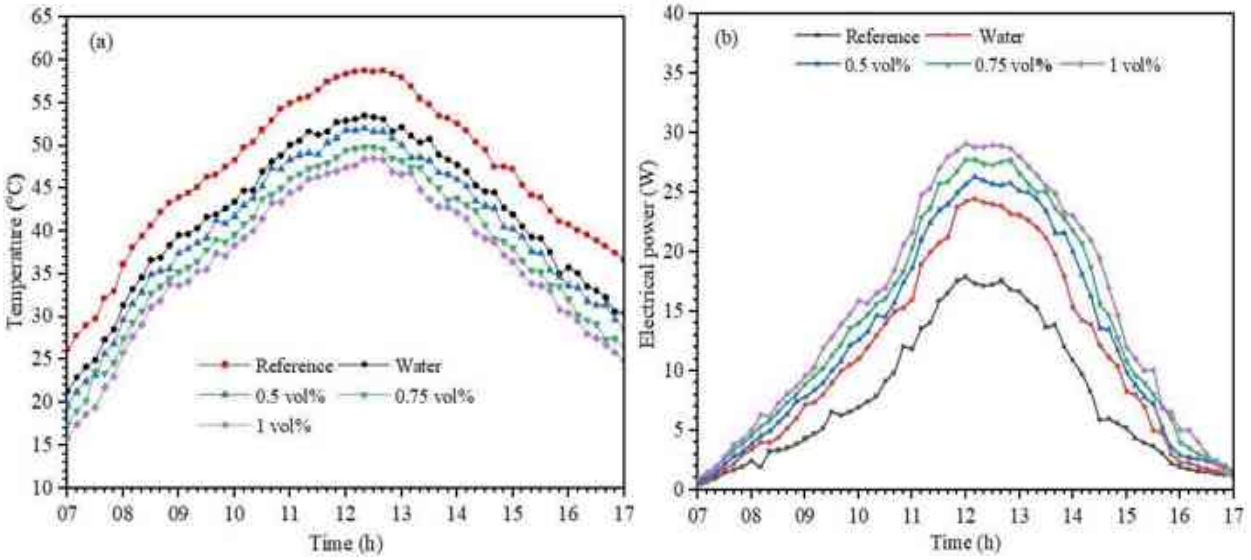

Figure 5.14: The average temperature of the PVT systems (a), (b)The electrical power output of the PVT modules.

Figure 5.15 shows the gradual increment in the thermal efficiency of the PVT system at different volume concentrations. The maximum thermal efficiency was 30.11% at 1 vol% compared with the cooling by DI water. This boosts the overall efficiency of the PVT system by up to 39.29% at 1 vol% compared with cooling by DI water. The increase of Reynolds number and volume concentration of WO_3 nanoparticles in the base fluid has been investigated to show the influence on the Nusselt number, heat transfer coefficient, friction factor and pressure drop. Figure B2.10 (a) shows the Nusselt number as a function of Reynold's number, and it can observe an increase in the Nusselt number with an increase in the value of Reynold's number at a gradual increase in the volume concentration. Adding WO_3 nanoparticles in the base fluid has enhanced the Nusselt number in which the maximum enhancement was about 51.21% at 1 vol% compared to the DI water. Dispersion of WO_3 nanoparticles in the base fluid leads to an enhancement of the thermal properties of the cooling fluid. The WO_3 nanofluid has higher Nusselt numbers than the base fluid, which positively increases the heat transfer efficiency. Figure B2.10 (b) indicates the variation of heat transfer coefficient values with Reynold's number at increased volume concentrations due to an increase in the thermal conductivity of the nanofluid. The increment of Reynolds number significantly increased the heat transfer coefficient of the nanofluid. In this regard, the heat transfer coefficient is enhanced by 5.30% compared to DI water at 1 vol%, consequently, nanofluids can increase the heat transfer coefficient and contribute to lower PV temperature more than DI water. Increasing the volume concentration of nanoparticles in the base fluid increases the nanofluid's density and thermal conductivity, which affects the pressure drop. Figure B2.11 (a) shows the decrease of friction factor with the increase of Reynolds number and volume concentration of WO_3 nanofluid. The friction factor of WO_3 nanofluids was

high due to the increased viscosity of nanofluids, more than that of the DI water. The friction factor decreases with the increased Reynolds number by 4.52%, 9% and 13.60%, respectively, at volume concentrations of 0.5 vol%, 0.75 vol% and 1 vol%. The concentration of nanoparticles in the base fluid increased the nanofluid's density and thermal conductivity, which impacted the pressure drop.

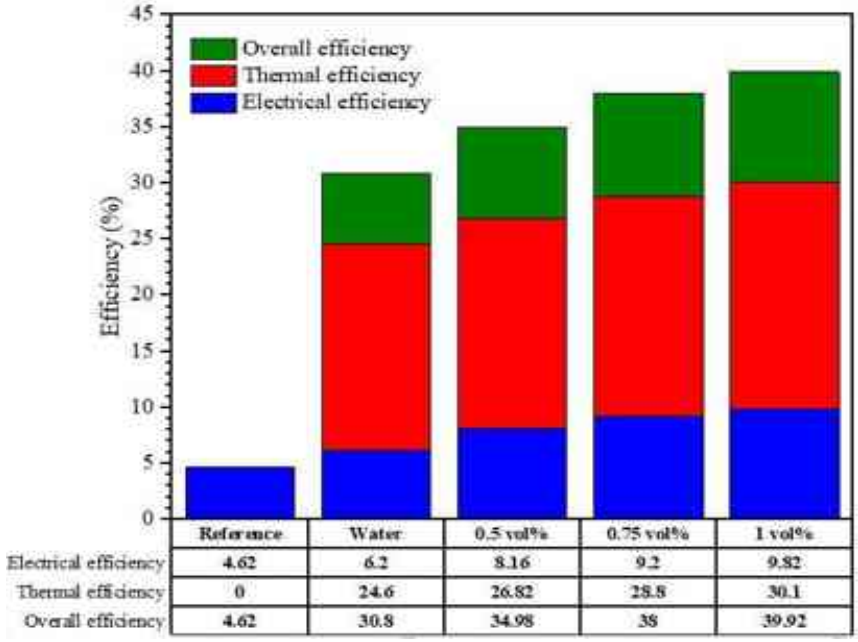

	Reference	Water	0.5 vol%	0.75 vol%	1 vol%
Electrical efficiency	4.62	6.2	8.16	9.2	9.82
Thermal efficiency	0	24.6	26.82	28.8	30.1
Overall efficiency	4.62	30.8	34.98	38	39.92

Figure 5.15: The overall efficiency of the PVT systems against the reference PV module

Figure B2.11 (b) shows the pressure drop increment with the increased Reynolds number at different volume concentrations. On the other hand, the increase in both density and viscosity has increased the pressure drop in the nanofluid compared with the base fluid. Besides, increasing the pressure drop of the nanofluid resulted from the flow resistance of nanoparticles compared to the case of the base fluid. Thus, the increased volume concentration and Reynolds number increased the pressure drop to 49.21% at 1 vol%, compared with the DI water.

5.4.1.2 Exergy and entropy generation results

This section assesses the effect of WO_3 nanofluid and water on the PVT system's exergy efficiencies, losses and entropy generation. According to Eq. (40), the input exergy of the solar radiation to the PVT system is calculated during experimental days wherein the maximum, average and minimum solar exergies were 947, 672.33 and 336.13 W/m^2, respectively. Figure 5.16 (a) shows the thermal exergy of the PVT system, which recorded a lower value than the electrical exergy, attributed to the close fluid outlet temperature to the ambient temperature. Furthermore, thermal exergy is impacted by the thermophysical properties of the nanofluid, such as the specific heat and the high thermal conductivity. Figure 5.16 (b) shows the effect of WO_3 nanofluid and DI water on the PVT system's thermal and electrical exergy efficiencies. The thermal exergy efficiency was remarkably low compared to the electrical exergy efficiency. This is attributed to the low quality of the thermal energy due to converging the outlet fluid temperature to ambient temperature, which was confirmed by our previous study [123]. Circulating the WO_3 nanofluid into the serpentine tube enhances the electrical exergy by reducing the PV module temperature and positively enhancing the electrical exergy efficiency. Increasing the vol% of WO_3 nanoparticles (0.5 vol%, 0.75 vol%, 1 vol%) in the base fluid has raised the electrical exergy efficiency by 26.90%, 42%, and 50%, respectively, to the DI water cooling. The evaluation of exergy loss and entropy generation is an important parameter in the PVT system for specifying their losses and irreversibilities.

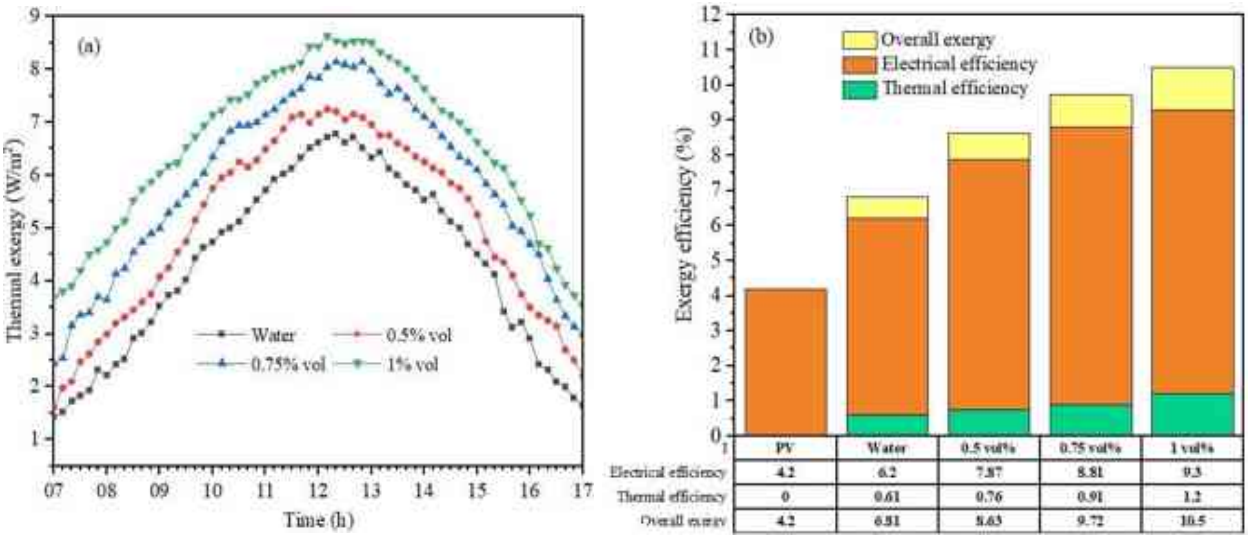

Figure 5.16: Average thermal exergy of the PVT system (a), (b) Average electrical and thermal exergy efficiency of the PVT system

According to Figure 5.17, the exergy loss in the reference PV module was high compared to the PVT system due to the cooling technique used in the PVT system. Moreover, using WO_3 nanofluids has effectively reduced the exergy loss due to enhancing the heat transfer coefficient. Compared to the reference PV module, a gradual increase in WO_3 nanoparticles vol% has reduced the exergy loss by 15.32% at 1 vol% due to the heat transfer enhancement. Minimizing the entropy generation rate is significant for determining the system's operating conditions and reducing the lost work. Increasing the temperature of the PV module increases the heat transfer between the system and the environment, thus, increasing the entropy generation. In the PVT system, entropy generation is affected by heat transfer and fluid friction into the PVT system. Figure 5.17 shows a substantial drop in the entropy generation value compared to the reference PV module due to the enhanced thermal properties of the WO_3 nanofluid. The gradual reduction of the entropy generation when using WO_3 nanofluid reached 53.51% compared to the reference PV module. Table B2.9 highlights the important results obtained by cooling with WO_3 nanofluid.

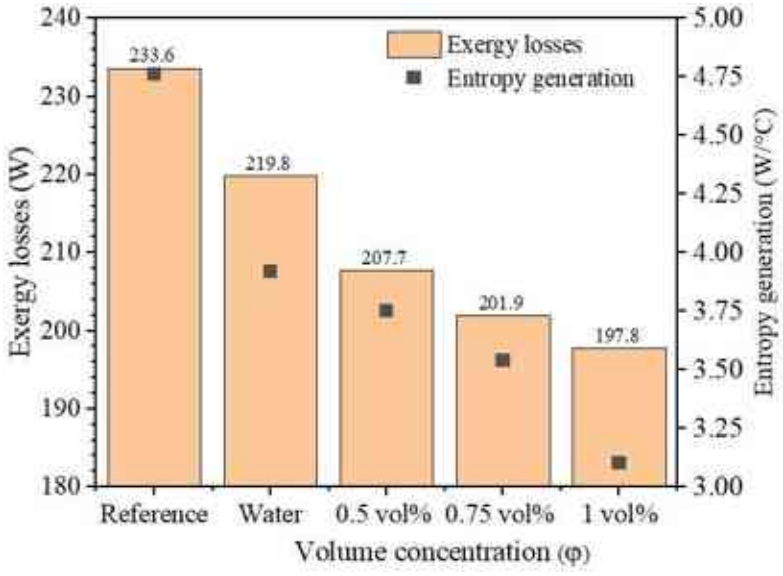

Figure 5.17: Exergy losses and entropy generation of the PVT system at different concentrations against the PV module

5.2.3 New contributions results

Contribution 2

The passive cooling applied in the first case showed sustained performance of the PV modules in hot conditions. The energy yield, efficiency and exergy analyses were investigated based on the results of the experiment as follows:

- The CWIWs attached to the backside of the PV module contributed to reducing the PV module temperature by 22% compared with the PV module without cooling. The moist condition resulting from the cotton bristles immersed in water and exposed to the wind has provided appropriate cooling that enhances efficiency to 7.25% and the power yield increment of about 16.31 W. The CWIWs technique applied has a lower cost and easy configuration with less water consumption.
- Using CWIWs decreases the entropy generation of the PV module by 14.32% due to reducing the losses exergy by 14% of the PV module compared to the PV module without cooling. The exergy efficiency of the PV module with evaporating cooling was higher than that of the PV module without cooling. The electrical energy (output power) was the same as the electrical exergy.
- The passive cooling enhanced the PV module's performance higher than in another similar study, making it more reliable for application.
- Significant power yield deterioration and the PV modules' efficiency were observed due to the PV cell's temperature increase to 56.4 °C.

Contribution 3

- Increasing the heat dissipation area of the back surface of the PV module by aluminium fins integrated with wet cotton bristles and exposed to air created a cooling environment during the experiment period, lowering the PV module's average temperature. The following conclusions are derived from the present work, as follows:
- The CWIRAFs passive cooling technique shows improved behaviour and significantly enhances the PV module performance by lowering its temperature by 137.78% than the active cooling technique.
- Reducing PV module temperature using the CWIRAF technique increased the power yield and efficiency by 13.78% and 8.86%, respectively, compared with the PVT collector.
- The active cooling technique showed lower performance than passive cooling under similar conditions. This result is attributed to heat transfer across different PVT collector layers, not directly, such as CWIRAFs cooling.
- The PVT collector enhances thermal energy by removing excess heat from the PV module's backside by circulating water inside pipes, improving the overall efficiency of the PVT collector.
- The economic analysis of the PVT system has achieved a good payback period within a short period compared with the conventional reference PV module, which confirms the feasibility of the cooling approach used. The cooling technique applied may be feasible for small installations of PV modules, such as a family house system.

Contribution 4

The second case investigated the effects of cooling PV modules using ZrO_2/water nanofluids and water on their thermal behaviour, energy, exergy and thermal parameters. Based on the results, the conclusions are summarized as follows:

- Improving the thermal conductivity of ZrO_2 nanofluid increases the heat absorption at the backside of the PV module, then reduces the PV module temperature to 21.20% compared to water. Reduced the PV module temperature effectively increased the electrical power to 33.72 W. The electrical and thermal efficiency was enhanced by using nanofluids, which

positively reflected the overall efficiency of the PVT system increased to 60% compared with water at 0.0275 vol%.

- Increasing the volume concentration of ZrO_2 nanoparticles in the base fluid increased Reynolds number has enhanced the heat transfer coefficient and Nusselt number due to the increase in the thermal conductivity of the nanofluid. On another side, the density and viscosity have increased, which causes reduced friction factors and increased pressure loss.
- Exergy analysis indicates lower thermal exergy of the PVT system than electrical exergy, which is attributable to the closing of the fluid outlet temperature of the PVT system to the ambient temperatures.
- The overall exergy efficiency is affected by the thermal and the electrical exergy efficiencies, which incremented with using nanofluid by 11.86 at 0.0275 vol% compared with water due to the high thermal conductivity enhancing of the convective heat transfer.
- Exergy losses and energy generation have reduced by 7% and 26% at 0.0275 vol% compared to water because of their effects on convective heat transfer.

Contribution 5

The increased volume concentration of WO_3 nanoparticles in the base fluid reduced the PV module temperature and improved its performance; the points below summarize the results obtained.

- The increased volume concentration of WO_3 nanoparticles in DI water reduced the temperature of the PV cells by 21% and enhanced the electrical power by 62% compared with DI water, which increased the electrical efficiency by 52%. The increase in volume concentration gradually increased thermal efficiency by 30.12%.
- Nusselt number and the heat transfer coefficient of the WO_3 nanofluid were improved by 51.23% and 5.30% with the increase of the volume concentration. Increasing volume concentration caused increased density and viscosity, which increased the pressure drop by 49.2% compared to DI water.
- The thermal exergy of the PVT system was lower than the electrical exergy due to the convergence of the fluid outlet temperature of the PVT system to the ambient temperature.
- The thermal exergy efficiency of the PVT system was low due to the drop in the quality of the thermal exergy. Thus, an increased volume concentration has positively influenced the thermal and electrical exergy efficiencies due to the enhanced nanofluid heat transfer coefficient. Using WO_3 nanofluids effectively reduced the exergy loss and entropy generation by 15.32% and 53.50% because of their heat transfer enhancement and reduced fluid friction in PVT systems.

Chapter 6

Effect of active cooling by nanofluids on the photovoltaic thermal system efficiency

This chapter consists of five experimental case studies, which applied mono nanofluids and a new hybrid nanofluid as cooling fluids, in addition to DI water as a reference cooling fluid used with a PVT system:
The first case study investigates the effects of Cuo nanoparticles at different volume concentrations that dispersion in DI water on the PVT system performance. The results obtained are compared with previous studies to show the effectiveness of the nanofluid prepared and the cooling method on the PVT energies produced.
The second case study investigates the effect of TiO_2 nanowire, which has been synthesized and prepared with specific mixing ratios to cool the PV cells and enhance their efficiency by reducing their temperature. Then exploit the heat extracted from the backside of the PV module to maximize the thermal energy depending on the improved thermal properties of TiO_2 nanofluid.
The third case study investigates the effect of Fe_2O_3 nanorod dispersion in DI water on the PVT system's electrical power generation and efficiency. Then determining the enhanced percentage of the electrical power and efficiencies of the PVT system at different volume concentrations.
The fourth and fifth cases investigate the effects of a new hybrid nanomaterials such as TiO_2-Fe_2O_3 and TiO_2-CuO at different volume concentrations that dispersion in DI water on the energy and exergy of the PVT system. These cases are characterized by the comprehensive study of the PVT system according to the laws of thermodynamics (first and second laws) to demonstrate the quantity and quality of the energies produced by the PVT system. Then compared, the result obtained by previous studies by considering parameters such as system size, nanofluid type, volume concentrations, and operating conditions to show the effectiveness of the new hybrid nanofluid as a cooling fluid in the PVT system.

6.1 Instruments used in experiments

Experiments were conducted in Miskolc city, Hungary, on typical sunny days from 8:30 am to 3:00 pm. Two polycrystalline PV modules of 50 W were used. The first PV module was referenced without cooling, and the second PV module was cooled with DI water as conventional fluid and then cooled with mono and hybrid nanofluids. The PVT modules consist of a copper absorber plate integrated with serpentine copper tubes soldering together and attached at the backside of the PV module by thermal grease HP, which has high thermal conductivity. High-performance insulation type SLENTEX was placed on the copper pipes, and an aluminium plate covered the PV module. The PV modules have fixed with a tilt angle of 14.8° towards the southern. Four thermocouples (T type) were placed on each surface, the backside of the PV modules, the PVT system, the inlet, the outlet of the PVT system, the inside nanofluid tank, and the water tank. The outlet of the PVT system is connected to a copper coil placed inside the water tank, and the coil outlet is linked to the nanofluid tank. Figure 6.1 shows the experimental setup of the reference PV module and PVT system. Data logger type National instrument model NI cDAQ-9178 consists of 24 channels for measuring temperatures, voltage, current of PV modules, solar radiation, and flow rate. The data logger connected with IN

SignalExpress 2015 software for recording and reading the data every 10 minutes; Table B3.1 shows the measurement devices and sensors' specifications used in the current study.

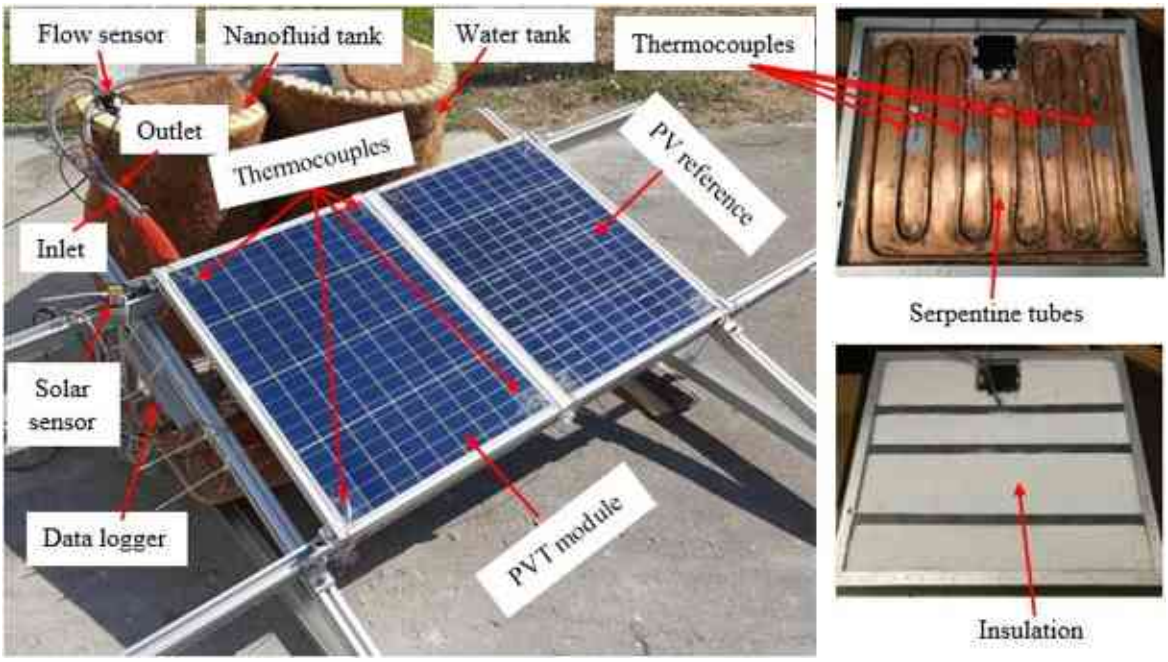

Figure 6.1: A sight of the experimental setup

6.2 Effect of deionized water on the photovoltaic thermal system efficiency

To the investigation effect of cooling the PV module on their performance, this case employed DI water as a cooling fluid of the PVT system and compared their performance with the reference PV module. Figure B3.1 (a) show the variation of solar radiation and ambient temperature; the maximum solar radiation was 940.17 W/m^{2,} and the ambient temperature was 37.6 °C. Rising PV cell temperature represents a critical problem facing the conversion efficiency of PV cells, which causes degradation in their performance. The direct incident solar radiation on the PV module raised the temperature of the PV cells to a high level, significantly decreasing their efficiency. Figure B3.1 (b) shows the reference PV module temperature, which rises to 55.6 °C at 12:20 pm; this temperature range cause lowers the PV module efficiency.
In contrast, the circulated DI water was into serpentine tubes soldered on absorb plate attached at the back side of the PV module to reduce the PV cell's temperature to 51.6 °C. Due to the removal of the heat from the backside of the PV module and the effect of the increase of heat convection between tubes and DI water into tubes, which helped to reduce the PV cell's temperature by 6.74% compared to the reference PV module. Figure 6.2 (a) shows the lowering of the electrical power of the reference PV module, which recorded 19.32 W. It is observed that the electrical efficiency of the PVT system was higher than the reference PV module due to cooling by DI water which helps to reduce the PV temperature and boosts the electrical power yield of the PVT system. Thus, cooling the PVT system with DI water at a constant mass flow rate of 1.4 L/min reduced PV module temperatures and contributed to enhancing the electrical power of the PVT to 22.19 W. Circulation of DI water in serpentine tubes helped to remove the heat of the PV cells and to maximize the thermal efficiency of the PVT system which recorded maximum value at noon is 30.25%. Figure 6.2 (b) shows the maximum electrical efficiency of the PVT system recorded at 12:30 pm is 6.32 %, while the reference PV module recorded 5. 11% reflects the DI water's capacity as a cooling fluid. The electrical and thermal efficiency significantly contributed to the increased overall efficiency of the PVT system to 36.57%.

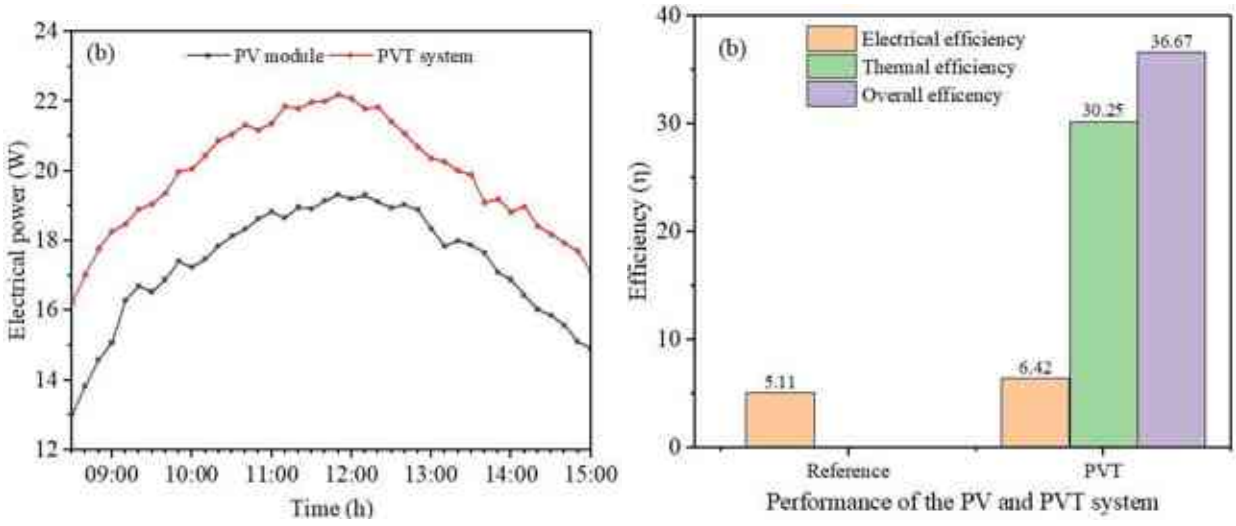

Figure 6.2: Performance of the PV, PVT system (a)electrical power, and (b) efficiency

6.3 Effect of copper oxide nanofluid on the photovoltaic thermal system efficiency

According to the climatic conditions of Miskolc city, the weather was sunny, and no significant variation was recorded regarding the solar radiation and the ambient temperature measured during the experiment period. The hourly variations of solar radiation and ambient temperature were recorded from 8:30 am. to 3 pm. Figure B3.2 (a) shows the maximum solar radiation values, which recorded 941.48 W/m^2, and the ambient temperature was 35.75 °C, specifically at 12:30 pm. It can be observed that the ambient temperature is directly proportional to solar radiation, which both reduced with sunset. Because of the direct exposure to intensive solar radiation and increased temperature, the reference PV module recorded a higher temperature, reaching 52.86 °C. The thermal properties of the CuO nanoparticle suspended in the base fluid have improved the convective heat transfer of the nanofluid. Thereby, using CuO nanofluid helps to reduce the temperature of the PVT system differently depending on the CuO volume concentration in the base fluid. Figure B3.2 (b) show the average temperature of the PV module and PVT system at 0.2 vol% and 0.3 vol% nanofluids, which reduced to 45.6 °C and 42.82 °C, respectively. The high thermal properties of nanofluid circulated in the serpentine tubes placed on the PVT system's backside helped reduce the temperature by 16% and 23.44% compared to the reference PV module. The electrical power of the PV module and PVT system is calculated by the voltage of the PV module, which is affected by the PV cell's temperature, and its current, which is affected by the intensity of solar radiation.

Figure 6.3 (a) illustrates the electrical power generated by PV, PVT system with CuO nanofluid and without cooling throughout the testing. The maximum PV module voltage recorded at 12:20 PM was 20.78 W, at 0.2 vol% of CuO in the base fluids helped to increment the PVT system power to 32.76 W. In contrast, at 0.3 vol%, the electrical power increment to 35.47 W. Thereby suspensions of CuO nanoparticles into DI water have proven their ability to withdraw the heat of the backside of the PV module and improve the electrical power by 70.60%, 57.65% compared to the reference PV module. Figure 6.3 (b) shows the efficiency of the PV module and PVT system; the intensity of solar radiances and rising temperature caused degradation of the electrical efficiency of the reference PV module, which was recorded by about 5.42%. Using CuO nanofluid improved the electrical power positively reflected in the electrical efficiency of the PVT system, which increments to 9.21%, 10.30% at 0.2 vol% and 0.3 vol, respectively. The heat of the backside of the PV module is dropped due to the circulated CuO nanofluid, which enhances the thermal energy of the PVT system and then improves the thermal efficiency of the PVT system. Figure 6.3 (b) shows the impact of CuO nanofluid on the thermal efficiency at different volume concentrations of CuO nanoparticles in the base fluids. The difference in temperature between the nanofluid's inlet and outlet and the nanofluid's higher thermal properties

improve thermal efficiency. Improving the thermal and electrical efficiencies increased the PVT system's overall efficiency exponentially with an increasing volume concentration of CuO nanoparticles. Table B3.2 compares current results with previous studies results in the literature that used CuO nanofluid for cooling PVT systems, the current results may not be the best among the results of other studies, but it was not the least.

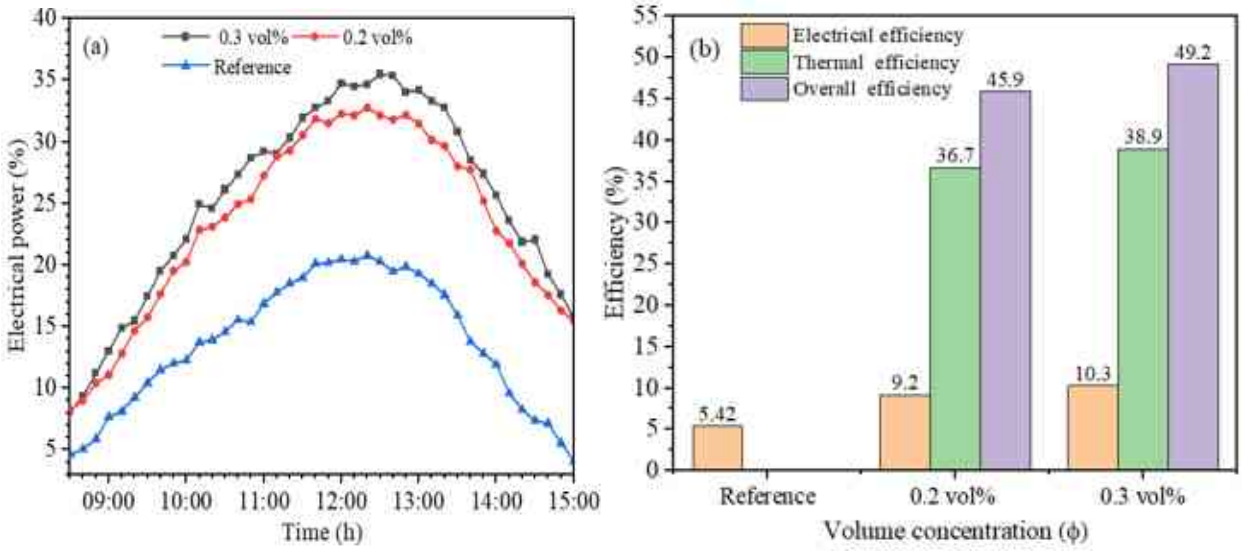

Figure 6.3: The performance of the PVT system (a) electrical power and (b) effect volume concentration on the efficiency

6.4 Effect of titanium dioxide nanofluid on the photovoltaic thermal system efficiency

In this case, TiO_2 nanofluid cools PV modules and PVT systems under different solar radiation and ambient temperature values. Figure B3.3 (a) presents the solar radiation values during the experiment period, which gradually increases with operation hours until 12:20 PM, which recorded the maximum solar radiation is 918.9 W/m^2, then lower with sunset. Rising the ambient temperature is associated with increased solar radiation intensity, in which the average ambient temperatures are variable along the experiment period. At the beginning of the experiment, the ambient temperature increased gradually, and the maximum ambient temperature was 34.16 °C at 12:20 PM. After that, it decreased to 30.83 °C when the experiment was over. The maximum temperature of the reference PV was recorded at 52.58 °C at 12:20 PM; this temperature range negatively influences the PV module performance. Conversely, using TiO_2 nanowires at different volume concentrations, 0.2 vol% and 0.3 vol% in the base fluid helps reduce the PVT system temperature to 47.31 °C and 46.11 °C compared with the reference PV module, as shown in Fig. B3.3 (b). The improved thermal properties of the TiO_2 nanowires suspended in the base fluid circulated in the serpentine tubes help to remove the heat of the backside of the PVT system. Thus, the PVT system temperature was reduced by about 5.27 °C at 0.2 vol%, while increasing the volume concentration to 0.3 vol% decreased the PVT system temperature by about 6.47 °C. Figure 6.4 (a) shows the PV module's electrical power drop compared with the PVT system cooled with TiO_2 nanofluid. Because of the rising PV module temperature, the maximum electrical power of the reference PV module was 21.15 W. Employing TiO_2 nanofluid contributed to the increment of the electrical power of the PVT system to 30.31 W at 0.2 vol% and 31.66 at 0.3 vol% due to improving thermal properties of the TiO_2 nanofluid. TiO_2 nanofluid reduced PVT system temperatures and improved the electrical power by 45.45% and 49.71%, compared with the reference PV module, at increased volume concentration of 0.2 vol% and 0.3 vol% nanowires in the base fluid. Figure 6.4 (b) shows an increase in the suspension of TiO_2 nanowires in base fluid at 0.2 vol% and 0.3 vol%, incrementing thermal efficiency to 32.70% and 34.63%; thus, the overall efficiency increased to 40.32% and 43%. The PVT system exhibits

a better performance with TiO_2 nanofluid as a cooling fluid by comparing reference PV modules, using TiO_2 nanowires at different volume concentrations, improving the PV module's thermal and electrical efficiency compared with DI water.

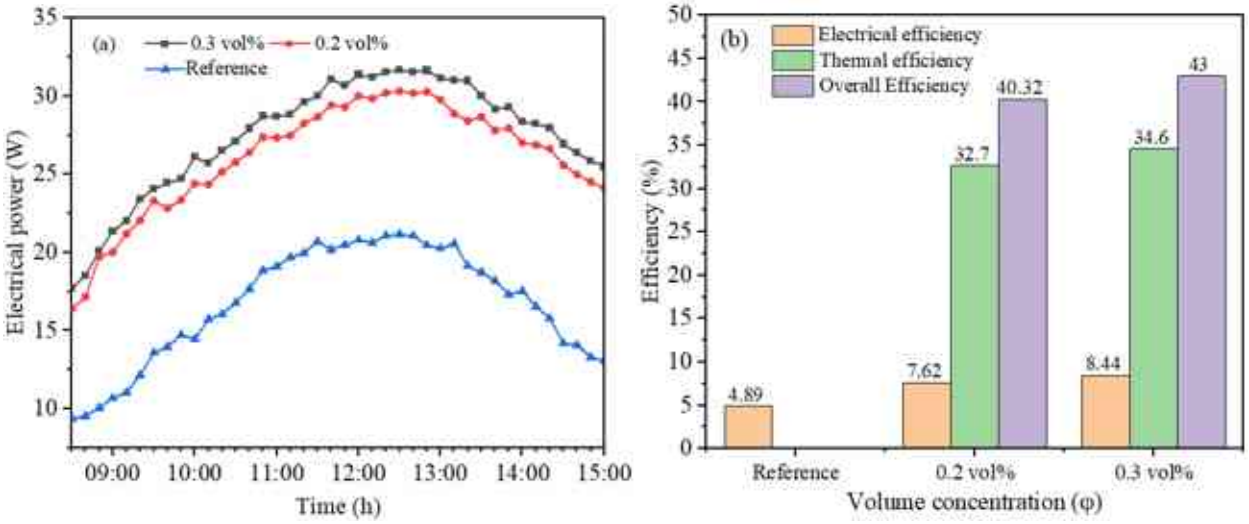

Figure 6.4: Performance of PVT system (a) electrical power, and (b) the overall efficiency

6.5 Effect of iron oxide nanofluid on the photovoltaic thermal system efficiency

A gradually increased solar radiation intensity was recorded from the first morning hours and continued to reach its maximum value of 925 W/m^2 at 12:30 PM. Increasing solar radiation intensity recorded the maximum ambient temperature at 12:40; the maximum ambient temperature was 32.97 °C. Figure B3.4 (a) shows the variation value of the solar radiation and ambient temperature during the experiment. In this case, iron oxide Fe_2O_3 nanofluid was used for cooling the PVT system, and two volume concentrations of Fe_2O_3 nanorod (0.2 vol% and 03 vol%) were suspended in the based fluid. The nanofluid is circulated inside serpentine tubes at 1.4 L/min to increase the PVT system backside heat removal. The performance of the reference PV module is degraded due to increased temperature which was 50.9 °C, as shown in Fig. B3.4 (b).

In contrast, using Fe_2O_3 achieved a remarkable decrease in the PVT system temperature. Suspended 0.2 vol% of Fe_2O_3 in base fluid improved the convection heat transfer, which helped to reduce the PVT system temperature to 42.6 °C. Increased the volume concentration to 0.3 vol% decreases the temperature to 39.26 °C; this confirms the ability to use Fe_2O_3 nanofluid for cooling and improve the PVT performance compared with water cooling. Thus, reducing the PVT system temperature by 19.45% and 29.64% led to improved PVT system performance.

Figure 6.5 (a) demonstrates that using Fe_2O_3 nanofluid improves the electrical power due to lowered PVT system temperature compared to the reference PV module. The reduced temperature is attributed to the enhancement of the Fe_2O_3 nanofluid thermal conductivity, then enhanced convective heat transfer between the Fe_2O_3 nanofluid circulated in tubes and the backside of the PVT system. It observed an increment of the electrical power of the PVT system with an increase in the Fe_2O_3 nanorod in the base fluid; at 0.2 vol and 0.3 vol%, the electrical power increased to 36.7 W and 37.76 W, respectively. The electrical power of the reference PV module was recorded at about 21.37 W. Thereby, using Fe_2O_3 nanofluid has improved the electrical power to 71.73% and 76.68% compared with the reference PV module. Thus, improved output electrical power of the PVT system has positively reflected the electrical efficiency. Figure 6.5 (b) shows the maximum electrical efficiency of the reference PV module, which was 5.75%, confirming the rising temperature's effect on the PV module efficiency. The maximum electrical efficiency of the PVT system using Fe_2O_3 nanofluid was 11.3% and 12.1 at 0.2 vol% and 0.3 vol%, respectively. Improved the heat transfer convection between the

backside of the PV module and the circulating nanofluid in the heat exchanger attached at the back side of the PVT system contributed to removing the heat of the PVT system. The maximum thermal efficiency recorded at 0.2 vol% was 40.80%, while at 0.3 vol%, the thermal efficiency increased to 43.32%. The overall efficiency of the PVT system is the summation of thermal and electrical efficiencies; with increasing the volume concentrations in the base fluid, the overall efficiency increments to 52.10% and 55.41%.

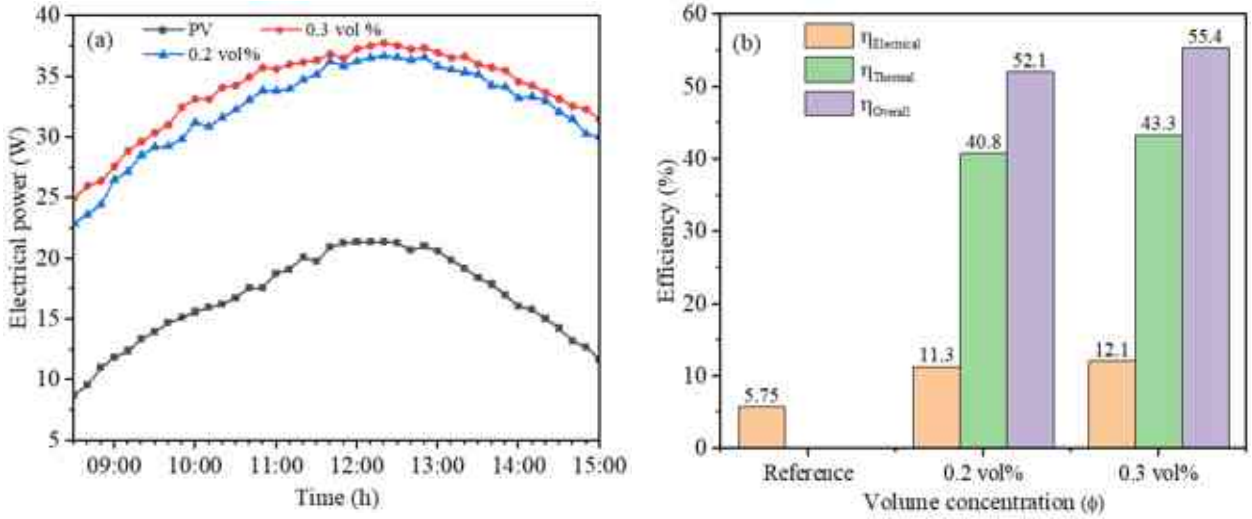

Figure 6.5: Performance of PVT system (a) electrical power, and (b) the overall efficiency

6.6 Effect of hybrid titanium dioxide-iron oxide nanofluid on the photovoltaic thermal system efficiency

6.6.1 Energy analysis results

A hybrid TiO_2-Fe_2O_3 nanofluid and DI water have been employed as a cooling fluid to improve the PVT system performance and compare their performance with the reference PV module. Figure B3.5 (a) shows the average solar radiation values and ambient temperature recorded during the experiment days. The maximum solar radiation recorded was 899.23 W/m^2 at 12:30 pm. The ambient temperature is about 32.76 °C. Thus, increased solar radiation coincides with rising ambient temperature, which affects the PV cells by reducing their conversion efficiency. Figure B3.5 (b) shows the temperature of the PV module and PVT system from the experiment's beginning until the period's end. The maximum temperature of the reference PV module was recorded at 49.85 °C at noon when the ambient temperature of 32.76 °C increased the PV cell's temperature and caused decreased electrical efficiency. Circulation of DI water in the PVT system reduces the temperature of the PV cells to 45 °C due to removing the heat from the backside of the PV module. Using hybrid nanofluid as a cooling fluid reduced the temperature of the PV cells, and loading of CuO NPs over the TiO_2 NWs has increased the surface area of the nanomaterials suspended in the base fluid and improved the thermal characteristics, which led to an increase in convective heat transfer and a decrease in the PV module temperature. The circulation of hybrid TiO_2-Fe_2O_3 nanofluid at volume concentrations 0.2 vol% and 0.3% inside the serpentine tubes helps to increase the heat transfer convection and extract excessive heat of the PV module, then reduced the temperature to 37.46 °C and 36.37 °C. Compared to the reference PV module, cooling by DI water decreased the PV module temperature by 10.71%, and cooling by hybrid nanofluid at 0.2 vol%, 0.3 vol% reduced the PV module temperature by 33% and 37% confirms the ability of hybrid TiO_2-Fe_2O_3 nanofluids as a cooling fluid.

Maximum electrical power was recorded at 23.14 W; reduced PV cells temperature helped to increment the electrical power. Figure 6.6 (a) shows the effect of DI water, hybrid nanofluid on the electrical power of the PV and PVT system, using DI water as a cooling fluid increment of

electrical power of the PVT system to 27.22 W. Increased TiO_2-Fe_2O_3 nanomaterials suspension in the base fluid enhanced the thermal properties of the working fluids, which positively reflected on the electrical power produced of the PVT system. Using nanofluids at different volume concentrations of 0.2 vol% and 0.3 vol% at constant mass flow rate incremented the electrical power output of the PVT system by 38.95 W and 39.71W, respectively. Compared with the electrical power of the reference PV module, using DI water and hybrid nanofluid at 0.2% and 0.3% enhanced the electrical power by 17.63%, 68.32% and 71.63%, respectively. Figure 6.6 (b) shows the reference PV module's electrical efficiency and cooling PVT system by DI water and hybrid nanofluid. At maximum solar radiation and ambient temperature, the electrical efficiency of the reference PV module was 5.72%. Enhanced electrical power of the PVT system directly affects the electrical efficiency of the PVT system due to cooling. The maximum electrical efficiency of the PVT system was 7.11%, 12.44% 12.62% at cooling by DI water and hybrid nanofluid at 0.2 vol% and 0.3 vol%.

Circulation of hybrid nanofluid into tubes helps to increase the heat removal by convection and increase thermal efficiency to 45.40% and 48.22% at 0.2 vol% and 0.3 vol% respectively, while used DI water has incremented thermal efficiency to 32.60%. The overall efficiency is the sum of thermal and electrical efficiencies; maximum overall efficiency has been recorded using a hybrid nanofluid at 57.84% and 59.82% compared with DI water, which was 39.70%. This is attributed to the high thermal properties of the hybrid TiO_2-Fe_2O_3 nanofluid. The results obtained are compared with previous studies to show the ability of TiO_2-Fe_2O_3 nanofluids as a cooling fluid to improve the PVT system performance, as shown in Table B3.3. Considering some factors, such as the size of the PVT system, the nanofluids used and volume concentrations of nanomaterials in the base fluid, measurement conditions, and their effect on temperature drop, the thermal and electrical energy efficiencies of the PVT system. The present results highlight a new type of nanofluid that can be used as a cooling fluid helps to improve the energy and exergy of the PVT system. This study investigated the influence of adding TiO_2-Fe_2O_3 nanomaterials at different volume concentrations in DI water on Reynolds number, heat transfer coefficient, Nusselt number, pressure drop and friction factor. Depending on the maximum, average and minimum, it has calculated heat transfer coefficient, Nusselt number, pressure drop, and fraction factor from Eq. (15-17).

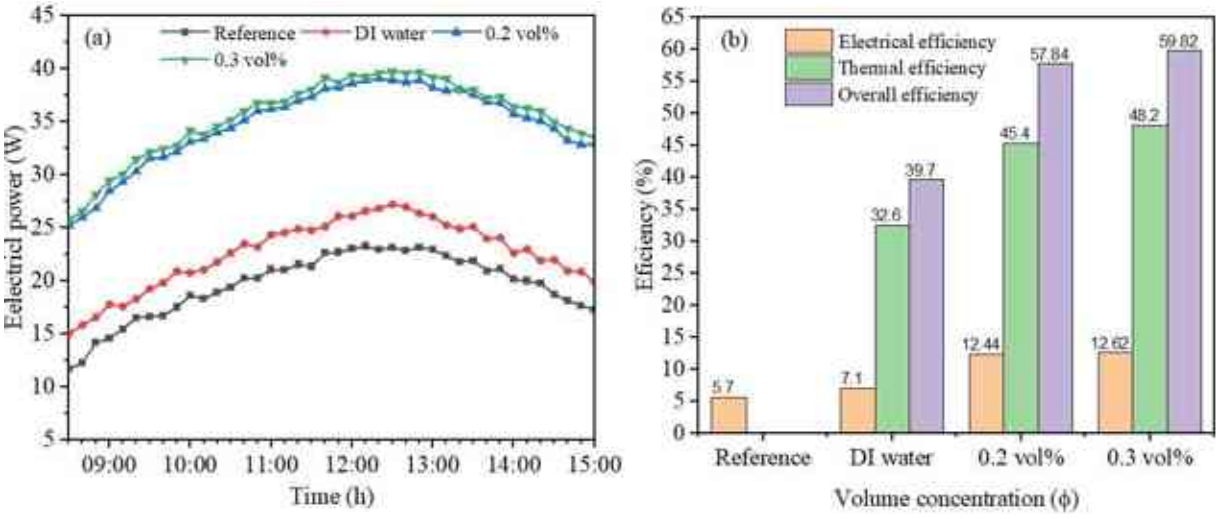

Figure 6.6: Performance of the PV and PVT system (a) electrical power, (b) overall efficiency

Figure B3.6 (a) show the effect of increased volume concentration of the TiO_2-Fe_2O_3 nanomaterials on the Nusselt number as a function of Reynold's number; it was gradually increased by Nusselt number with increased Reynold's number. Suspension of TiO_2-Fe_2O_3 nanomaterials by 0.2 vol% and 0.3 vol% in the base fluid enhanced the Nusselt number by 25% at 0.3 %vol compared to the DI water. An increase in Nusselt numbers of the TiO_2-Fe_2O_3

nanofluid has positively increased the heat transfer coefficient. The increase in the Reynolds number has enhanced the heat transfer coefficient of the nanofluid. Figure B3.6 (b) shows the increase of the heat transfer coefficient with Reynold's number increased at different volume concentrations, which is attributed to the high thermal conductivity of the hybrid nanofluid. Adding 0.2 vol% and 0.3 vol% in DI water enhanced the heat transfer coefficient of hybrid nanofluid by 28.95% and 43.33% contributing to lower PV temperature more than in DI water. Despite increasing the heat transfer coefficient due to increasing thermal conductivity, the density of the hybrid nanofluid is increased because of the volume concentration, which influences the pressure drop. Thus, the nanofluid's increased density and viscosity increased the pressure drop using a hybrid nanofluid compared to DI water, as shown in Fig. B3.7 (a). The nanomaterials dispersed in DI water worked to the resistance of the flow and increased the pressure drop, increasing the volume concentration of nanomaterials pressure drop by 23.61% and 36.12% as a function of increased Reynolds number. Figure B3.7 (b) shows the decreased friction factor of the TiO_2-Fe_2O_3 nanofluid with increased Reynolds number and volume concentration of nanomaterials in DI water. The friction factor dropped by 5.26% and 10.52% at increased Reynolds number and volume concentration by 0.2 vol%, 9% and 0.3 vol %, respectively.

6.6.2 Exergy analysis results

The thermal exergy of the system is proportional to the specific heat of the cooling fluid, the flow rate, and the exit temperature of the cooling fluid. Figure 6.7 (a) shows the thermal exergy of using TiO_2-Fe_2O_3 nanofluid compared with DI water, where increasing the TiO_2-Fe_2O_3 nanomaterials in base fluid increments the thermal exergy of the system. This is attributed to enhanced cooling fluid thermal conductivity reflected on enhanced convective heat transfer between circulating cooling fluid and tubes placed on the absorbing plate. It can notice that the thermal exergy system's value is lower than the electrical exergy because of its higher quality compared to the thermal energy [70]. Thus, enhancing thermal properties such as specific heat and increasing the flow rate of the cooling fluid may achieve comparable with electrical exergy. According to Eq. (43), the thermal exergy efficiency of the system is influenced by the outlet fluid temperature. Figure 6.7 (b) shows that the relative increase of the nanomaterials in DI water led to a gradual increment of the thermal exergy efficiency to 2.43%, 2.28%, at 0.2 vol% and 0.3 vol%, respectively, compared with DI water which recorded 1.48%. Thereby, it can be observed that the thermal exergy efficiency was much lower than the electrical exergy efficiency. This is attributed to the outlet temperature of the fluids being closer to the ambient temperature, which agrees with [124]; the low quality of the thermal exergy is one of the reasons that causes reduced thermal exergy efficiency.

The electrical exergy efficiency is relatively enhanced with increased volume concentrations; maximum electrical exergy recorded was 12.41%, 11.52% at 0.3 vol% and 0.2 vol%, respectively, while cooling with DI water recorded at about 6.8%, as shown in Fig. 6.7 (b). Thus, using TiO_2-Fe_2O_3 nanofluid increments the electrical exergy efficiency of the PVT system by 82.30%, 69.41% with increased the TiO_2-Fe_2O_3 nanomaterials in DI water by 0.3% and 0.2% compared with DI water. It can be observed that increasing the volume concentration of TiO_2-Fe_2O_3 nanomaterials in base fluid increased the overall exergy efficiency to 14.83% and 13.80% at 0.3% and 0.3%, respectively, while used DI water achieved 8.28%. Compared with previous studies that used different PVT system sizes, volume concentrations, and types of nanomaterials, Table B3.4 shows the effect of hybrid TiO_2-Fe_2O_3 nanofluid on the thermal and electrical efficiencies of the PVT system. The exergy analysis results show the effect of hybrid TiO_2-Fe_2O_3 nanofluid on the thermal and electrical exergy efficiencies, which achieved quite results.

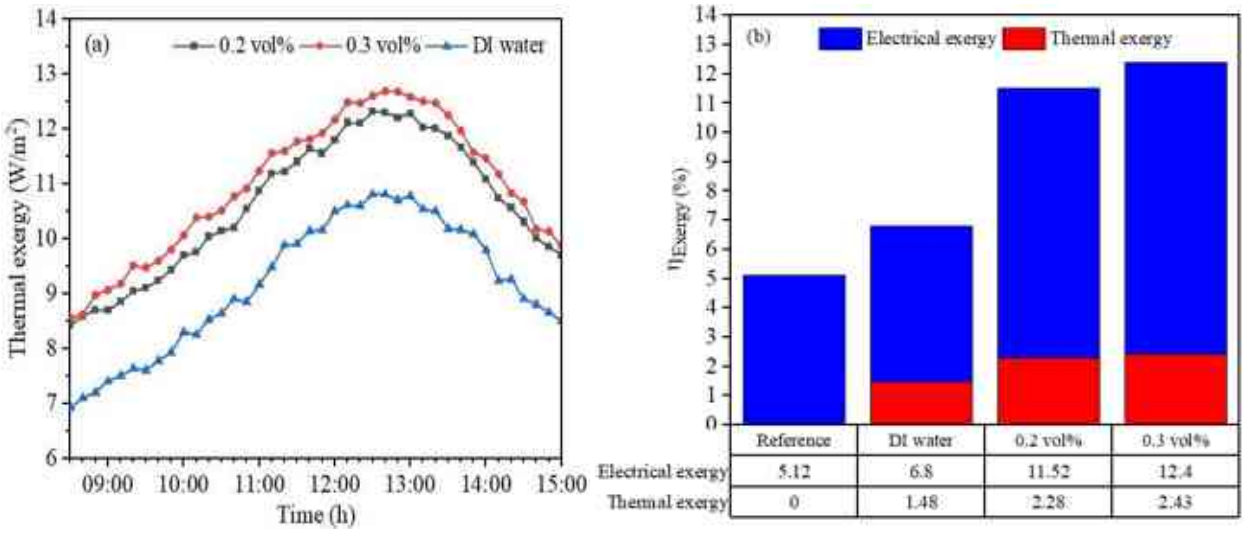

Figure 6.7: Exergy performance of the PV and PVT system (a) thermal exergy, (b) overall exergies

The PVT system's exergy loss and entropy generation are calculated using Eq. (46) using DI water and hybrid nanofluid at different volume concentrations. Rising the PV module temperature means increased exergy losses; employing hybrid nanofluid help in reducing the exergy losses due to enhanced thermal properties. Using a hybrid TiO_2-Fe_2O_3 nanofluid reduced the exergy losses in the PVT system by converting the heat generated by the PV cells to useful thermal energy due to the circulating of the hybrid nanofluid in tubes. Figure 6.8 shows the relatively reduced exergy losses of the PVT system compared with the reference PV module using DI water and hybrid nanofluid at 0.2 vol%, 0.3 vol% the exergy losses reduced to 13.57%, 42.33% and 47.30%, respectively. On the other side, the reference PV module has the highest entropy generation due to rising temperature because of the increase in the heat transfer between the PVT system and the environment. Figure 6.15 shows the influence of DI water and hybrid nanofluid by reducing the entropy generation by 18.15%, 60.92% and 70.47%, respectively, compared with the reference PV module. Thereby, both the exergy losses and entropy generation of the PVT system have lowered at cooling the hybrid nanofluid was higher than cooling by DI water; this is important to reducing the work lost in the PVT system.

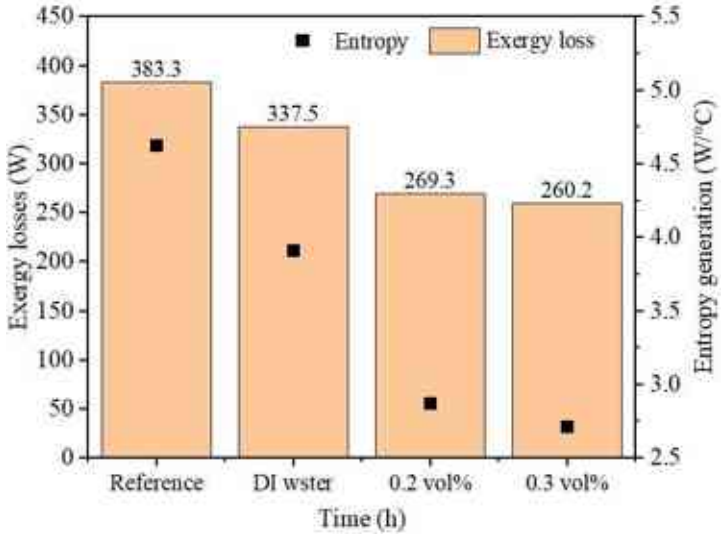

Figure 6.8: Exergy losses and entropy generation

6.6.3 Economic analysis of the photovoltaic thermal system

The economic analysis of the proposed cooling approach is important to show the payback period [20], the feasibility of a hybrid PVT system for the long term and compare it with conventional PV modules. Considering the daily maintenance, which may be non-existent on some days of the month, operation cost, including pump and flow sensor electrical consumption and others. Synthesizing nanomaterials in the laboratory and preparing the nanofluid helped significantly reduce the cost of nanofluid compared to purchasing from companies, as well as the purity and morphology of nanomaterials that can be improved. The nanofluid cost was calculated each day after dividing the total price by days in the year. The configuration of the PVT system includes an absorbing part, copper tubes, an aluminium cover, insulation, a pump, a flow sensor, plastic tanks, etc. The net profit is calculated from Eq. (5.1) [122] depending on the cost of each element mentioned in Table B3.5 Compared with conventional PV modules, the hybrid PVT system used hybrid nanofluid achieved less payback period of 630 days than conventional PV modules with a payback period of about 727 days with more than 3 months difference. This difference is logically acceptable and confirms the effectiveness of using nanofluids in improving the PVT system efficiency and its economic feasibility.

6.7 Effect of hybrid titanium dioxide-iron oxide nanofluid on the PVT system efficiency

6.7.1 Energy analysis results

In this case, using a hybrid TiO_2-CuO nanofluid as a cooling fluid improves the efficiency of the reference PV module by decreasing its temperature. During the experiment, the sky was clear, and no significant variation in solar radiation or temperature was recorded. The reference PV module and PVT system were oriented to face south with installed at a 14.8° tilt angle. Figure B3.8 (a) shows the average ambient temperature and solar radiation; at the beginning, the temperature and solar radiation values were low, then increased at noon to reach maximum values and dropped with sunset. The maximum ambient temperature and solar radiation recorded between 12:20 PM to 1:50 PM were 32.6 °C and 903.5 W/m^2. The mechanism of conduction heat transfer from the backside of the PV modules to the absorbing plate, then to serpentine tubes and by heat convection to hybrid nanofluids that pass inside tubes has reduced the temperature rise in the PV module. Figure B3.8 (b) shows the peak temperature of the reference PV module was 51.63 °C; with cooling by DI water, the average temperature decreased to 48.85 °C, at 0.2 vol% and 0.3 vol% of hybrid nanomaterials in the base fluid, the average temperature dropped to 37.91 °C and 37.13 °C, respectively. The loaded of CuO NPs over the TiO_2 NWs increased their surface area and improved the thermal characteristics of the hybrid nanofluid, which led to an increase in convective heat transfer and a decrease in the PV module temperature. The flowing hybrid nanofluid at different volume concentrations inside the serpentine tubes attached beneath the PV module helps extract the excessive heat and reduce the PV module temperature by 36.11%, 39%, compared to the reference PV module. Cooling by water slightly decreased temperature by 5.62% compared to the reference PV module, confirming the efficient hybrid nanofluids proposed as cooling fluids.

Figure 6.9 (a) shows the maximum electrical power generated by the reference PV module, PVT system at cooling by water and hybrid nanofluid at different volume concentration. The reference PV module has recorded lower electrical power, about 21.92 W, which confirms the degradation of the PV cell's work due to increased temperature. Circulation water inside serpentine tubes with absorb plate helps slightly increment the electrical power to 24.2 W. Using hybrid nanofluids at 0.2 vol % and 0.3 vol %, the electrical power of the PVT system increments to 38.1 W and 38.88 W, respectively. The load of CuO NPs on TiO_2 NWs at equal ratios and dispersion in DI water helped improve the hybrid nanofluid's thermal properties by increasing the hybrid nanofluid's thermal conductivity and heat capacity. The electrical power produced was enhanced by 73.95% and 77.52% with the hybrid nanofluid at 0.2 vol% and 0.3 vol%, while the DI water improved by 10.40% compared to the reference PV module. The effectiveness of

hybrid nanofluid caused a decrease in the PV cell's temperature and an increment in electrical power generation of the PVT system hence positively reflecting the electrical efficiency of the PVT system. Figure 6.9 (b) it can observe the electrical efficiency of the reference PV module was 5.82% due to a drop in the electrical power; with DI water cooling, the electrical efficiency of the PVT system is an increment to 6.41%. The improvement of electrical power of the PVT system with the used hybrid nanofluid led to an increment in the PVT electrical efficiency to 12.28%, 12.40%, at 0.2 vol% and 0.3 vol%, respectively, that attributed to reducing PV module temperature. The higher heat transfer capacity of using hybrid nanofluids caused decreasing the PV module operation temperature, thus incrementing the thermal efficiency of the PVT system. Figure 6.9 (b) shows the variation of thermal efficiency increase in the volume concentration of nanomaterials in DI water; the increase in volume concentration achieved a relative increase in thermal efficiency due to the increased thermal conductivity of nanofluids. Compared with DI water, using a hybrid nanofluid led to an increment in thermal efficiency to 44.22% and 45.83% with increased volume concentration by 0.2 vol% and 0.3 vol%. Thus, increasing the overall efficiency of the PV module to 54.11%, 58.80%, compared with cooling by DI water. Compared with previous studies in the literature, Table B3.6 compares the current study with previous studies that used mono nanofluids such as CuO, TiO_2 and hybrid nanofluids for cooling PVT systems. It can remark that the hybrid TiO_2-CuO fluid achieved good performance by temperature drops and increment in the electrical and thermal efficiency attributed to the improving thermal characteristics of hybrid nanofluids.

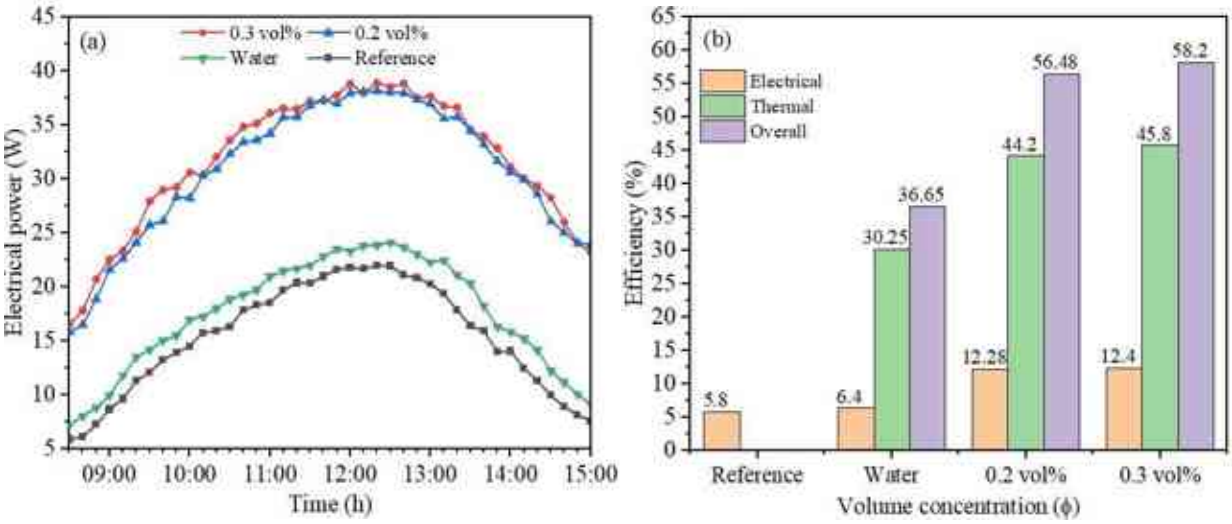

Figure 6.9: Performance of the PV and PVT system (a) electrical power, (b) overall efficiencies

6.7.2 Exergy analysis results

Exergy analysis is important for appearing the actual work and determining the losses of the PVT system. Similar to the energy analysis of the PVT system, the exergy analysis shows the effect of an increase in the solar radiance and the ambient temperature on the exergy performance of the PVT system. Based on Eq. (40), the solar exergy calculated for the maximum, average, and minimum values during experiments days were 897 W/m^2, 654.33W/m^2 and 320.58 W/m^2, respectively. According to Eq. (41), the electrical exergy was equal to the electrical power produced by the PVT system. The electrical exergy produced was higher than the thermal exergy, in contrast to thermal energy in energy analysis, which is attributed to the outlet fluid's temperature convergence with an ambient temperature. Based on Eq. (42), it can observe the thermal exergy depends on the difference between the $T_{f\,\mathrm{out}}$, $T_{f\,\mathrm{in}}$ fluid temperature, ambient temperature, the logarithm of $\left(\frac{T_{f\,\mathrm{out}}}{T_{f\,\mathrm{in}}}\right)$, and the specific heat of fluids applied. The convergence of $T_{f\,\mathrm{out}}$ to ambient temperature leads to dropping thermal exergy and influencing

thermal exergy efficiency. Nevertheless, using nanofluid achieved a remarkable improvement of thermal exergy to 11.86 %, 12.18, at 0.2 vol% and 0.3 vol%, while cooling by DI water was 8.8 W/m^2, as shown in Fig. B3.9. Circulating the hybrid nanofluid into the serpentine tubes helps to remove excess heat from the backside of the PV module and reduces their temperature, which improves the electrical exergy. Figure 6.10 (a) shows the effect of DI water and hybrid nanofluid at 0.2 vol% and 0.3 vol% by increasing electrical exergy efficiency to 5.41%, 11.33%, and 12.18%, respectively. The thermal exergy drop influences the thermal exergy efficiency because of the low quality of the thermal exergy. Enhancing hybrid nanofluid's thermal properties increments the PVT system's overall exergy efficiency to 13.44% and 14.97% at different volume concentrations. In contrast, overall exergy efficiency with cooling by DI water does not exceed 6.28%. Increasing the volume concentration of hybrid nanomaterials in the base fluid remarkably influences the increment of the overall exergy efficiency. It is important to evaluate exergy loss and entropy generation for specifying the PVT system losses and irreversibilities. The exergy loss increases with the rising temperature of the PV module surface. Enhancing the thermal characteristics of hybrid nanofluids helped to reduce the exergy losses; Fig. 6.10 (b) shows a reduction of exergy losses by 38.40%, 44.32% at 02 vol% and 0.3 vol%. In contrast, using DI water has reduced entropy generation by about 4.50% compared to the reference PV module. Rising the temperature of the PV module causes increased entropy generation due to increased heat transfer between the PVT system and the environment. Minimizing the entropy generation is necessary to reduce the work lost in the system. Figure 6.10 (b) shows the effect of hybrid nanofluid by lowering the entropy generation; compared with the reference PV module, hybrid nanofluid reduced the entropy generation by 62.20% and 69.61%, while DI water by 8.46%, which confirms the effectiveness of hybrid nanofluid used.

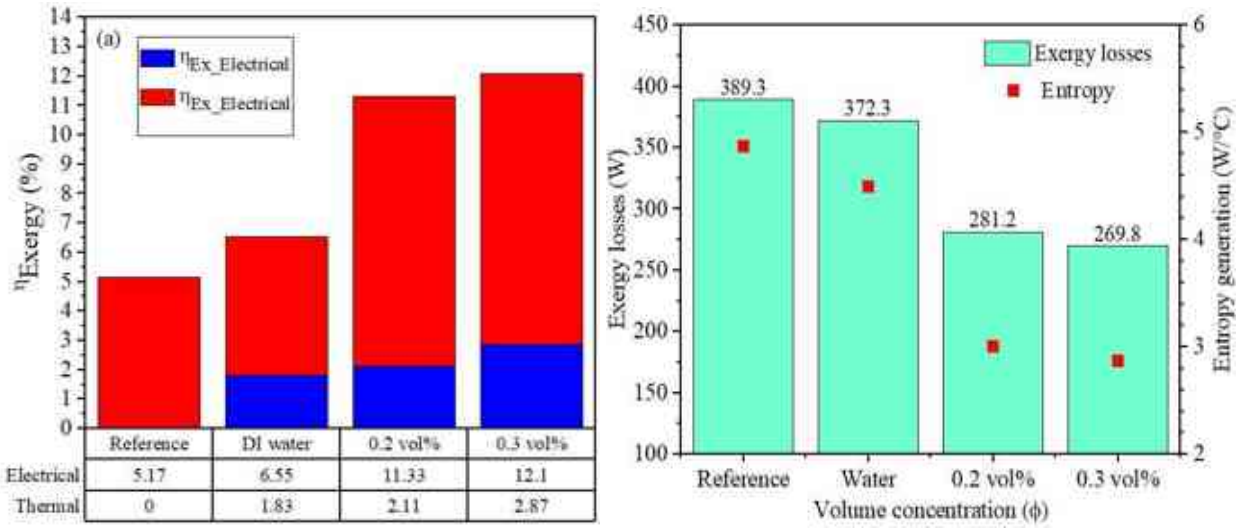

Figure 6.10: Exergy performance of the PV and PVT system (a) exergy efficiencies, (b) exergy losses and entropy generation

6.8 New contributions results

Contribution 6

- Dispersion of CuO nanofluid at different volume concentrations for cooling the PVT system gives good results by improving the PVT system performance. Copper oxide nanoparticles are characterized by higher thermal conductivity, which is positively reflected by a reduced PVT system temperature of 23.44% and an increment in the electrical power from 20.78 W to 35.47 W at 0.3 vol%. Thus, enhancing the electrical efficiency from 5.43% to 10.3% and increasing thermal efficiency to 38.91% confirms the nanofluid's effectiveness.
- TiO_2 nanowires have been adopted to prepare nanofluids, which are characterized by having a surface area to help increase heat absorption. Compared with the reference PV module,

using TiO_2 nanofluid decreased the PVT system temperature to 14% at 0.3 vol% and increased the electrical power to 49.70% and increased electrical power to 49.70% and increased electrical efficiency by 27.51%. Increasing the thermal conductivity of nanofluid increases heat absorption from PV cells and then increases thermal efficiency to 34.63%.

- Suspension of 0.3 vol% of Fe_2O_3 nanoparticles in DI water improved the convection heat transfer, which helped to reduce the PVT system temperature by 29.64%. Compared with DI water, the electrical power increased from 21.37 W to 37.76 W, that is, by 76.68%, and enhanced the electrical efficiency to 12.10%. Thermophysical properties of Fe_2O_3 nanoparticles significantly help to improve the heat transfer convection between the backside of the PV module and the heat exchanger, which increases thermal efficiency to 43.31%.
- Table B3.7 shows the effect of different cooling fluids on the PVT system; all nanofluids applied to contribute to reducing the PV cell temperature and increasing the efficiency of the PVT system higher than DI water. At 0.3 vol%, the Fe_2O_3 nanofluids achieved better performance than other nanofluids. This is attributed to the high thermal conductivity of Fe_2O_3 nanofluids compared to CuO and TiO_2 nanofluids. CuO nanofluid achieved higher performance than TiO_2 nanofluid because of their high thermal properties, which positively reflected the PVT system performance.

Contribution 7

The hybrid TiO_2-Fe_2O_3 nanofluid consisting of 50% nanowires and 50% nanoparticles has created a new hybrid nanofluid having new thermophysical properties that help improve the hybrid nanofluid performance used with PVT system more than mono nanofluid, which positively reflected enhanced the PVT system performance as follows:

- Compared to the reference PV module, circulation of DI water decreased the PV module temperature by 9.67%, using hybrid nanofluid at 0.2 vol%, 0.3 vol% reduced the PV module temperature by 25% and 33.63%. Due to decreased PV cell temperature, the PVT system's electrical power has increased by 17.63%, 68.32% and 71.60% at DI water and hybrid nanofluids, respectively.
- Increment in the electrical power has enhanced the electrical efficiency of the PVT systems to 7.12%, 12.44%, and 12.62% at cooling by DI water and hybrid nanofluid at different volume concentrations compared with the reference PV module. Increasing the volume concentrations in the base fluid has increased the nanofluid heat transfer coefficient, then enhanced the thermal efficiency of the PVT system by 39.26% and 47.85% compared to used DI water.
- Compared with DI water, a hybrid nanofluid enhanced the Nusselt number by 25% at 0.3 %vol. An increase in Nusselt numbers has positively increased the heat transfer coefficient by 43.33% at 0.3 vol%, which helped lower PV temperature and increased thermal efficiency. Increased volume concentration causes increased nanofluid density and effect by the pressure drop of about 36.12%; increased Reynolds number and volume concentrations lead to dropping the fraction factor to 10.52%.
- The thermal exergy is affected by the specific heat of the cooling fluid, flow rate and temperature. An increase in the TiO_2-Fe_2O_3 nanomaterials in base fluid increments the thermal exergy by 17.29% and 13.87% compared to DI water. The relative increase of the volume concentrations increases the thermal exergy efficiency to 2.43%, 2.28% compared with DI water.
- The increment of electrical exergy has a positive reflection to enhance the electrical exergy efficiency of the PVT system by 69.40% and 82.30% compared to cooling by DI water. The exergy losses increase with the rising PV module temperature. Compared to cooling by DI water, employing hybrid nanofluid helps reduce the exergy losses by 13.57% and 42.33%.

Thereby reducing entropy generation by 60.9% and 70.47%, reducing the work lost in the PVT system.

- Compared with previous studies, which adopted different sizes of the PVT system, the nanofluids and volume concentrations of the nanomaterials. The employed hybrid TiO_2-Fe_2O_3 nanofluid enhanced the energy and exergy of the PVT system better than previous studies. The economic analysis of cooling by hybrid nanofluid achieved a satisfying payback period compared to the reference PV module with a difference of more than 3 months.

Contribution 8

Energy and exergy of the PVT system have been conducted to evaluate the quantity and quality of the PVT system's productivity. The following points summarized the new findings of using hybrid TiO_2-CuO nanofluid as follows:

- The effectiveness of the hybrid nanofluid at different volume concentrations helps to extract the excessive heat and reduces PV module temperature by 36.10% and 39%, while DI water by 5.61% compared with the reference PV module. The electrical power improved of the PVT system by 73.95% and 77.50% at increased volume concentrations due to improving the hybrid nanofluid's thermal properties, while using DI water improved it by 10.41%. Thus, the electrical efficiency of the PVT system increased by 12.28% and 12.41%.
- The high thermal characteristics of hybrid nanofluids increment heat transfer convection and then improve the thermal efficiency of the PVT system to 56.48% and 58.20%, then increment the overall efficiency of the PV module, reaching 36.25% and 56.48%.
- Convergence of the outlet fluids temperature with ambient temperature causes decreased thermal exergy and thus reduced thermal exergy efficiency. Cooling by hybrid nanofluid has improved the electrical exergy efficiency by 11.33% and 12.18%, while a slight improvement was recorded using DI water. The exergy efficiency has increased to 13.44 %, 14.97% and 6.28 % at different nanomaterials volume concentrations and DI water.
- The exergy losses were reduced by 32.30% and 37.91% due to enhancing the thermal characteristics of hybrid nanofluids, while used DI water was reduced by 4.52% compared to the reference module. The effective cooling by hybrid nanofluid causes reduced entropy generation by 62.23% and 69.60%, compared with DI water.
- Loading Fe_2O_3 nanorods over TiO_2 nanowires and loading CuO nanoparticles over TiO_2 nanowires produced new hybrid nanomaterials with higher thermal properties than mono nanomaterials. Dispersion of the hybrid nanomaterials in DI water achieved high performance than the mono nanofluids; Table 18 shows the improvement of the PVT system at 0.3 vol% of TiO_2-Fe_2O_3 and TiO_2-CuO nanofluids compared with mono nanofluid used, as mentioned in Table B3.8. TiO2-Fe2O3 nanofluid achieved higher performance than TiO2-CuO due to the high specific heat and low density of Fe_2O_3 nanorods that help enhance the thermal properties of the TiO_2 nanowire, and the results in Table 6.8 confirm the effectiveness of hybrid nanofluid as a cooling fluid.

Chapter 7

Numerical simulation of the photovoltaic thermal system by using different nanofluids

In this chapter, a numerical simulation on the effects of ZrO_2/water nanofluid and TiO_2-Fe_2O_3 hybrid nanofluid as cooling fluids on the temperature, energy efficiency, exergy efficiency, heat transfer coefficient, Nusselt number, Reynold number, and pressure drops in system PVT system. The methodology of this chapter involved a numerical simulation via ANSYS Fluent 19.2 software by (computational fluid dynamics (CFD)) of a 3D model. The proposed model involved a PV module, an absorber plate and serpentine tubes attached at the backside of the PV module. The numerical results are validated by comparing the experimental results obtained. The numerical simulation results of the PVT system cooled by ZrO_2/water nanofluid have been compared with experimental results conducted according to the Iraq condition, while the TiO_2-Fe_2O_3 hybrid nanofluid according to experimental results conducted in Hungary condition.

7.1 The model geometry and assumptions

The proposed model consists of a glass cover, photovoltaic cells, absorb plate, and tubes directly in contact with the absorbing plate. Figure 7.1 shows the geometry of the PVT system used for the current simulation. The geometry model is created by SolidWorks with all dimensions and then imported to ANSYS 19.2; Table B4.1 presents the properties of the geometry model proposed. The effect of the cover glass and the PV module are indirectly used through the boundary conditions; the solar radiation value received by the copper absorber plate depends on the transmissivity of the cover glass section beside and the absorptivity of the PV module, which is interpreted as constant heat flux and that agrees with [125]. The conduction heat transfer among absorber plates and tubes and the convection heat transfer of the fluid circulation inside the tube are important mechanisms in this chapter employed by CFD in the numerical domain proposed. The assumptions below have been applied to the numerical simulation model:

-The fluid is steady-state, uniform and incompressible.

- Part of the absorbed solar radiation by PV cells converts to electrical, whereas the rest part cause is rising in PV cell temperature.

-In reality, the nanoparticles and base fluid are two-phase; in calculations, both are in thermal equilibrium and single phase; this assumption is repeatedly in literature [126-129].

- Due to the lowering of temperature in the PVT system, the radiation heat loss is neglected.

- The contact area between the surface tubes and the bottom surface of the absorber plate is adiabatic.

- The thermal grease thickness between the PV module and the copper absorber plate is ignored.

-Assumed a perfect contact between the PV module and absorber plate. Thus, the temperature is the same in these layers, which agrees with [130, 128].

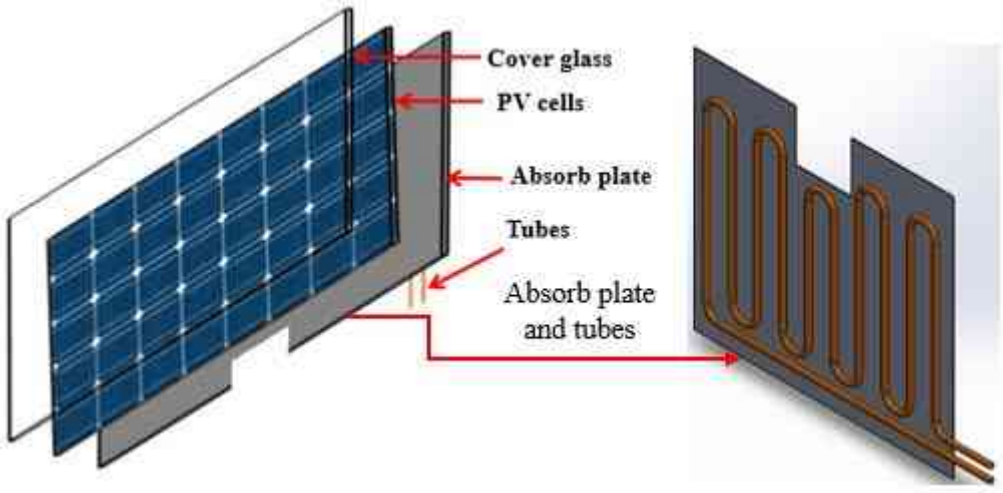

Figure 7.1: Sketch of the initial model and its components

7.2 Boundary conditions and numerical procedure

In this numerical study, the computational fluid dynamic (CFD) approach was used to investigate the performance of the PVT system cooled by nanofluids. According to the assumption above, the fluid flow inside the tubes is steady and incompressible, and the PVT system is considered the control volume; the governing equations adopted in the simulation are energy, continuity, and momentum [92]. These equations represent the boundary conditions for the current cases in a simple form.

Energy equation $$\nabla \cdot \left(\rho_{nf} U_{nf} C_{p_{nf}} T\right) = \nabla \cdot \left(k_{nf} \nabla T\right) \quad (7.1)$$

Continuity equation $$\nabla\left(\rho_{nf} U_{nf}\right) = 0 \quad (7.2)$$

Momentum equation $$\nabla \cdot \left(\rho_{nf} U_{nf} U_{nf}\right) = -\nabla \mathrm{P} + \nabla\tau + \rho_{nf} g \quad (7.3)$$

The equations are solved using the finite volume method through the ANSYS Fluent 19.2 software. According to the boundary condition, the heat flux value has been set and specified the fluid velocity at the inlet and temperature of the inlet fluid, then the specification method of the turbulent intensity from Eq (7.4) and the hydraulic diameter. At the tube outlet, the outflow is adapted as a fully developed fluid flow. For the flow regime, the k-epsilon model has been used through the calculations with activation of the enhanced wall treatment for both pressure gradient and thermal effects. The properties of the PVT system component and thermophysical properties of the nanofluids have been inserted from a fluent database. The boundary conditions of the external tube surface and the backside of the absorbing plate are an adiabatic wall, and the heat flux is zero. The heat generation rate on the top surface of the PVT system (geometry model) as a wall is equal to the value of absorbed solar irradiation, with the assumption that this wall transfers heat to the surrounding in a convection and radiation mechanism. The three-dimensional meshing generation is important to the conducted computational domain of the proposed CFD simulation model. The absorber plate and tubes were meshed with a mesh element size of 0.1mm, as shown in Fig. B4.1; the number of meshes elements was 779755 with high smoothing. Using the expression of the Re, Nu, and heat transfer coefficient, we calculated theirs for minimum, average and maximum values to compare with experimental results. The gravitational acceleration is an important parameter that works as a function of the system setup tilt angle and affects buoyancy force convection terms. This feature has been activated in the

simulation and is defined in Eq (7.7-7.9) [86]. For turbulent flow in tubes and a smooth surface and fully turbulent conditions, the Dittus-Boelter equation used Eq. (7.5).

$$I = 0.16\ Re^{\frac{1}{8}} \tag{7.4}$$

$$Nu = 0.023\ Re^{\frac{4}{5}}\ Pr^{n} \tag{7.5}$$

$$Pr = \frac{C_p\ \mu}{k} \tag{7.6}$$

$$g_x = -g\ \text{Sin}\ \theta \tag{7.7}$$

$$g_y = 0 \tag{7.8}$$

$$g_z = +g\cos\ \theta \tag{7.9}$$

7.3 Results and discussions

To validate the results of the simulation model, it has been compared with experimental studies that adopt ZrO_2/DI water and TiO_2-Fe_2O nanofluid. In this chapter, the simulation results are validated with results obtained according to Iraq and Hungary conditions by using ZrO_2/DI water nanofluid and Fe_2O_3/DI water nanofluid.

7.3.1 Temperature distribution on the proposed model

Figure 7.2 (a) shows the temperature distribution on the absorber plate directly in contact with tubes at used TiO_2-Fe_2O_3 nanofluid; a similar trend was observed with cooling by ZrO_2 nanofluid. It can be observed that the gradual temperature distribution increased at the end of the outlet fluid due to heat accumulated during nanofluid flow inside the serpentine tubes. The temperature distribution on the absorber plate was conducted at the tilt angle of 26 when 0.2vol% nanofluid enters the inlet tube at 0.323 m/s, 295 K, and solar radiation of 900 W/m^2. Thus, the cooling fluid's effect on the temperature distribution of the absorbing plate is positively reflected by decreased PV cells temperature. Figure 7.2 (b) shows the thermal behaviour of the cooling fluid inside the tubes that enters the inlet tube at low temperatures. Then it increases gradually due to heat transfer conduction from absorbing plate to tubes and by heat transfer convection to circulated fluid. By entering the cooling fluid inside the tubes, the temperature of the PV cells at the entrance area is reduced due to decreased absorb plate temperature. The cooling fluid temperature is gradually raised by circulating the coolant fluid through the tubes, which gain heat from the PV cells by the absorbing plate. Figure B4.2 shows a simplification of one tube contacted with absorb plate taken from the tubes connected to the entire absorbed plate, which can show the gradual temperature of a nanofluid along the tube tested under the same condition. Temperature contour shows the temperature path increased from the tube wall to fluid, which was high at the contact area of the tube and absorbed plate because there was no cooling effect at this area.

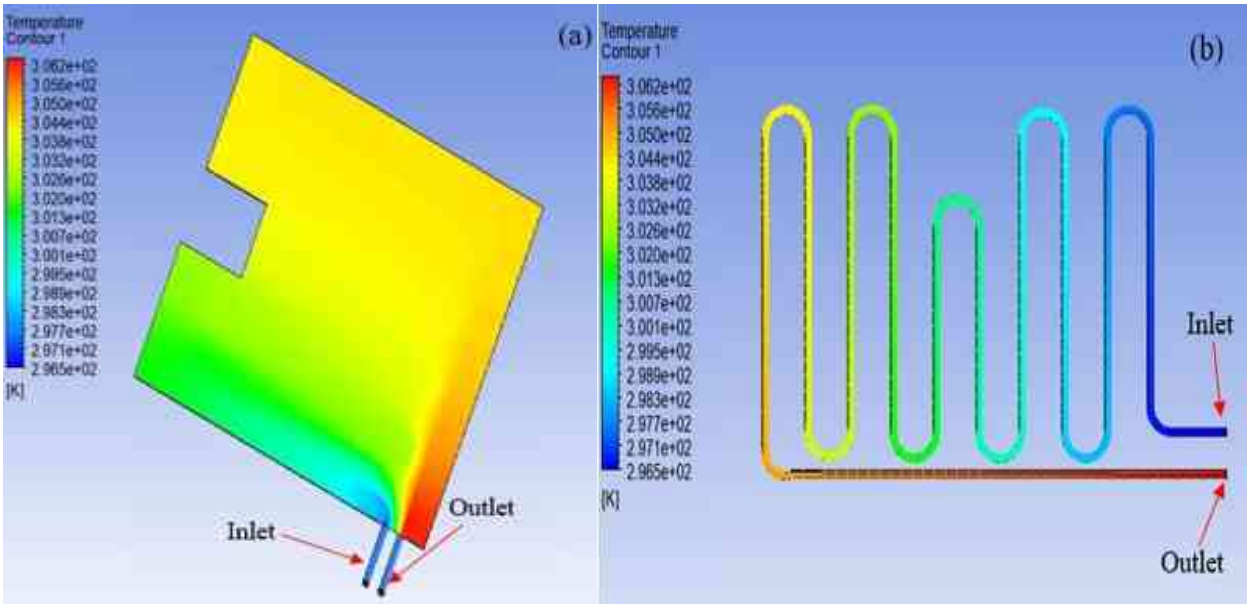

Figure 7.2: Temperature distribution contour (a) absorb plate and (b) serpentine tube

7.3.2 Energy evaluation of the photovoltaic thermal model

Figure 7.3 (a) and (b) shows the effect of the increase in the volume concentration of nanomaterials on the PVT temperature. The gradual volume concentration increases in base fluid enhanced the thermal conductivity of nanofluid and then increased the heat absorbed by the backside of the PV module. Using ZrO_2/DI water nanofluid for cooling the PV module helps decrease its temperature. Figure 7.3 (a) and (b) show the simulation results of maximum, average and minimum PVT system temperature, recorded at 0.015 vol%, 0.025 vol%, and 0.0275% were 51.93 °C, 50.32 °C and 48.8 °C, respectively. A gradual decrease in the temperature to the increased thermal conductivity of nanofluid can be observed due to an increase in the volume concentration of nanoparticles in base fluid compared with the PVT system cooled by DI water. Validation of the numerical simulation results with experimental results regarding the PVT system temperature was performed in May according to Iraq conditions. The deviation of the maximum, average, and minimum simulation results were 1.70%, 2.32% and 2.71%; this percentage is reasonable. Using a hybrid TiO_2-Fe_2O_3 nanofluid achieved a remarkable decrease in the PVT system temperature due to enhanced thermal properties. Suspension 0.2 vol% and 0.3 vol% of hybrid nanomaterials in base fluid helped decrease the PVT system temperature compared with cooling by DI water. Thus, cooling by hybrid nanofluid achieved a maximum reduction of the PVT system at 38.7 °C, 38 °C at 0.2 vol% and 0.3 vol% compared to cooling by DI water. By validation with experimental results obtained according to Hungary conditions in August, the maximum, average, and maximum deviation between the simulation and experimental results regarding PVT system temperature was 2.86%, 2.73 and, respectively. The energy efficiency of the PVT system is an important parameter to demonstrate the quantitative performance of the PVT system, which consists of electrical and thermal efficiencies.

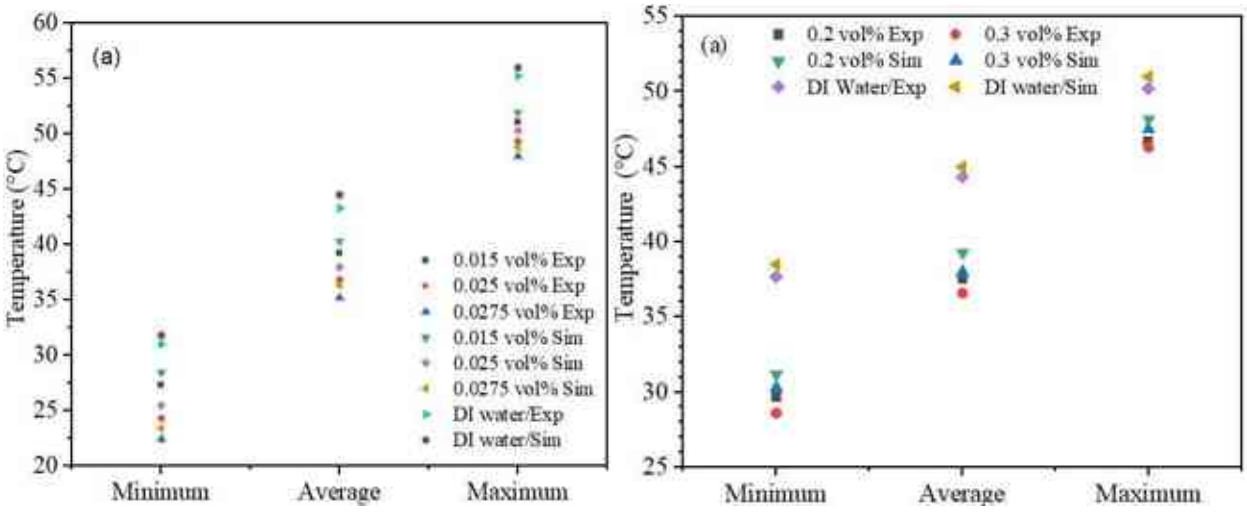

Figure 7.3: The numerical and experimental results of the effect of coolinb by nanofluid on the PVT system temperature (a) ZrO_2 nanofluid and (b) TiO_2-Fe_2O_3 nanofluid

Circulating the fluids at the backside of the PV module reduces the PV cell's temperature and enhances the PV cells' conversion efficiency. The cooling of the PVT system ZrO_2 nanofluid contributed by reducing the temperature and positively reflected by increased electrical efficiency. Figure 7.4 (a) shows the increase in the electrical efficiency of the PVT system cooled by ZrO_2 nanofluid at different volume concentrations compared to cooling by DI water. Enhancing the thermal conductivity of the nanofluid helps increase the excess absorbing heat at the backside of the PV module, then gradually increases the electrical efficiency. Compared with DI water, the ZrO_2 nanofluid improved electrical efficiency by 11.40% at 0.0275 vol%. Dispersion of ZrO_2 nanoparticles in the base fluid has enhanced thermal conductivity and then increased the absorption of excess heat, which causes an increase in the thermal efficiency of the PVT system. Thermal efficiency depends on mass flow rate, the specific heat of fluid used, and the temperature variation between inlet and outlet fluid. The maximum thermal efficiency achieved by cooling with ZrO_2 nanofluid was 30.79% at 0.0275 vol% compared to DI water, with achieved 26.81%. Compared with experimental results, the deviation of simulation results is about 2.70% of the electrical efficiency and 2.83%.

On the other hand, using the new hybrid nanofluid at different volume concentrations has noticeably improved electrical and thermal efficiencies. The new synthesis of TiO_2-Fe_2O_3 nanomaterials dispersed into DI water significantly helped to decrease the PV cell's temperature more than mono nanofluid, then improved the electrical efficiency to 12.93% at 0.3 vol% compared to DI water which achieved 7.31%. The high thermophysical properties of the hybrid nanofluid caused more heat absorption at the backside of the PV module, which reflected to increase in the thermal efficiency to 49.51% at 0.3 vol%. The simulation result of electrical and thermal efficiencies is validated with experimental results as shown in Fig. 7.4 (b); the deviation of electrical efficiency was 3.61% 2.98% of ZrO_2 and hybrid nanofluid, while thermal efficiency was 2.95 %, 3.11% which confirms the reasonable result of the module proposed. Dispersion of nanomaterials in the base fluid improves their thermal properties because the nanomaterials have higher thermal properties than fluids.

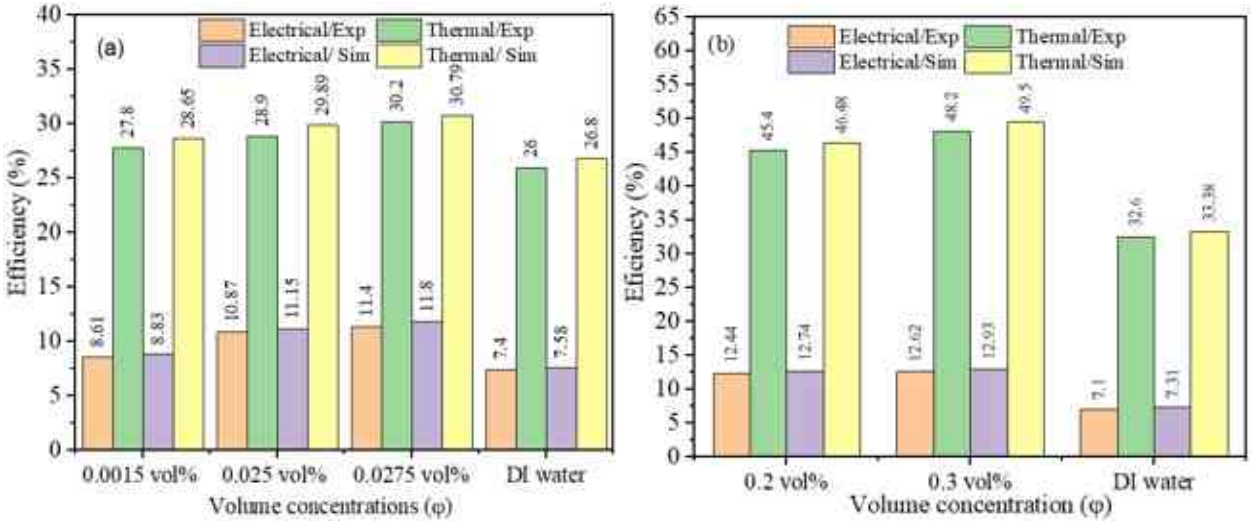

Figure 7.4: The electrical and thermal efficiencies of the PVT system cooled by (a) ZrO_2 nanofluid and (b) hybrid TiO_2-Fe_2O_3 nanofluid

This chapter investigated the influence of adding ZrO_2 nanoparticles and TiO_2-Fe_2O_3 nanomaterials at different volume concentrations in DI water on Reynolds number, heat transfer coefficient, Nusselt number, and pressure drop. Depending on the maximum, average and minimum, it has calculated heat transfer coefficient, Nusselt number, and pressure drop from Eq. (15-17). Figure B4.3 (a) and (b) shows the effect of increased volume concentration of the ZrO_2 and TiO_2-Fe_2O_3 nanomaterials on the Nusselt number as a function of Reynold's number. There was a gradually increased Nusselt number with increased Reynold's number with increased nanomaterials in the base fluid. Suspension of ZrO_2 nanoparticles at 0.015 vol%, 0.025 vol% and 0.0275 vol% enhanced the Nusselt number by 12.61%, 17.36% and 19.60% compared to DI water. In contrast, the suspension of TiO_2-Fe_2O_3 nanomaterials by 0.2 vol% and 0.3 vol% in the base fluid enhanced the Nusselt number by 25 % at 39.47% compared to the DI water. Increasing Nusselt numbers positively affects the heat transfer coefficient; thus, increasing the Reynolds number enhances the hybrid nanofluid's heat transfer coefficient. The maximum deviation between simulation and experimental results regarding using ZrO_2 nanofluid was 2.46%, and with TiO_2-Fe_2O_3 was 2.35%.

Figure B4.4 (a) shows the increment of the heat transfer coefficient with Reynold's number increased at different volume concentrations due to the high thermal conductivity of the thermophysical properties of the nanofluid. The gradual increase of ZrO_2 volume concentrations in host fluid enhanced the heat transfer coefficient by 9.11%, 10.75%, and 12.34 % compared with DI water. On the other side, Fig. B4.4 (b) show that adding 0.2 vol% and 0.3 vol% of TiO_2-Fe_2O_3 nanomaterials in DI water enhanced the heat transfer coefficient of hybrid nanofluid by 28.95% and 43.33%, which contributes to lower PV temperature more than DI water. Despite increasing the heat transfer coefficient due to increasing thermal conductivity, the density of the hybrid nanofluid is increased because of the volume concentration, which influences the pressure drop. The deviation between experimental and simulation results is recorded at 2.65% at the used ZrO_2 nanofluid and with the used TiO_2-Fe_2O_3 nanomaterials at 2.96%. Despite the remarkable enhancement in thermal conductivity of nanofluid and the enhancement of the Nusselt number and heat transfer coefficient with the increase in volumetric concentration, there was a percentage increase in the nanofluid density, which effect on the pressure drop. Figure B4.5 (a) shows the pressure drop values when increased Reynolds number due to the increase in the nanofluid density at adding ZrO_2 nanoparticles at different volume concentrations in the DI water. Thus, the nanofluid's increased density and viscosity increased the pressure drop using

ZrO_2 nanofluid to 18.70% at 0.0275 vol% compared to DI water. Figure B4.5 (b) shows the effect of the TiO_2-Fe_2O_3 nanomaterials dispersed in DI water, which worked to the flow's resistance and increased the pressure drop. Increasing the volume concentration of nanomaterials in the base fluid increased the pressure drop by 22.97% and 35.12% compared with DI water. Thereby the deviation of pressure drop in the simulation result was higher than the experimental result by 3.11% for the ZrO_2 nanofluid and 2.6% for the TiO_2-Fe_2O_3 hybrid nanofluid.

7.3.3 Exergy evaluation of the photovoltaic thermal module

The outlet fluid temperature, the volume concentrations of nanomaterials in the DI water and the mass flow rate influence the thermal exergy efficiency of the PVT system. Figure 77 (a and b) shows that the relative increase of the ZrO_2 nanoparticles and TiO_2-Fe_2O_3 nanomaterials in DI water led to a gradual increment of the thermal exergy efficiency higher than used DI water. Thereby, it can be observed that the thermal exergy efficiency was much lower than the electrical exergy efficiency. This is attributed to the outlet temperature of the fluids being closer to the ambient temperature, which agrees with [92]; the low quality of the thermal exergy is one of the reasons that causes reduced thermal exergy efficiency. The electrical exergy efficiency has relatively enhanced with increased volume concentrations and due to the enhanced heat transfer coefficient of the nanofluid. Figure 7.5 (a) shows the gradual increment of the electrical exergy with increased volume concentrations, where the maximum electrical exergy recorded at used ZrO_2 nanofluid to 10.32% at 0.0274 vol% compared to DI water. Figure 7.5 (b) demonstrates the ability of the TiO_2-Fe_2O_3 nanofluid to enhance the electrical exergy of the PVT system, adding 0.2 vol% and 0.3 vol% nanomaterials in base fluid increased the electrical exergy to 11.82% and 12.62%, respectively, compared by cooling with DI water.

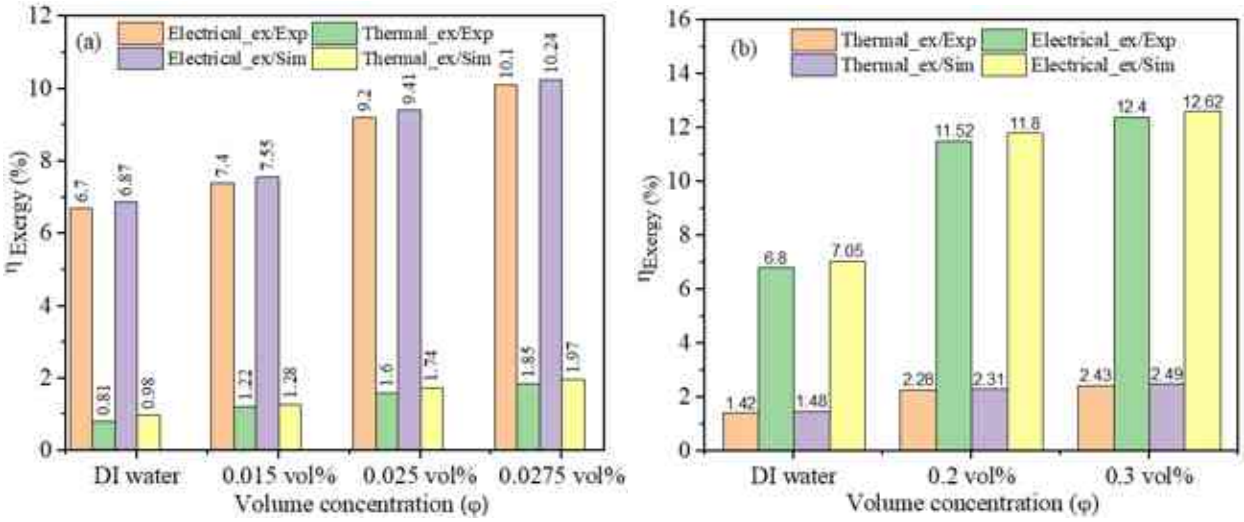

Figure 7.5: The exergy efficiency of the PVT system cooled by (a) ZrO_2 nanofluid, (b) TiO_2-Fe_2O_3 nanofluid

Nevertheless, using TiO_2-Fe_2O_3 nanofluid increments the electrical exergy efficiency of the PVT system by 82.32%, 69.41% with increased the TiO_2-Fe_2O_3 nanomaterials in DI water by 0.3% and 0.2% compared with DI water. Increment in the electrical energy efficiency significantly increased the overall exergy of the PVT system than thermal exergy efficiency; Fig. 7.5 (b) shows the exergy efficiency of the PVT system cooled with DI water and hybrid TiO_2-Fe_2O_3. This is attributed to enhanced cooling fluid thermal conductivity reflected on enhanced convective heat transfer between circulating cooling fluid and tubes placed on the absorbing plate. The variation between simulation results, electrical and thermal exergy efficiencies of using ZrO_2 nanofluid and experimental results were 2.61% and 3.12%respactivly. While using

hybrid nanofluid has recorded 2.87% thermal exergy efficiency and 3.32% electrical exergy efficiency.

7.4 New contributions results

Contribution 9

This chapter presents a numerical simulation study to investigate the effect of TiO_2-Fe_2O_3 nanofluid and ZrO_2 nanofluid at different volume concentrations on the energy and exergy. The important results of the simulation study are summarized as points below:

- Improving the thermal properties of nanofluid help accelerates heat exchange between circulated nanofluids in tubes and absorbing plate, which decreases the PV cell's temperature by 14.75% at cooling with ZrO_2 nanofluid at 0.0275 vol% and by 20.74% by cooling with hybrid nanofluid at 0.3 vol%, which affects by increased energy and exergy efficiency.
- Improvement of the heat transfer coefficient between the absorbing plate and the backside of the PV module, which has a high temperature, helped decrease the temperature and increased the electrical efficiency to 55.60% and 76.82% using ZrO_2 and TiO_2-Fe_2O_3 nanofluid. The heat absorption by absorb plate has maximized the thermal efficiency of the PVT system by 15% of ZrO_2 nanofluid and 28.29% of TiO_2-Fe_2O_3 hybrid compared to DI water.
- The thermal parameters have improved with an increased volume concentration of nanofluid; increasing Nusselt number led to an increase of heat transfer coefficient by 12.34% at used ZrO_2 nanofluid and 43.33% with hybrid nanofluid. An increase in volumetric concentration affects the pressure drop due to an increase in the nanofluid density, then increased the pressure drop by 18.72% using ZrO_2 nanofluid, while using TiO_2-Fe_2O_3 nanofluid increased the pressure drop to 35.12%.
- The exergy efficiency of the PVT system improved with the dispersion of nanomaterial in the DI water, which caused of increase in the exergy efficiency of the PVT system due to improving heat exchange. Improving the nanofluid's thermal conductivity helped increase the electrical exergy by 10.32% with ZrO_2 nanofluid and 12.62% using hybrid nanofluid. The low quality of the thermal exergy is due to the closer of the outlet temperature to the ambient temperature.
- For validating the simulation result work, a comparison study has been implemented between the simulation and experimental results, as shown in Table B4.2; reasonable conformity was observed between the numerical and experimental results.

Chapter 8

Contributions to the scientific knowledge

This dissertation presents new scientific results that contribute to increasing the knowledge of readers and researchers about new methods that help increase the efficiency of PV modules and PVT systems. Thus, demonstrating the quantity and quality of the PVT system produced using different cooling approaches and operation conditions. The points below summarize the new scientific results:

8.1 Prediction of photovoltaic module thermal and electrical behaviour under different conditions

It's necessary to study the thermal behaviour of PV modules under different conditions to know their influence on the electrical behaviour and then specify the weak points that affect their performance. I found that the electrical power and efficiency of the PV module dropped with a low solar radiation value of 176 W/m^2 and temperature between a maximum of 15.4 °C and a minimum of 11.9 °C; this range did not cause damage to the PV cells but lowering the performance. Increasing solar radiation to 735 W/m^2 with an ambient temperature of 35 °C causes an increase in the PV module temperature, affecting the open circuit voltage and output power. Thus, this range of solar radiation and ambient temperature caused to increase in the PV module temperature to 84.6 °C, which may lead to damage to PV cells. MATLAB-Simulink has investigated the electrical behaviour of the PV module by modelling the governing equations, which predict the P-V and V-I values of the PV cell depending on the various weather conditions and under STC operation. I found that, at a constant temperature of 25 °C and variable solar radiation from 820, 535, and 185 W/m^2, the current of the PV module has reduced to 21.50%, 82.33%, and 414.7%, respectively.
In contrast, the voltage was reduced to 13.63%, 78.57% and 455.55%, respectively, compared with the STC condition. Furthermore, at constant solar radiation 1000 W/m^2, various temperature values at 35 °C, 24 °C, and 18 °C, the current of the PV cells is slightly decreased at 35 °C by 12% and voltage by 19% compared with STC. The reduced temperature has enhanced the current and voltage of the PV module; the better condition was at 1000W/m^2 and 24 °C. Both simulations help us know the thermal and electrical behaviour of the PV module under different conditions, thus specifying the best methods to improve their performance.

8.2 Effect of passive cooling approaches applied

The passive cooling approach represented by cotton wicks immersed in water (CWIWs) generated continuous evaporative cooling, which decreased the PV module temperature by 22.34% and made it near ambient temperature. The generation of evaporative cooling helped increment the output power and efficiency by 114.81% and 113.22%, respectively, which were higher than the previous studies that used similar approaches. The electrical energy and exergy efficiency has improved by 29.80% and 7.23 %, respectively. The exergy losses have dropped to 14%, while entropy generation has by 14.32% due to temperature reduction. The reason returned to the type of cotton wicks used and the setting of the PV module. The internal structure consists of four small sub-cotton wicks collected together and covered with a cotton cover that helps

absorb water, which adequately transmits and distributes water to all CWs at the backside of the PV module. The tilt angle and the height of the PV module from the ground allow great air to circulate on the backside of PV modules. Thus, the flowing of the air over the wetted surface of the cotton wicks causes water to evaporate and cools the air that absorbs the heat from the PV module by forced convection and transfers it to air, which the productivity of the PV module enhances. In addition, water supplied to cotton wicks by gravity helped to sustain wet cotton wicks throughout the experiment and avoid using external power.
Cooling by cotton wicks integrated with rectangular aluminium fins (CWIRAFs). This case study compares passive (CWIRAF) and active cooling (circulated water) and their effect on the PV module's performance. Integrating wetted cotton wicks with aluminium fins that made direct contact with the backside of the PV module helped increase the heat transfer dissipation and reduced the PV module temperature higher than the first approach (without aluminium fins). The cooler aluminium fins' higher thermal conductivity helps enhance the heat exchanger at the backside of the PV module. Then it increases the conversion efficiency of the PV cells due to a temperature drop of 46.34%. Thereby, integrated cotton wicks by aluminium fins as on cooling approach achieved effective evaporative cooling applicable in hot conditions. The CWIRAFs cooling approach shows improved behaviour, which significantly enhanced the output power and efficiency of the PV module by 199.82% and 175.62% compared with the reference PV module.
Nevertheless, some cons of utilizing cotton wicks, such as the water consumption in hot weather; thus, this approach may not be feasible for large-scale installations. The active cooling approach performed less than passive cooling under similar conditions. This is attributed to indirect cooling, heat transfer across different PVT system layers, the thermal resistance of the layers, and the low thermal conductivity of the fluid circulated in tubes.

8.3 Effect of active cooling approaches applied

Active cooling approaches are represented by different circulated types of mono and new hybrid nanofluids applied to improve the PVT system's design, which is mentioned in chapter 6. According to hot climate conditions, new mono nanofluids not used by other researchers or studies, such as (ZrO_2 and WO_3) have been used as a cooling fluid to reduce the PV cells' high temperature and increase the PVT system energy and exergy. Using ZrO_2 nanofluid helps decrease the PV cell temperature by 21.20% and increasing the volume concentrations of the nanomaterials in the host fluid causes to enhance the heat transfer coefficient and Nusselt number by 13% and 51.70%. Thus, increased heat exchange between the absorbing plate (less hot) and the backside of the PV module (The hottest) helps increase the electrical power and efficiency to 87.31% and 54%, respectively. On the other hand, increased the exergy efficiency by 11.86% due to lowering the temperature, and the exergy losses and entropy generation were improved by 7% and 26%, respectively. Using WO_3 nanofluid helped to reduce the temperature of the PV cells by 21%, which was reflected in enhanced electrical power and electrical efficiency by 62% and 52% due to improved heat transfer coefficient to 5.31% with increased volume concentration to 1%. Increased volume concentration and Reynolds number caused an improved Nusselt number by 51.20% and increased the pressure drop by 49.23% compared to DI water. The exergy efficiency increased with the temperature low, effectively reducing the exergy loss and entropy generation by 15.32% and 53.52% because of their heat transfer enhancement and reduced fluid friction in PVT systems. Using both ZrO_2 and WO_3 nanofluids, the thermal exergy was lower than the electrical exergy because of the convergence of the fluid outlet temperature to the ambient temperature.
Therefore, both nanofluids enhanced PVT system performance due to reduced PV cell temperature and increased electrical power. A slightly better variation has been observed of the PVT system performance at used ZrO_2 nanofluid higher than WO_3 nanofluid, and this is because the thermal conductivity of ZrO_2 nanoparticles, which reflected heat transfer convection between absorb plate and circulated nanofluid. Thus, using ZrO_2 nanofluids has effectively enhanced the

exergy efficiency and reduced the exergy loss due to enhancing the heat transfer coefficient. Enhancing the heat transfer and reducing fluid friction led to a drop in the PVT system's entropy generation compared to the reference PV module. Cooling by different improving types of mono nanofluids represented by dispersion of the CuO in DI water has improved the performance of the PVT system due to the decreased temperature of the PV cells by 23.44%, and this is attributed to the effectiveness of CuO synthesized, which have high purity, and high thermal properties contribute to enhance the heat transfer convection between tubes and CuO nanofluid. Thus, increased the electrical power and efficiency of the PVT system by 70.72% and 90%, which was higher than the previous studies that used conventional approaches cooling by CuO nanofluid. This returns to the effective PVT system design and effectiveness of CuO synthesized. Dispersion TiO_2 in DI water achieved higher performance of the PVT system than ZrO_2 and WO_3 nanofluid due to their low thermophysical properties compared with TiO_2 nanofluid. On another side, using TiO_2 nanofluid achieved lower performance of the PVT system compared with CuO nanofluid, despite the low density and increased specific heat of the TiO_2 NWs, but the thermal conductivity of CuO has a major role by enhancing the heat transfer of nanofluid, which reflected of performance of the PVT system. Nevertheless, cooling with TiO_2 nanofluid reduced the PV cell reaches by 14%, reflecting an increment of power produced by 49.69%, then improved the electrical efficiency to 72.63% compared with DI water. Dispersion Fe_2O_3 in DI water achieved the highest performance of the PVT system than all the mono nanofluids used because of their high thermal properties. The gradually increased Fe_2O_3 in the base fluid caused an increase in heat transfer convection between the Fe_2O_3 nanofluid and tubes, which caused a lower temperature of the absorbing plate due to direct contact between tubes and the absorbing plate by 29.64%. Thus, heat transfers from the hot body (backside of the PV module) to a relatively cold body (absorb plate). This heat transfer mechanism decreases the PV cell's temperature and then improves the electrical power and efficiency of the PVT system by 76.70% and 110.43%, respectively, compared with DI water. Thereby, using Fe_2O_3 nanofluid achieved higher temperature reduction of the PVT system than CuO and TiO_2 nanofluids by 26.45% and 111.7%, respectively.

In contrast, electrical power and electrical efficiency of the PVT system cooled with Fe_2O_3 nanofluid were higher than cooling by CuO and TiO_2 nanofluids by 8.48%, 54.35%, 22.70% and 52.12%, respectively, which confirm the effectiveness of Fe_2O_3 nanofluid as a cooling fluid. The new hybrid nanomaterials synthesized positively affect the nanofluid preparation by improving its thermal properties. Loading TiO_2 NWs over Fe_2O_3 NPs and TiO_2 NWs over CuO NPs led to the hybrid nanomaterials increased surface area, thermal conductivity, and specific heat. Improving the nanomaterials thermophysical properties significantly affects the heat transfer coefficient, Nusselt number, and Reynolds Number of nanofluids, which affects PVT system performance. I have found that dispersion of TiO_2-Fe_2O_3 hybrid nanomaterials in DI water increased the heat transfer coefficient by 25% of nanofluid; this caused a lowering of the absorb plate temperature that dropped the temperature of the PV cells by 37.06% due to heat exchange. The electrical power output has enhanced by 71% and the overall efficiency of the PVT system by 50.68%, compared with DI water; I found that using TiO_2-Fe_2O_3 reduced the exergy loss and entropy generation by 47.32% and 70.47% due to temperature reduction, which led to increments in the exergy efficiency of the PVT system by 79.10%. Also found increased the pressure drop value by 36.12% with increased volume concentration in DI water, which caused an increase in the density and viscosity, then increased flow resistance of nanoparticles compared with cooling by DI water.

I found that using TiO_2-CuO nanofluid helps improve the energy and exergy efficiency of the PVT system, which is not less effective than TiO_2-Fe_2O_3 nanofluid. The loading of TiO_2 NWs over the CuO NPs achieved higher thermal conductivity and less density than TiO_2-Fe_2O_3 nanomaterials, which decreased the PV cell's temperature by 39.16%, which was higher than the other nanofluids used. Then enhanced the energy and exergy efficiencies by 113.8% and 78.6%, with fewer exergy losses than TiO_2-Fe_2O_3 by 44.3%. Lowering the PV cell's temperature reduced

the entropy generation by 69.61% more than DI water. It was observed that lower thermal exergy efficiency, which also attributed to the low quality of the thermal exergy. Compared with mono nanofluids, I found that hybrid nanofluid has a higher ability as a cooling fluid than mono nanofluids because of their new thermophysical properties and the new morphology of the nanomaterials shape. Preparation of the volume concentrations selected in DI water helped enhance the performance of nanofluid. It was found that the PVT system's performance is convergent at both hybrid nanofluids with slight variation in temperature drop and electrical power at using TiO_2-CuO nanofluid, which is slightly higher than used TiO_2-Fe_2O_3 nanofluid. This is attributed to the slight increase in thermal conductivity of the TiO_2-CuOnanofluid than TiO_2-Fe_2O_3 nanofluid.

8.4 Numerical simulation effect nanofluids on the photovoltaic thermal system performance

The numerical simulation has been conducted for a proposed model consisting of PVT components by ANSYS Fluent 19.2; the numerical simulation results have been validated with the experimental results. Dispersion of nanomaterials in base fluid improves the thermal properties of the nanofluid due to the high thermal conductivity of solid materials, which leads to improved thermal parameters of nanofluids with increased volume concentrations. By increasing the volume concentration, the Nusselt number increased and improved heat transfer coefficient by 12.34 % and 43.33% at used ZrO_2 and hybrid nanofluid. It was observed increased the pressure dropped by 18.7% and 35.12% at using ZrO_2 and hybrid nanofluid because the increased volume concentration caused to increase in the nanofluid density. The simulation results show that the adopted ZrO_2 nanofluid helped decrease the PV cell's temperature to 14.75%, while a hybrid TiO_2-Fe_2O_3 nanofluid reduced the temperature by 20.70%. The maximum deviation regarding decreased PV cell temperature between simulation results and experimental results was 2.79%. Improving the heat transfer coefficient has positively affected the heat exchange between the hot backside of the PV module and the absorbing plate, which have a lower temperature, which causes reduced temperature and improves the electrical efficiency by 55.62% and 76.80% using ZrO_2 and hybrid nanofluid. While absorbing the excess heat from the absorb plate has maximized the thermal efficiency by 15% and 28.29% at used ZrO_2 nanofluid and TiO_2-Fe_2O_3 nanofluid. The deviation was 3.93% and 3.02% between the simulation and experimental results for the electrical and thermal efficiencies. Improved heat exchange area due to enhancing the thermal conductivity of nanofluid led to increasing the electrical exergy by 10.32% at using ZrO_2 nanofluid; this percentage is an increment to 12.62% with using hybrid nanofluid. Thermal exergy efficiency was lower than electrical exergy efficiency, which was proven in experimental results due to the low quality of the thermal exergy. The maximum deviation of the thermal and electrical exergy efficiencies was 3.28% and 2.86% between the simulation and experimental results.

Bibliography

Papers published in international journals

[J1] Alktranee M, Péter B. Energy and exergy analysis for photovoltaic modules cooled by evaporative cooling techniques. Energy Reports. Elsevier; 2023;9:122–32.
[J2] Alktranee M, Shehab MA, Németh Z, Bencs P, Hernadi K, Koós T. Energy and Exergy Assessment of Photovoltaic-Thermal System Using Tungsten Trioxide Nanofluid: An Experimental Study. Int J Thermofluids. Elsevier; 2022;100228.
[J3] Alktranee M, Shehab MA, Németh Z, Bencs P, Hernadi K. Effect of zirconium oxide nanofluid on the behaviour of photovoltaic–thermal system: An experimental study. Energy Reports. Elsevier; 2023;9:1265–77.
[J4] Alktranee M, Bencs P. Experimental comparative study on using different cooling techniques with photovoltaic modules. J Therm Anal Calorim. Springer; 2023;1–13.
[J5] Alktranee M, Bencs P. Effect of Evaporative Cooling on Photovoltaic Module Performance. Process Integr Optim Sustain. Springer; 2022;1–10.
[J6] Alktranee M, Bencs P. Applications of nanotechnology with hybrid photovoltaic/thermal systems: A review. J Appl Eng Sci. 2021;19:292–306.
[J7] Alktranee M, Bencs P. Test the mathematical of the photovoltaic model under different conditions by use Matlab–Simulink. J Mech Eng Res Dev. 2020;43:514–21.
[J8] Bencs P, Alktranee M. The potential of vehicle cooling systems. J Phys Conf Ser. IOP Publishing; 2021. p. 12012.

Papers published in Hungarian journals

[J1] Alktranee, M. & Bencs, P. Simulation study of the photovoltaic panel under different operation conditions. ACTA IMEKO 10, 62–66 (2021).
[J2] Alktranee, M. & Bencs, P. Overview of the hybrid solar system. Analecta Tech. Szeged. 14, 100–108 (2020).
[J3] Bencs, P., Al-Ktranee, M. & Mészáros, K. M. Effects of solar panels on electrical networks. Analecta Tech. Szeged. 14, 50–60 (2020).
[J4] Péter, B., Dávid, F. & Alktranee, M. Áramlás-és Hőtechnikai fejlesztések az EFOP-361 projekt keretében. Multidiszcip. Tudományok 11, 107–115 (2021).

Conferences participation

[J1]Alktranee M, Bencs P. Factors affecting nanofluids behaviour: A review. Int Rev Appl Sci Eng. Akadémiai Kiadó Budapest; 2023;
[J2] Alktranee M, Bencs P. Simulation study of the photovoltaic panel under different operation conditions. ACTA IMEKO. 2021;10:62–6.
[J3] Alktranee M, Bencs P. Overview of the hybrid solar system. Analecta Tech Szeged. 2020;14:100–8.
[J4] Bencs P, Al-Ktranee M, Mészáros KM. Effects of solar panels on electrical networks. Analecta Tech Szeged. 2020;14:50–60.
[J5] Péter B, Dávid F, Alktranee M. Áramlás-és Hőtechnikai fejlesztések az EFOP-361 projekt keretében. Multidiszcip Tudományok. 2021;11:107–15.

References

[1] P. A. Østergaard, N. Duic, Y. Noorollahi, H. Mikulcic, and S. Kalogirou, "Sustainable development using renewable energy technology," *Renewable Energy*, vol. 146. Elsevier, pp. 2430–2437, 2020.

[2] P. J. T. Straatman and W. G. Van Sark, "A new hybrid ocean thermal energy conversion–Offshore solar pond (OTEC–OSP) design: A cost optimization approach," *Sol. Energy*, vol. 82, no. 6, pp. 520–527, 2008.

[3] M. Ball, M. Wietschel, and O. Rentz, "Integration of a hydrogen economy into the German energy system: an optimising modelling approach," *Int. J. Hydrogen Energy*, vol. 32, no. 10–11, pp. 1355–1368, 2007.

[4] P. Yilmaz, M. H. Hocaoglu, and A. E. S. Konukman, "A pre-feasibility case study on integrated resource planning including renewables," *Energy Policy*, vol. 36, no. 3, pp. 1223–1232, 2008.

[5] D. Das, P. Kalita, and O. Roy, "Flat plate hybrid photovoltaic-thermal (PV/T) system: A review on design and development," *Renew. Sustain. Energy Rev.*, vol. 84, pp. 111–130, 2018.

[6] D. H. W. Li, L. Yang, and J. C. Lam, "Zero energy buildings and sustainable development implications–A review," *Energy*, vol. 54, pp. 1–10, 2013.

[7] A. Hepbasli, "A key review on exergetic analysis and assessment of renewable energy resources for a sustainable future," *Renew. Sustain. energy Rev.*, vol. 12, no. 3, pp. 593–661, 2008.

[8] M. Alktranee and P. Bencs, "Overview of the hybrid solar system," *Analecta Tech. Szeged.*, vol. 14, no. 1, pp. 100–108, 2020, doi: 10.14232/analecta.2020.1.100-108.

[9] A. Dawar, A. Wakif, T. Thumma, and N. A. Shah, "Towards a new MHD non-homogeneous convective nanofluid flow model for simulating a rotating inclined thin layer of sodium alginate-based Iron oxide exposed to incident solar energy," *Int. Commun. Heat Mass Transf.*, vol. 130, p. 105800, 2022.

[10] N. Kannan and D. Vakeesan, "Solar energy for future world:-A review," *Renew. Sustain. Energy Rev.*, vol. 62, pp. 1092–1105, 2016.

[11] V. Tomar, B. Norton, and G. N. Tiwari, "A novel approach towards investigating the performance of different PVT configurations integrated on test cells: An experimental study," *Renew. Energy*, vol. 137, pp. 93–108, 2019.

[12] Y. Wang, M. L. Kamari, S. Haghighat, and P. T. T. Ngo, "Electrical and thermal analyses of solar PV module by considering realistic working conditions," *J. Therm. Anal. Calorim.*, vol. 144, no. 5, pp. 1925–1934, 2021.

[13] A. F. Abed, D. M. Hachim, and S. E. Najim, "A Novel Hybrid PV/T System for Sustainable Production of Distillate Water from the Cooling of the PV Module," in *IOP Conference Series: Materials Science and Engineering*, 2021, vol. 1094, no. 1, p. 12049.

[14] Z. Fu, X. Liang, Y. Li, L. Li, and Q. Zhu, "Performance improvement of a PVT system using a multilayer structural heat exchanger with PCMs," *Renew. Energy*, vol. 169, pp. 308–317, 2021.

[15] J. Siecker, K. Kusakana, and et B. P. Numbi, "A review of solar photovoltaic systems cooling technologies," *Renew. Sustain. Energy Rev.*, vol. 79, pp. 192–203, 2017.

[16] S. Odeh and M. Behnia, "Improving photovoltaic module efficiency using water cooling,"

Heat Transf. Eng., vol. 30, no. 6, pp. 499–505, 2009.
[17] M. Aghaei *et al.*, "Review of degradation and failure phenomena in photovoltaic modules," *Renew. Sustain. Energy Rev.*, vol. 159, p. 112160, 2022.
[18] I. W. G. on the E. of C. R. to Humans, "Solar and ultraviolet radiation," *Radiation*, 2012.
[19] L. J. Piotrowski, M. G. Simões, and F. A. Farret, "Feasibility of water-cooled photovoltaic panels under the efficiency and durability aspects," *Sol. Energy*, vol. 207, pp. 103–109, 2020.
[20] D. C. Jordan, S. R. Kurtz, K. VanSant, and J. Newmiller, "Compendium of photovoltaic degradation rates," *Prog. Photovoltaics Res. Appl.*, vol. 24, no. 7, pp. 978–989, 2016.
[21] M. Suthar, G. K. Singh, and R. P. Saini, "Performance evaluation of sun tracking photovoltaic systems: a case study," 2013.
[22] W. Luo *et al.*, "Potential-induced degradation in photovoltaic modules: a critical review," *Energy Environ. Sci.*, vol. 10, no. 1, pp. 43–68, 2017.
[23] B. V Chikate, Y. Sadawarte, and B. Sewagram, "The factors affecting the performance of solar cell," *Int. J. Comput. Appl.*, vol. 1, no. 1, pp. 975–8887, 2015.
[24] K. Sudhakar, N. Jain, and S. Bagga, "Effect of color filter on the performance of solar photovoltaic module," in *2013 International Conference on Power, Energy and Control (ICPEC)*, 2013, pp. 35–38.
[25] P. Dwivedi, K. Sudhakar, A. Soni, E. Solomin, and I. Kirpichnikova, "Advanced cooling techniques of P.V. modules: A state of art," *Case Stud. Therm. Eng.*, vol. 21, no. June, p. 100674, 2020, doi: 10.1016/j.csite.2020.100674.
[26] N. Abdollahi and M. Rahimi, "Potential of water natural circulation coupled with nano-enhanced PCM for PV module cooling," *Renew. Energy*, vol. 147, pp. 302–309, 2020.
[27] Y. Xu, Y. Xuan, and L. Yang, "Full-spectrum photon management of solar cell structures for photovoltaic–thermoelectric hybrid systems," *Energy Convers. Manag.*, vol. 103, pp. 533–541, 2015.
[28] I. A. Hasan and D. A. Attar, "Effect of evaporative cooling combined with heat sink on PV module performance," *J. Univ. Babylon Eng. Sci.*, vol. 27, no. 2, pp. 252–264, 2019.
[29] V. Baran *et al.*, "A comprehensive study on a stand-alone germanium (Ge) solar cell," *J. Electron. Mater.*, vol. 49, pp. 1249–1256, 2020.
[30] Z. Zhou, W. Liu, Y. Guo, H. Huang, and X. Ding, "Design Simulation and Optimization of Germanium-Based Solar Cells with Micro-Nano Cross-Cone Absorption Structure," *Coatings*, vol. 12, no. 11, p. 1653, 2022.
[31] M. Chandrasekar, S. Rajkumar, and D. Valavan, "A review on the thermal regulation techniques for non integrated flat PV modules mounted on building top," *Energy Build.*, vol. 86, pp. 692–697, 2015.
[32] A. S. Abdelrazik, F. A. Al-Sulaiman, R. Saidur, and R. Ben-Mansour, "A review on recent development for the design and packaging of hybrid photovoltaic/thermal (PV/T) solar systems," *Renew. Sustain. Energy Rev.*, vol. 95, pp. 110–129, 2018.
[33] G. S. Menon, S. Murali, J. Elias, D. S. Aniesrani Delfiya, P. V. Alfiya, and M. P. Samuel, "Experimental investigations on unglazed photovoltaic-thermal (PVT) system using water and nanofluid cooling medium," *Renew. Energy*, vol. 188, pp. 986–996, 2022, doi: 10.1016/j.renene.2022.02.080.
[34] H. Fayaz, R. Nasrin, N. A. Rahim, and M. Hasanuzzaman, "Energy and exergy analysis of the PVT system: Effect of nanofluid flow rate," *Sol. Energy*, vol. 169, pp. 217–230, 2018.
[35] M. Sardarabadi, M. Hosseinzadeh, A. Kazemian, and M. Passandideh-Fard, "Experimental investigation of the effects of using metal-oxides/water nanofluids on a photovoltaic thermal system (PVT) from energy and exergy viewpoints," *Energy*, vol. 138, pp. 682–695, 2017, doi: 10.1016/j.energy.2017.07.046.
[36] M. I. Hussain, J.-H. Kim, and J.-T. Kim, "Nanofluid-powered dual-fluid photovoltaic/thermal (pv/t) system: Comparative numerical study," *Energies*, vol. 12, no. 5, p. 775, 2019.

[37] A. H. Alami, “Effects of evaporative cooling on efficiency of photovoltaic modules,” *Energy Convers. Manag.*, vol. 77, pp. 668–679, 2014.
[38] M. Chandrasekar and T. Senthilkumar, “Passive thermal regulation of flat PV modules by coupling the mechanisms of evaporative and fin cooling,” *Heat Mass Transf. und Stoffuebertragung*, vol. 52, no. 7, pp. 1381–1391, 2016, doi: 10.1007/s00231-015-1661-9.
[39] L. J. Simpson, J. Woods, N. Valderrama, A. Hill, N. Vincent, and T. Silverman, “Passive Cooling of Photovoltaics with Desiccants,” in *2017 IEEE 44th Photovoltaic Specialist Conference (PVSC)*, 2017, pp. 1893–1897.
[40] P.-L. Paradis, D. R. Rousse, L. Lamarche, and H. Nesreddine, “A hybrid PV/T solar evaporator using CO2: Numerical heat transfer model and simulation results,” *Sol. Energy*, vol. 170, pp. 1118–1129, 2018.
[41] A. D. Tuncer, A. Khanlari, İ. Aytaç, E. Çiftçi, A. Sözen, and H. İ. Variyenli, “Passive thermal management of photovoltaic panel by using phase change material-filled aluminum cans: an experimental study,” *Heat Transf. Res.*, vol. 53, no. 5, 2022.
[42] Z. Arifin, S. Suyitno, D. D. D. P. Tjahjana, W. E. Juwana, M. R. A. Putra, and A. R. Prabowo, “The effect of heat sink properties on solar cell cooling systems,” *Appl. Sci.*, vol. 10, no. 21, p. 7919, 2020.
[43] T. Nabil and T. M. Mansour, “Augmenting the performance of photovoltaic panel by decreasing its temperature using various cooling techniques,” *Results Eng.*, p. 100564, 2022.
[44] A. Parthiban, K. S. Reddy, B. Pesala, and T. K. Mallick, “Effects of operational and environmental parameters on the performance of a solar photovoltaic-thermal collector,” *Energy Convers. Manag.*, vol. 205, p. 112428, 2020.
[45] Z. Wang, J. Wei, G. Zhang, H. Xie, and M. Khalid, “Design and performance study on a large-scale hybrid CPV/T system based on unsteady-state thermal model,” *Sol. Energy*, vol. 177, pp. 427–439, 2019.
[46] A. Rahaei, R. Rafee, and M. R. Zargarabadi, “A photovoltaic thermal system with a complete contact between water and PV modules suitable for district heating and electric power generation,” *Sustain. Energy Technol. Assessments*, vol. 47, p. 101325, 2021.
[47] S. Misha, A. L. Abdullah, N. Tamaldin, M. A. M. Rosli, and F. A. Sachit, “Simulation CFD and experimental investigation of PVT water system under natural Malaysian weather conditions,” *Energy Reports*, vol. 6, pp. 28–44, 2020.
[48] P. Chidambaram, R. Govindan, and K. C. Venkatraman, “Study of Thermal Comfort Properties of Cotton / Regenerated Bamboo Knitted Fabrics,” vol. 4, no. 2, pp. 60–66, 2012, doi: 10.5829/idosi.ajbas.2012.4.2.1032.
[49] A. Fudholi, K. Sopian, M. H. Yazdi, M. H. Ruslan, A. Ibrahim, and H. A. Kazem, “Performance analysis of photovoltaic thermal (PVT) water collectors,” *Energy Convers. Manag.*, vol. 78, pp. 641–651, 2014.
[50] S. M. Shalaby, M. K. Elfakharany, B. M. Moharram, and H. F. Abosheiasha, “Experimental study on the performance of PV with water cooling,” *Energy Reports*, vol. 8, pp. 957–961, 2022.
[51] S. Aghakhani, M. Afrand, A. Karimipour, R. Kalbasi, and M. M. Razzaghi, “Numerical study of the cooling effect of a PVT on its thermal and electrical efficiency using a Cu tube of different diameters and lengths,” *Sustain. Energy Technol. Assessments*, vol. 52, p. 102044, 2022.
[52] T. Le Ba *et al.*, “Experimental Study of Halloysite Nanofluids in Pool Boiling Heat Transfer,” *Molecules*, vol. 27, no. 3, p. 729, 2022, doi: 10.3390/molecules27030729.
[53] M. Firoozzadeh, A. H. Shiravi, M. Lotfi, S. Aidarova, and A. Sharipova, “Optimum concentration of carbon black aqueous nanofluid as coolant of photovoltaic modules: A case study,” *Energy*, vol. 225, 2021, doi: 10.1016/j.energy.2021.120219.
[54] S. Aberoumand, S. Ghamari, and B. Shabani, “Energy and exergy analysis of a photovoltaic thermal (PV/T) system using nanofluids: An experimental study,” *Sol.*

Energy, vol. 165, no. January, pp. 167–177, 2018, doi: 10.1016/j.solener.2018.03.028.
[55] G. S. Menon, S. Murali, J. Elias, D. S. A. Delfiya, P. V Alfiya, and M. P. Samuel, "Experimental investigations on unglazed photovoltaic-thermal (PVT) system using water and nanofluid cooling medium," *Renew. Energy*, vol. 188, pp. 986–996, 2022.
[56] S. Diwania, R. Kumar, S. K. Singh, G. S. Dua, and P. Khetrapal, "Performance assessment of a serpentine tube PVT system using Cu and TiO2 nanofluids: an experimental study," *J. Brazilian Soc. Mech. Sci. Eng.*, vol. 44, no. 2, pp. 1–18, 2022, doi: 10.1007/s40430-022-03366-5.
[57] M.-W. Tian *et al.*, "Energy, exergy and economics study of a solar/thermal panel cooled by nanofluid," *Case Stud. Therm. Eng.*, vol. 28, p. 101481, 2021.
[58] S. Diwania, A. S. Siddiqui, S. Agrawal, and R. Kumar, "Modeling and assessment of the thermo-electrical performance of a photovoltaic-thermal (PVT) system using different nanofluids," *J. Brazilian Soc. Mech. Sci. Eng.*, vol. 43, no. 4, pp. 1–18, 2021, doi: 10.1007/s40430-021-02909-6.
[59] S. R. Abdallah, H. Saidani-Scott, and O. E. Abdellatif, "Performance analysis for hybrid PV/T system using low concentration MWCNT (water-based) nanofluid," *Sol. Energy*, vol. 181, pp. 108–115, 2019.
[60] T. Venkatesh, S. Manikandan, C. Selvam, and S. Harish, "Performance enhancement of hybrid solar PV/T system with graphene based nanofluids," *Int. Commun. Heat Mass Transf.*, vol. 130, p. 105794, 2022, doi: 10.1016/j.icheatmasstransfer.2021.105794.
[61] J. A. Duffie and W. A. Beckman, *Solar engineering of thermal processes*. John Wiley & Sons, 2013.
[62] O. Rejeb, H. Dhaou, and A. Jemni, "Parameters effect analysis of a photovoltaic thermal collector: Case study for climatic conditions of Monastir, Tunisia," *Energy Convers. Manag.*, vol. 89, pp. 409–419, 2015.
[63] T. T. Chow, "Performance analysis of photovoltaic-thermal collector by explicit dynamic model," *Sol. Energy*, vol. 75, no. 2, pp. 143–152, 2003.
[64] O. Rejeb, H. Dhaou, and A. Jemni, "A numerical investigation of a photovoltaic thermal (PV/T) collector," *Renew. Energy*, vol. 77, pp. 43–50, 2015.
[65] A. Whillier and G. Saluja, "Effect of materials and construction details on the thermal performance of solar water heaters," *Sol. Energy*, vol. 9, no. 1, pp. 21–26, 1965, doi: https://doi.org/10.1016/0038-092X(65)90156-8.
[66] O. Rejeb, M. Sardarabadi, C. Ménézo, M. Passandideh-Fard, M. H. Dhaou, and A. Jemni, "Numerical and model validation of uncovered nanofluid sheet and tube type photovoltaic thermal solar system," *Energy Convers. Manag.*, vol. 110, pp. 367–377, 2016.
[67] M. Sardarabadi and M. Passandideh-Fard, "Experimental and numerical study of metal-oxides/water nanofluids as coolant in photovoltaic thermal systems (PVT)," *Sol. Energy Mater. Sol. Cells*, vol. 157, pp. 533–542, 2016.
[68] M. I. Hussain and J.-T. Kim, "Performance optimization of unglazed nanofluid photovoltaic/thermal system: Energy and exergy analyses," *Int. J. Photoenergy*, vol. 2018, 2018.
[69] D. L. Evans, "Simplified method for predicting photovoltaic array output," *Sol. energy*, vol. 27, no. 6, pp. 555–560, 1981.
[70] M. Hosseinzadeh, M. Sardarabadi, and M. Passandideh-Fard, "Energy and exergy analysis of nanofluid based photovoltaic thermal system integrated with phase change material," *Energy*, vol. 147, pp. 636–647, Mar. 2018, doi: 10.1016/j.energy.2018.01.073.
[71] S. Dubey, J. N. Sarvaiya, and B. Seshadri, "Temperature dependent photovoltaic (PV) efficiency and its effect on PV production in the world–a review," *Energy Procedia*, vol. 33, pp. 311–321, 2013.
[72] F. Abbas *et al.*, "Towards convective heat transfer optimization in aluminum tube automotive radiators: Potential assessment of novel Fe2O3-TiO2/water hybrid nanofluid," *J. Taiwan Inst. Chem. Eng.*, vol. 124, pp. 424–436, 2021.

[73] M. Alktranee and P. Bencs, “Applications of nanotechnology with hybrid photovoltaic/thermal systems: A review,” *J. Appl. Eng. Sci.*, vol. 19, no. 2, pp. 292–306, 2021, doi: 10.5937/jaes0-28760.
[74] P. Naphon, “Heat transfer characteristics and pressure drop in channel with V corrugated upper and lower plates,” *Energy Convers. Manag.*, vol. 48, no. 5, pp. 1516–1524, 2007.
[75] A. H. A. Al-Waeli, M. T. Chaichan, H. A. Kazem, K. Sopian, and J. Safaei, “Numerical study on the effect of operating nanofluids of photovoltaic thermal system (PV/T) on the convective heat transfer,” *Case Stud. Therm. Eng.*, vol. 12, pp. 405–413, 2018.
[76] S. Devireddy, C. S. R. Mekala, and V. R. Veeredhi, “Improving the cooling performance of automobile radiator with ethylene glycol water based TiO2 nanofluids,” *Int. Commun. heat mass Transf.*, vol. 78, pp. 121–126, 2016.
[77] A. M. Hussein, R. A. Bakar, K. Kadirgama, and K. V Sharma, “Experimental measurement of nanofluids thermal properties,” *Int. J. Automot. Mech. Eng.*, vol. 7, p. 850, 2013.
[78] Z. Qiu, X. Zhao, P. Li, X. Zhang, S. Ali, and J. Tan, “Theoretical investigation of the energy performance of a novel MPCM (Microencapsulated Phase Change Material) slurry based PV/T module,” *Energy*, vol. 87, pp. 686–698, 2015.
[79] Y. Demirel, “Thermodynamic analysis,” *Arab. J. Sci. Eng.*, vol. 38, no. 2, pp. 221–249, 2013.
[80] T. T. Chow, G. Pei, K. F. Fong, Z. Lin, A. L. S. Chan, and J. Ji, “Energy and exergy analysis of photovoltaic–thermal collector with and without glass cover,” *Appl. Energy*, vol. 86, no. 3, pp. 310–316, 2009.
[81] A. Fudholi *et al.*, “Energy and exergy analyses of photovoltaic thermal collector with∇-groove,” *Sol. Energy*, vol. 159, pp. 742–750, 2018.
[82] S. R. Maadi, A. Kolahan, M. Passandideh-Fard, M. Sardarabadi, and R. Moloudi, “Characterization of PVT systems equipped with nanofluids-based collector from entropy generation,” *Energy Convers. Manag.*, vol. 150, no. August, pp. 515–531, 2017, doi: 10.1016/j.enconman.2017.08.039.
[83] A. Farzanehnia and M. Sardarabadi, “Exergy in photovoltaic/thermal nanofluid-based collector systems,” in *Exergy and Its Application-Toward Green Energy Production and Sustainable Environment*, IntechOpen, 2019.
[84] M. A. Shehab *et al.*, “Preparation and Photocatalytic Performance of TiO2 Nanowire-Based Self-Supported Hybrid Membranes,” *Molecules*, vol. 27, no. 9, p. 2951, 2022.
[85] M. Sołtys-Mróz, K. Syrek, J. Pierzchała, E. Wiercigroch, K. Malek, and G. D. Sulka, “Band gap engineering of nanotubular Fe2O3-TiO2 photoanodes by wet impregnation,” *Appl. Surf. Sci.*, vol. 517, p. 146195, 2020.
[86] Y. Li, S. Tung, E. Schneider, and S. Xi, “A review on development of nanofluid preparation and characterization,” *Powder Technol.*, vol. 196, no. 2, pp. 89–101, 2009.
[87] M. Awais, A. A. Bhuiyan, S. Salehin, M. M. Ehsan, B. Khan, and M. H. Rahman, “Synthesis, heat transport mechanisms and thermophysical properties of nanofluids: A critical overview,” *Int. J. Thermofluids*, vol. 10, p. 100086, 2021.
[88] M. Milanese, G. Colangelo, A. Cretì, M. Lomascolo, F. Iacobazzi, and A. De Risi, “Optical absorption measurements of oxide nanoparticles for application as nanofluid in direct absorption solar power systems–Part II: ZnO, CeO2, Fe2O3 nanoparticles behavior,” *Sol. Energy Mater. Sol. Cells*, vol. 147, pp. 321–326, 2016.
[89] N. Gupta, S. M. Gupta, and S. K. Sharma, “Synthesis, characterization and dispersion stability of water-based Cu–CNT hybrid nanofluid without surfactant,” *Microfluid. Nanofluidics*, vol. 25, no. 2, pp. 1–14, 2021.
[90] N. S. Binti Rukman, A. Fudholi, N. F. Mohd Razali, M. Hafidz Ruslan, and K. Sopian, “Investigation of TiO2 and MWCNT Nanofluids-based Photovoltaic-Thermal (PV/T) System,” *IOP Conf. Ser. Earth Environ. Sci.*, vol. 268, no. 1, 2019, doi: 10.1088/1755-1315/268/1/012076.

[91] A. H. A. Al-Waeli, M. T. Chaichan, H. A. Kazem, and K. Sopian, “Evaluation and analysis of nanofluid and surfactant impact on photovoltaic-thermal systems,” *Case Stud. Therm. Eng.*, vol. 13, p. 100392, 2019.
[92] Y. Khanjari, F. Pourfayaz, and A. B. Kasaeian, “Numerical investigation on using of nanofluid in a water-cooled photovoltaic thermal system,” *Energy Convers. Manag.*, vol. 122, pp. 263–278, 2016.
[93] Y. Xuan and W. Roetzel, “Conceptions for heat transfer correlation of nanofluids,” *Int. J. Heat Mass Transf.*, vol. 43, no. 19, pp. 3701–3707, 2000.
[94] S. M. S. Murshed, K. C. Leong, and C. Yang, “Thermophysical and electrokinetic properties of nanofluids–a critical review,” *Appl. Therm. Eng.*, vol. 28, no. 17–18, pp. 2109–2125, 2008.
[95] D. A. Vincely and E. Natarajan, “Experimental investigation of the solar FPC performance using graphene oxide nanofluid under forced circulation,” *Energy Convers. Manag.*, vol. 117, pp. 1–11, 2016.
[96] Z. Said, M. H. Sajid, M. A. Alim, R. Saidur, and N. A. Rahim, “Experimental investigation of the thermophysical properties of AL2O3-nanofluid and its effect on a flat plate solar collector,” *Int. Commun. heat mass Transf.*, vol. 48, pp. 99–107, 2013.
[97] A. N. Al-Shamani, K. Sopian, S. Mat, H. A. Hasan, A. M. Abed, and M. H. Ruslan, “Experimental studies of rectangular tube absorber photovoltaic thermal collector with various types of nanofluids under the tropical climate conditions,” *Energy Convers. Manag.*, vol. 124, pp. 528–542, 2016.
[98] M. J. Muhammad, I. A. Muhammad, N. A. C. Sidik, M. N. A. W. M. Yazid, R. Mamat, and G. Najafi, “Retracted: the use of nanofluids for enhancing the thermal performance of stationary solar collectors: a review.” Elsevier, 2016.
[99] M. R. Safaei, A. Hajizadeh, M. Afrand, C. Qi, H. Yarmand, and N. W. B. M. Zulkifli, “Evaluating the effect of temperature and concentration on the thermal conductivity of ZnO-TiO2/EG hybrid nanofluid using artificial neural network and curve fitting on experimental data,” *Phys. A Stat. Mech. its Appl.*, vol. 519, pp. 209–216, 2019.
[100] T.-K. Hong, H.-S. Yang, and C. J. Choi, “Study of the enhanced thermal conductivity of Fe nanofluids,” *J. Appl. Phys.*, vol. 97, no. 6, p. 64311, 2005.
[101] R. Mehmood, S. Nadeem, and N. Sher Akbar, “Non-aligned ethylene-glycol 30% based stagnation point fluid over a stretching surface with hematite nano particles,” *J. Appl. Fluid Mech.*, vol. 9, no. 3, pp. 1359–1366, 2016.
[102] R. L. Hamilton and O. K. Crosser, “Thermal conductivity of heterogeneous two-component systems,” *Ind. Eng. Chem. Fundam.*, vol. 1, no. 3, pp. 187–191, 1962.
[103] S. K. Verma and A. K. Tiwari, “Progress of nanofluid application in solar collectors: a review,” *Energy Convers. Manag.*, vol. 100, pp. 324–346, 2015.
[104] R. S. Vajjha and D. K. Das, “Measurements of specific heat and density of Al 2 O 3 nanofluid,” in *AIP Conference Proceedings*, 2008, vol. 1063, no. 1, pp. 361–370.
[105] O. Arthur and M. A. Karim, “An investigation into the thermophysical and rheological properties of nanofluids for solar thermal applications,” *Renew. Sustain. Energy Rev.*, vol. 55, pp. 739–755, 2016.
[106] S. Armstrong and W. G. Hurley, “A thermal model for photovoltaic panels under varying atmospheric conditions,” *Appl. Therm. Eng.*, vol. 30, no. 11–12, pp. 1488–1495, 2010.
[107] P. I. Cooper, “The absorption of radiation in solar stills,” *Sol. energy*, vol. 12, no. 3, pp. 333–346, 1969.
[108] “Weather and climate, Miskolc, Hungary,” 2021.
[109] J. A. D. Deceased and W. A. Beckman, *Solar engineering of thermal processes*, vol. 3, no. 3. 1982. doi: 10.1016/0142-694x(82)90016-3.
[110] H. C. Hottel, “A simple model for estimating the transmittance of direct solar radiation through clear atmospheres,” *Sol. energy*, vol. 18, no. 2, pp. 129–134, 1976.
[111] I. Bodnár, P. Iski, D. Koós, and Á. Skribanek, “Examination of electricity production loss

of a solar panel in case of different types and concentration of dust," in *Advances and Trends in Engineering Sciences and Technologies III*, CRC Press, 2019, pp. 313–318.
[112] M. Premkumar, K. Chandrasekaran, and R. Sowmya, "Mathematical modelling of solar photovoltaic cell/panel/array based on the physical parameters from the manufacturer's datasheet," *Int. J. Renew. energy Dev.*, vol. 9, no. 1, p. 7, 2020.
[113] H. Bellia, R. Youcef, and M. Fatima, "A detailed modeling of photovoltaic module using MATLAB," *NRIAG J. Astron. Geophys.*, vol. 3, no. 1, pp. 53–61, 2014.
[114] F. Abbas *et al.*, "Towards convective heat transfer optimization in aluminum tube automotive radiators: Potential assessment of novel Fe2O3-TiO2/water hybrid nanofluid," *J. Taiwan Inst. Chem. Eng.*, vol. 124, pp. 424–436, 2021, doi: 10.1016/j.jtice.2021.02.002.
[115] S. M. Peyghambarzadeh, S. H. Hashemabadi, M. Naraki, and Y. Vermahmoudi, "Experimental study of overall heat transfer coefficient in the application of dilute nanofluids in the car radiator," *Appl. Therm. Eng.*, vol. 52, no. 1, pp. 8–16, 2013.
[116] E. M. C. Contreras, G. A. Oliveira, and E. P. Bandarra Filho, "Experimental analysis of the thermohydraulic performance of graphene and silver nanofluids in automotive cooling systems," *Int. J. Heat Mass Transf.*, vol. 132, pp. 375–387, 2019.
[117] K. S. Hanumanth Ramji, J. Vinoth Kumar, and A. Amar Karthik, "Experimental Investigation of Automobile radiator using Tungsten trioxide Nano-fluid," *IOP Conf. Ser. Mater. Sci. Eng.*, vol. 995, no. 1, 2020, doi: 10.1088/1757-899X/995/1/012017.
[118] Z. A. Haidar, J. Orfi, and Z. Kaneesamkandi, "Photovoltaic panels temperature regulation using evaporative cooling principle: Detailed theoretical and real operating conditions experimental approaches," *Energies*, vol. 14, no. 1, p. 145, 2020.
[119] R. S. Hansen, C. S. Narayanan, and K. K. Murugavel, "Performance analysis on inclined solar still with different new wick materials and wire mesh," *Desalination*, vol. 358, pp. 1–8, 2015.
[120] J. Kim, S. Bae, Y. Yu, and Y. Nam, "Experimental and numerical study on the cooling performance of fins and metal mesh attached on a photovoltaic module," *Energies*, vol. 13, no. 1, p. 85, 2019.
[121]: : "Agrometeorological Network::" http://www.agromet.gov.iq/stations.php?id=6 (accessed Jun. 24, 2022).
[122] P. Pounraj *et al.*, "Experimental investigation on Peltier based hybrid PV/T active solar still for enhancing the overall performance," *Energy Convers. Manag.*, vol. 168, pp. 371–381, 2018.
[123] M. Alktranee, M. A. Shehab, Z. Németh, P. Bencs, and K. Hernadi, "Effect of zirconium oxide nanofluid on the behaviour of photovoltaic–thermal system: An experimental study," *Energy Reports*, vol. 9, pp. 1265–1277, 2023.
[124] M. Sardarabadi, M. Passandideh-Fard, and S. Z. Heris, "Experimental investigation of the effects of silica/water nanofluid on PV/T (photovoltaic thermal units)," *Energy*, vol. 66, pp. 264–272, 2014.
[125] C. D. Corbin and Z. J. Zhai, "Experimental and numerical investigation on thermal and electrical performance of a building integrated photovoltaic–thermal collector system," *Energy Build.*, vol. 42, no. 1, pp. 76–82, 2010.
[126] A. H. Mahmoudi, M. Shahi, A. M. Shahedin, and N. Hemati, "Numerical modeling of natural convection in an open cavity with two vertical thin heat sources subjected to a nanofluid," *Int. Commun. Heat Mass Transf.*, vol. 38, no. 1, pp. 110–118, 2011.
[127] K. C. Lin and A. Violi, "Natural convection heat transfer of nanofluids in a vertical cavity: Effects of non-uniform particle diameter and temperature on thermal conductivity," *Int. J. Heat Fluid Flow*, vol. 31, no. 2, pp. 236–245, 2010.
[128] H. Demir, A. S. Dalkilic, N. A. Kürekci, W. Duangthongsuk, and S. Wongwises, "Numerical investigation on the single phase forced convection heat transfer characteristics of TiO2 nanofluids in a double-tube counter flow heat exchanger," *Int. Commun. Heat Mass Transf.*, vol. 38, no. 2, pp. 218–228, 2011.

[129] E. Ekramian, S. G. Etemad, and M. Haghshenasfard, “Numerical analysis of heat transfer performance of flat plate solar collectors,” *J. Fluid Flow, Heat Mass Transf.*, vol. 1, pp. 38–42, 2014.
[130] S. O. Giwa, M. Sharifpur, and J. P. Meyer, “Experimental study of thermo-convection performance of hybrid nanofluids of Al2O3-MWCNT/water in a differentially heated square cavity,” *Int. J. Heat Mass Transf.*, vol. 148, p. 119072, 2020, doi: 10.1016/j.ijheatmasstransfer.2019.119072.
[131] B. yuan Han *et al.*, “WO3 thermodynamic properties at 80–1256 K revisited,” *J. Therm. Anal. Calorim.*, vol. 142, no. 4, pp. 1533–1543, 2020, doi: 10.1007/s10973-020-09345-z.
[132] E. B. Öğüt, “Natural convection of water-based nanofluids in an inclined enclosure with a heat source,” *Int. J. Therm. Sci.*, vol. 48, no. 11, pp. 2063–2073, 2009.
[133] A. H. A. Al-Waeli, M. T. Chaichan, H. A. Kazem, and K. Sopian, “Comparative study to use nano-($Al2O_3$, CuO, and SiC) with water to enhance photovoltaic thermal PV/T collectors,” *Energy Convers. Manag.*, vol. 148, pp. 963–973, 2017.
[134] M. Faizal, R. Saidur, S. Mekhilef, and M. A. Alim, “Energy, economic and environmental analysis of metal oxides nanofluid for flat-plate solar collector,” *Energy Convers. Manag.*, vol. 76, pp. 162–168, 2013.
[135] A. B. Colak, “Experimental study for thermal conductivity of water-based zirconium oxide nanofluid: developing optimal artificial neural network and proposing new correlation,” *Int. J. Energy Res.*, vol. 45, no. 2, pp. 2912–2930, 2021.
[136] Y. Wang and J. Zhang, “Ultrafine TiO_2 (B) nanowires for ultrahigh-rate lithium-ion batteries,” *Ionics (Kiel).*, vol. 26, no. 3, pp. 1159–1164, 2020.
[137] A. Mulik, P. Hegade, S. Mulik, and M. Deshmukh, “CuO nanoparticles and nanobelts catalyzed potent synthesis of benzopyran derivatives,” *Res. Chem. Intermed.*, vol. 45, no. 11, pp. 5641–5647, 2019.
[138] C. Han, J. Han, Q. Li, and J. Xie, “Wet chemical controllable synthesis of hematite ellipsoids with structurally enhanced visible light property,” *Sci. World J.*, vol. 2013, 2013.
[139] P. Chidambaram, R. Govindan, and K. C. Venkatraman, “Study of thermal comfort properties of cotton/regenerated bamboo knitted fabrics,” *African J. Basic Appl. Sci.*, vol. 4, no. 2, pp. 60–66, 2012.
[140] A. Pandey, S. Chakrabarti, and P. Daghe, “A systematic approach for a better thermal management of photovoltaic systems-a review,” *J. Comput. Appl. Res. Mech. Eng.*, vol. 10, no. 1, pp. 1–24, 2020, doi: 10.22061/JCARME.2019.5814.1734.
[141] M. Chandrasekar and T. Senthilkumar, “Experimental demonstration of enhanced solar energy utilization in flat PV (photovoltaic) modules cooled by heat spreaders in conjunction with cotton wick structures,” *Energy*, vol. 90, pp. 1401–1410, 2015, doi: 10.1016/j.energy.2015.06.074.
[142] M. Firoozzadeh, A. H. Shiravi, and S. S. Chandel, “An experimental analysis of enhancing efficiency of photovoltaic modules using straight and zigzag fins,” *J. Therm. Anal. Calorim.*, 2022, doi: 10.1007/s10973-021-11178-3.
[143] M. Alktranee and P. Bencs, “Effect of Evaporative Cooling on Photovoltaic Module Performance,” *Process Integr. Optim. Sustain.*, pp. 1–10, 2022, doi: https://doi.org/10.1007/s41660-022-00268-w.
[144] P. Jidhesh, T. V Arjunan, and N. Gunasekar, “Thermal modeling and experimental validation of semitransparent photovoltaic-thermal hybrid collector using CuO nanofluid,” *J. Clean. Prod.*, vol. 316, p. 128360, 2021.
[145] M. Chandrasekar, S. Suresh, T. Senthilkumar, and M. Ganesh Karthikeyan, “Passive cooling of standalone flat PV module with cotton wick structures,” *Energy Convers. Manag.*, vol. 71, pp. 43–50, 2013, doi: 10.1016/j.enconman.2013.03.012.
[146] N. Hooshmandzade, A. Motevali, S. R. M. Seyedi, and P. Biparva, “Influence of single and hybrid water-based nanofluids on performance of microgrid photovoltaic/thermal

system," *Appl. Energy*, vol. 304, p. 117769, 2021.
[147] H. Adun *et al.*, "Synthesis and application of ternary nanofluid for photovoltaic-thermal system: Comparative analysis of energy and exergy performance with single and hybrid nanofluids," *Energies*, vol. 14, no. 15, p. 4434, 2021.
[148] I. Wole-Osho, H. Adun, M. Adedeji, E. C. Okonkwo, D. Kavaz, and M. Dagbasi, "Effect of hybrid nanofluids mixture ratio on the performance of a photovoltaic thermal collector," *Int. J. Energy Res.*, vol. 44, no. 11, pp. 9064–9081, 2020.
[149] R. Sathyamurthy, A. E. Kabeel, A. Chamkha, A. Karthick, A. Muthu Manokar, and M. G. Sumithra, "Experimental investigation on cooling the photovoltaic panel using hybrid nanofluids," *Appl. Nanosci.*, vol. 11, no. 2, pp. 363–374, 2021.
[150] M. Alktranee, M. A. Shehab, Z. Németh, P. Bencs, K. Hernadi, and T. Koós, "Energy and Exergy Assessment of Photovoltaic-Thermal System Using Tungsten Trioxide Nanofluid: An Experimental Study," *Int. J. Thermofluids*, p. 100228, 2022.
[151] M. Hosseinzadeh, M. Sardarabadi, and M. Passandideh-Fard, "Energy and exergy analysis of nanofluid based photovoltaic thermal system integrated with phase change material," *Energy*, vol. 147, pp. 636–647, 2018.
[152] N. S. B. Rukman, A. Fudholi, N. F. M. Razali, M. H. Ruslan, and K. Sopian, "Energy and exergy analyses of photovoltaic-thermal (PV/T) system with TiO2/water nanofluid flow," in *IOP Conference Series: Earth and Environmental Science*, 2019, vol. 268, no. 1, p. 12075.
[153] T. K. Murtadha, A. A. dil Hussein, A. A. H. Alalwany, S. S. Alrwashdeh, and M. Ala'a, "Improving the cooling performance of photovoltaic panels by using two passes circulation of titanium dioxide nanofluid," *Case Stud. Therm. Eng.*, vol. 36, p. 102191, 2022.

Appendix A

Synthesized mono nanomaterials

Nanomaterials are the main part of nanofluids; all the nanomaterials used to prepare nanofluids have been synthesized in the faculty of materials and chemical engineering at the University of Miskolc, except ZrO_2 nanoparticles, which were purchased. The thermophysical properties of all mono nanomaterials are shown in Table A1.

Table A.1: Thermophysical properties of mono nanomaterials

Properties	DI Water [130]	Fe_2O_3 [72]	WO_3 [117][131]	TiO_2 [72][132]	CuO [133][134]	ZrO_2 [135]
Density (kg/m^3)	997	5240	7160	3900	6310	5890
Thermal conductivity (W/m·K)	0.613	20	1.63	8.9	32.9	2.7
Heat capacity (J/kg·K)	4179	650	335	686	551	0.455

A.1 Tungsten trioxide

Hydrothermal treatment is used to fabricate tungsten trioxide nanoparticles (WO_3 NPs), which involves dissolving 5 g of sodium tungstate dihydrate ($Na_2WO_4{\cdot}2H_2O$) into 200 mL of DI water under continuous stirring (500 rpm) for 2 hours. Then Hydrochloric acid (HCl) was dropwise by 3 M into the solution even tungsten acid was precipitated thoroughly, thus putting the solution into a Teflon-lined autoclave with a capacity of 500 ml, then sealed and maintained the autoclave at 150 °C for 12 hours. Left the autoclave to cool to room temperature naturally after the reaction was completed; after that, washed with DI water several times by centrifuge to reach pH 7. Moreover, the solution is dried in an oven at 100 ºC for 1 hour and calcination under 500 ºC for 2 hours. Figure A.1 shows the steps of nanoparticle WO_3 synthesis.

Figure A.1: Schematic of the synthesis process of WO_3 nanopowder by hydrothermal method

The crystal structure of the prepared samples was determined using X-ray powder diffraction (XRD) (Bruker D8 Advance diffractometer) at (CuK α= 0.15418 nm) (40 kV and 40 mA) in parallel beam geometry (Göbel mirror) with a position-sensitive detector (Vantec1, 1°opening).

On top-loaded specimens in zero-background WO_3 sample containers, measurements were made in the 2-100° (2 Theta) range using a 0.007° (2 Theta)/14-sec goniometer speed. Based on the qualitative phase analysis of WO_3 synthesized by the hydrothermal method, the sample consists of a hexagonal lattice WO_3 phase found in more significant amounts, and there are few monoclinic lattice WO_3. Based on the Rietveld refinement, the sample is 100% crystalline with green colour with no amorphous phase found; Fig. A.2 (a) shows the XRD pattern of WO_3 nano-powder. Figure A.2 (b) shows the shape and distribution of the WO_3 nano-powder sample synthesized by the scanning electron microscope (SEM). The morphology of WO_3 appeared as nanoflakes formed in irregular shapes.

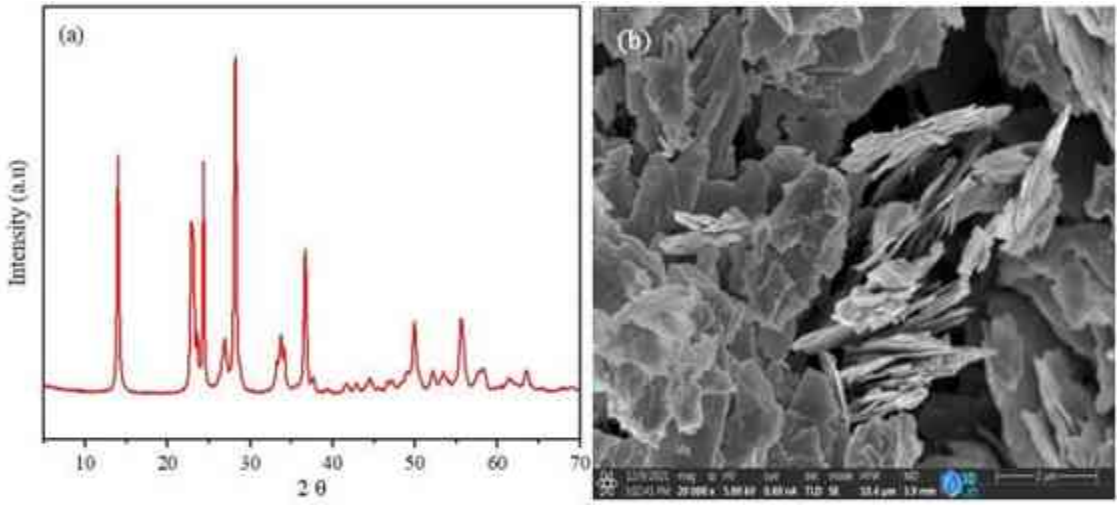

Figure A.2: The XRD pattern of the synthesized WO_3 (a) and (b) SEM image of WO_3 nanoflakes

A.2 Titanium oxide nanowires

As published in our earlier work, titanium oxide nanowires (TiO_2 NWs) were produced using a hydrothermal method. The homogenous suspension was formed using 3 g of TiO_2 nanoparticles, dissolved in 100 mL KOH aqueous solution (10 M), kept stirred for 30 min, then transferred to a Teflon-lined autoclave at 160 °C for 24 h. The product was collected using vacuum filtration and washed several times with 0.1 M HCl and DI water until the pH was 7. After drying the products overnight in a furnace, the white TiO_2 NWs powder was obtained and calcined at 400 °C for 1 h. XRD has been performed to identify and describe the crystal structure of TiO_2 NWs, as shown in Fig. A.3 (a). The diffraction peaks are located at 33.8°, 39.2°, 48°, 54.2°, 56.5°, 66.4° and 68.8°, corresponding to (211), (220), (200), (105), (213), (004) and (403) refer to anatase phase (JCPDS 21-1272). The other peaks located at 27.4°, 36.1° and 41.2° index to (110), (101) and (111) relate to the rutile phase (JCPDS no-21-1276). Furthermore, the diffraction peaks located at 11.4°, 24.1°, 29.2°, 42.9° and 59.8° corresponding to (200), (002), (310), (602) and (610) refer to $K_2Ti_6O_{13}$ (PDF no. 40-0403). All these results agreed with [84] [136]. A transmission electron microscope TEM technique is used for investigations of the surface morphology of TiO_2, which is shown as nanowires, as shown in Fig. A.3 (b).

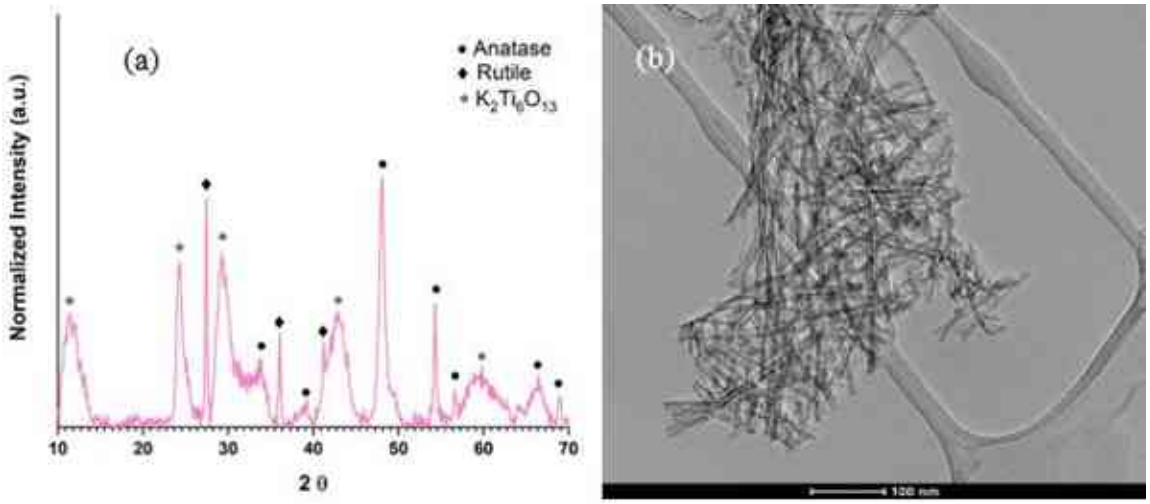

Figure A.3: The XRD pattern of the synthesized TiO_2 (a) and (b) TEM image of TiO_2 nanowires

A.3 Copper oxide nanoparticles

In order to produce the copper oxide (CuO NPs), a calculated amount of (Cu $(CH_3COO)_2 \cdot H_2O$) was dissolved in 100 mL of ethanol and stirred vigorously for 30 min. Then poured into an autoclave and thermally treated at 150 °C for 12 h. The finished product was collected, vacuum-filtered, washed, and then calcined at 500 °C for 2 h, similar to the method conducted by [84]. Figure A.4 (a) shows XRD analysis of CuO, the diffraction peaks located at 32.5°, 35.5°, 38.7°, 48.8°, 53.4°, 58.3°, 61.5°, 65.8°, 66.2° and 68° corresponding to (110), (-111), (111), (-202), (020), (202), (-113), (022), (-311) and (220) refer to copper oxide (JCPDS card number 45-0937), which agree with [137]. A transmission electron microscopy TEM technique is used for investigations of the surface morphology of CuO, which is shown as nanoparticles, as shown in Fig. A.4 (b).

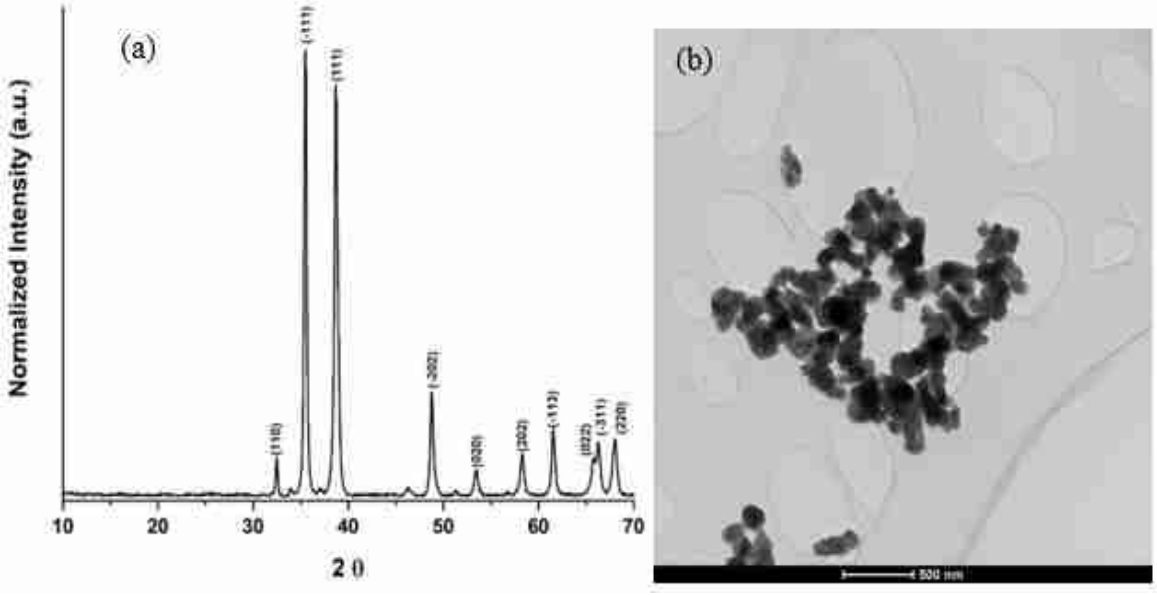

Figure A.4: The XRD pattern of the synthesized CuO (a) and (b) TEM image of CuO nanoparticles

A.4 Iron oxide nanorods

Iron oxide (Fe_2O_3) nanorod production by a similar method used by [84], $FeC_{l3} \cdot 6H_2O$ precursor was dissolved in 100 mL of distilled water to gain a homogeneous solution. NaOH solution was added dropwise under stirring until the solution became base and then transferred to the

autoclave at 90 °C for 9 h. To neutral pH, the product was washed with distilled water, dried and calcinated at 500 °C for 2 h. XRD analysis was performed to identify crystal structure, as shown in Fig. A.5 a, the peaks located at 24.1°, 33.1°, 35.6°, 40.8°, 49.4°, 54°, 57.6°, 62.4°, 64° and 67.4° index to (012), (104), (110), (113), (024), (116), (018), (214), (300) and (442) originating to Hematite iron oxide (α-Fe_2O_3) (JCPDS 33-0664). This results in good agreement with [138]. A transmission electron microscope TEM technique is used to investigate the surface morphology of Fe_2O_3, shown as nanorods, as shown in Fig. A.5 b.

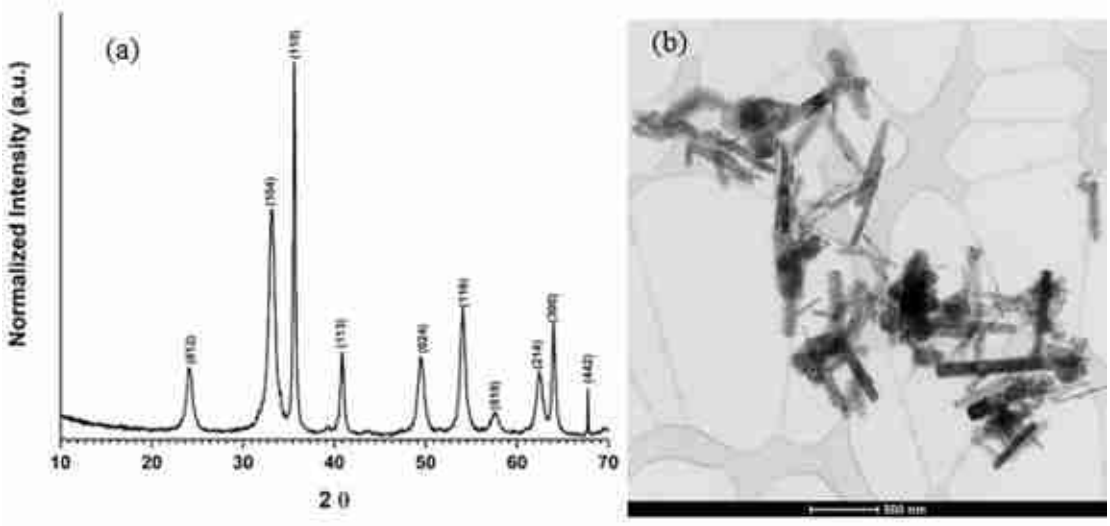

Figure A.5: The XRD of the synthesized Fe_2O_3 (a) and (b) TEM image of Fe_2O_3 nanorods

A.5 Zirconium Oxide nanoparticles (ZrO_2 NPs)

The ZrO_2 nanoparticles were supplied by (Research Nanomaterials, Inc., Houston, TX, USA) with a particle size of 20 nm, white colour, with 99.95% purity, and the SEM image in Fig. A.6 shows the morphology of the ZrO_2 according to provided by the vendor.

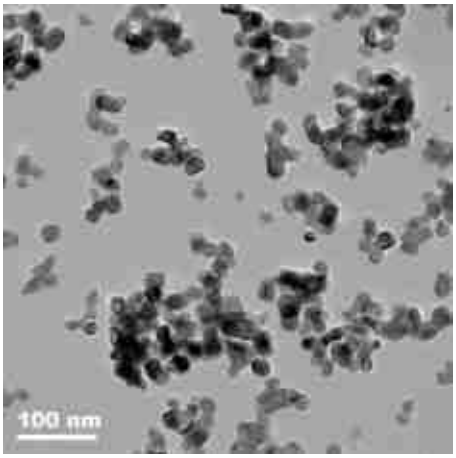

Figure A.6: TEM image of the ZrO_2 nanoparticle

Appendix B1

Effect of iron oxide and tungsten trioxide nanofluids on the boiler system behaviour

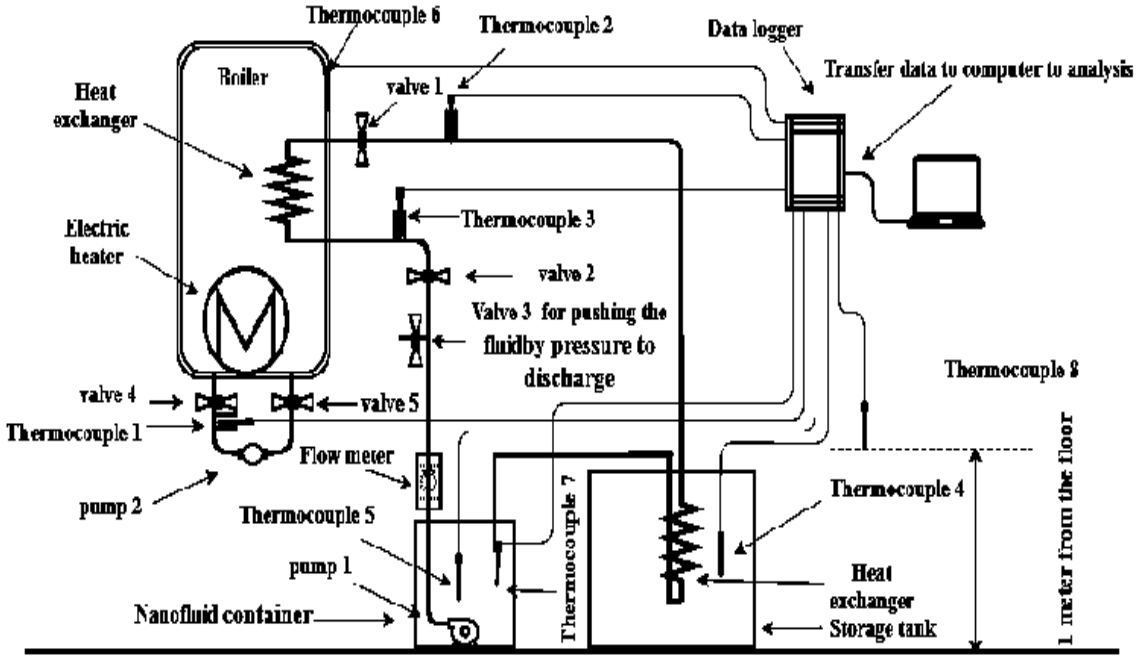

Figure B1.1: Schematic diagram of the boiler system

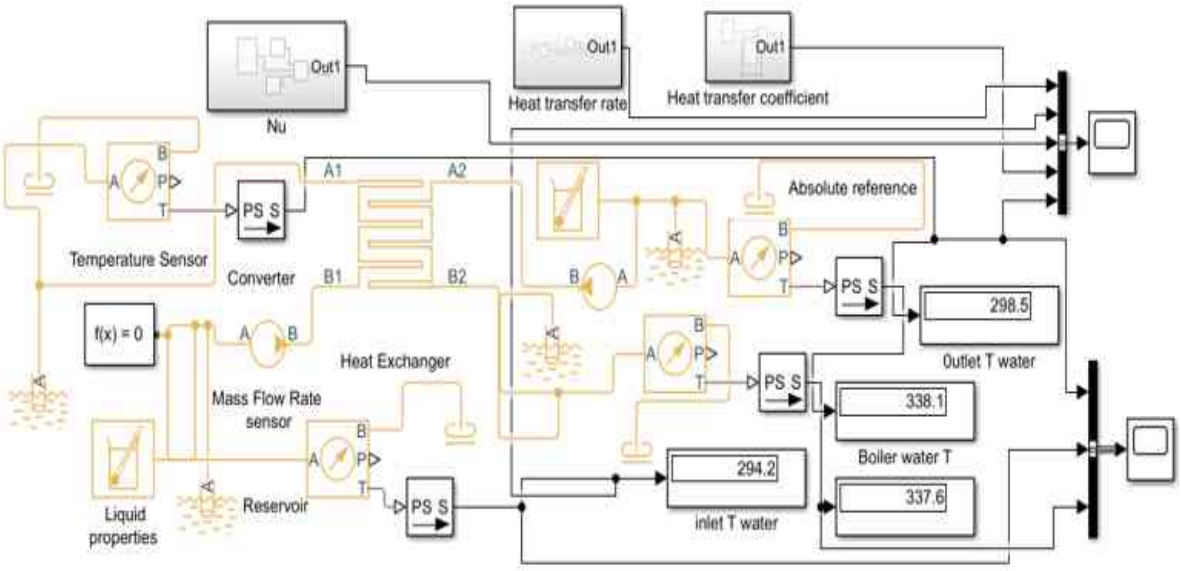

Figure B1.2: Simulink model of the heat exchanger

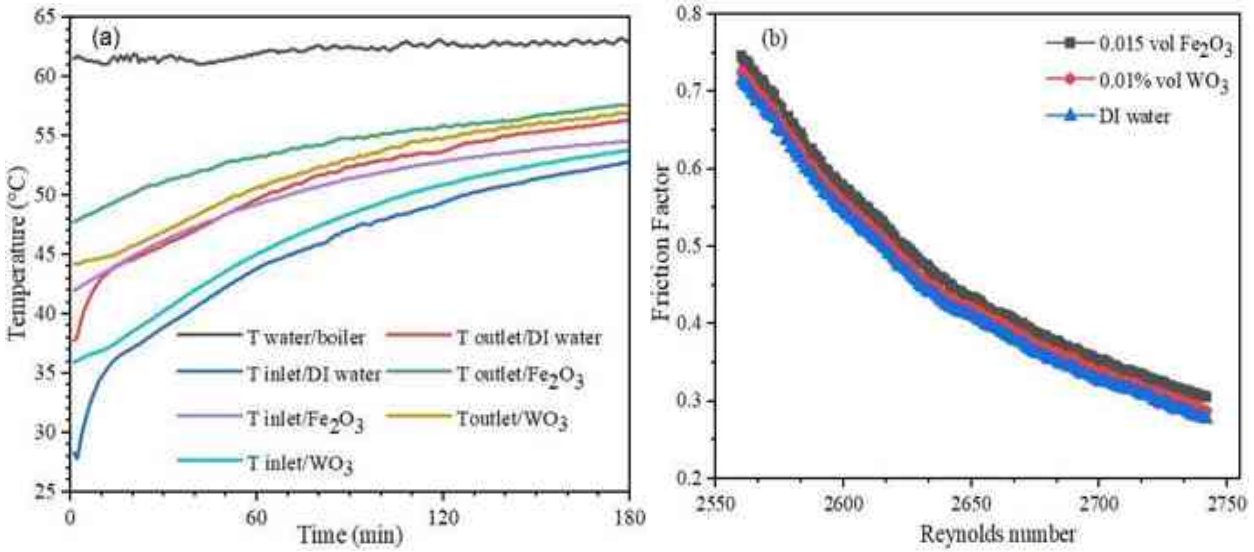

Figure B1.3: The temperature profile of working fluid (a) and (b) influence of Reynolds number on friction factor

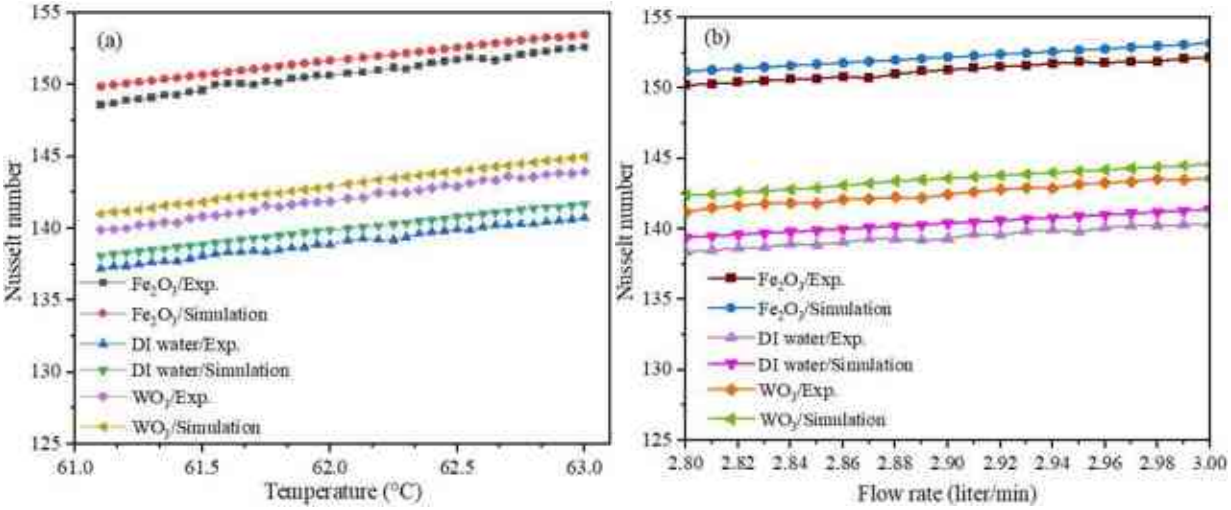

Figure B1.4: Influence Nusselt number by (a) inlet temperatures and (b) flow rate

Appendix B2

Effect of evaporative cooling and nanofluids cooling on the photovoltaic performance

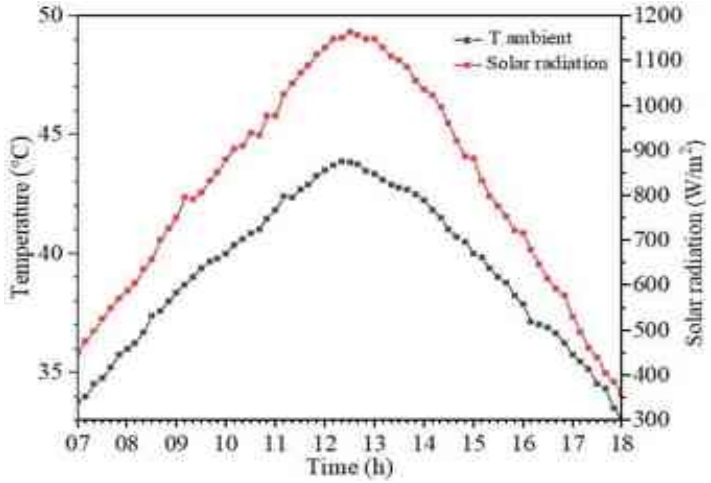

Figure B2.1: Average solar radiation and ambient temperature

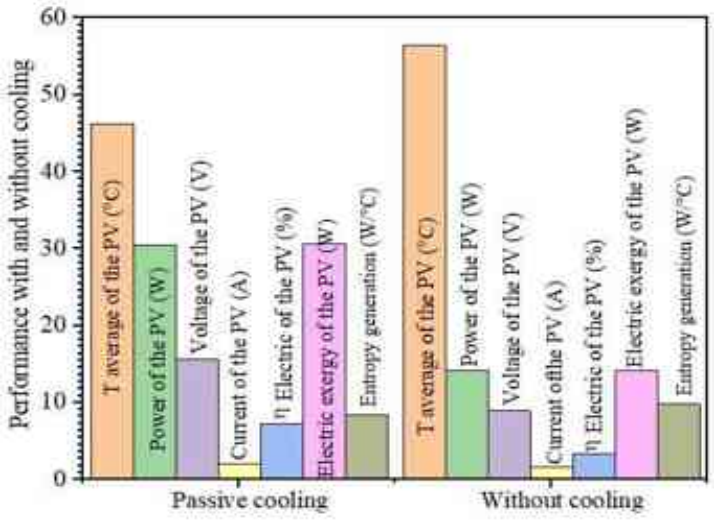

Figure B2.2: Comparison of PV module's performance

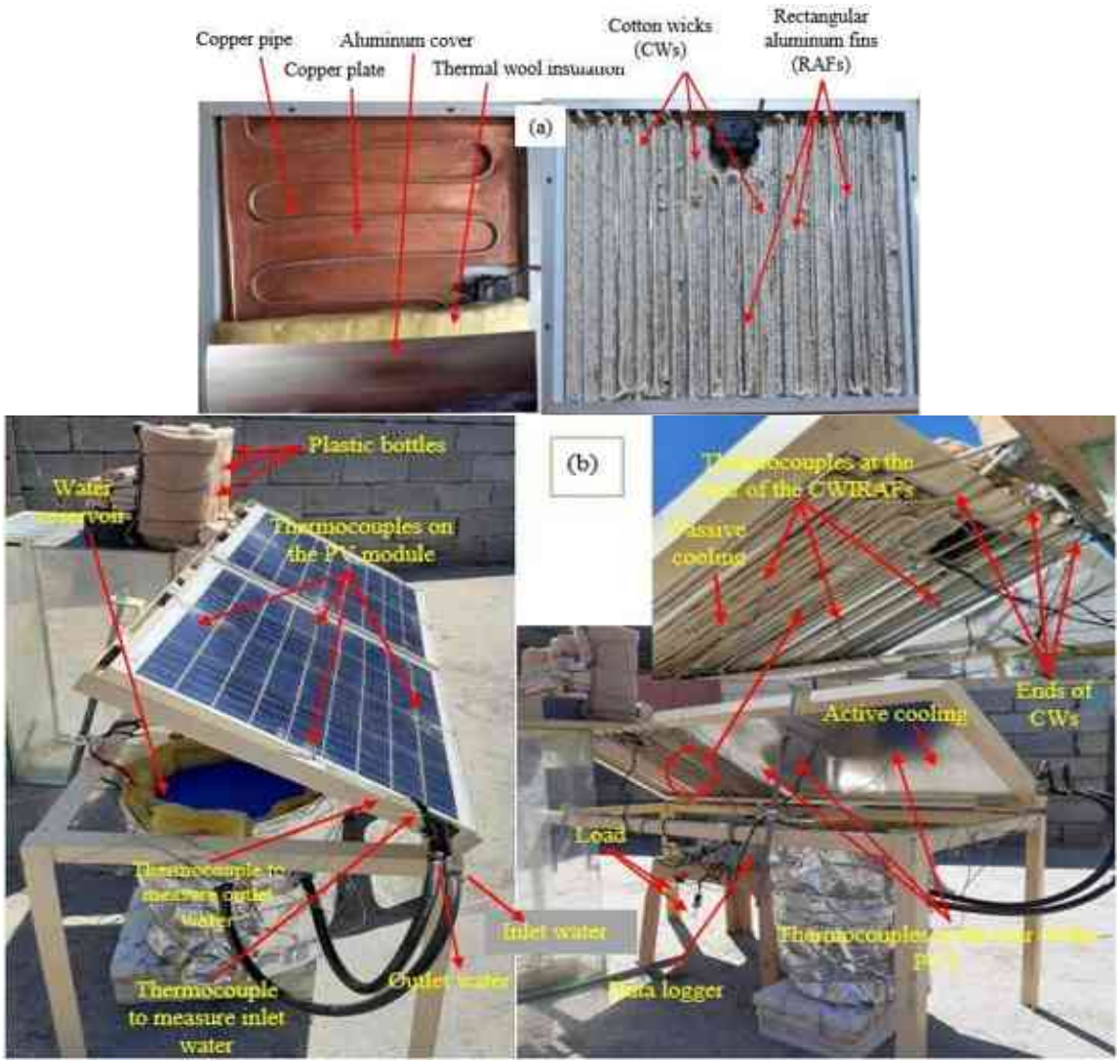

Figure B2.3: Configurations of PV with CWIRAFs and PVT collector (a) and (b) using passive and active cooling with PV modules

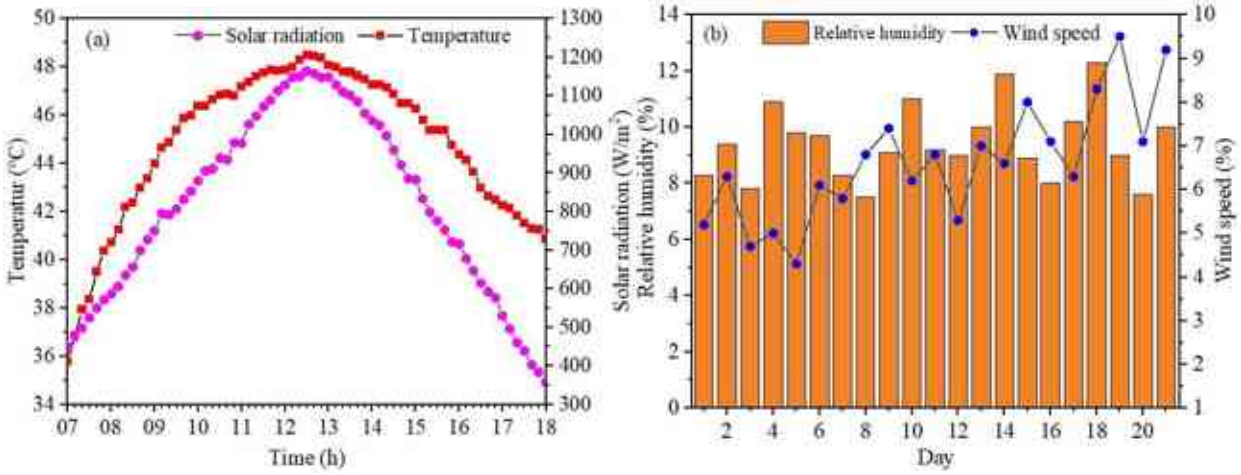

Figure B2.4: The operational parameters (a) ambient temperature and solar radiation, (b) wind speed and humidity throughout the experiments

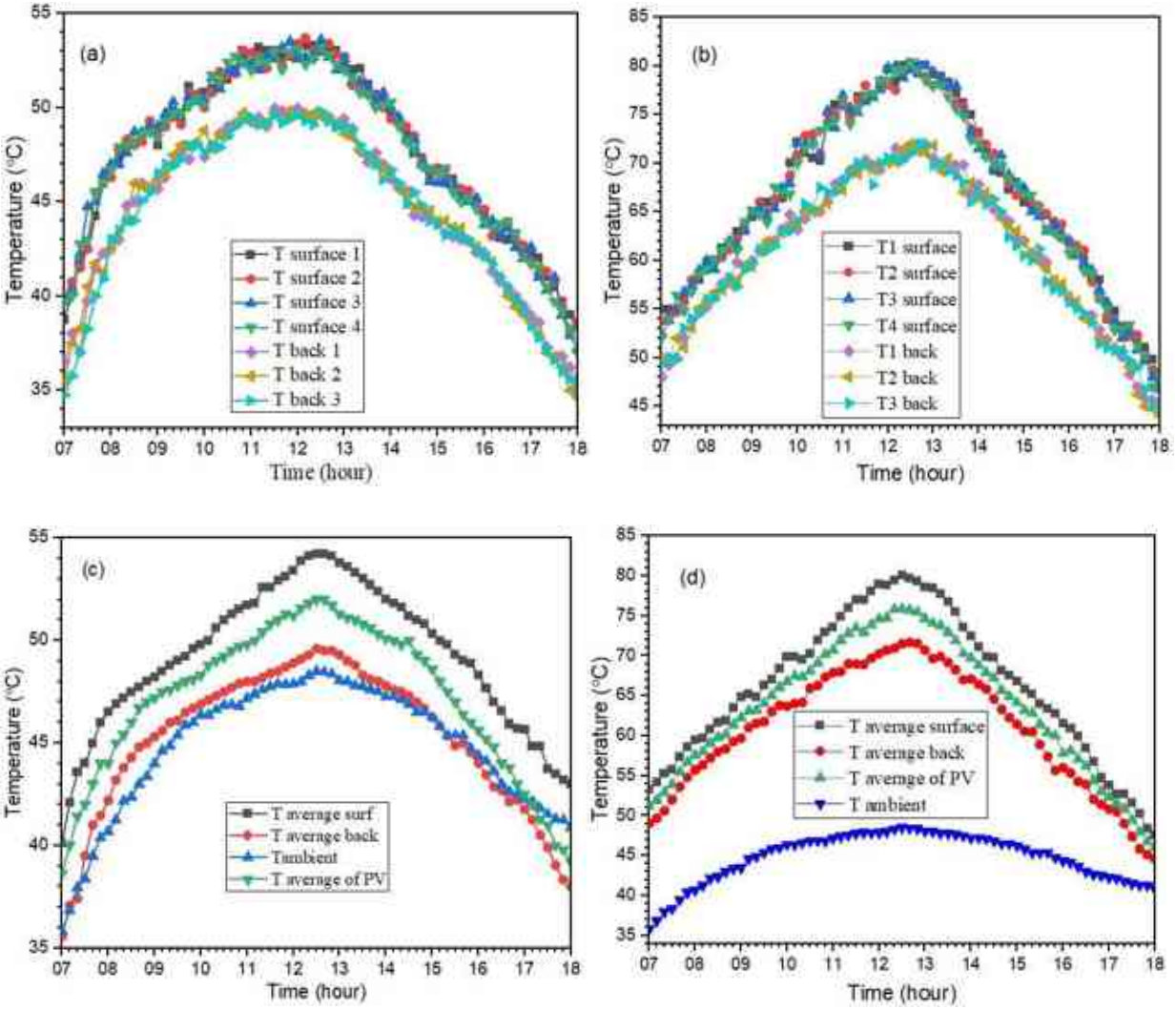

Figure B2.5: Temperature distribution on PV modules (a) with cooling, (b) without cooling, Average temperature of PV module (c) with cooling and (d) without cooling

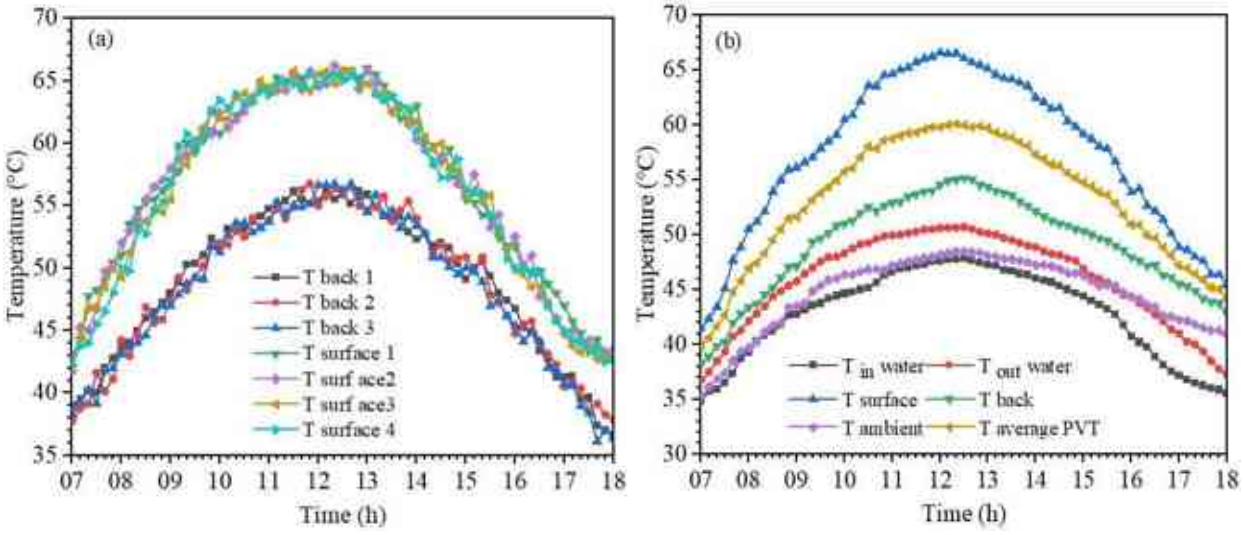

Figure B2.6: The temperature profile of the PVT collector (a) surface, backside temperature (b) average temperature of the PVT collector.

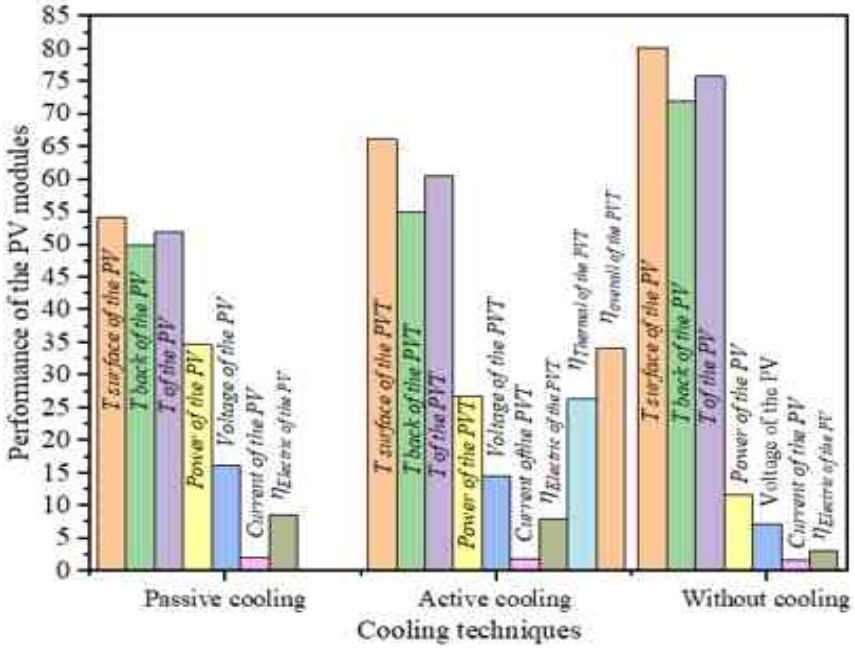

Figure B2.7: Comparison of PV module's performance under different cooling techniques

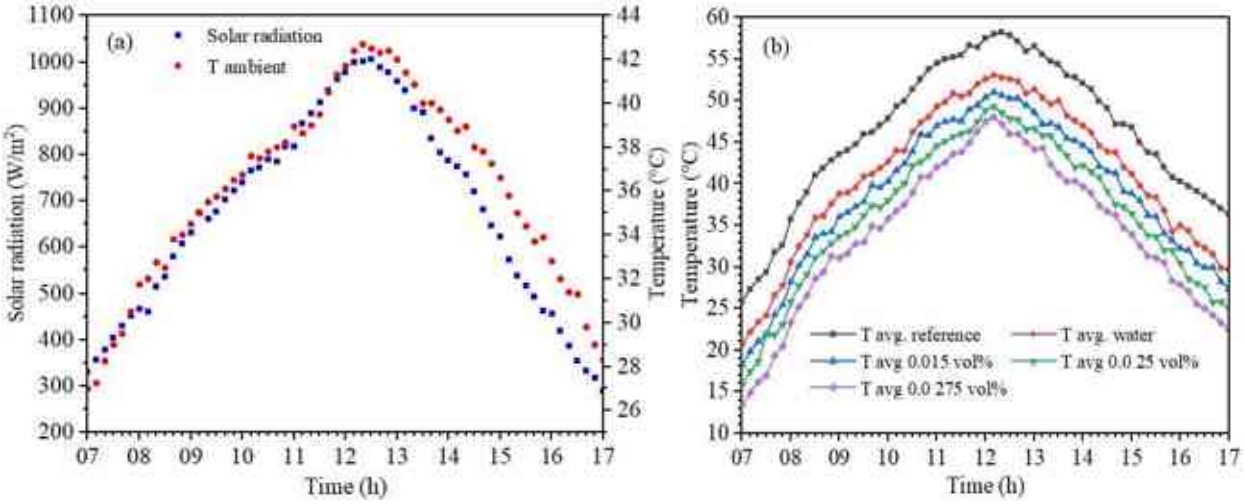

Figure B2.8: Average ambient temperature and solar radiation and (b) The temperature of the PVT system cooling by ZrO_2 nanofluid

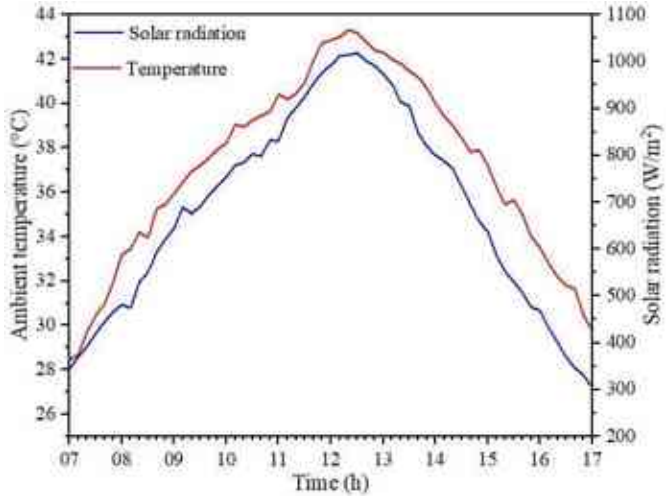

Figure B2.9: Average daily ambient temperature and incident solar radiation during the test period.

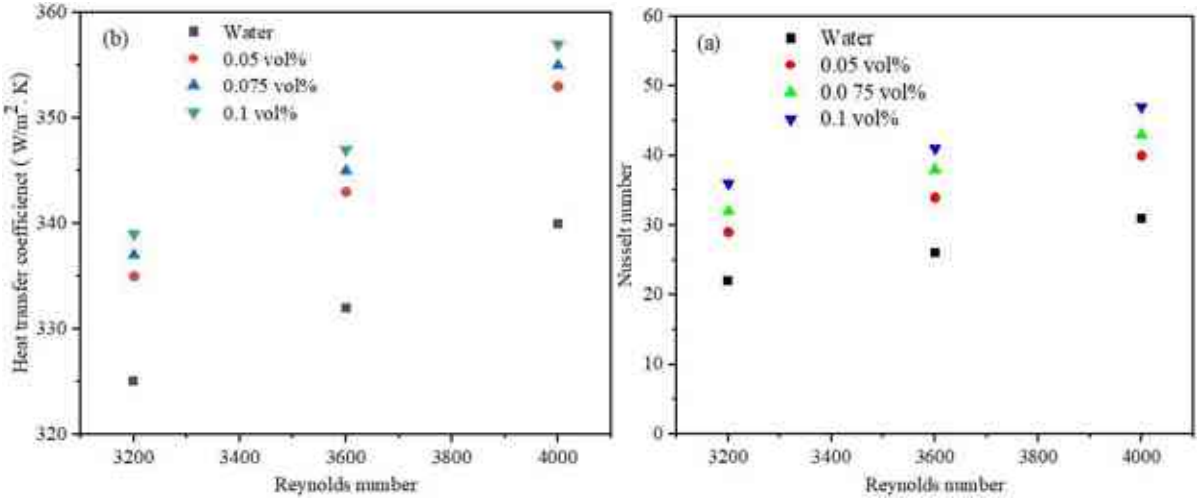

Figure B2.10: Effect of Reynolds number and volume concentration on (a) Nusselt number and (b) heat transfer coefficient

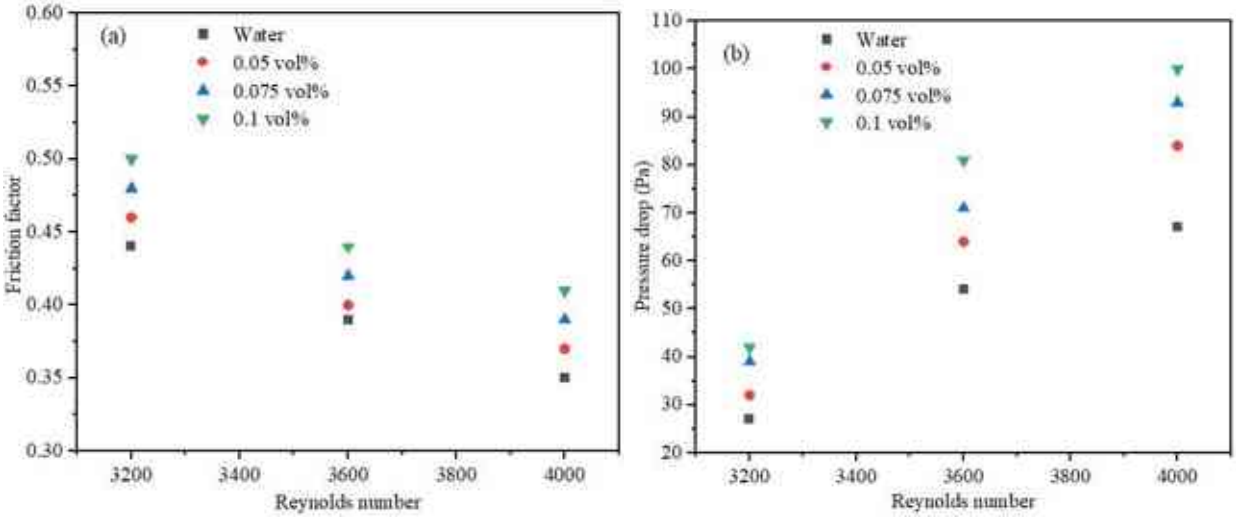

Figure B2.11: Effect of Reynolds number and volume concentration on (a) fraction factor and (b) pressure drop

Table B2.1: The properties of the cotton wicks

[119] [139]	Cotton wick diameter	Cotton wick length	Thermal conductivity	Heat transfer coefficient
	8 mm	50 m	0.048W/m·K	36 W/m °C

Table B2.2: Specifications of the measurement devices and sensors.

Item	Model/Brand	Range	Accuracy
Thermocouples	K (2 m length)	−200 °C to 1350 °C	0.25 °C
Solar power meter	SM206	1-3999 W/m^2	±0.1 W/m^2
Current sensor	ACS712	up to 30 A	0.04 A
Voltage sensor	Module 25V	up to 25 V	0.02445 V
Flow rate sensor	YF-S201	1-30 L/min	---------
Electronic scale	BOECO BAS	3 Kg	0.0001g
Ultrasonication	Bransonic	240V, Vf: 48kHz	----------

Table B2.3: The PV module performance compared with previous studies

Ref.	Passive cooling techniques	$\eta_{electric}$ increment	Power increment (W)	Temperature reduction (°C)
Current study	Cooling by CWWs/ PV 50W	7.25	16.3	10.3
[118]	Inclined duct with water flows on a piece of cloth/PV 130W	6.7	5	10
[140]	Evaporative cooling by a wool/ PV 80 W	0.6	9.7	12
[42]	Aluminium fins / PV 50 W	2.3	20	5.5
[141]	Cotton wick structures/ PV 25W	1.4	12.2	5.9

Table B2.4: The variation of energy and exergy analysis

Performance of PV module	PV with CWWs
Electrical energy (power output)	30.5 W
Efficiency	7.25 %
electrical exergy	29.8 W
Exergy efficiency	7.2 %

Table B2.5: Material specifications used for passive cooling

Rectangular fins		Cotton wick	
Material	Aluminum	Cotton wick diameter	8 mm
Number of fins	20	Cotton wick length	50 m
Thermal conductivity	237 W/m·K	Thermal conductivity	0.048 W/m·K
Specific heat	903 J/kg·K	Heat transfer coefficient	36 W/m °C
Density	2702 kg/m^3	-	-

Table B2.6: Comparing the PV module's performance with other passive previous studies

Ref.	Cooling techniques	Power increment %	Temperature reduction %	Electrical efficiency increment %
[118]	Passive cooling	5	10	6.7
[28]	Passive cooling	32.7	16	31.7
[142]	Passive cooling	14	27.2	14.5
[143]	Passive cooling	16.2	22	7.25
Current study	Passive cooling	66.6	31.4	63.7

Table B2.7: Comparing the PV module's performance with other active previous studies

Ref.	Cooling techniques	Thermal efficiency %	Electrical efficiency %	Temperature reduction %
[120]	Active cooling	25	8	16
[49]	Active cooling	52	13	9.8
Current study	Active cooling	26.3	8.1	20.8

Table B2.8: Effect of ZrO_2 nanofluid on energy and exergy of the PVT system

Volume concentrations	0.015 vol%	0.025 vol%	0.0275 vol%	DI water
Temperature drops %	14	18.1	21.2	9.7
Power increment W	29.4	32.7	33.72	26.5
Electrical efficiency increment%	8.62	10.87	11.4	7.4
Thermal efficiency increment%	27.8	28.9	30.2	26
Electrical exergy efficiency increment%	7.4	9.2	10.01	6.3
Thermal exergy efficiency increment%	1.22	1.6	1.85	0.81
Exergy losses reduced	203.7	198.8	195.6	209.3
Entropy generation reduced	3.41	3.22	3	3.86

Table B2.9: Effect of WO_3 nanofluid on energy and exergy of the PVT system

Volume concentrations	0.5 vol%	0.75 vol%	1 vol%	DI water
Temperature drops %	13	18	21	9.9
Power increment W	25.71	27.79	28.99	23.86
Electrical efficiency increment%	8.16	9.2	9.82	6.2
Thermal efficiency increment%	26.82	28.8	30.1	24.6
Electrical exergy efficiency increment%	7.87	8.81	9.3	6.2
Thermal exergy efficiency increment%	0.76	0.91	1.2	0.61
Exergy losses reduced	207.2	201.9	197.8	219.8
Entropy generation reduced	3.75	3.54	3.1	3.92

Appendix B3

Effect of mono and hybrid nanofluids on the photovoltaic thermal system efficiency

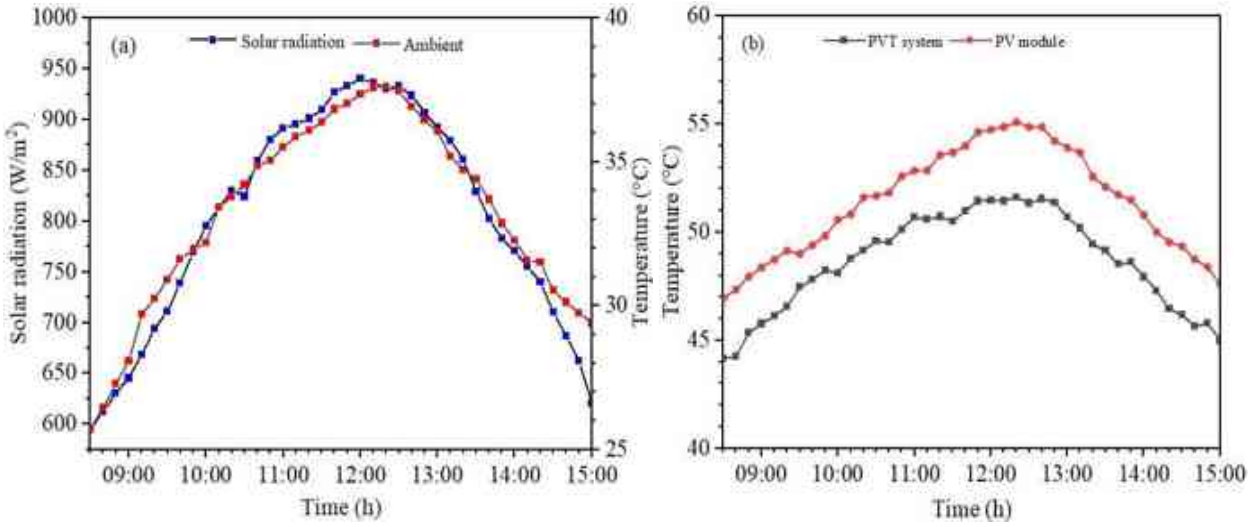

Figure B3.1: The various values of (a) solar radiation and ambient temperature and (b) temperature of the PV module

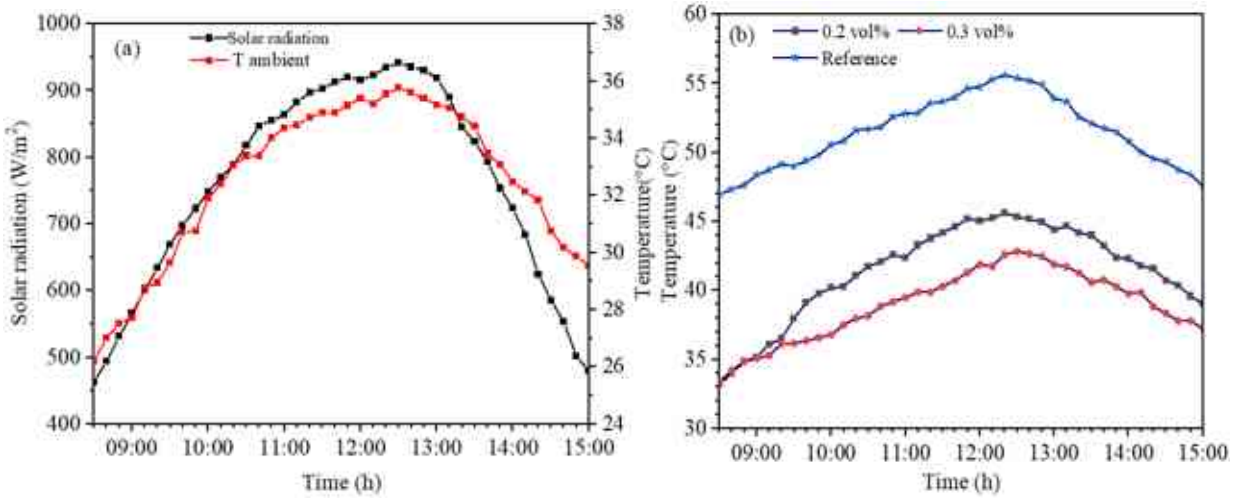

Figure B3.2: The average values of (a) ambient temperature and solar radiation, and (b) PV, PVT system temperature

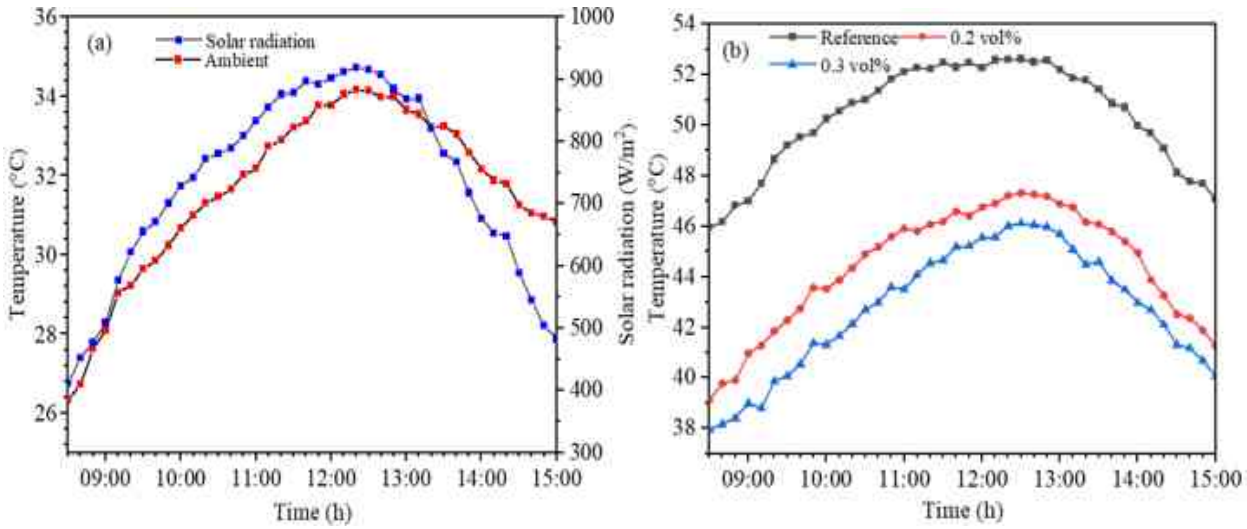

Figure B3.3: The variation values of (a) solar radiation and ambient temperature, and (b) temperature of the PV, PVT system

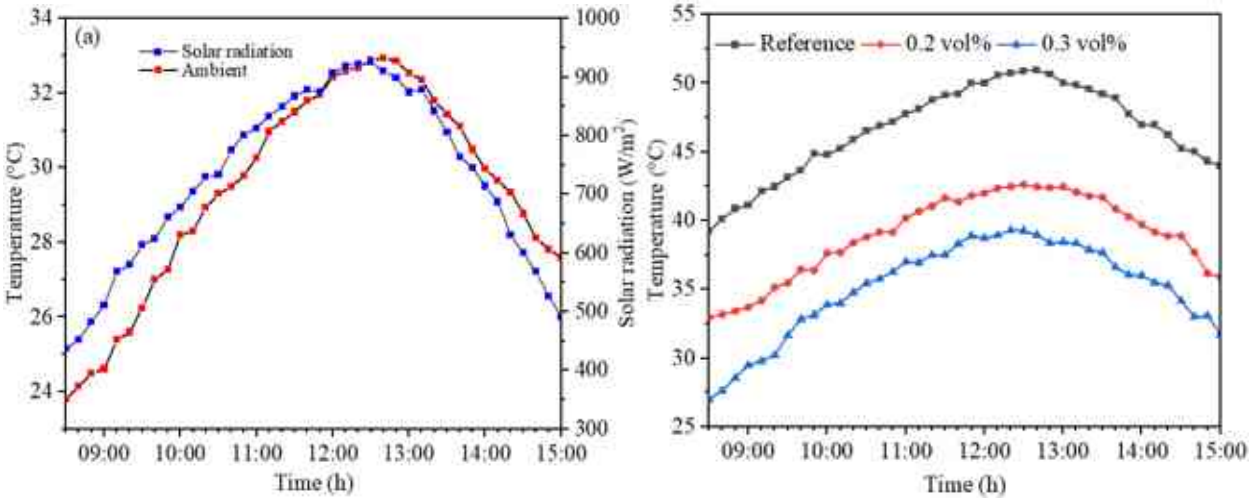

Figure B3.4: The variation value of (a) Solar radiation and ambient temperature, and (b) temperature of the PV, PVT system

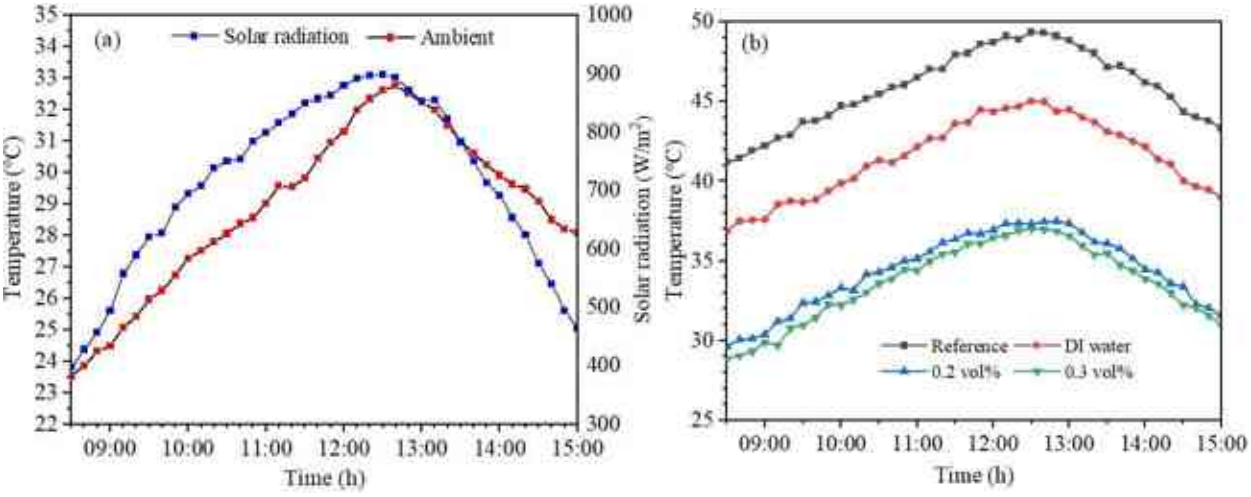

Figure B3.5: The variation values of (a) solar radiation and ambient temperature, (b) temperature of PV and PVT system

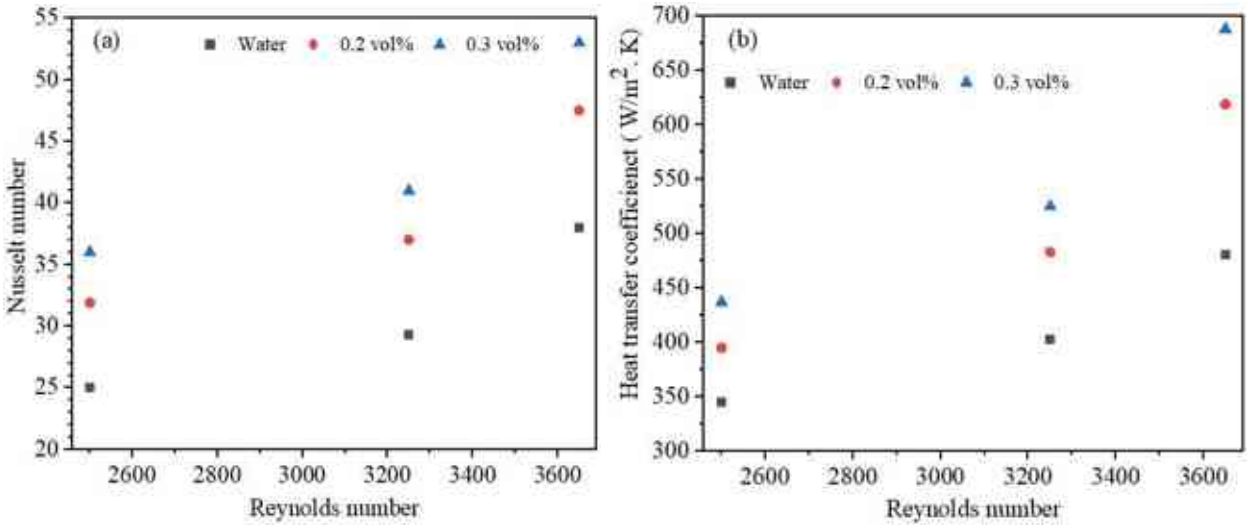

Figure B3.6: The effect volume concentration of TiO_2-Fe_2O_3 on (a) Nusselt number and (b) heat transfer coefficient

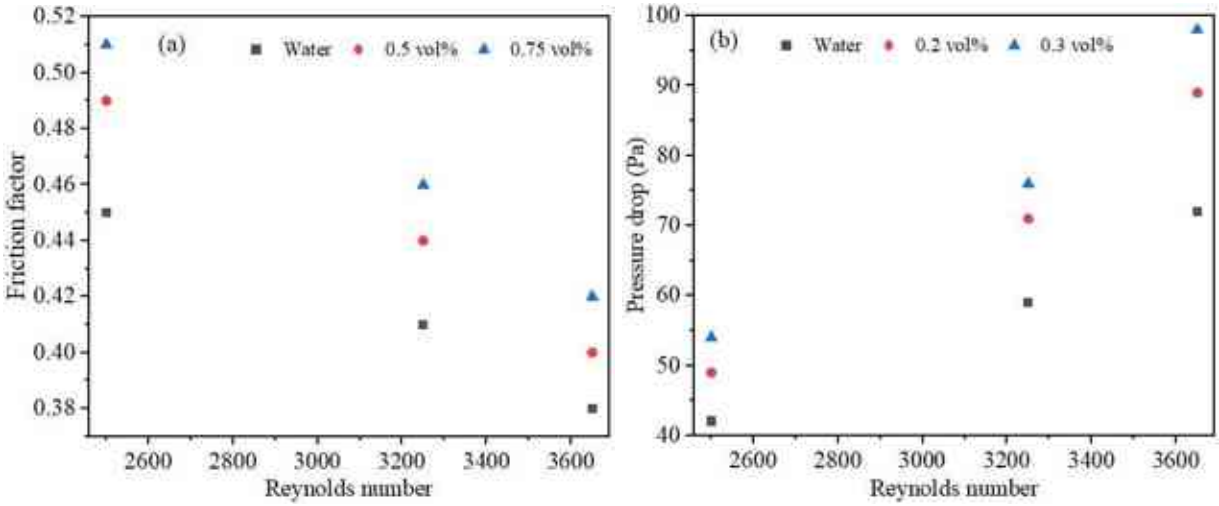

Figure B3.7: The effect of volume concentration of TiO_2-Fe_2O_3 on (a) fraction factor and (b) pressure drop

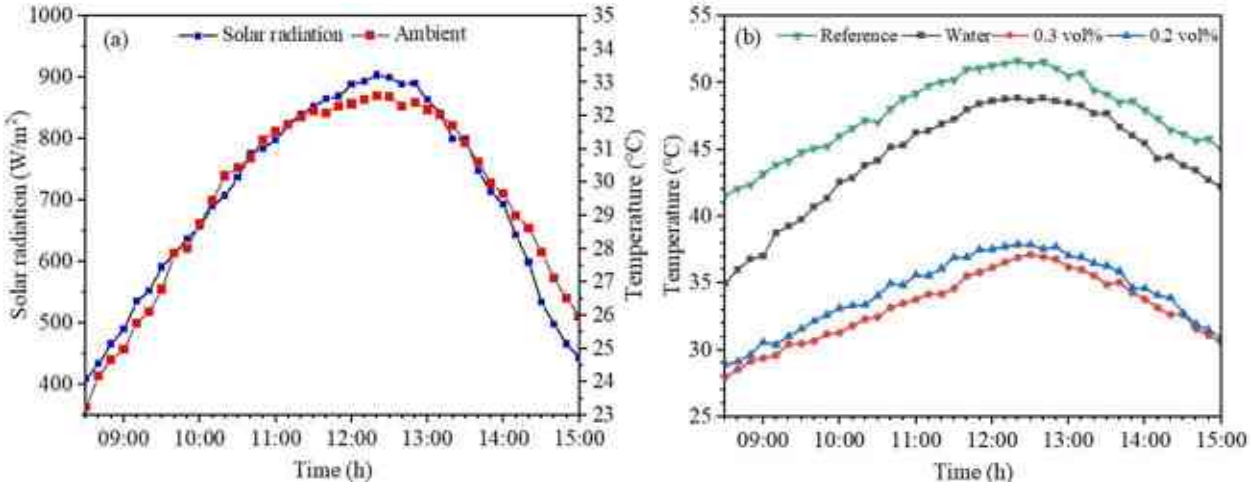

Figure B3.8: Variations values of (a) solar radiation and ambient temperature, (b) temperature of the PV and PVT system

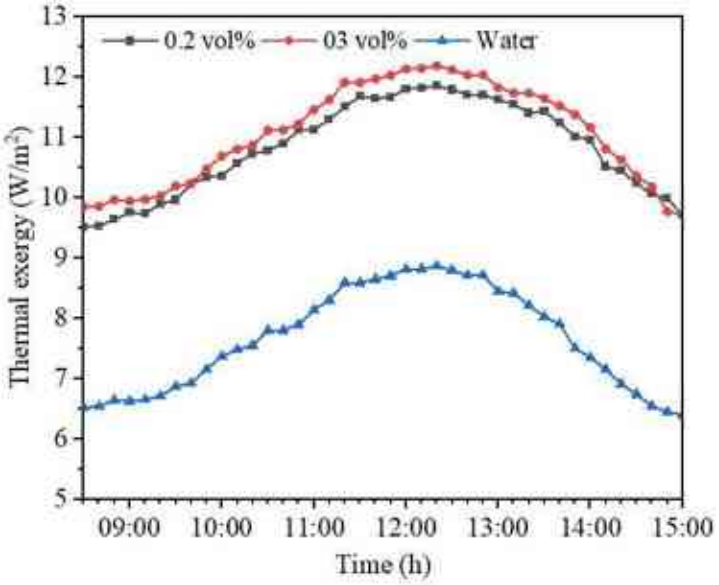

Figure B3.9: Thermal exergy of the PVT system

Table B3.1: Specifications of the measurement devices and sensors

Item	Model/Brand	Range	Accuracy
Thermocouples	T-type 0.2 mm	-250°C to 400°C	± 0.5 °C
Solar sensor	SS11.303	1-3999 W/m^2	± 0.1 W/m^2
Flow rate sensor	YF-S201	1-30 L/min	±10%
Electronic scale	BOECO BAS	3 kg	0.0001 g
Current sensor	ACS712	up to 30 A	0.04 A
Voltage sensor	Module 25V	up to 25 V	0.02445 V
Pump	AD20P-1230C	240 L/H	---------
Ultrasonication	Bransonic	240V, Vf: 48 kHz	----------

Table B3.2: Performance of the PVT system compared with previous studies

Ref.	PV module power	Volume concentration (vol%)	Temperature reduction (°C)	Power increased (W)	Electrical efficiency (%)	Thermal efficiency (%)
Current study	50 W	0.2	7.2	11.9	9.2	36.7
		0.3	10.06	14.6	10.3	38.9
[144]	250 W	0.2	12	9.5	11.2	43
[33]	100 W	0.05	15	11.2	12.9	71. 7
[145]	50 W	0.1	6	3.6	9.5	-

Table B3.3: Compare the energy result obtained by other previous studies

Ref.	PV module peak power	Type of nanofluid	Volume concentration %	Temperature drop %	Electrical efficiency %	Thermal efficiency %
Current study	50 Watts	TiO_2-Fe_2O_3	0.2	12.04	12.44	45.4
		TiO_2-Fe_2O_3	0.3	12.45	12.62	48.2
[146]	35 Watts	$Al2O_3/SiO_2$	0.5	19.2	1.99	9.09
[147]	250 Watts	Al_2O_3/ZnO-Fe_3O_4	1	5.14	13.43	54.11
[148]	250 Watts	$Al2O_3$/ZnO	1.7	21	13.8	55.9
[149]	150 Watts	CNT/Al_2O_3	2	15	17.2	27.23

Table B3.4:The exergy performance compared with previous studies

Ref.	PV module peak power	Type of nanofluid	Volume concentration %	Thermal exergy %	Electrical exergy %
Current study	50 W	TiO_2-Fe_2O_3	0.2	2.28	11.52
			0.3	2.43	12.4
[150]			0.5	0.76	7.87
	50 W	WO_3	0.75	0.91	8.81
			1	1.2	9.3
[35]		Al_20_3	0.2	1.01	10.87
	40 W	ZnO	0.2	1.18	10.99
		TiO_2	0.2	0.91	11.02
			0.1	0.25	15.25
[53]	60 W	Carbon black	0.2	0.52	15.98
			0.3	0.34	15.55
			0.4	0.19	14.45
[151]		ZnO	0.2	0.89	11.48
	40 W	PCM	-	1.6	12.01

Table B3.5: Economic analysis of PV module and PVT system cooled by hybrid nanofluid

Element cost	PVT system costs $	Conventional PV costs $
Configuration	179.86 $	39.76 $
Maintenance	0.007 $/ day	0.00397 $/day
Nanofluid supply	0.06 $/day	-
Operation cost	0.00363 $/ day	-
Energy productivity	0.356 $/day	0.0587 $/day
Net profit	0.285	0.0547
Payback period	630 days	727 days

Table B3.6: The energy analysis of the PVT system compared with previous studies

Ref.	PV module peak power	Type of nanofluid	Temperature drop %	Electrical efficiency %	Thermal efficiency %
Current study	50 Watts	TiO_2-CuO/0.2 vol%	13.7	12.28	44.2
		TiO_2-CuO/ 0.3vol%	14.5	12.4	45.8
[144]	250 W	CuO	12	11.2	43
[33]	100 W	CuO	15	12.9	71.1
[152]	80 W	TiO_2	12.3	7.32	41
[153]	50 W	TiO_2	9.6	18.8	45
[149]	150 Watts	CNT/Al_2O_3	15	17.2	27.23
[146]	35 Watts	$Al2O_3/SiO_2$	19.2	1.99	9.09
[148]	250 Watts	$Al2O_3$/ZnO	21	13.8	55.9
[147]	250 Watts	Al_2O_3/ZnO-Fe_3O_4	5.14	13.43	54.11

Table B3.7: Effect of different nanofluids on the PVT system performance

Cooling applied	PV_{ref}	Cooling by DI water	PV_{ref}	Cooling by CuO nanofluid	PV_{ref}	Cooling by TiO_2 nanofluid	PV_{ref}	Cooling by Fe_2O_3 nanofluid
T_{PV} °C	55.6	-	52.86	-	52.57	-	50.9	-
T_{PVT} °C	-	51.6	-	42.82	-	46.11	-	39.26
P_{PV} W	19.3	-	20.78	-	21.15	-	21.37	-
P_{PVT} W		22.19		35.47	-	31.66	-	37.76
η_{ele-PV} %	5.11	-	5.42	-	4.89	-	5.75	-
$\eta_{ele-PVT}$ %	-	6.32	-	10.3	-	8.44	-	12.1
$\eta_{ther-PVT}$ %	-	30.25	-	49.2	-	43	-	55.4

Table B3.8. Effect of hybrid nanofluid on the PVT system performance

Cooling applied	PV_{ref}	Cooling by TiO_2-Fe_2O_3 nanofluid	PV_{ref}	Cooling by TiO_2-CuO nanofluid
T_{PV} °C	49.85	-	51.63	-
T_{PVT} °C	-	36.37	-	37.1
P_{PV} W	23.14	-	21.9	-
P_{PVT} W		39.71		38.88
η_{ele-PV} %	5.7	-	5.8	-
$\eta_{ele-PVT}$ %	-	12.62	-	12.4
$\eta_{ther-PVT}$ %	-	59.82	-	58.2

Appendix B4

Numerical investigation of cooling the photovoltaic thermal system by different nanofluids

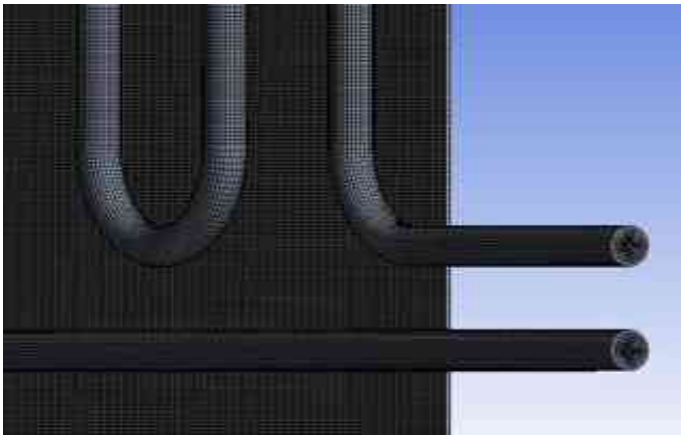

Figure B4.1: The meshing of the model proposed

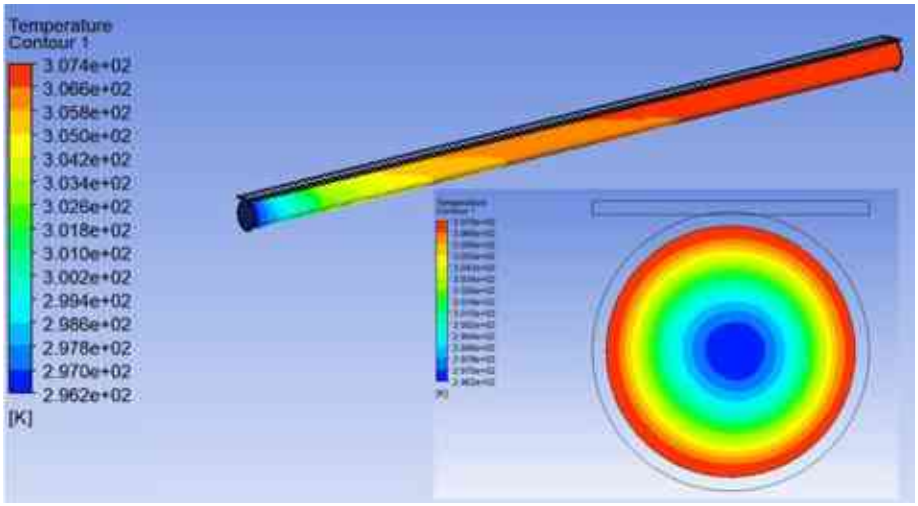

Figure B4.2: Gradual heat transfer

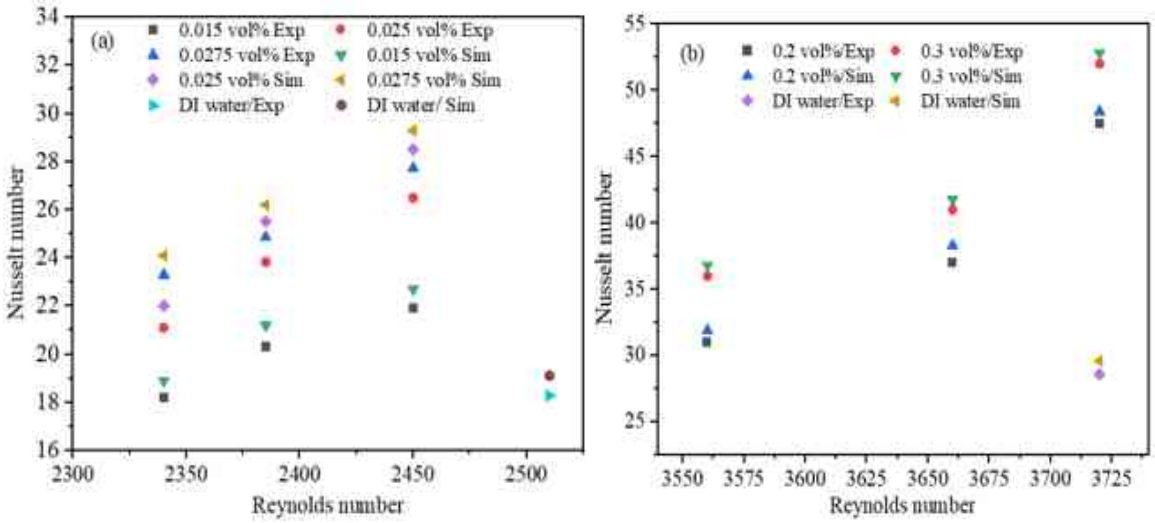

Figure B4.3: Effect of Reynolds number and volume concentration on Nusselt number at used (A) ZrO_2 nanofluid and (b) TiO_2-Fe_2O_3 nanofluid

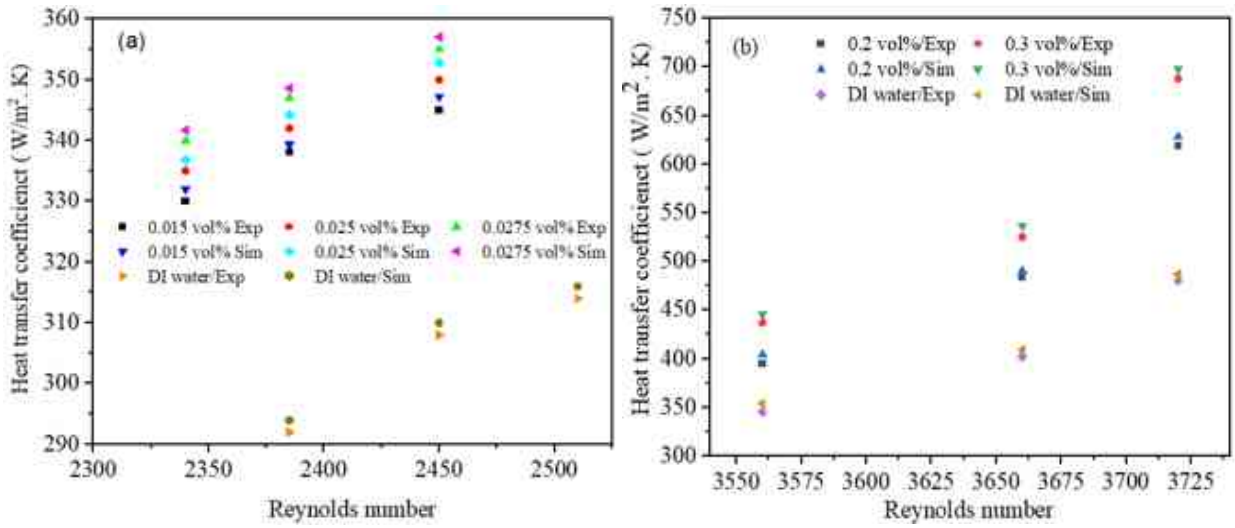

Figure B4.4: Effect of Reynolds number and volume concentration on heat transfer coefficient at used (A) ZrO_2 nanofluid and (b) TiO_2-Fe_2O_3 nanofluid

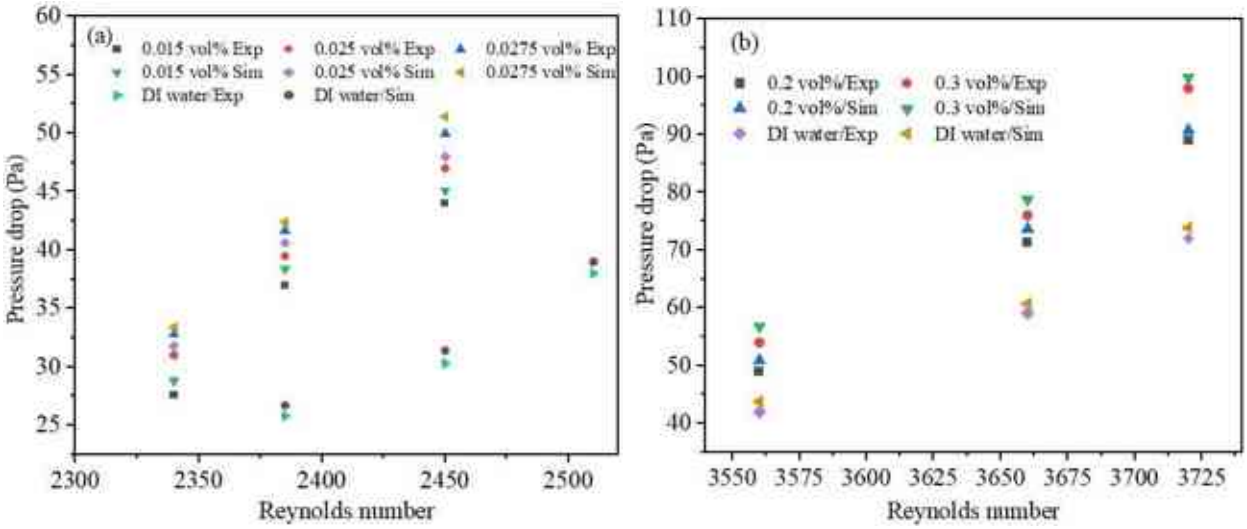

Figure B4.5: Effect of Reynolds number and volume concentration on pressure drop using (a) ZrO_2 nanofluid and (b) TiO_2-Fe_2O_3 nanofluid

Table B4.1: The model component's characteristics

Glass	Emissivity 0.88
PV module	Number of riser cells: 60 Area: 0.355 m^2 Absorptance: 0.9 Emissivity: 0.88 η_r = 15% β_r= 0.0045 $°C^{-1}$
Absorb plate	Area: 0.2928 m^2 Thickness: 0.002 m Material: Copper C_p= 381 J/kg K, k = 387.6 W/m K, ρ = 8978 kg/m^3
Tubes	Length of tubes: 5 m The thickness of the tube: 0.001 m Outer diameter: 0.01 m Material: Copper

Table B4.2: The variation between simulation and experiments results

Nanofluid	Temperature	Electrical efficiency	Thermal efficiency	Heat Transfer coefficient	Nusselt number	Pressure drops	Electrical exergy efficiency	Thermal exergy efficiency
ZrO_2	2.86%	3.61%	2.95	2.46	2.56	3.1	2.61	2.87
TiO_2-Fe_2O_3	2.73%	2.98%	3.1	2.3	2.96	2.6	3.12	3.3